

HYDROGENATION AND POLYMER MODIFICATION IN SUPERCRITICAL FLUIDS

Thesis submitted for the degree of
Doctor of Philosophy
at the University of Leicester

by

Wayne Eltringham BSc (Leicester)
Department of Chemistry
University of Leicester

August 2004

UMI Number: U188370

All rights reserved

INFORMATION TO ALL USERS

The quality of this reproduction is dependent upon the quality of the copy submitted.

In the unlikely event that the author did not send a complete manuscript and there are missing pages, these will be noted. Also, if material had to be removed, a note will indicate the deletion.



UMI U188370

Published by ProQuest LLC 2013. Copyright in the Dissertation held by the Author.
Microform Edition © ProQuest LLC.

All rights reserved. This work is protected against
unauthorized copying under Title 17, United States Code.



ProQuest LLC
789 East Eisenhower Parkway
P.O. Box 1346
Ann Arbor, MI 48106-1346

HYDROGENATION AND POLYMER MODIFICATION IN SUPERCRITICAL FLUIDS

WAYNE ELTRINGHAM
UNIVERSITY OF LEICESTER

2004

ABSTRACT

The aim of this work was to investigate the applicability of using supercritical (sc) hydrofluorocarbons (HFCs) as alternative solvents for hydrogenation and polymer modification processes. Solubility studies in binary and ternary systems have been carried out using both dielectrometry and gravimetric techniques and results show that a range of unsaturated carboxylic acids (crotonic acid, 6-methoxy-1-tetralone, methylsuccinic acid, α -acetamido-cinnamic acid and itaconic acid) have a high degree of solubility in 1,1,1,2-tetrafluoroethane (HFC 134a). The solubility results were modelled successfully using the Peng-Robinson equation of state (PR EOS) and this model was used to devise a separation methodology for itaconic acid and methylsuccinic acid. It is suggested that HFC 134a can be used as both the reaction medium and the extracting solvent, which enables in-line separation of compounds during sc synthesis.

The homogeneous asymmetric hydrogenation of a range of unsaturated substrates (itaconic acid, dimethyl itaconate, α -acetamido-cinnamic acid and *trans*-2-methyl-2-pentenoic acid) has been studied using a rhodium/MonoPhos catalytic system. High yields and enantiomeric excesses (ee's) have been observed and this, coupled with the separation technique, provides an effective method of asymmetric reduction, which greatly enhances the commercial applicability of this technology.

The infusion of difluoromethane (HFC 32) into polystyrene (PS) and polyethylene (PE) has been characterised and the results have been compared to those obtained for carbon dioxide. Significant plasticization was observed in the polymeric materials and it was shown that manipulation of the experimental temperature, pressure and depressurisation rate could cause significant changes in the morphology of the samples.

It is concluded that sc HFCs are promising alternatives to conventional organic solvents and are useful for a variety of processes. These media have accessible critical constants, relatively high dielectric constant values and are able to facilitate the dissolution of polar solutes and rhodium based catalysts without the need for co-solvents or fluorinated ponytails. Furthermore, the investigation suggests that reactions carried out in the sc regime can allow facile reagent/product separation and it is logical to assume that a similar methodology can be applied to catalyst recovery.

ACKNOWLEDGENTS

Firstly I'd like to thank my supervisor, Dr. Andrew Abbott, for his continued support over the last three years. His seemingly endless optimism and enthusiasm have been invaluable. I would like to thank Prof. Eric Hope and members of the Leicester Fluorine Group for their help during my research. In particular I'd like to thank Dave Adams and Andy West for useful discussions and for instruction in techniques new to me. I would also like to express my gratitude to Advanced Phytonics Ltd. for supporting this project financially.

It has been a pleasurable and memorable experience working in the Abbott group and a thank you must go to Glen and Ray; not for any relevant contributions or useful discussions but for being such unique characters and making my second spell in Leicester an enjoyable one. Ev, cheers for supplying me with "brain oil" during long stints at my desk.

A big thank you goes to Keith Wilkinson and John Weale for the construction and repair of the high-pressure kit, even when they had a massive workload. There are far too many to mention and a general thanks goes to all the departmental staff that have helped me during my time in Leicester.

I'm ever so grateful to my parents for their financial and moral support over the last eight years. It's been a long haul but I'm finally leaving "school" at the age of twenty-six.....Thank you!

Finally and most of all I'd like to thank Nicky. Her patience during the last six months of my PhD has been akin to that of a saint! There are so many more things I'd like to thank Nicky for and this is the basis of "future work."

“The most exciting phrase to hear in science, the one that heralds new discoveries, is not ‘Eureka!’ (‘I found it!’) but rather ‘hmm....that’s funny’...”

— *Isaac Asimov*

CONTENTS

	Page
CHAPTER 1 Introduction	1
1.1 Introduction	2
1.2 Supercritical Fluids	2
1.3 Hydrofluorocarbons	6
1.4 Supercritical Fluid Applications	9
1.4.1 Chromatography	9
1.4.2 Extraction and Separation Processes	10
1.4.3 Chemical Reactions using Supercritical Fluids	12
1.5 References	19
 CHAPTER 2 Experimental	 25
2.1 Materials	26
2.1.1 Solvents	26
2.1.2 Solutes, Reagents and Catalysts	26
2.1.3 Polymers	26
2.2 Instrumentation	28
2.2.1 General Apparatus	28
2.2.2 Dielectrometry Apparatus	28
2.2.3 Quartz Crystal Microbalance Apparatus	30
2.2.4 Hydrogenation Apparatus	31
2.3 Experimental Methods	33
2.3.1 Solubility Studies	33
2.3.2 Hydrogenation Reactions	35
2.3.3 Polymer Modification	39
2.4 References	40
 CHAPTER 3 Solubility Studies of Solutes in Hydrofluorocarbon Solvents	 41
3.1 Introduction	42
3.1.1 Solubility in Supercritical Fluids	42
3.1.2 Measurement Techniques	44
3.1.3 Solubility Modelling	46
3.1.4 Separation Science using Supercritical Fluids	49
3.2 Results and Discussion	50
3.2.1 Solubility of Solids in Supercritical HFC 134a	50
3.2.2 Modelling Solubility in Supercritical HFC 134a	58
3.2.3 Designing a Separation Process	62
3.3 Conclusion	73
3.4 References	75

CHAPTER 4 Hydrogenation in Hydrofluorocarbon Solvents	78
4.1 Introduction	79
4.1.1 Hydrogenation Reactions	79
4.1.2 Catalytic Systems for Asymmetric Hydrogenation	80
4.1.3 Heterogeneous Hydrogenation using Supercritical Fluids	82
4.1.4 Homogeneous Hydrogenation using Supercritical Fluids	83
4.1.5 Asymmetric Hydrogenation using Supercritical Fluids	87
4.1.6 Continuous Hydrogenation using Supercritical Fluids	91
4.2 Results and Discussion	93
4.2.1 Evaluating HFC 134a as a Solvent for Hydrogenation Processes	93
4.2.2 Asymmetric Hydrogenation in Supercritical HFC 134a	98
4.3 Conclusion	109
4.4 References	110
 CHAPTER 5 Polymer Modification using Supercritical Fluids	 113
5.1 Introduction	114
5.1.1 Solid-State Properties of Polymers	114
5.1.2 Polymer Processing with Supercritical Fluids	117
5.1.3 Gas Sorption of Polymers	119
5.1.4 The Measurement of Gas Sorption using a Quartz Crystal Microbalance	122
5.1.5 Modelling Gas Sorption	123
5.2 Results and Discussion	127
5.2.1 Measurement of Gas Sorption by Polymers	127
5.2.2 Modelling the Gas Sorption Data	147
5.2.3 Kinetics of Gas Sorption	153
5.3 Conclusion	160
5.4 References	162
 CHAPTER 6 Summary and Future Work	 166
6.1 Summary	167
6.1.1 Solubility Studies	167
6.1.2 Hydrogenation Reactions	167
6.1.3 Polymer Modification	168
6.2 Future Work	169
6.2.1 Solubility and Separation Studies	169
6.2.2 Hydrogenation Reactions	169
6.2.3 Polymer Processing	169
 APPENDIX	 170

CHAPTER 1

INTRODUCTION

1.1 Introduction

1.2 Supercritical Fluids

1.3 Hydrofluorocarbons

1.4 Supercritical Fluid Applications

1.4.1 Chromatography

1.4.2 Extraction and Separation Processes

1.4.3 Chemical Reactions using Supercritical Fluids

1.5 References

1.1 Introduction

There is increasing political, social, economic and environmental demand on the chemical industry to develop new, cleaner, more acceptable chemical processes. The obvious target area for process moderation is the solvent. It is well known that the solvent can have a significant effect on the mechanism and kinetics of a reaction¹ and the ideal solvent should:

- Homogenise reactants
- Allow reaction control and selectivity
- Provide a means of temperature control
- Allow simple product isolation
- Be environmentally benign
- Be recyclable
- Be economically viable

Supercritical (sc) fluids are promising alternatives for use as solvents in chemical processing. This work investigates the use of sc fluids as solvents for hydrogenation reactions and as polymer modifying agents. In particular the hydrofluorocarbon (HFC) solvents 1,1,1,2-tetrafluoroethane (HFC 134a) and difluoromethane (HFC 32) are studied.

1.2 Supercritical Fluids

Baron Cagniard de La Tour discovered sc fluids in 1822² and researchers have been aware of their enhanced solvent properties for over a century.³ However, it is only within the last two decades that sc fluids have been the focus of a number of research and development programs.

A sc fluid is defined as a substance exceeding its critical temperature (T_c) and pressure (P_c) but below the pressure required to condense the substance into a solid. The critical point represents the highest temperature and pressure at which a substance can exist as a liquid vapour at equilibrium. A typical phase diagram is shown in Figure 1.1. The curves show where two phases coexist and the triple point represents the coexistence of the solid, liquid and gas phases.

If we move along the liquid-gas coexistence curve (the boiling curve), increasing both temperature and pressure, then the liquid becomes less dense due to thermal expansion and the gas becomes more dense as the pressure is increased. The

point at which these two densities become equal and converge is the critical point, beyond which the substance is in the sc state.

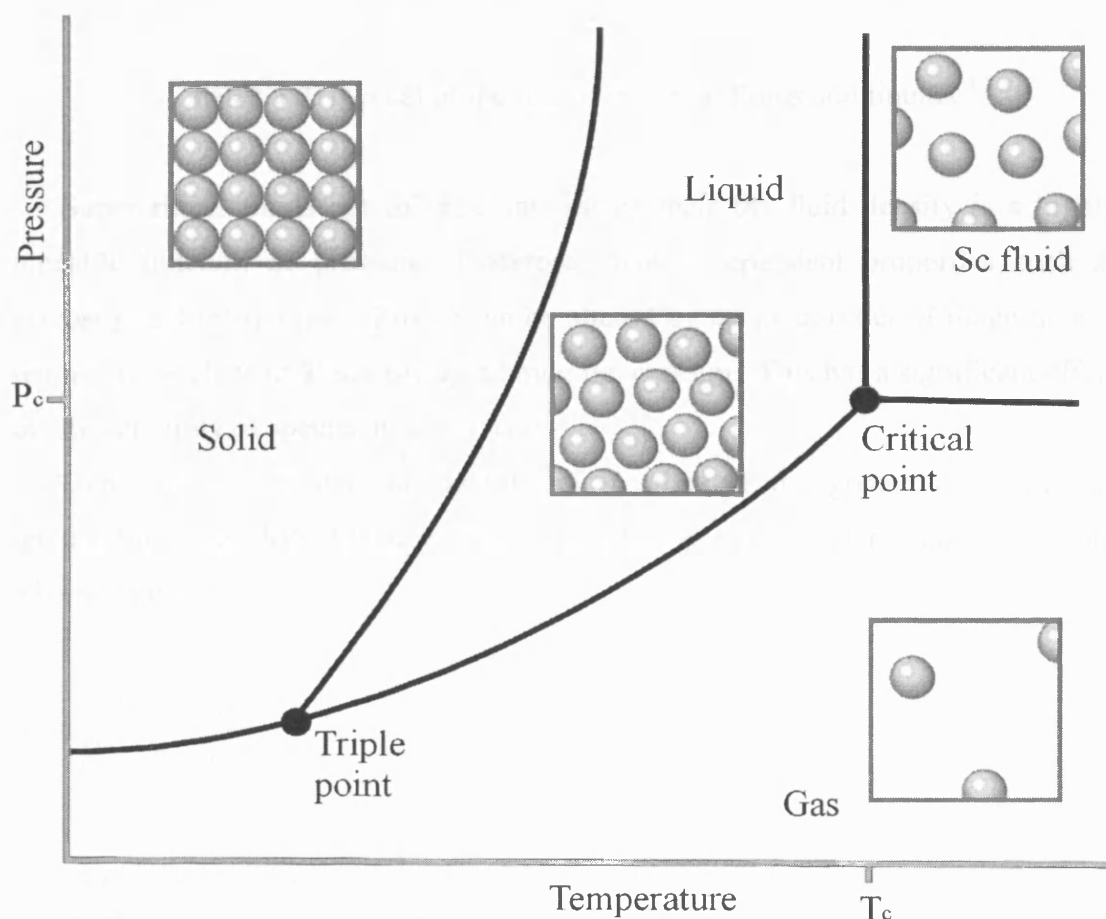


Figure 1.1 A typical phase diagram showing the sc region and a density representation of each phase.

A sc fluid has some properties that are between those of liquids and gases. Some typical values of selected physical properties of sc fluids are compared to those of gases and liquids in Table 1.1.^{4,5} As a result of these intermediate properties sc fluids have gas-like transport properties but a density, which provides large solute-solvent interactions affording liquid-like solvating power. Other properties such as compressibility and heat capacity are significantly higher near the critical point than they are in liquids or gases.

Property	Gas	Sc fluid	Liquid
Density (g cm^{-3})	10^{-3}	0.4	1
Viscosity ($\text{g cm}^{-3} \text{s}^{-1}$)	10^{-5}	10^{-4}	10^{-3}
Diffusivity ($\text{cm}^2 \text{s}^{-1}$)	10^{-1}	10^{-3}	10^{-5} - 10^{-6}

Table 1.1 Typical properties of gases, sc fluids and liquids.^{4,5}

Supercritical fluids are of great interest because the fluid density is a highly tuneable function of pressure. Therefore, density-dependent properties such as viscosity and relative permittivity can be altered by up to an order of magnitude at temperatures close to T_c simply by altering the pressure. This has a significant effect on the solubility of species in sc solvents.

Generally the greater the polarity of a substrate the greater is its critical temperature⁶ and this can be explained in terms of the van der Waals equation,⁷ which is given by

$$p = \frac{RT}{V_m - b} - \frac{a}{V_m^2} \quad (1.1)$$

where p is the gas pressure, R is the ideal gas constant, T is the temperature, V_m is the molar volume and a and b are the van der Waals coefficients; a relates to the attractive forces of the molecules and b is a correction to the volume due to molecular repulsive forces. The critical constants can be related to the van der Waals coefficients by interpretation of the corresponding isotherms. For $T < T_c$, the calculated isotherms pass through a minimum followed by a maximum. As T approaches T_c these two extremities converge and coincide at $T = T_c$ giving a flat inflection point in the isotherm. From the properties of curves it is known that the first and second derivatives are equal to zero at such inflection points. It is, therefore, possible to calculate the critical constants by finding these derivatives and setting them equal to zero (Equations 1.2 and 1.3).

$$\frac{dp}{dV_m} = -\frac{RT}{(V_m - b)^2} + \frac{2a}{V_m^3} = 0 \quad (1.2)$$

$$\frac{d^2 p}{dV_m^2} = \frac{2RT}{(V_m - b)^3} - \frac{6a}{V_m^4} = 0 \quad (1.3)$$

The solutions of these two equations to give the critical constants are

$$V_c = 3b, \quad p_c = \frac{a}{27b^2} \quad \text{and} \quad T_c = \frac{8a}{27Rb} \quad (1.4)$$

For polar molecules a is the dominant and more positive coefficient and, therefore, the critical parameters are higher.

Water (H₂O) would be an ideal solvent due to its high polarity but unfortunately it has critical constants ($T_c = 647.35$ K, $P_c = 220.5$ bar)⁸ that make it impractical for widespread industrial applications. Water has also been shown to be highly corrosive in the sc state.^{9,10}

Supercritical CO₂ has received the most attention to date because it has relatively low critical parameters ($T_c = 304.25$ K, $P_c = 73.8$ bar),¹¹ is environmentally benign and is available in high purity at low cost. Unfortunately, due to the low polarity of CO₂, its applications are limited to low-to-medium molecular weight, non-polar solutes. The solvating power of CO₂ can be enhanced by the addition of a co-solvent (or polar modifier), which modifies the characteristics of the sc CO₂ so that they are more like those of the solute.¹¹ However, the more modifier that is added, the more sc CO₂ moves away from being the ideal solvent. It is also possible that the modifying agents could be left as residues, which could be problematic if the end product is for human consumption.¹²⁻¹⁴ Other common sc media with low critical parameters ($T_c < 308.15$ K) include xenon, ethane and ethane. These fluids are also non-polar, which precludes the dissolution of more polar solutes.¹⁵

More recently it has been suggested that hydrofluorocarbons (HFCs) are a promising class of sc fluids because they are non-toxic, inert and can be polar yet still exhibit low critical constants.¹⁶

1.3 Hydrofluorocarbons

Following the discovery of the ozone hole over Antarctica in the mid-1980's, chlorofluorocarbons (CFCs) were implicated as the primary agent responsible for ozone depletion. This led to movements calling for the reduction and elimination of ozone-depleting substances. The Montreal Protocol¹⁷⁻¹⁹ was a landmark, international agreement, originally signed in 1987, which stipulated that the production and consumption of ozone depleting compounds were to be phased out by 2005.

Chlorofluorocarbons were used in a variety of applications including refrigeration, air-conditioning, insulation, medical products and cleaning of precision engineering components. It was, therefore, important for effective alternatives to be found and HFCs have replaced some CFCs in the refrigeration and propellant industries.^{20,21} Some of these HFCs are shown in Table 1.2.²² HFCs retain many of the properties of CFCs but there was some uncertainty regarding their environmental effects. The Alternative Fluorocarbons Environmental Acceptability Study (AFEAS) reviewed these affects in 1989.²³

The study concluded that the ozone depleting potential and global warming potential for HFCs were much smaller than those for CFCs. The fact that HFCs contain no chlorine means they will not contribute to ozone depletion and the presence of hydrogen in their structure means they are largely removed in the lower atmosphere by natural processes. For most of the compounds the decomposition products will be simple, inorganic species already present in the atmosphere.^{23,24} Some HFCs have the ability to form trifluoroacetyl halides that will dissolve in water to give trifluoroacetate (TFA) salts.^{23,25} These salts are present in rain or surface water but are degraded by microorganisms naturally present in soils and sediments. TFA salts were detected at low levels in rainwater and tropospheric air samples even before significant amounts of HFCs were used.^{26,27}

The rates at which CO₂, CFCs and HFCs are removed from the atmosphere differ greatly (Table 1.3).²⁸ It can be seen that the lifetimes of some commonly used HFCs are much shorter than those for CO₂ and CFCs. The destruction of HFCs in the lower atmosphere, along with their relatively short lifetime, means they do not accumulate and, therefore, have a smaller potential to contribute to the greenhouse effect.

Hydrofluorocarbon	Abbreviation	Application
1,1,1,2-Tetrafluoroethane	HFC 134a	Refrigeration, aerosol, foam blowing and medical
1,1-Difluoroethane	HFC 152a	Aerosol
Difluoromethane	HFC 32	Refrigeration blends
1,1,1-Trifluoroethane	HFC 143a	Refrigeration blends
Pentafluoroethane	HFC 125	Refrigeration blends
1,1,1,2,3,3,3-Heptafluoropropane	HFC 227ea	Aerosol propellant and fire fighting agent
1,1,1,3,3,3-Hexafluoropropane	HFC 236fa	Foam blowing

Table 1.2 Some common HFCs and their uses.²²

Compound	Abbreviation	Estimated Atmospheric Lifetime (years)
Carbon dioxide	CO ₂	50-500 ^a
Trichlorofluoromethane	CFC 11	45 ^b
Dichlorodifluoromethane	CFC 12	100 ^b
1,2-dichlorotetrafluoroethane	CFC 114	300 ^b
Chloropentafluoroethane	CFC 115	1700 ^b
1,1-Difluoroethane	HFC 152a	1.4 ^b
Difluoromethane	HFC 32	5 ^b
1,1,1,2-Tetrafluoroethane	HFC 134a	13.8 ^b
1,1,1,2,3,3,3-Heptafluoropropane	HFC 227ea	33 ^b

Table 1.3 Atmospheric lifetimes of CO₂ and some selected CFCs and HFCs.²⁸

^a Variable due to different CO₂ removal processes ^b Data taken from the Intergovernmental Panel on Climate Change (IPCC) 2001.

More recently HFCs have been studied for applications outside the refrigeration and propellant industries including dry-cleaning,²⁹⁻³¹ natural product extraction,³² HPLC mobile phases³³⁻³⁵ and their use as solvents.³² They have been studied as potential replacements for conventional solvents and the more commonly used sc solvent CO₂. Supercritical CO₂ has been widely studied and employed due to its environmental and economic benefits. The problem associated with using CO₂ as a solvent for extraction and reaction processes is its inability to dissolve polar solutes due to its low polarity. This may result in the use of large volumes of solvent and high pressures, thus increasing cost and energy contributions. If the cost and energy factors become too high then the beneficial aspects of employing CO₂ can be negated. It has been reported that some fluids such as HFC 134a and HFC 32 are relatively polar solvents in the sc state³⁶⁻³⁸ and this allows them to be used as efficient solvents for extraction and reaction processes. Table 1.4 shows the critical parameters³⁹⁻⁴⁰ and dipole moments (μ)^{20,21} of HFCs 134a, 32 and 125. They all have a critical temperature below 375 K and dipole moments greater than 1.5 D. Some conventional solvents are shown for comparison⁴¹ and it can be seen, based on dipole moments, that these HFCs are promising alternatives for use as extraction and reaction media.

Solvent	Abbreviation	T _c (K)	P _c (bar)	μ (D)
1,1,1,2-Tetrafluoroethane	HFC 134a	374.21	40.59	2.058
Diffuoromethane	HFC 32	351.26	57.82	1.98
Pentafluoroethane	HFC 125	339.33	36.29	1.563
Toluene	-	591.80	41.06	0.31
Dichloromethane	DCM	510.00	61.71	1.14
Ethyl acetate	-	523.30	37.81	1.82
1,2-Dichloroethane	1,2-DCE	561.00	53.70	1.83

Table 1.4 The critical constants and dipole moments of HFC 134a, HFC 32 and HFC 125. Some conventional solvents are shown for comparison.^{20,21,39-41}

1.4 Supercritical Fluid Applications

The ability to vary the solvating power of sc fluids by simple manipulation of temperature and/or pressure offers a means of control and selectivity for various chemical applications. This has resulted in their exploitation for use in chromatography (section 1.4.1),^{42,43} extraction (section 1.4.2)^{44,45} and reaction processes (section 1.4.3).¹¹

1.4.1 Chromatography

It has been recognised that sc fluids can be employed as mobile phases for chromatographic analysis.^{46,47} Supercritical fluid chromatography (SFC) uses sc gases to transport compound mixtures over the stationary phase and takes advantage of the liquid-like solvating power and gas-like transport properties of these fluids. The solvent power of sc gases is determined by density and can easily be modified by pressure.⁴⁸ Furthermore, separation of the eluted compounds is easily achieved by pressure release.¹¹ The enhanced mass transport properties of the sc mobile phase allows the dissolution and separation of high molecular weight compounds, even at relatively low temperatures.⁴⁹ Supercritical fluid chromatography is therefore an important analytical technique that can provide information on solubility and separation conditions of a wide range of molecular mass compounds, which is essential in designing chemical processes. Hupe *et al.* have reviewed the theory and fundamentals of SFC in detail.⁵⁰

As awareness of SFC has increased so has the research. Earlier studies include the separation of oligomers,⁵¹ polystyrene⁵² and high molecular mass compounds.⁵³ Analyses of plant materials⁵⁴ and aromatics in diesel fuel⁵⁵ have also been carried out using SFC. A review by Chester and Pinkston⁵⁶ describes some of the most recent applications of SFC and these include applications in forensic science^{57,58} and separations in the natural product and food industries.

The most commonly used mobile phase in SFC is sc CO₂^{49,59,60,61} but many applications require the addition of co-solvents to this non-polar fluid.⁶²⁻⁶⁴ Some research groups have investigated the use of HFC 134a for chromatographic applications in both the liquid and sc state.^{32,33} They reported that HFC 134a offered improved resolution for many separations when compared to those given by sc CO₂. The scale-up of the SFC process employing HFC 134a is potentially easier and more cost effective than that for sc CO₂ due to the lower pressures involved.³²

1.4.2 Extraction and Separation Processes

Supercritical fluids are of interest for extraction because of the marked changes that can occur in solvent properties following modest changes in temperature or pressure.^{6,42-45} It is therefore very important to characterize the effect of physical conditions on solvent properties and over the last few decades the solubilities of solids and liquids in sc fluids have been studied extensively. Solubility data is important in process design and is influenced by the substrate functionality, solvent nature and the operating conditions. Unfortunately, such information does not always provide an accurate prediction for the efficiency of a supercritical fluid extraction (SFE) for a particular matrix. Early SFE studies based extraction conditions on temperatures and pressures that gave maximum solubility of target analytes in the absence of a matrix.⁴⁵ It was suggested by King⁶⁵ that the concept of threshold solubility could be considered for the target analyte (i.e. the conditions at which the analyte becomes significantly soluble). Although the extractability of a particular compound is governed by different molecular interactions (i.e. solute-solvent interactions versus solute-matrix or solute-solute interactions) the threshold solubility can act as a useful guide in determining the feasibility of a SFE process.

The ideal extraction process should be rapid, simple, cost effective and should provide quantitative recovery of the analyte without loss or degradation. The recovered sample should be ready for direct analysis without the need for additional concentration or fractionation steps and no additional laboratory waste should be produced. These key factors are important considering the political, social, economic and environmental demands placed on the chemical industries of today. Liquid solvent extraction techniques fail to meet a number of these goals and SFE is emerging as a promising tool to overcome these difficulties.

The literature shows that approximately 98 % of developed SFE applications have employed CO₂ as the extracting solvent due to its relatively low critical parameters, its environmentally benign nature and its low cost. Unfortunately due to the low polarity of CO₂ difficulties arise when polar analytes are to be extracted. The solvent power of CO₂ can be increased by the addition of a co-solvent or another alternative is to simply use a more polar fluid as the extracting solvent.⁶⁶

In the 1960's researchers began to develop SFE for the extraction of spices,^{67,68} herbs,⁶⁹ coffee^{44,45,70} and tea^{44,45,71} using mainly sc CO₂. Over the next twenty years there was rapid development of SFE for the extraction of hops,⁷²⁻⁷⁴ cholesterol from

food products,⁷⁵⁻⁷⁷ perfumes and flavours from natural products,⁷⁸ and unsaturated fatty acids from fish oils.^{79,80} There are several large-scale SFE processes in operation around the world. The most important of these processes are the decaffeination of coffee and tea and the extraction of hops. For the decaffeination of coffee the CO₂ must be moistened in order to free the caffeine, which is chemically bound to the chlorogenic acid structure present in the green coffee beans.⁴⁴ Tea is fermented prior to caffeine extraction and the SFE process for hops has replaced the conventional methylene chloride process.⁴⁵ The extraction of hops is an important industrial process because the removal of the bitter flavours, in the form of a syrup-like substance, reduces the cost of storage, air conditioning and transport.

Cholesterol occurs in foods of animal origin such as eggs, meat, fish and dairy products. Increasing awareness of health risks posed by cholesterol intake has prompted manufacturers to develop low-cholesterol products and researchers to develop methods of determining the sterol content in foodstuffs. Supercritical fluid extraction is a promising tool for this determination.⁷⁵ Table 1.5 shows the number and locations of commercial SFE plants as of 2000.⁸¹ Other examples include the treatment of soil and waste⁸²⁻⁸⁴ and SFE has been identified as a possible alternative to CFCs for the cleaning of metals, plastics, composites, ceramics and optical materials.^{66,81}

Supercritical fluid extraction is also an attractive alternative to conventional methods of product purification for pharmaceuticals, vitamins and high value products.⁸⁵ However, the technical application of SFE is mainly restricted to the food industry for extraction from natural materials⁸⁶ and in some cases for the fractionation of the products.⁸⁷ For example, in paprika extraction⁸⁸ the first step involves separation of oleoresins and this is followed by the separation of aroma and essential oils.

Research into the use of sc fluids for extraction purposes is still a rapidly growing area of interest and another potential application under investigation is the purification of polymers. This takes advantage of the variation in polymer solubility, which is governed by chain length and operating conditions. Supercritical fluid extraction has also been successfully employed for the dyeing of textiles. The dyestuff is dissolved in the sc fluid and the mixture penetrates the whole fibre. By controlled pressure release the dyestuff remains on the fibre and no residual solvent

remains in the sample. For a more detailed treatment of the basics and applications of SFE the reader is directed to the works of McHugh, Krukonis⁴⁴ and Taylor.⁴⁵

Commercial Application	Number of Plants	America 	Asia/Australia 	Europe 
Coffee & Tea	5	1	0	4
Hops	7	4	1	2
Nicotine	3	1	1	1
Chemistry	5	3	1	1
Environmental	5	2	3	0
Spices	12	1	5	6
Fats & Oils	8	0	3	5
Medicinal Plants	7	0	1	6
Flavours	7	0	3	4
Total	59	12	18	29

Table 1.5 Commercial SFE plants as of 2000.⁸¹

1.4.3 Chemical Reactions using Supercritical Fluids

The demand for more environmentally benign, efficient and cost effective processes has initiated a great deal of research into the use of sc fluids as reaction media. Most work has been carried out over the last twenty years, although the first reactions in sc fluids are reported from the early nineteenth century. It was Baron Cagniard de La Tour in 1822 who noticed in that near-critical H₂O was particularly reactive.² His pioneering work led to a great deal of research using sc H₂O over the next few decades, as reviewed in great detail by Morey.⁸⁹ There are numerous advantages associated with the use of sc fluids as reaction solvents, all of which are based on the unique properties of these media.¹¹ Different types of reactions may benefit particularly from specific fluid properties.

Enhanced reaction rates have been observed^{90,91} and there are several factors that account for this. Firstly, because of the high temperatures usually involved in sc

synthesis, reaction rates change exponentially in accordance with the Arrhenius equation (Equation 1.1)⁹² where R is the gas constant, A is the pre-exponential factor and E_A is the activation energy.

$$k = Ae^{\frac{-E_A}{RT}} \quad (1.5)$$

Secondly, the low viscosity of sc fluids allows diffusion-controlled processes, such as free-radical and enzymatic reactions, to proceed at higher rates.⁹³ Solvent polarity has also been shown to have an influence on the rates of reaction.⁹⁴

Fox *et al.* demonstrated that the rate of Michael addition of piperidine to methyl propiolate in polar sc fluoroform (CHF_3) and non-polar sc ethane depends on fluid density.⁹⁵ A difference in rate constants was observed between the two solvents, the higher being observed for the reactions in sc CHF_3 , and this was attributed to the reaction dependence on the solvent dielectric constant. The reaction proceeds through a highly polar transition state and this is better stabilized in the more polar sc CHF_3 solvent.

Reactions have been reported in which product selectivity, controlled by variation in sc fluid density, have been far superior compared to those reported using conventional solvents. This has led to a number of studies to determine the influence of either the bulk or local density variations on stoichiometric reactions.⁹⁶⁻⁹⁸ An example is the Diels-Alder reaction, where the endo/exo and ortho/para selectivity appears to be controlled to some extent by variation of the bulk density.⁹⁹⁻¹⁰⁴ One of the earliest reported synthetic reactions in sc fluids was a Diels-Alder reaction carried out by Paulaitis and Alexander.⁹⁹ They studied the effect of sc CO_2 pressure on the reaction rate of maleic anhydride and isoprene. The reaction mechanism was thought to be the same irrespective of the solvent medium and the results showed that the reaction rate increased slightly with increasing pressure.

A later study by Kim and Johnston carried out the Diels-Alder reaction of cyclopentadiene and methyl acrylate.¹⁰⁰ Both endo and exo products are formed in this reaction and they studied product selectivity as a function of sc fluid density. They discovered that endo selectivity increases with increasing fluid density at constant temperature. At constant pressure it was shown that the selectivity decreased with decreasing temperature. They attributed their observations to the

difference in dipole moments between the endo and exo products with the endo being the more polar of the two. Since these early studies wide ranges of sc fluid phase reactions have been reported including inorganic, organic, photochemical, polymerisation and catalytic. A few are discussed here but for a more thorough treatise of this subject the reader is directed to other literatures.^{5,11,105-108}

Sc fluids are gas-like in the fact they have no surface tension. They diffuse rapidly to occupy the entire volume of the system, as do any other gases introduced into that same system. Therefore, the sc fluid and the added gases will be completely miscible in contrast to liquids, in which gases have only slight solubility. Increased gas miscibility can offer optimum selectivity, increased reaction rate and very high conversion.^{5,11,109-111} Several processes including hydroformylation,^{5,11,91,112} oxidation^{5,11,113} and hydrogenation^{5,11,90,114-116} are able to take advantage of this complete miscibility.

Synthetic chemists see dioxygen and air as the ideal oxidants because they are readily available, inexpensive and produce water as the only by-product. An example is the sc water oxidation (SCWO) process,¹¹⁷⁻¹¹⁹ which is an effective means for the complete oxidation of many organic wastes. The SCWO technique has been developed to treat organics in industrial wastewater streams and is an extension of wet air oxidation (WAO), which operates at subcritical temperatures and pressures.¹⁰⁸ Carrying out the oxidation above the critical point offers enhanced reaction rates, a single fluid phase and complete miscibility of non-polar organics with sc H₂O. The subject of hydrogenation is discussed in greater detail in Chapter 4.

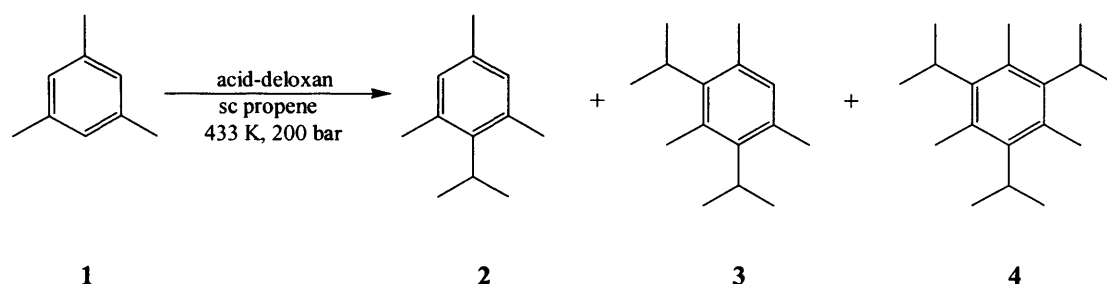
There have been numerous examples of organic reactions that exploit the unique properties associated with sc fluids and these include amination,¹²⁰ the Fischer-Tropsch (FT) synthesis,¹⁰⁸ alkylation^{121,122} and esterification.¹²³⁻¹²⁸

Fischer and co-workers carried out the amination of amino-1-propanol in a continuous tubular reactor.¹²⁹ The reaction was carried out at 463 K in the near critical region of ammonia ($T_c = 405.55$ K, $P_c = 114.8$ bar) and was catalysed by a Co-Fe catalyst. Only very small changes in conversion were observed but the corresponding selectivity showed a 10-fold increase near the critical region of ammonia. The increase in selectivity was explained in terms of an increased

concentration of ammonia at the surface, which favours the amination with ammonia and suppresses hydrogenolysis-like side reactions.

The classical Fischer-Tropsch synthesis route involves an exothermic, gas phase reaction and therefore efficient heat removal is essential. Another problem is the condensation of higher hydrocarbons formed within the catalyst pores and this can cause catalyst deactivation.¹⁰⁸ In the liquid phase these problems are overcome due to improved heat transfer and enhanced solubility of higher hydrocarbons. This however can lead to lower overall reaction rates due to mass transfer limitations in the liquid phase. It is the gas-like diffusivity and liquid-like solubility of sc fluids that has driven the research of the Fischer-Tropsch synthesis under sc conditions.

Poliakoff *et al.*¹³⁰ carried out the continuous Friedel-Crafts alkylation of mesitylene **1** in sc propene ($T_c = 365.04$ K, $P_c = 46.0$ bar) (Scheme 1.1). The propene acted as both the solvent and the alkylating agent and the reaction was catalysed with a heterogeneous Deloxan[®] catalyst in a small fixed-bed reactor. Although the mono-alkylated species **2** was the major product, selectivity and conversion was low (25% yield with 6% selectivity towards **2**). This selectivity was improved when the reaction was carried out in sc CO₂ with propan-2-ol as the alkylating agent. This gave 100% selectivity for the mono-alkylated product with a 42% conversion.

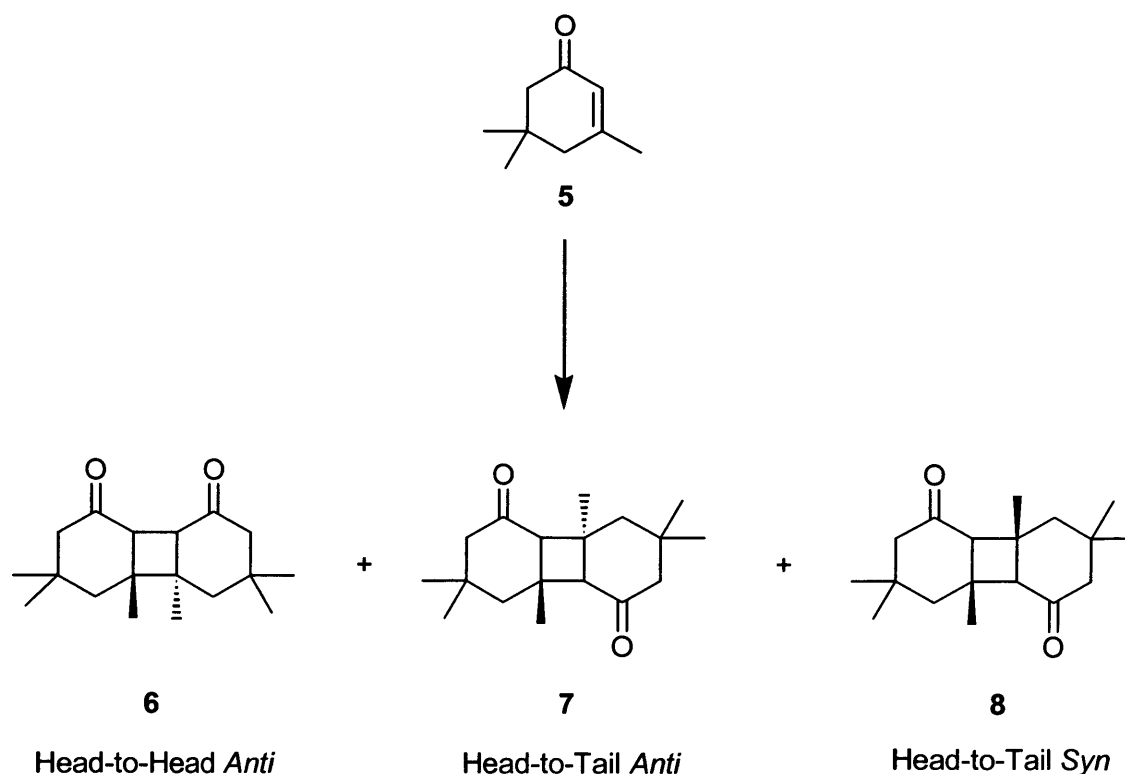


Scheme 1.1

Vieville *et al.* investigated the sulfonic acid catalysed esterification of oleic acid with methanol in sc CO₂.¹³¹ The reaction was found to proceed faster in sc CO₂ than in *n*-hexane. They suggested that due to the hydrophobic nature of the resins, the reactants do not diffuse to the catalytic sites within the resin macropores and the esterification only takes place at the catalyst surface via adsorption of oleic acid.

Therefore the reaction in *n*-hexane appeared to be limited by external diffusion and desorption of reactants and products. The higher reaction rate in sc CO₂ was attributed to the increased solubility of methyloleate and higher diffusivity within the sc reaction media.

Johnston and co-workers report the photodimerisation of isophorone **5** in sc CHF₃ and CO₂ as a function of pressure (Scheme 1.2).¹³² Three possible reaction products are formed. The head-to-head dimer **6** is more polar (5.08 D) than the head-to-tail dimers **7** and **8** (1.03 and 1.09 D respectively). Results were consistent with the fact that the more polar product should be formed in the more polar solvent and *vice versa*. They were also able to show that the regioselectivity of dimers **6** and **7** was a distinct function of pressure in both sc CHF₃ and CO₂ with the anti configuration **7** being the most favoured. They concluded that the relative degree of solvent reorganisation required for the *anti* **7** versus *syn* **8** configurations accounted for this observation.



Scheme 1.2

There are several reviews in the literature on the use of both homogeneous¹⁰⁵⁻¹⁰⁷ and heterogeneous¹⁰⁸ catalysis in sc fluids. The industrial uses of sc fluids as reaction media are becoming more prolific and examples include the synthesis of ammonia, low density polyethylene and more recently, the first multi-purpose industrial scale sc fluid plant has been commissioned (Thomas Swan & Co. Ltd., County Durham, UK).¹³³ Reactions carried out at the Thomas Swan plant include hydrogenations, Friedel-Crafts alkylations, hydroformylations, etherifications and esterifications.

This first chapter is intended to provide the reader with general background material pertaining to sc fluid processes. Chapter 2 describes the experimental methodologies used for data collection and the results are presented in Chapters 3, 4 and 5. Each data chapter contains a subject specific introduction, which is followed by a results and discussion section.

One of the major potential advantages of using HFCs is one of process intensification arising from higher solute solubilities. Therefore, in Chapter 3, the solubilities of a range of carboxylic acids in HFC 134a are discussed in order to assess the suitability of this solvent for sc homogeneous asymmetric hydrogenation processes. Carrying out asymmetric hydrogenation reactions in sc fluids offers the advantage of being able to significantly vary the concentration of hydrogen gas (due to complete gas miscibility with these media), which can enable enantioselective control over reaction products. Solubilities were obtained using both dielectric and gravimetric techniques and a separation methodology for reagents and products is also proposed based upon the results.

After confirming the solubility of substrates, hydrogenation reactions were carried out in sc HFC 134a and the results are presented in Chapter 4. Initial studies were carried out using Wilkinson's catalyst and styrene as a test reaction. Promising results were obtained during this initial investigation and it was shown that catalytic species have sufficient solubility, affording homogeneous reaction conditions, and that reaction rates comparable to those in liquid solvents can be obtained. The asymmetric hydrogenation of a range of carboxylic acid substrates using a rhodium/monodentate-phosphine based catalyst (Section 2.3.2) in HFC 134a was also investigated. Preliminary results suggest that HFCs are promising alternatives for such processes.

It was noted during the hydrogenation and solubility experiments that the sc HFCs caused considerable swelling and deformation of several polymeric components within the high-pressure apparatus due to the high diffusivity of these fluids within these materials. These observations prompted the investigation into the swelling of polymers with HFCs and some results for carbon dioxide (CO₂) were obtained for comparison. The data was obtained *in situ* using a quartz crystal microbalance (QCM) technique and the results are presented in Chapter 5.

1.5 References

1. Buncel, E.; Straits, R.; Wilson, H. *The Role of the Solvent in Chemical Reactions*, Oxford University Press, Oxford, **2003**.
2. Cagniard de La Tour C. *Ann. Chim. Phys.* **1822**, 127.
3. Hannay, J. B.; Hogarth, J. *Proc. R. Soc. London*, **1879**, 29, 324.
4. Van Wasen, U.; Swaid, I.; Schneider, G. M. *Angew. Chem. Int. Ed. Engl.* **1980**, 19, 575.
5. Oakes, R. S.; Clifford, A. A.; Rayner, C. M. *J. Chem. Soc. Perkin Trans. 1.* **2001**, 917.
6. Savage, P. F.; Gopalan, S.; Mizan, T. I.; Martino, C. J.; Brock, E. E. *AIChE. J.* **1995**, 41, 1723.
7. Atkins, P. W. *Physical Chemistry* fifth edition, Oxford University Press, **1994**.
8. Stanley, H. E. *Phase Transitions and Critical Phenomena*, Clarendon Press, Oxford, **1987**.
9. Berry, W. E. *Int. Corros. Conf. Ser.* **1976**, NACE-4, 48.
10. Vermilyea, D. A.; Indig, M. E. *J. Electrochem. Soc.* **1972**, 119, 39.
11. Jessop, P. G.; Leitner, W. *Chemical Synthesis using Supercritical Fluids*, Wiley-VCH, Weinheim, **1999**.
12. Anitescu, G.; Tavlerides, L. L. *J. Supercrit. Fluids* **1997**, 11, 37.
13. Anitescu, G.; Tavlerides, L. L. *J. Supercrit. Fluids* **1999**, 14, 197.
14. Foster, N. R.; Singh, H.; Yun, J. S. L.; Tomasko, D. L.; MacNaughton, S. J. *Ind. Eng. Chem. Res.* **1993**, 32, 2849.
15. Smith, R. D.; Frye, S. L.; Yonker, C. R.; Gale, R. W. *J. Phys. Chem.* **1987**, 91, 3059.
16. Olsen, S. A.; Tallman, D. E. *Anal. Chem.* **1996**, 68, 2054.
17. Morrisette, P. M. *Nat. Res. J.* **1989**, 29, 793.
18. Haas, P. M. *Global Environ. Change*, **1991**, 1, 224.
19. Benedick, R. *Ozone Diplomacy: New Directions in Safeguarding the Planet*, Cambridge, MA: Harvard University Press, **1991**.
20. Meyer, C. W.; Morrison G. *J. Phys. Chem.* **1991**, 95, 3860.
21. Meyer, C. W.; Morrison G. *J. Chem. Eng. Data*, **1991**, 36, 409.
22. Noakes, T. *J. Fluor. Chem.* **2002**, 118, 35.
23. <http://www.afeas.org/>

-
24. Ravishankara, A. R. *Science*. **1994**, 263, 71.
 25. Frank, H.; Christoph, E. H.; Holm-Hansen, O.; Bullister, J. L. *Environ. Sci. Technol.* **2002**, 36, 12.
 26. Jordan, A.; Frank, H. *Environ. Sci. Tech.* **1999**, 33, 522.
 27. Ellis, D. A.; Mabury, S. A.; Martin, J. W.; Muir, D. C. G. *Nature*, **2001**, 412, 321.
 28. <http://www.grida.no/>
 29. Mount, D. J.; Rothman, L. B.; Robey, R. J.; Ali, M. K. *Solid State Tech.* **2002**, July, 103.
 30. Schollmeyer, E.; Knittel, D.; Buschmann, H. J.; Kosfeld, R. *Ger. Offen.* **1990**, DE 3904514.
 31. Woerlee, G. F.; Van Roosmalen, M.; Breijer, A.; Van Ganswijk, J. W.; Wichhart, M. *PCT Int. Appl.* **2003**, WO 2003062520.
 32. Corr, S. J. *Fluor. Chem.* **2002**, 118, 55.
 33. Vayisoglu-Giray, E. S.; Johnson, B. R.; Frere, B. G. A. M.; Bartle, K. D.; Clifford, A. A. *Fuel* **1998**, 77, 1533.
 34. Handley, A. J.; Clarke, R. D.; Powell, R. L. US 5824225 **1998**.
 35. Cantrell, G. O.; Blackwell, J. A. *J. Chromatogr. A* **1997**, 782, 237.
 36. Abbott, A. P.; Eardley, C. A. *J. Phys. Chem. B* **1998**, 102, 8574.
 37. Abbott, A. P.; Eardley, C. A.; Tooth, R. J. *J. Chem. Eng. Data* **1999**, 44, 112.
 38. Abbott, A. P.; Eardley, C. A. *J. Phys. Chem. B* **1999**, 103, 2504.
 39. Tillner-Roth, R.; Baehr, H. D. *J. Phys. Chem. Ref. Data* **1994**, 23, 657.
 40. Tillner-Roth, R.; Yokozeki, A. *J. Phys. Chem. Ref. Data* **1997**, 26, 1273.
 41. Riddick, J. A.; Bunger, W. B.; Sakano, T. K. *Organic Solvents: Physical Properties and Methods of Purification*, 4th ed.; J. Wiley & Sons: New York, **1986**.
 42. Wright, B. W.; Smith, R. D. *Chromatographia* **1984**, 18, 542.
 43. Yonker, C. R.; Wright, B. W.; Udseth, H. R.; Smith, R. D. *Ber. Bunsen-Ges. Phys. Chem.* **1984**, 88, 908.
 44. McHugh, M.; Krukoni, V. J. *Supercritical Fluid Extraction*, 2nd ed.; Butterworth-Heinemann: Boston, **1994**.
 45. Taylor, L. T. *Supercritical Fluid Extraction*; J. Wiley & Sons: New York, **1996**.

-
46. Klesper, E.; Corwin, A. H.; Turner, D. A. *J. Org. Chem.* **1962**, 27, 700.
 47. Conaway, J. E.; Graham, J. A.; Rogers, L. B. *J. Chromatogr. Sci.* **1978**, 16, 102.
 48. Giddings, J. C.; Myers, M. N.; McLaren, L.; Keller, R. A. *Science* **1968**, 162, 67.
 49. Smith, R. M. *Supercritical Fluid Chromatography*; Royal Society of Chemistry: London, **1988**.
 50. Hupe, K. P.; McNair, H. M.; Kok, W. T.; Bruin, G. J.; Poppe, H.; Poole, C.; Chester, T. L.; Wimalasena, R. L.; Wilson, G. S. *LC-GC* **1992**, 10, 211
 51. Schmitz, F. P.; Klesper, E. *Polymer Bulletin* **1981**, 14, 679.
 52. Schmitz, F. P. *Polymer Comm.* **1983**, 24, 142.
 53. Jackson, W. P.; Markides, K. E.; Lee, M. L. *J. High Resolut. Chromatogr., Chromatogr. Comm.* **1986**, 9, 213.
 54. Namiesnik, J.; Gorecki, T. *JPC-J. Planar Chromat-Mod. TLC* **2000**, 13, 404.
 55. Brooks, M. W.; Uden, P. C. *J. Chromatogr.* **1993**, 637, 179.
 56. Chester, T. L.; Pinkston, J. D. *Anal. Chem.* **2002**, 74, 2801.
 57. McAvoy, Y.; Dost, K.; Jones, D. C.; Cole, M. D.; George, M. W.; Davidson, G. *Forensic Sci. Int.* **1999**, 99, 123.
 58. Radcliffe, C.; Maguire, K.; Lockwood, B. *J. Biochem. Biophys. Methods* **2000**, 43, 261.
 59. Grob, K. *J. High. Res. Chromatogr.* **1983**, 6, 178.
 60. Wheeler, J. R.; McNally, M. E. *J. Chromatogr.* **1987**, 410, 343.
 61. Wu, N.; Chen, Z.; Medina, J. C.; Bradshaw, J. S.; Lee, M. L. *J. Microcolumn Sep.* **2000**, 12, 454.
 62. Brenner, B. A. *Anal. Chem.* **1998**, 70, 4594.
 63. Gritti, F.; Felix, G.; Archard, M-F.; Hardouin, F. *Chromatographia* **2001**, 53, 201.
 64. Pyo, D. *Microchem. J.* **2001**, 68, 183.
 65. King, J. W. *J. Chromatogr. Sci.* **1989**, 27, 355
 66. Gamse, T.; Marr, R. *Preceedings of the 2nd European School on Industrial Applications of Supercritical State Fluid Technology* **2001**, Barcelona.
 67. Illes, V.; Daood, H. G.; Biacs, P. A.; Gnayfeed, M. H.; Meszaros, B. *J. Chromatogr. Sci.* **1999**, 37, 345.

-
68. Lack, E.; Seidlitz, H. *Process Technol. Proc.* **1996**, 12, 253.
 69. Ma, X.; Yu, X.; Zheng, Z.; Mao, J. *Chromatographia* **1991**, 32, 40.
 70. Dean, J. R.; Liu, B.; Ludkin, E. *Methods Biotechnol.* **2000**, 13, 17.
 71. Chang, C. J.; Chiu, K.-L.; Chen, Y.-L. *Food Chem.* **1999**, 69, 109.
 72. Smith, G. W. *Eur. Patent Appl.* **1995** EP679419
 73. Verschuene, M.; Sandra, P.; David, F. J. *Chromatogr. Sci.* **1992**, 30, 388.
 74. Sieves, U.; Eggers, R. *Chem. Eng. Proc.* **1996**, 35, 239.
 75. Jimenez-Carbona, M. M.; Luque de Castro, M. D. *Anal. Chem.* **1998**, 70, 2100.
 76. Wehling, R. L. *Adv. App. Biotechnol. Ser.* **1991**, 12, 133.
 77. Froning, G. W. *Adv. App. Biotechnol. Ser.* **1991**, 12, 277.
 78. Hawthorne, S. B.; Krieger, M. S.; Miller, D. J. *Anal. Chem.* **1988**, 60, 472.
 79. Imanishi, N.; Fukuzato, R.; Furuta, S.; Ikawa, N. *R&D, Research and Development, Kobe Steel Ltd.* **1989**, 39, 29.
 80. Lucien, F. P.; Liong, K. K.; Cotton, N. J.; Macnaughton, S. J.; Foster, N. R. *Australas. Biotechnol.* **1993**, 3, 143.
 81. Gamse, T. *High Pressure Chemical Engineering Processes: Basics and Applications Summer School 2002*, University of Technology Graz/University of Maribor, June 27th.
 82. Laitnen, A.; Michaux, A.; Aaltanen, O. *Environ. Technol.* **1994**, 15, 715.
 83. Misch, B.; Firus, A.; Brunner, G. J. *Supercrit. Fluids* **2000**, 17, 227.
 84. Sahle-Demessie, E. *Environ. Technol.* **2000**, 21, 447.
 85. Chester, T. L.; Pinkston, J. D.; Raynie, D. E. *Anal. Chem.* **1998**, 70, 301.
 86. Steytler, D. *Sep. Processes Food Biotechnol. Ind.* **1996**, 17.
 87. Zosel, K. *Angew. Chem. Int. Ed. Engl.* **1978**, 17, 702.
 88. Vesper, H.; Nitz, S. *Adv. Food Sci.* **1997**, 17, 172.
 89. Morey, G. W.; Niggli, P. *J. Am. Chem. Soc.* **1913**, 35, 1086.
 90. Jessop, P. G.; Ikariya, T.; Noyori, R. *Nature* **1994**, 368, 231.
 91. Rathke, T. W.; Klinger, R. J.; Krause, T. R. *Organometallics* **1991**, 10, 1350.
 92. Benson, S. W. *The Foundations of Chemical Kinetics*, McGraw-Hill, **1960**.
 93. Mesiano, A. J.; Beckman, E. J.; Russell, A. J., *Chem. Rev.*, **1999**, 99, 623.
 94. Zhang, X.; Sui, Q.; Han, B.; Yan, H.; Wang, Y. *J. Supercrit. Fluids* **2000**, 17, 171.

-
95. Rhodes, T. A.; O'Shea, K.; Bennett, G.; Johnston, K. P.; Fox, M. A. *J. Phys. Chem.* **1995**, 99, 9903.
 96. Thompson, R. L.; Glaser, R.; Bush, D.; Liotta, C. L.; Eckert, C. A. *Ind. Eng. Chem. Res.* **1999**, 38, 420.
 97. Reaves, J. T.; Roberts, C. B. *J. Chem. Soc., Chem. Eng. Comm.* **1999**, 171, 117.
 98. Dillow, A. K.; Brown, J. S.; Liotta, C. L.; Eckert, C. A. *J. Phys. Chem. A* **1998**, 102, 7609.
 99. Paulaitis, M. E.; Alexander, G. C. *Pure Appl. Chem.* **1987**, 59, 61.
 100. Kim, S.; Johnston, K. P.; *J. Chem. Soc., Chem. Eng. Comm.* **1988**, 63, 49.
 101. Isaacs, N. S.; Keating, N. *J. Chem. Soc., Chem. Comm.* **1992**, 876.
 102. Ikushima, Y.; Saita, N.; Arai, M.; Blanch, H. W. *J. Phys. Chem.* **1995**, 99, 8941.
 103. Weinstein, R. D.; Renslo, A. R.; Vanheiser, R. L.; Harns, J. G.; Terter, J. W. *J. Phys. Chem.* **1996**, 100, 12337.
 104. Korzenski, M. B.; Kalis, J. W. *Tetrahedron Lett.* **1997**, 38, 5611.
 105. Brennecke, J. F.; Chataeuneuf, J. E. *Chem. Rev.* **1999**, 99, 433.
 106. Jessop, P. G.; Ikariya, T.; Noyori, R. *Chem. Rev.* **1999**, 99, 475.
 107. Jessop, P. G. *Topics in Catalysis* **5** **1998**, 95.
 108. Baiker, A.; *Chem. Rev.* **1999**, 99, 453.
 109. Jessop, P. G.; Hsiao, Y.; Ikariya, T.; Noyori, R. *J. Am. Chem. Soc.* **1994**, 116, 8851.
 110. Hitzler, M.; Smail, F. R.; Ross, S. K.; Poliakoff, M. *Org. Proc. Res. Dev.* **1998**, 2, 137.
 111. Hitzler, M.; Poliakoff, M. *J. Chem. Soc., Chem. Comm.* **1997**, 1667.
 112. Koch, D.; Leitner, W. *J. Am. Chem. Soc.* **1998**, 120, 13398.
 113. Nelson, W. M.; Puri, I. K. *Ind. Eng. Chem. Res.* **1997**, 36, 3449.
 114. Tsang, C. Y.; Streett, W. B. *Chem. Eng. Sci.* **1981**, 36, 993.
 115. Jessop, P. G.; Hsiao, Y.; Ikariya, T.; Noyori, R. *J. Am. Chem. Soc.* **1996**, 118, 344.
 116. Xiao, J.; Nefkens, S. C. A.; Jessop, P. G.; Ikariya, T.; Noyori, R. *Tetrahedron Lett.* **1996**, 37, 2813.
 117. Kritzer, P.; Dinjus, E. *Chem. Eng. J.* **2001**, 83(3), 207.

-
118. Koda, S.; Kanno, N.; Fujiwara, H. *Ind. Eng. Chem. Res.* **2001**, 40(18), 3861.
119. Portela, J. R.; Nebot, E.; de la Ossa, E. M. *J. Supercrit. Fluids* **2001**, 21(2), 135.
120. Fischer, A.; Mallet, T.; Baiker, A. *J. Catal.* **1999**, 182(2), 289.
121. Gao, Y.; Liu, H-Z.; Shi, Y-F.; Yuan, W-K. *The 4th International Symposium on Supercritical Fluids*, Sendai, Japan, **1997**, 531.
122. Gao, Y.; Shi, Y-F.; Zhu, Z-N.; Yuan, W-K. *3rd International Symposium on High-Pressure Chemical Engineering*, Zurich, Switzerland, **1996**, 151.
123. Ellington, J. B.; Park, K. M.; Brennecke, J. F. *Ind. Eng. Chem. Res.* **1994**, 33, 965.
124. Brown, J. S.; Lesutis, H. P.; Lamb, D. R.; Bush, D.; Chandler, K.; West, B. L.; Liotta, C. L.; Eckert, C. A. *Ind. Eng. Chem. Res.* **1999**, 38, 3622.
125. Goddard, R.; Bosley, J.; Al-Duri, B. *J. Supercrit. Fluids*. **2000**, 18, 121.
126. Mori, T.; Funasaki, M.; Kobayashi, A.; Okahata, Y. *Chem. Comm.* **2001**, 1832.
127. Zhenshan Hou, Buxing Han, Xiaogang Zhang, Haifei Zhang, Zhimin Liu. *J. Phys. Chem. B*, **2001**, 105, 4510-4513.
128. Abbott, A. P.; Corr, S.; Durling, N. E.; Hope, E. G. *J. Phys. Chem. B*, **2004**, 108, 4922.
129. Fischer, A.; Mallet, T.; Baiker, A. *Angew. Chem. Int. Ed. Engl.* **1999**, 38(3), 351.
130. Hitzler, M.; Smail, F. R.; Ross, S. K.; Poliakov M. *Chem. Comm.* **1998**, 359.
131. Vieville, C.; Mouloungiu, Z.; Gaset, A. *Ind. Eng. Chem. Res.* **1993**, 32, 2065.
132. Hrnjez, B. J.; Mehta, A. J.; Fox, M. A.; Johnston, K. P.; Fox, M. A. *J. Am. Chem. Soc.* **1989**, 111, 2662.
133. <http://www.thomas-swan.co.uk>

CHAPTER 2

EXPERIMENTAL

2.1 Materials

2.1.1 Solvents

2.1.2 Solutes, Reagents and Catalysts

2.1.3 Polymers

2.2 Instrumentation

2.2.1 General Apparatus

2.2.2 Dielectrometry Apparatus

2.2.3 Quartz Crystal Microbalance Apparatus

2.2.4 Hydrogenation Apparatus

2.3 Experimental Methods

2.3.1 Solubility Studies

2.3.2 Hydrogenation Reactions

2.3.3 Polymer Modification

2.4 References

2.1 Materials

2.1.1 Solvents

The solvents used in this work are shown in Table 2.1. The commercial source and purity of each is shown.

Solvent	Abbreviation	Source	Assay
1,1,1,2-Tetrafluoroethane ^a	HFC 134a	Ineos Fluor	>99.9%
Difluoromethane ^a	HFC 32	Ineos Fluor	>99.9%
Carbon dioxide ^a	CO ₂	BOC Ltd.	>99.9%
Dichloromethane ^b	DCM	Fisher	>99%
Ethyl acetate ^b	EtOAc	Fisher	>99%
Toluene ^b	-	Fisher	>99%
Diethyl ether ^b	DE	Fisher	>99%

Table 2.1 Solvents used in this work. ^aUsed as received. ^bDried and degassed before use.

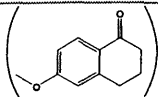
2.1.2 Solutes, Reagents and Catalysts

The solutes, reagents and catalysts used in this work are shown in Table 2.2. The commercial source is shown and each was used as received.

2.1.3 Polymers

The polyethylene (PE) and the polystyrene (PS) used in the polymer modification study were supplied by Rapra Technology. Each was received in pellet form, which were then formed into solid polymer blocks as described in Section 2.3.3.

Table 2.2 Solutes, reagents and catalysts used in this work.

Chemical	Alternative name	Formula	Source	Assay
3,4-Dihydro-6-methoxy-1-naphthalene	6-Methoxy-1-tetralone	$C_{11}H_{12}O_2$ 	Acros Organics	99%
Methylenesuccinic acid	Itaconic acid	$HO_2CCH_2C(=CH_2)CO_2H$	Aldrich	>99%
2-Butenoic acid	Crotonic acid	$CH_3CH=CHCO_2H$	Fluka	>97%
Methylsuccinic acid	-	$HO_2CCH_2CH(CH_3)CO_2H$	Aldrich	99%
Styrene	-	$C_6H_5CHCH_2$	Aldrich	>99%
Hydrogen	-	H_2	BOC Ltd.	
α -Acetamido-cinnamic acid	-	$C_6H_5CH=C(NHCOCH_3)CO_2H$	Aldrich	98%
Dimethyl itaconate	-	$CH_3CO_2CH_2C(=CH_2)CO_2CH_3$	Aldrich	97%
Trans-2-methyl-2-pentenoic acid	-	$C_2H_5CH=C(CH_3)CO_2H$	Aldrich	97%
Chlorotris(triphenylphosphine) rhodium (I)	Wilkinson's catalyst	$RhCl[P(C_6H_5)_3]_3$	Aldrich	99.99%
Bis(1,5-cyclooctadiene) rhodium (I) tetrafluoroborate hydrate	-	See structure 9 in Section 2.3.2	Aldrich	97%
Hexamethylphosphorous triamide	HMPT	$P[N(CH_3)_2]_3$	Aldrich	97%
(R)-(+)-1,1-Bi(2-naphthol)	(R)-BINOL	See structure 11 in Section 2.3.2	Aldrich	99%

2.2 Instrumentation

2.2.1 General Apparatus

The high-pressure cells were constructed from 316 stainless steel and were heated using 240 V, 250 W band heaters supplied by Walton Ltd. The temperature was controlled and maintained (± 0.5 K) using CAL 9900 heater/controllers fitted with an iron/constantan thermocouple, the tip of which was in contact with the solvent close to the centre of the cell. The high-pressure seals between the body of the cells and the cell tops were provided by Teflon[®] supported, standard nitrile o-rings. The cells had 3 cm thick walls, a maximum working pressure of 1 kbar and were rated to 1.5 kbar. Each high-pressure system was fitted with pressure relief valves set to 300 bar for safety.

Pressure was applied using two different pumps; a model 10-600 hydraulic pump (Hydraulic Engineering Corp., Los Angeles, USA), driven by compressed air, and a Thar Technologies P-Series piston pump. The P-Series pump was electrically driven and used two pistons to give a pulse free delivery of solvent. The seals in both pumps were changed to polytetrafluoroethane (PTFE) composites in order to accommodate the use of hydrofluorocarbon (HFC) solvents. A more detailed description of each high-pressure system is given in the sections that follow.

2.2.2 Dielectrometry Apparatus

The high-pressure system used for the capacitance measurements is shown in Figure 2.1. The cell top contained a parallel plate capacitor consisting of two rectangular, stainless steel plates with an area of 6.6 cm^2 held 1 mm apart by Teflon[®] spacers as shown in Figure 2.2. The plates were attached to electrical feed-throughs supplied by RS Components Ltd. and were sealed with Swagelok fittings. The cell was used to determine the solvent and solution dielectric constant, ϵ , which was given by

$$C = \epsilon C_o \quad (2.1)$$

where C is the measured capacitance and C_o is the cell capacitance.

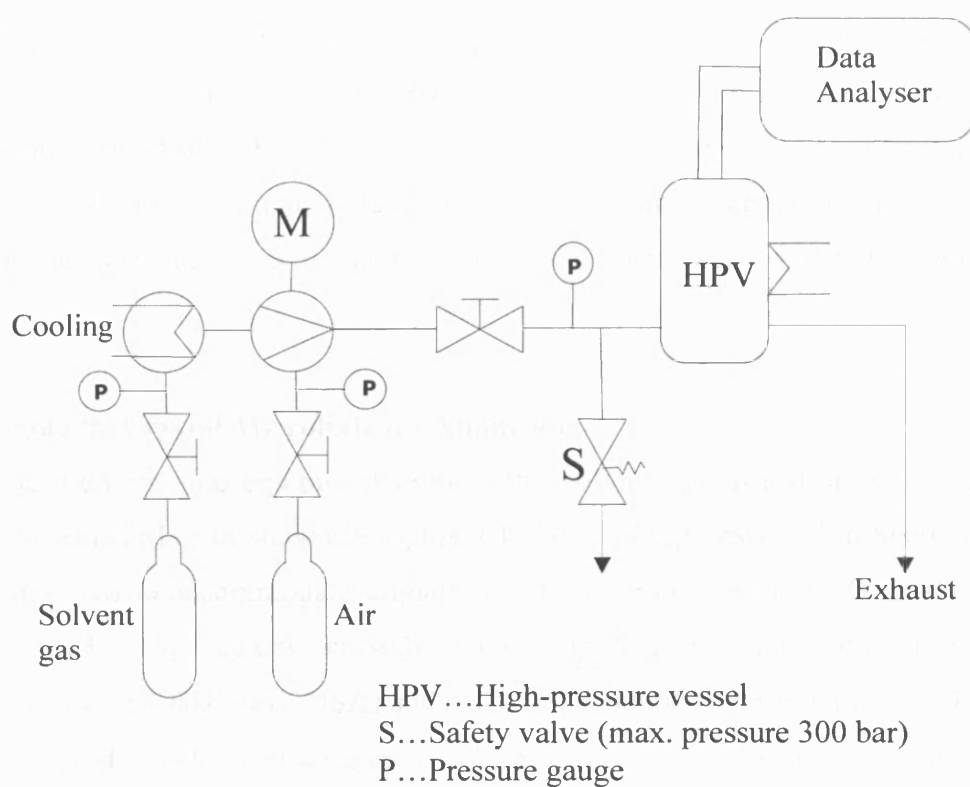


Figure 2.1 Schematic layout of the dielectrometry apparatus.

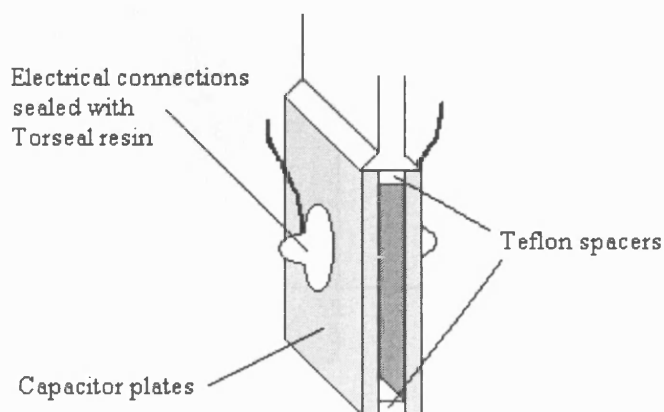


Figure 2.2 The capacitor used in the dielectrometry solubility studies.

Capacitances were measured at 65 kHz with a 20 mV ac voltage amplitude using a 1254 frequency response analyser and a 1286 potentiostat (both Solartron instruments) controlled by ZPLOT software. The acquired data was analysed using ZVIEW software and the uncertainty of each capacitance measurement was 50 fF. The capacitance cell was manufactured in-house and was validated in previous work.¹

2.2.3 Quartz Crystal Microbalance Apparatus

The high-pressure equipment used in the polymer modification work had the same schematic layout shown in Figure 2.1. The cell top described in Section 2.2.2 was modified to accommodate a quartz crystal microbalance (QCM) as shown in Figure 2.3. The quartz crystals were supplied by International Crystal Manufacturing (Oklahoma, USA) and had a fundamental frequency of 10 MHz. The gold electrodes had a surface area of 0.3 cm^2 and were $<5 \text{ }\mu\text{m}$ thick. Admittances were measured over a frequency range of 1 MHz (centred on 10 MHz) using a Hewlett Packard 8751A network analyser controlled by HP VEE v.5 software.

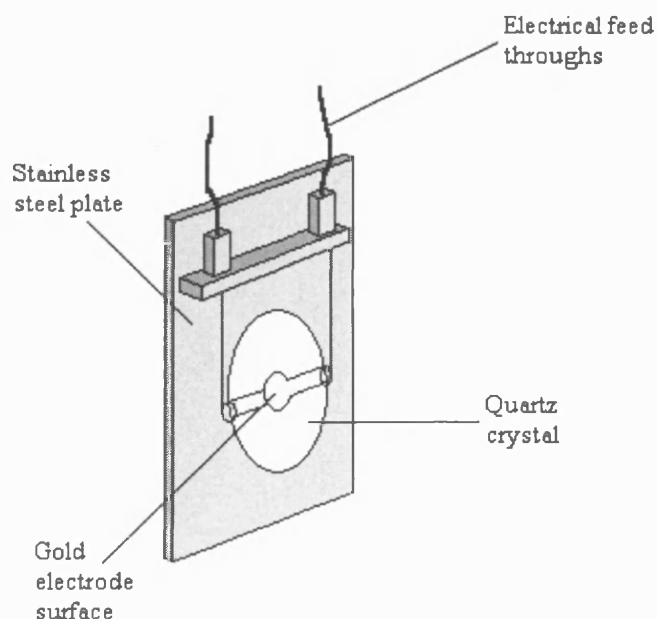
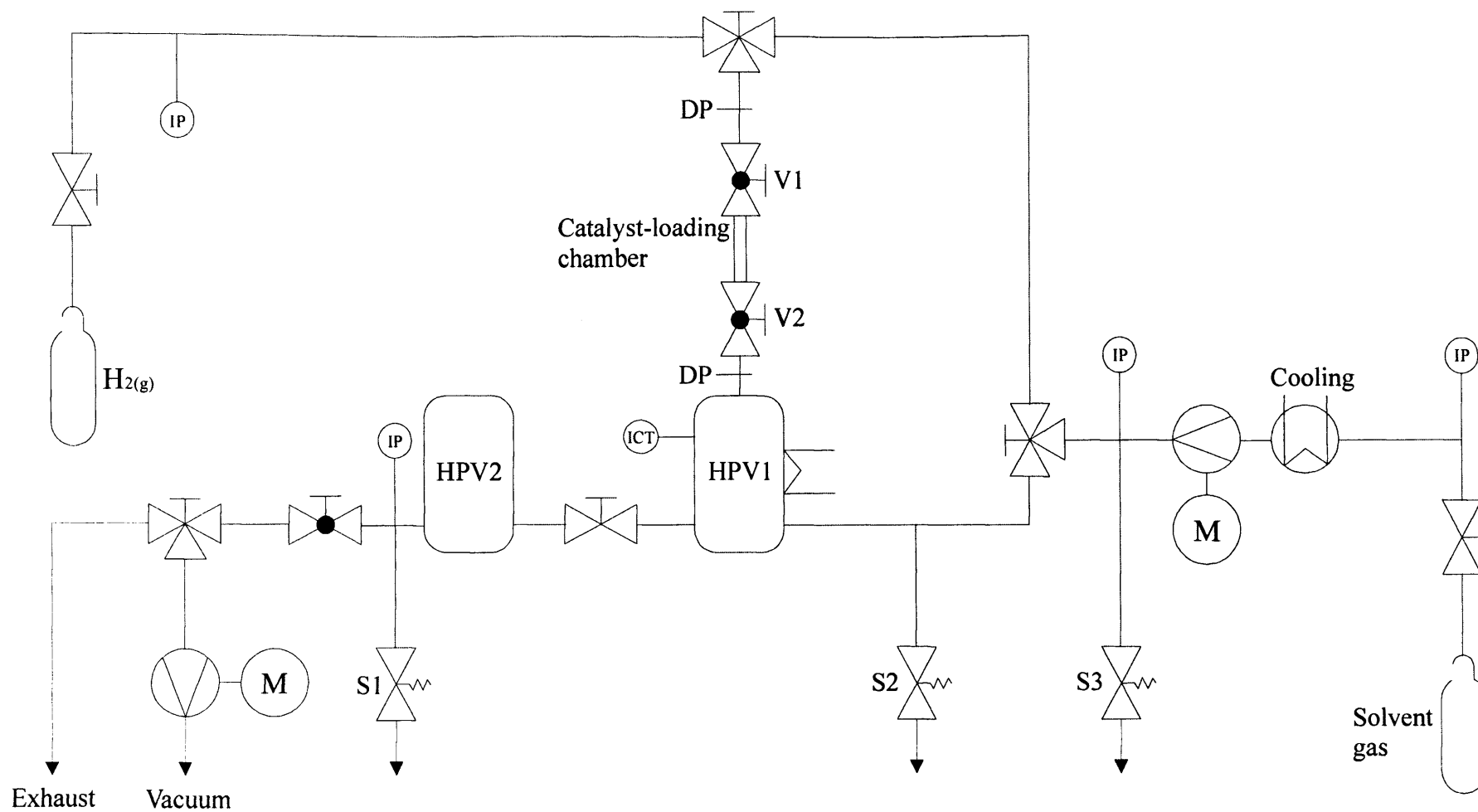


Figure 2.3 Configuration of the high-pressure quartz crystal.

2.2.4 Hydrogenation Apparatus

The high-pressure system used for the hydrogenation work is shown schematically in Figure 2.4. The catalyst-loading chamber is a 3 x 0.3 cm length of stainless steel pipe sealed at each end by a valve. V_1 is a two-way needle valve and V_2 is a two-way ball valve with a polychlorotrifluoroethylene (PCTFE) seat.



HPV1...High-pressure reaction vessel
 HPV2...High-pressure collection vessel
 S1 to S3...Safety valves (max. pressure 300 bar)

IP...Inspection of pressure
 ICT...Inspection and control of temperature
 DP...Detach point

2.3 Experimental Methods

2.3.1 Solubility Studies

Two different methods of solubility determination were used in this work. The first was a dielectrometry technique, which employed the cell shown in Figure 2.5. Excess solute (to ensure saturation of the solvent) was placed between the two metal sieves. The capacitance was measured as described in Section 2.2.2 as a function of pressure along an isotherm. The method used to calculate the solubility values is discussed in Section 3.2.1 (page 48).

The second technique was a gravimetric one and used the apparatus shown in Figure 2.6. Excess solute was placed into the stainless steel base and the weight was recorded. The gauze cover was screwed in place and the solute container was placed into the high-pressure cell. The cell was heated to the desired temperature and pressurised using the appropriate solvent. Once equilibration had been reached the cell was depressurised, the gauze cover was removed and the base was re-weighed.

The qualitative phase equilibria and solubility investigations were carried out using the high-pressure view cell shown in Figure 2.7. The cell is constructed from 316 stainless steel and is fitted with sapphire windows.

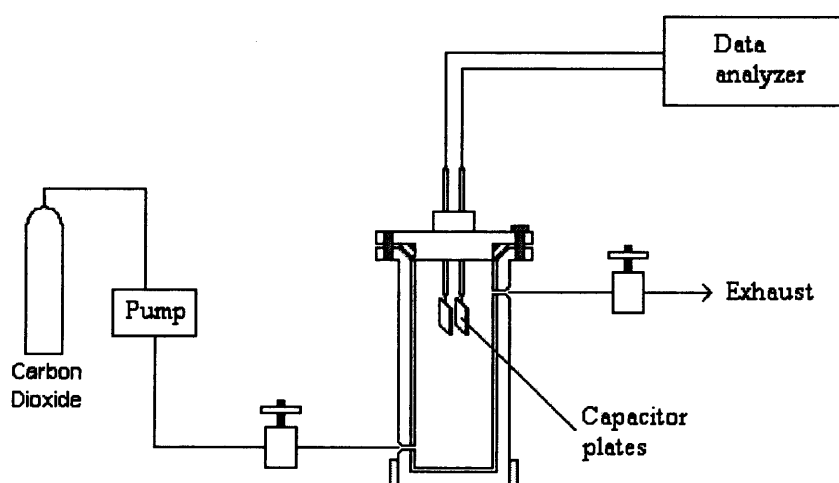


Figure 2.5 The cell used for the dielectrometry solubility determinations.

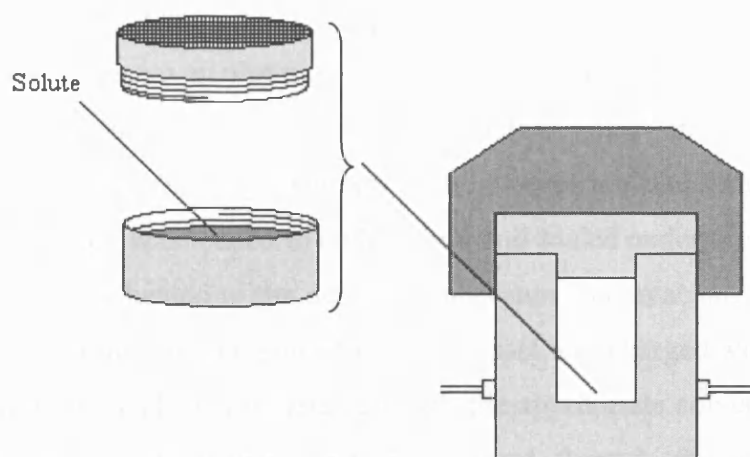


Figure 2.6 The apparatus used for the gravimetric solubility determinations.

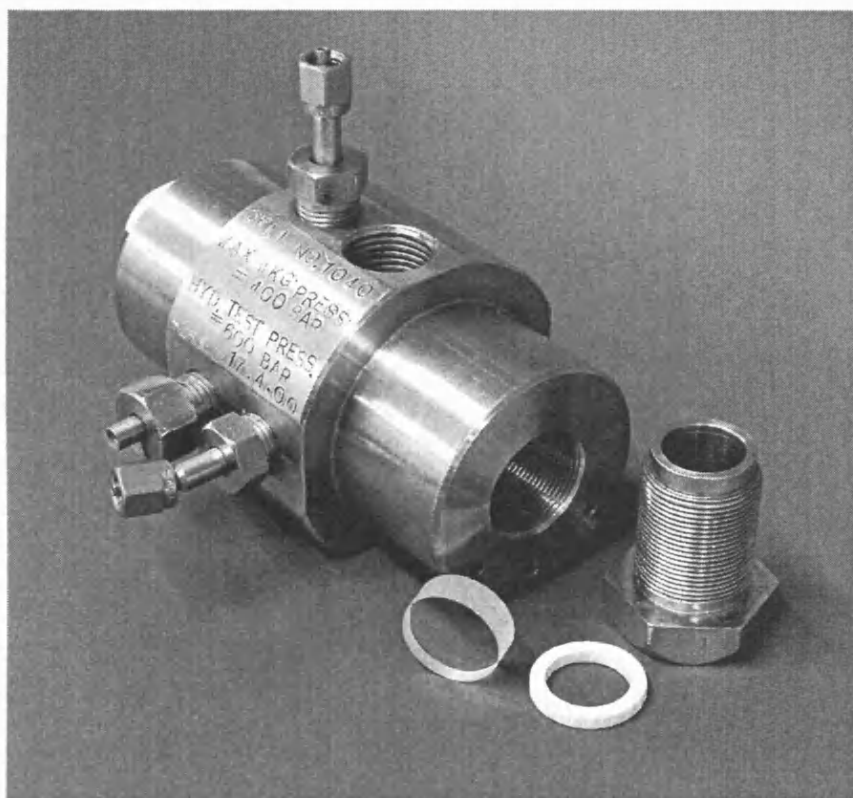


Figure 2.7 The high-pressure view cell used in the qualitative phase equilibria and solubility investigations.

2.3.2 Hydrogenation Reactions

The apparatus shown in Figure 2.4 was used to carry out the hydrogenation reactions. The substrate was placed into the reaction vessel and the catalyst was loaded into the catalyst-loading chamber. In the case of air- and moisture-sensitive catalysts the chamber was loaded in a glove box and sealed under nitrogen using V_1 and V_2 . The cell was heated to the desired temperature and evacuated to ensure the reaction vessel was air- and moisture-free. The vessel was charged with the required amount of hydrogen and then pressurised with the appropriate solvent using the P-Series piston pump. The solvent gas was passed through the catalyst-loading chamber, which flushed the catalyst into the reaction vessel, thus starting the reaction. When using HFC solvents cooling was applied before the gas entered the pump because the pump is more efficient at pumping liquids. The reaction was left for the desired amount of time and the products/unreacted starting materials were collected by depressurisation into the larger volume collection vessel. The products were analysed using NMR (DPX 300), GC-MS (Perkin Elmer) and GC (Perkin Elmer Autosystem XL controlled by Turbochrom software).

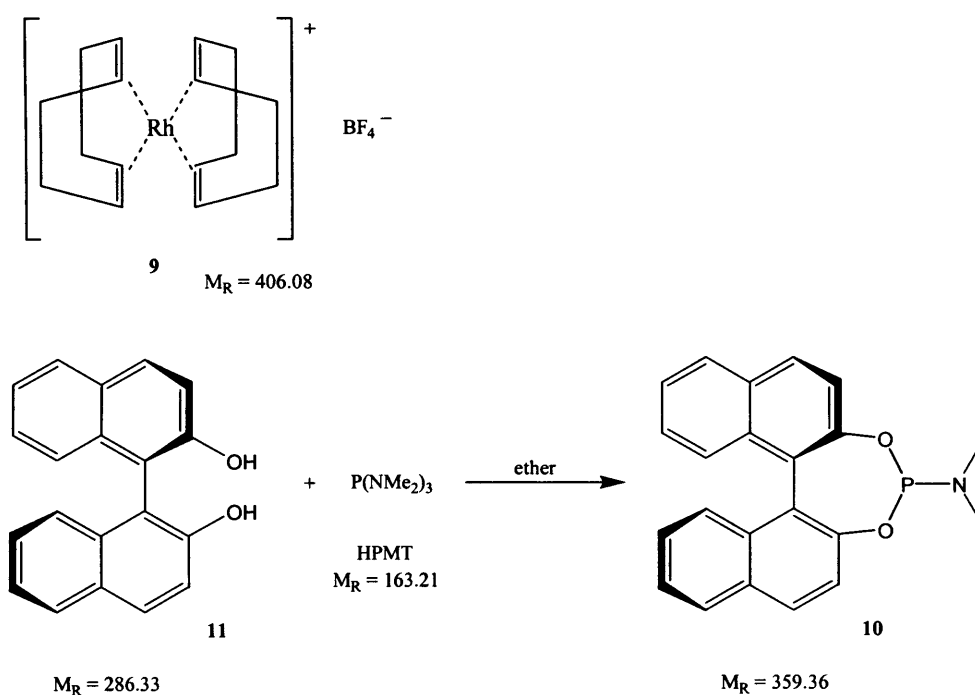
The rhodium asymmetric catalytic system was prepared *in situ* using $[\text{Rh}(\text{COD})_2\text{BF}_4]$ **9** (Bis(1,5-cyclooctadiene) rhodium (I) tetrafluoroborate) and (*R*)-MonoPhos **10** ((*R*)-2,2-*O,O*-(1,1-Binaphthyl)-*O,O*-dioxo-*N,N*-dimethylphospholide). The first preparation of the MonoPhos ligand was described by Feringa *et al.*² A typical example preparation used in this work is given below and the reaction is shown in Scheme 2.1. The purity of the synthesised (*R*)-MonoPhos ligand was tested by NMR (^1H , ^{13}C , ^{31}P), polarimetry and melting point tests and the results showed that a ligand of high purity had been synthesised:

(*R*)-MonoPhos purity data:

$[\alpha]_D^{20} = -570$ (c 0.06, CHCl_3); m.p. = 491-493 K; ^1H NMR (CDCl_3): δ 2.75 (d, $^3J_{\text{PH}} = 9.2$ Hz, 18H), 7.25-8.00 (m, 12H); ^{13}C NMR (CDCl_3): δ 35.81 (d, $^3J_{\text{PC}} = 22.0$ Hz, CH_3), 121.83 (d, $^3J_{\text{PC}} = 1.0$ Hz, CH), 123.02 (d, $^3J_{\text{PC}} = 84.0$ Hz, C), 124.93 (d, $^4J_{\text{PC}} = 15.1$ Hz, CH), 125.94 (s, CH), 126.78 (d, $^4J_{\text{PC}} = 6.0$ Hz, CH), 128.14 (d, $^7J_{\text{PC}} = 6.0$ Hz, CH), 130.01 (d, $^6J_{\text{PC}} = 36.0$ Hz, CH), 130.80 (d, $^4J_{\text{PC}} = 47.4$ Hz, C), 132.67 (d, $^3J_{\text{PC}} = 2.0$ Hz, C), 149.51 (d, $^2J_{\text{PC}} = 38.3$ Hz, C); ^{31}P NMR (CDCl_3): δ 148.72.

Example (*R*)-MonoPhos preparation:

The preparation was carried out using standard Schlenk techniques. 2.010 g (7.02×10^{-3} moles) of (*R*)-BINOL **11** ((*R*)-1,1-Bi(2-naphthol)) was dissolved in 20 mL of ether and 1.6 mL (8.80×10^{-3} moles) of HPMT (Hexamethylphosphorous triamide) was added. The mixture was stirred at room temperature for 2.5 hours. The product was filtered and washed with hexane giving 2.298g (6.40×10^{-3} moles) of product (91% yield).



Scheme 2.1

The reagent amounts for the constant mole fraction asymmetric hydrogenation studies are given in Table 2.3 for reactions conditions of 100 bar and 383 K. All other reactions were based on these mole fraction values.

Small quantities of reagents were introduced into the cell by dissolving the solid in an appropriate organic solvent and transferring the solution using a Gilson pipette. The air-sensitive catalyst was dissolved in dried and degassed solvents and transferred into the catalyst-loading chamber in a flush box. The number of moles of hydrogen was converted to pressure values using data from the Nist Chemistry WebBook.³

	Substrate / moles	MonoPhos / moles	Rh(COD)₂BF₄ / moles	H_{2(g)} / moles
Itaconic acid	8.25E-5	8.25E-7	4.13E-7	1.65E-4
Dimethyl itaconate	8.22E-5	8.22E-7	4.11E-7	1.64E-4
α -Acetamido-cinnamic acid	8.25E-5	8.25E-7	4.13E-7	1.65E-4
<i>trans</i> -2-Methyl-2-pentenoic acid	8.24E-5	8.24E-7	4.12E-7	1.65E-4

Table 2.3 Reagent amounts for the constant mole fraction asymmetric hydrogenation studies for reactions conditions of 100 bar and 383 K.

The enantiomeric excess values for dimethyl itaconate, α -acetamido-cinnamic acid and *trans*-2-methyl-2-pentenoic acid were determined by GC using a Chiraldex B-DM column and the conditions are shown in Table 2.4. The enantiomeric excess values for itaconic acid were determined using polarimetry and were taken from Figure 2.8. Absolute configurations for the itaconic acid and dimethyl itaconate hydrogenation products (methylsuccinic acid and dimethyl succinate) were determined using commercially available enantiomerically pure products and those for α -acetamido-cinnamic acid and *trans*-2-methyl-2-pentenoic acid (acetylalanine and 2-methylpentanoic acid) were determined using GC literature data.⁴

Substrate	Oven temp. / K	Detector temp. / K	Injector temp. / K
Dimethyl itaconate	393	523	513
α -Acetamido-cinnamic acid	403	513	493
<i>trans</i> -2-Methyl-2-pentenoic acid	353	513	493

Table 2.4 GC separation conditions for the determination of enantiomeric excess.

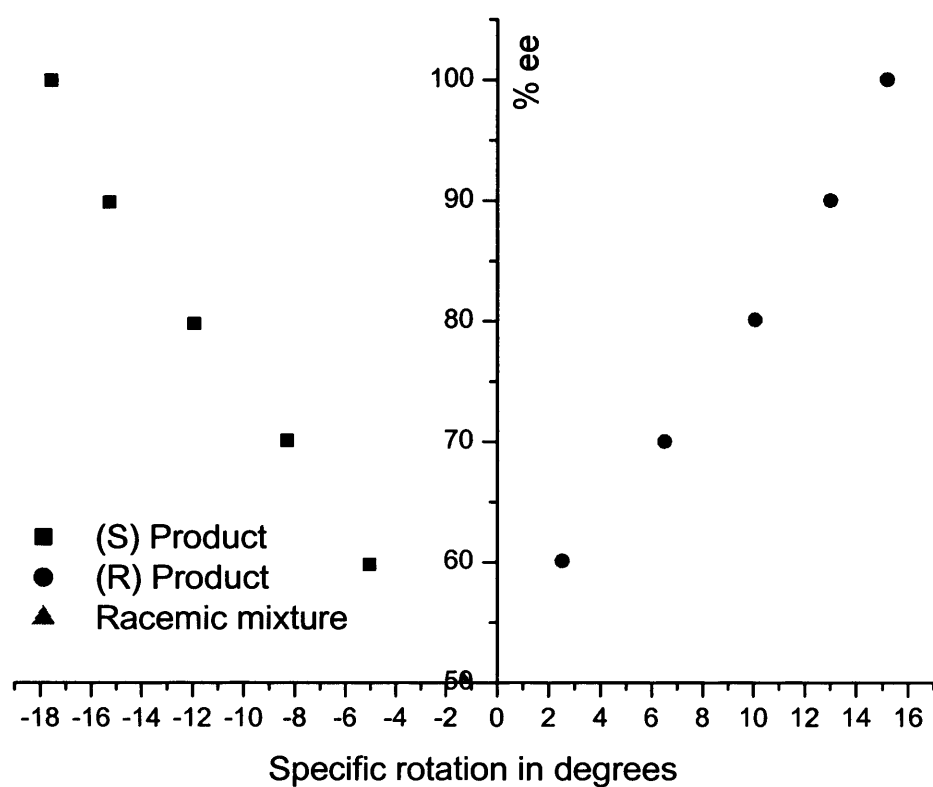


Figure 2.8 Plot used to determine the enantiomeric excess values for dimethylsuccinic acid.

2.3.3 Polymer Modification

For each set of experiments a scan was taken of the clean crystal prior to polymer attachment. The PE and PS pellets were heated and moulded into homogeneous, rectangular blocks and were set into place between the steel plate and the crystal shown in Figure 2.3.

The polymer/crystal configuration was placed into the cell and heated to the desired temperature. The cell was pressurised to the desired pressure and the system was allowed to reach equilibrium, which was indicated by the cessation of peak shift in the QCM scans. Each set of experiments was carried out on a newly cast sample.

2.4 References

1. Abbott, A. P.; Corr, S.; Durling, N. E.; Hope, E. G. *J. Chem. Eng. Data* **2002**, 47, 900.
2. Hulst, R.; Koen de Vries, N.; Feringa, B. L. *Tetrahedron Assym.* **1994**, 5, 699.
3. <http://webbook.nist.gov/chemistry/>
4. α -Acetamido-cinnamic acid and *trans*-2-methyl-2-pentenoic are test substrates used by ChiralDEX and the order of elution and separation conditions for the ChiralDEX B-DM column are given in the ChiralDEX handbook. Absolute configurations were determined using the handbook data.

CHAPTER 3

SOLUBILITY STUDIES OF SOLUTES IN HYDROFLUOROCARBON SOLVENTS

3.1 Introduction

3.1.1 Solubility in Supercritical Fluids

3.1.2 Measurement Techniques

3.1.3 Solubility Modelling

3.1.4 Separation Science using Supercritical Fluids

3.2 Results and Discussion

3.2.1 Solubility of Solids in Supercritical HFC 134a

3.2.2 Modelling Solubility in Supercritical HFC 134a

3.2.3 Designing a Separation Process

3.3 Conclusion

3.4 References

3.1 Introduction

The overall aim of the project was to evaluate the use of sc HFC 134a as a reaction medium for asymmetric hydrogenation and this was carried out using a range of unsaturated carboxylic acids. The effect of pressure (hence, dielectric constant) and hydrogen concentration on reaction conversion and enantioselectivity was investigated and the results are reported in Chapter 4.

One of the major potential advantages of using HFCs is one of process intensification arising from higher solute solubilities. Hence, the focus of this chapter is the effect of temperature, pressure and solute structure on the solubility of various potential substrates and their reduced products.

The substrates were chosen for their varying degrees of polarity, structure and location of unsaturation within the molecule. The study includes methylsuccinic acid in order to evaluate the difference in solubility between an unsaturated substrate (itaconic acid) and the hydrogenated product.

Both dielectrometry and gravimetric techniques were used in the determination of the solubility results and it is shown that HFC 134a is a suitable solvent for reactions involving polar substrates. The Peng-Robinson equation of state was used to model the solubility results for binary and ternary systems and acceptable correlations were obtained. The discussion is extended and the solubility information was used to model a counter-current extraction process for the separation of reagents and products.

3.1.1 Solubility in Supercritical Fluids

The ability of sc fluids to dissolve solids was first reported by Hannay and Hogarth¹ in the 19th century when they studied the solubility of inorganic salts in sc ethanol. Subsequent work by Buckner² showed that the solubility of organic solutes in sc CO₂ was orders of magnitude higher than those predicted by vapour pressure considerations alone. Over the last few decades the solubilities of solids and liquids in sc fluids have been studied extensively.³⁻⁷ Such information forms an important part of establishing the feasibility of any sc fluid process be it chromatography, extraction or chemical synthesis.

Carbon dioxide is by far the most commonly employed sc solvent but solutes are limited to non-polar or highly volatile compounds. Branching and fluorination are known to enhance the solubility of solutes whilst unsaturation, acidic protons

and phenyl substituents or phenyl-substituted ligands decrease solubility in sc CO₂.^{8,9} The restriction to non-polar reagents and/or catalysts with non-aromatic ligands poses a serious problem to the synthetic chemist and several strategies for increasing the solubility of compounds in non-polar fluids have been developed. These include the use of CO₂-philic tails, counter-ions and co-solvents.

The addition of CO₂-philic tails such as fluoroalkyl, fluoroether and silicone groups to conventional ligands has been shown to enhance the solubility of complexes in less polar media.⁹⁻¹³ The electron withdrawing effect of fluoroalkyl groups can be prevented by the insertion of alkyl spacers between the binding functional group and the fluorinated section.^{9,10} Although salts are generally insoluble in sc CO₂, careful choice of counter-ions can greatly increase the solubility of charged complexes.^{9,14} Some counter-ions most commonly employed include [BArF]⁻ (Figure 3.1) and [CF₃SO₃]⁻.^{12,15}

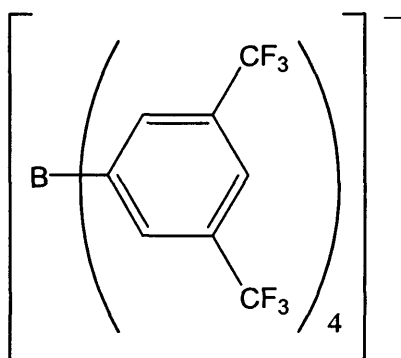


Figure 3.1 The structure of the commonly used counter-ion, [BArF]⁻.

It is well known that the addition of polar co-solvents to sc CO₂ can greatly enhance the solubility of polar solutes¹⁶⁻¹⁸ and this is generally attributed to the strong interaction between the co-solvent and solute. This explanation is based on results from spectroscopic studies^{19,20} and molecular simulations.²¹ Han *et al.*²² carried out an investigation into the mechanism of solubility enhancement by the addition of co-solvents using sc CO₂, chlorodifluoromethane and acetone. They found that although solubility is enhanced by the addition of co-solvents, the dissolution process (enthalpy of solution) becomes less exothermic. They concluded that the increase in entropy of solution is the dominant contribution to the solubility enhancement since

$$\Delta G = \Delta H - T\Delta S \quad (3.1)$$

where ΔG is the Gibbs free energy, ΔH is the enthalpy of solution and ΔS is the entropy of solution. Higher solubility values are associated with lower ΔG values. It should be noted that this conclusion only applies to systems in which the local density of the sc solvent around the solute and co-solvent is larger than that of the bulk density.

The low solubilities of substrates in CO₂ can be overcome by using sc HFCs as outlined in Sections 1.2 and 1.3. These solvents have only recently found significant use and solubility measurements in sc HFCs are very limited. Durling measured the solubilities of several *p*-benzoic acids and *p*-phenols in HFC 32 and found that solubility was largely dependent on the identity of the functional group at the *para* position.²³ Stahl and Willing measured the solubilities of different alkaloids in sc CO₂, NO₂ and CHF₃.²⁴ They found that the solubility of the alkaloids was higher in CHF₃ than in the other two solvents. Taylor and co-workers determined the solubility of sulphur-containing solutes in sc CO₂, CHF₃ and HFC 134a.²⁵ Their results showed that the solutes had much higher solubilities in HFC 134a when compared to the other solvents. It has been shown by Abbott *et al.* that HFC 134a is a relatively polar solvent, even in the sc state, and this may enhance the solubility of polar solutes.²⁶⁻²⁸ The increased solubility in sc HFC 134a is thought to be a consequence of the higher dielectric constant and polarisability of this medium.

For a more thorough treatise of solubility studies using sc fluids the reader is directed to a review by Bartle *et al.*, which covers work up to 1989.²⁹

3.1.2 Measurement Techniques

Several methods for the determination of solubility data in sc fluids are reported in the literature and the three most common include gravimetric, chromatographic and spectroscopic techniques. The gravimetric method developed by Eckert,³⁰ Paulaitis,³¹ Reid³² and their co-workers is by far the most commonly employed technique. This method requires solution saturation by passing the sc fluid at constant flow rate through an extraction cell loaded with the solute. The saturated solution is expanded to atmospheric pressure across a heated metering valve and the solute is precipitated and collected in a cold trap. Solute collection is carried out for

a given period of time and the solubility can be determined from knowing the solvent flow rate during that time period. Trapping the precipitated solute for analysis is often the most problematic part of the gravimetric technique. Compounds with high volatility are likely to form aerosols on depressurisation and some solute may be lost, suggesting that *in situ* techniques for solubility determination would be advantageous.

Most chromatographic techniques are extensions of gravimetric methods, where the chromatograph is used in conjunction with the flow apparatus for sc solution analysis.²⁹ There are many variants of this technique and it is particularly advantageous for studies related to mixed solute solubilities. Data accuracy in sc fluid solubility studies is heavily dependent on maintaining constant pressure and it is, therefore, essential to avoid pressure drop whilst obtaining samples for chromatographic analysis. Although this can lead to technical difficulties, results comparable to those obtained using the gravimetric method have been reported.³³

The spectroscopic techniques can be used to carry out more convenient, *in situ* analysis by taking measurements directly in a high-pressure cell.²⁹ They are however, limited to studies of solutes that have one or more absorption bands in the UV, VIS or IR wavelength ranges, which can then be used to determine solution concentration. Another limitation is the inapplicability to turbid solutions or solution concentrations greater than around $10^{-1} \text{ mol dm}^{-3}$.

In the late 1990's it was proposed that dielectrometry could be used to measure the solubility of polar solutes in sc fluids.³⁴⁻³⁶ The dissolution of polar solutes in the fluid causes a change in the solution dielectric constant, ϵ , and this can be measured directly using capacitance. The extent of the dielectric constant change of the saturated solution with respect to that of the pure solvent (at the same temperature and pressure) can be related to solute concentration and hence solubility. This is a precise, simple, inexpensive and *in situ* technique, which can be used even if the solution is turbid or solubilities are high.

Fedotov *et al.* used the dielectrometry method to measure the solubility of several compounds in sc CO₂ including acetonitrile, acetone and manganese cyclopentadienyltricarbonyl as a function of pressure.^{35,36} A later study by Hourri and co-workers studied the solubility of naphthalene in sc CO₂ as a function of

temperature and pressure in order to assess the validity of the dielectrometry technique.³⁴ They compared their data to previously published results and achieved agreement to better than $\pm 4\%$.

The low solubility of polar solutes in sc CO₂ means the overall change in the dielectric constant will be relatively small and this may inhibit the use of the dielectrometry technique for these systems. It is shown in this work and a previously published study²³ that the technique can be used effectively with HFC solvents due to the large dielectric constants exhibited by these media.

3.1.3 Solubility Modelling

There is a wealth of information in the literature pertaining to the solubility of solutes in a wide range of sc fluids. Solubility is dependent on a number of variables including the properties of the sc fluid and solute under investigation, the temperature and the experimental pressure. The solute vapour pressure has a significant influence on the solubility of that solute. Data is often reported in terms of the enhancement factor, E :

$$y_2 = E \frac{p_2}{p} \quad (3.2)$$

where y_2 is the observed solubility, p_2 is the vapour pressure of the pure solid and p is the system pressure. The enhancement factor represents the solubility increase in the sc solvent over that in the ideal gas mixture.³⁷ The large number of variables determining the solubility of solutes means there is a large demand for experimental data in order to assess the feasibility of sc processes. The ability to correlate and predict the solubility (or enhancement factor) of solids in sc fluids greatly reduces this demand and several methods for solubility prediction have been employed.

There are several equations of state (EOS) reported in the literature to describe solubility in sc fluids. Simple virial EOS models have been used to successfully correlate the dependence of solubility on thermodynamic variables.^{38,39} There are several other methods reported in the literature^{40,41} including a method using the spread of the electrostatic potential on the solute surface, which describes the solubility fundamentally in terms of the changes in vapour pressure of the pure

solute.⁴² Cubic EOS are the most commonly employed models and these have been used to describe solubilities at different temperatures and pressures. These are limited by the need to employ a combining rule, which can be used to describe the mixture parameters. An example is the Redlich-Kwong EOS but this fails to adequately describe solubilities for densities at high pressure.⁴³ Guigard and Stiver introduced an EOS using a density-dependent solute solubility parameter, which requires the critical pressure and density of the sc fluid along with the melting point, liquid molar volume and enthalpy of fusion for the solute.⁴⁴ If the solute properties are unknown then the most successful method for solubility correlation is that proposed by Chrastil.⁴⁵

The most widely used technique for the prediction of solubilities is the Peng-Robinson (PR) EOS, which requires knowledge of the solute properties.⁴⁶ The PR EOS is given by

$$P = \frac{RT}{\nu - b} - \frac{a(T)}{\nu(\nu + b) + b(\nu - b)} \quad (3.3)$$

where ν is the molar volume, a accounts for the intermolecular interactions for the species in the mixture and b accounts for the size difference between the species in the mixture. The component parameters a and b can be given by

$$a = \left(\frac{0.45724 R^2 T_c^2}{p_c} \right) \alpha \quad (3.4)$$

and

$$b = \frac{0.07780 RT_c}{p_c} \quad (3.5)$$

where T_c and p_c are the critical temperature and pressure respectively and α is a temperature dependent quantity determined from pure component vapour pressures:

$$\alpha(T) = \left[1 + m(1 - T_r^{0.5}) \right]^2 \quad (3.6)$$

and

$$m = 0.37464 + 1.54226\omega - 0.26992\omega^2 \quad (3.7)$$

where T_r is the reduced temperature ($T_r = T / T_c$) and ω is the acentric factor.

The acentric factor represents the acentricity or nonsphericity of a molecule. For monotomic gases ω is essentially zero and increases for higher-molecular weight hydrocarbons. To obtain values for ω , the reduced vapour pressure ($P_{vpr} = P / P_c$) at $T_r = 0.7$ is required and ω is given by

$$\omega = -\log P_{vpr} - 1 \quad (3.8)$$

Values of α determined from vapour pressures of saturated liquids are generally not suitable for the solvent in the sc region or for extrapolation to the sublimation curve.³⁷ The main problem associated with the use of the PR EOS for the calculation of solid-fluid phase equilibria is the lack of known vapour pressures for relatively non-volatile solutes.

It is necessary to describe a relationship between the EOS parameters for the pure components and those for component mixtures, which are dependent on the mixture composition. There are several mixing rules available in the literature for use with the PR EOS^{47,48} but in this work parameter a is given by a quadratic mixing rule and b is given by a linear one:

$$a(T) = \sum_i \sum_j y_i y_j a_{ij} \quad (3.9)$$

and

$$b = \sum_i y_i b_i \quad (3.10)$$

The combining rule for a_{ij} is given by

$$a_{ij} = \sqrt{a_{ii}a_{jj}}(1 - k_{ij}) \quad (3.11)$$

where a_{ii} and b_i are the pure component parameters and k_{ij} is an adjustable binary interaction parameter. The interaction parameter is usually determined from experimental data.

3.1.4 Separation Science using Supercritical Fluids

Supercritical fluids have received much attention over the last two decades for use as solvents in separation processes. The initial studies involved the investigation of capillary chromatography and it was thought that sc fluid techniques could rival gas-liquid chromatography and HPLC. From this initial research general interest in applications grew and this developed rapidly into applications for packed column separations and extraction processes. A thorough treatise of this initial work is given in a review by Smith.⁴⁹

Supercritical fluid extraction (SFE) is initially introduced in Section 1.4.2 and here we discuss extraction from liquid mixtures. The extraction of liquid mixtures with sc fluids is comparable to liquid-liquid extraction with the compressed gas acting instead of an organic solvent. While in liquid extraction the pressure process is negligible, it plays an important role in high-pressure extraction because it can influence fluid density, viscosity, surface tension and system phase behaviour. One advantage of SFE is that in counter-current processes (Section 3.2.3) the densities of the two counter-current flowing phases can be adjusted, which can only be achieved in liquid-liquid extraction by altering the temperature.

Another advantage offered is simple solvent regeneration. For liquid-liquid extraction solvent regeneration often includes a re-extraction or distillation step, which can have high energy requirements and be uneconomical. Therefore, the use of SFE as an in-line technique for the separation of post reaction materials could prove to be an efficient, convenient and cost effective method of solvent/starting material regeneration.

3.2 Results and Discussion

3.2.1 Solubility of Solids in Supercritical HFC 134a

Two different methods of solubility determination were used in this work as described in Chapter 2. The dielectrometry technique measures the change in dielectric constant of the solution as the solute is dissolved and has been previously reported by Hourri *et al.*⁵⁰ The reliability and validity of the dielectrometry technique and the equipment used has been reported in previous work.²³

The theoretical approach for the calculation of solubility used by Hourri and co-workers⁵⁰ had to be modified slightly so that it could be employed for polar solutes. The first dielectric virial coefficient is given by

$$A_{\epsilon}^s = \frac{4\pi N_A}{3} \left(\alpha + \frac{\mu^2}{3k_B T} \right) \quad (3.12)$$

where N_A is Avogadro's number, α is the molecular polarisability, μ is the permanent dipole moment, k_B is the Boltzmann constant and T is the experimental temperature. Lack of published data of μ for some of the selected substrates meant that μ values had to be approximated using the Spartan Pro⁵¹ molecular modelling computer program. The values for α were ignored as they were assumed to be negligible in comparison to μ and would therefore have little effect on the second term in Equation 3.12. The working relation used for the solubility determination is

$$\rho^s = \frac{CM' - CM''}{A_{\epsilon}^s} \quad (3.13)$$

where

$$CM = \frac{(\epsilon - 1)}{(\epsilon + 2)} \quad \text{Clausius-Mossotti function (3.14)}$$

and ϵ is the dielectric constant.

The primed quantities in Equation 3.13 pertain to the saturated sc solution and the double primed ones are associated with the pure sc solvent.

The capacitance values used in Equation 2.1 for the calculation of the dielectric constant were averaged from 5 replicate readings, which were found to vary by no more than ± 0.005 pF. The dielectric constant values varied by no more than ± 0.03 and this results in a maximum error of $\pm 2\%$ in the mole fraction solubility. Further uncertainty in the value of the mole fraction solubility arises from the calculation of the first dielectric virial coefficient. The error in the permanent dipole moment values used in Equation 3.12 are unknown but if a theoretical value of 5% uncertainty is used then the error in the mole fraction solubility is found to increase to $\pm 6\%$ although the actual value is likely to be less than this. Dielectric constant and density values for pure HFC 134a were taken from previously published data.⁵²

The dielectric constant for HFC 134a is considerably higher than that for CO₂ at similar temperatures and pressures and this is indicative that HFC 134a is a more polar solvent than CO₂. This means that polar solutes should have a higher solubility in HFC 134a than in CO₂ and this is investigated in this work. There is a large change in the dielectric constant of HFC 134a with increasing pressure, especially around the critical point, where there is a large change in density.

Before any new solubility measurements could be carried out using the gravimetric technique it was necessary to test the reliability of this method. The solubility of naphthalene in sc CO₂ was measured at 318 K and a variety of pressures and the results are compared to literature values in Figure 3.2. It can be seen that there is good agreement between this work and the results obtained in previous studies using an analytical open-flow⁵³ and a dielectrometry method⁵⁰ and this verifies the validity of the gravimetric method used here.

The experimentally calculated solubilities, obtained using the dielectrometry technique, for a variety of solutes in HFC 134a at 378 K and varying pressures are shown in Figure 3.3 and Tables 1-5 of the appendix. Some results using CO₂ as the solvent are shown for comparison in Figure 3.4 and it can be seen that the solvating power of HFC 134a is much higher than that of CO₂ for these solutes. If the solubility of crotonic acid at 378 K and 50 bar is taken as an example, it can be shown that this is a very significant result.

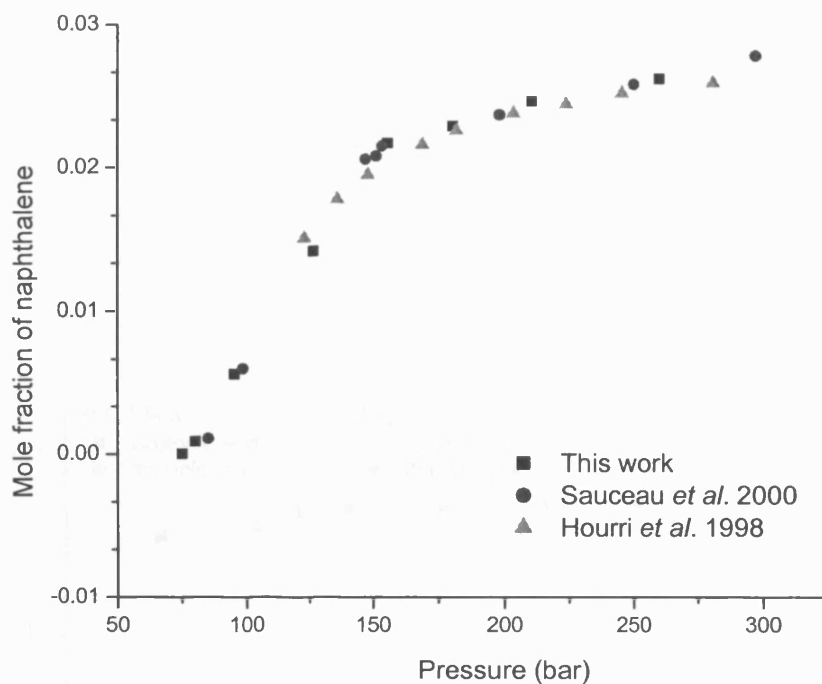


Figure 3.2 Comparison between this work and previously published data^{50,53} for the solubility of naphthalene in sc CO₂ at 318 K and a variety of pressures.

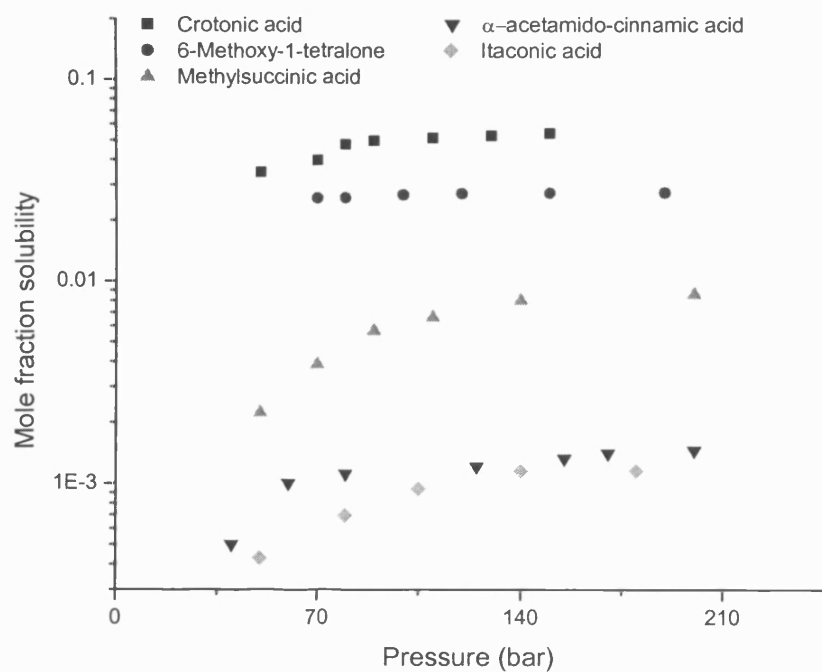


Figure 3.3 Comparison of solubilities for various substrates in HFC 134a at 378 K and a variety of pressures.

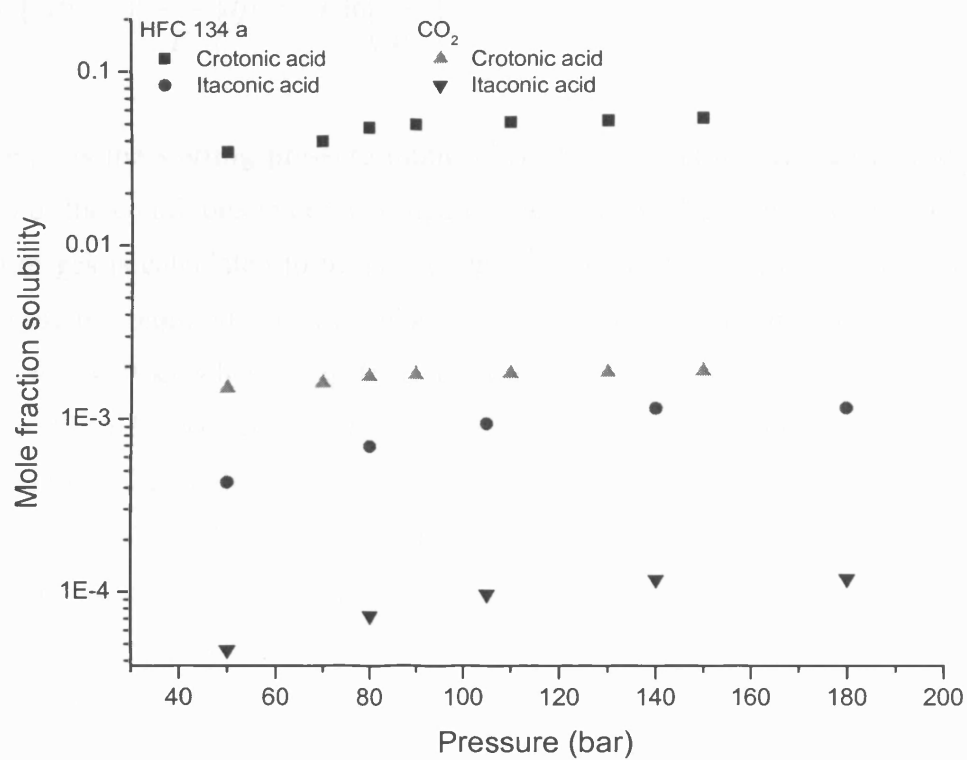


Figure 3.4 Comparison of crotonic acid and itaconic acid solubilities in HFC 134a and CO₂ at 378 K and a variety of pressures.

The solubility of crotonic acid in HFC 134a at 378 K and 50 bar is 2.62×10^{-1} mol L⁻¹ whereas the solubility in CO₂, under the same conditions, is two orders of magnitude lower at 2.72×10^{-3} mol L⁻¹. This means that 3.8 L of HFC 134a and 367.9 L of CO₂ would be needed to dissolve one mole of crotonic acid. At 50 bar and 378 K these volumes of HFC 134a and CO₂ correspond to 27.9 and 661.0 moles respectively. The work required to compress one mole of gas is given by

$$w = \int V dp = \int \left(\frac{RT}{p} \right) dp = RT \ln \left(\frac{p_2}{p_1} \right) \quad (3.15)$$

where p_1 is the starting pressure (atmospheric) and p_2 is the desired pressure (50 bar). For the conditions under investigation here the work required to compress one mole of gas is calculated to be 12.3 kJ mol⁻¹. This means that the work needed to compress the required volumes of gas, in order to dissolve one mole of crotonic acid, are 341.9 kJ when using HFC 134a and 8×10^3 kJ when using CO₂ as the solvent. It can be seen that the energy requirement for the process involving CO₂ is an order of magnitude higher than the same process involving HFC 134a. This result shows that HFCs are promising solvents for processes involving polar substrates in terms of energy requirements, economy and equipment design, since lower reaction volumes are required.

It can be seen from Figure 3.3 that the mole fraction solubility increases with increasing pressure for all of the solutes studied and it has been reported in a previous study²³ that solute solubility decreases with increasing polarity. Table 3.1 shows the permanent dipole moments and melting points (m.p.) for the solutes shown in Figure 3.3. Figure 3.5 is a representation of the trend of dipole moments and the mole fraction solubility of the solutes studied in this work.

Figure 3.5 shows that crotonic acid, 6-methoxy-1-tetralone and methylsuccinic acid have reversed solubility trends based on polarity considerations alone. This is attributed to the fact that the experimental temperatures used in this work are higher than the melting points for crotonic acid and 6-methoxy-1-tetralone and hence these solutes are in the liquid state.

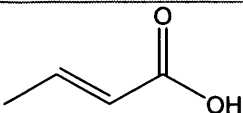
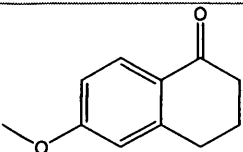
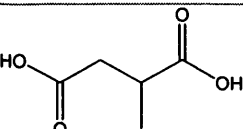
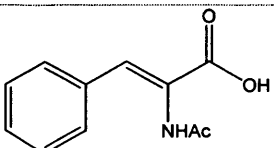
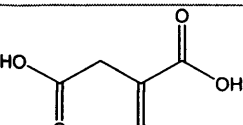
Solute	Structure	m.p. ⁵⁴ / K	μ^{51} / D
Crotonic acid		343-345	1.528
6-Methoxy-1-tetralone		350-352	1.113
Methylsuccinic acid		387-390	1.076
α -Acetamido-cinnamic acid		466-468	2.829
Itaconic acid		439-440	3.327

Table 3.1 The melting points and permanent dipole moments for the solutes shown in Figure 3.3.^{51,54}



Decreasing polarity 	Itaconic acid α -Acetamido-cinnamic acid Crotonic acid 6-Methoxy-1-tetralone Methylsuccinic acid	Itaconic acid α -Acetamido-cinnamic acid Methylsuccinic acid 6-Methoxy-1-tetralone Crotonic acid	Increasing solubility 
--	---	---	--

Figure 3.5 The trend of permanent dipole moments with solubility for the solutes studied in HFC 134a at 378 K.

Not only do these solutes have a higher vapour pressure in the liquid state (at 378 K: 1.08×10^{-1} bar for crotonic acid and 2.97×10^{-4} bar for 6-methoxy-1-tetralone *c.f.* 1.54×10^{-5} for methylsuccinic acid)⁵⁵ but also the energy of dissolution is lower due to the reduced solute-solute interactions in the liquid when compared to those in the solid state.

Generally, increasing the hydrostatic pressure increases the melting points of pure solids, but it is possible that the reverse is observed when solids are compressed in sc fluids and this effect is analogous to the freezing point depression of water when salt is added to it. As pressure is increased an increased amount of sc fluid dissolves in the liquid phase at the surface of the solid and therefore the temperature needed to freeze the solute to the solid phase decreases, since the liquid-solvent solution at the surface of the solid is not easily accommodated into the bulk solid lattice.

Since methylsuccinic acid has a melting point only 10 K higher than the experimental temperature, the phase behaviour of this solute was observed by placing an excess amount of solid in a windowed vessel (Figure 2.7), which was then subjected to the experimental conditions employed in this study. The solute remained solid under all conditions studied and this compliments the explanation given above for the solubility trends of crotonic acid, 6-methoxy-1-tetralone and methylsuccinic acid.

Figures 3.6 and 3.7 show several solubility isotherms for itaconic acid and methylsuccinic acid respectively. The data is compiled from Tables 3 and 5 of the appendix and the data for all temperatures greater than 378 K was obtained using the gravimetric method. The error associated with the balance readings is ± 0.0001 g and this leads to maximum errors of ± 2 % for itaconic acid and ± 0.5 % for methylsuccinic acid. It can be seen that solubility increases with increasing temperature for both solutes studied.

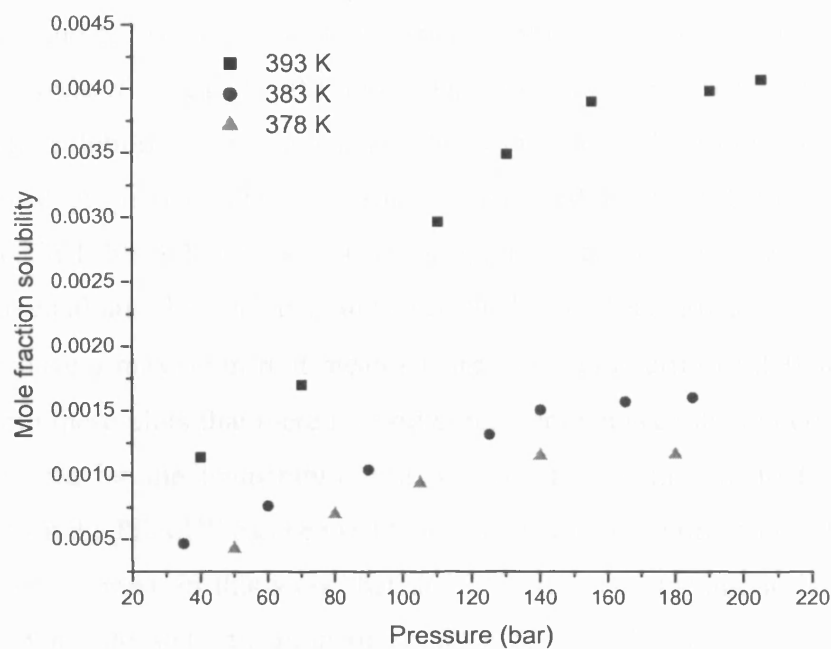


Figure 3.6 Temperature comparisons for itaconic acid in HFC 134a and a variety of pressures.

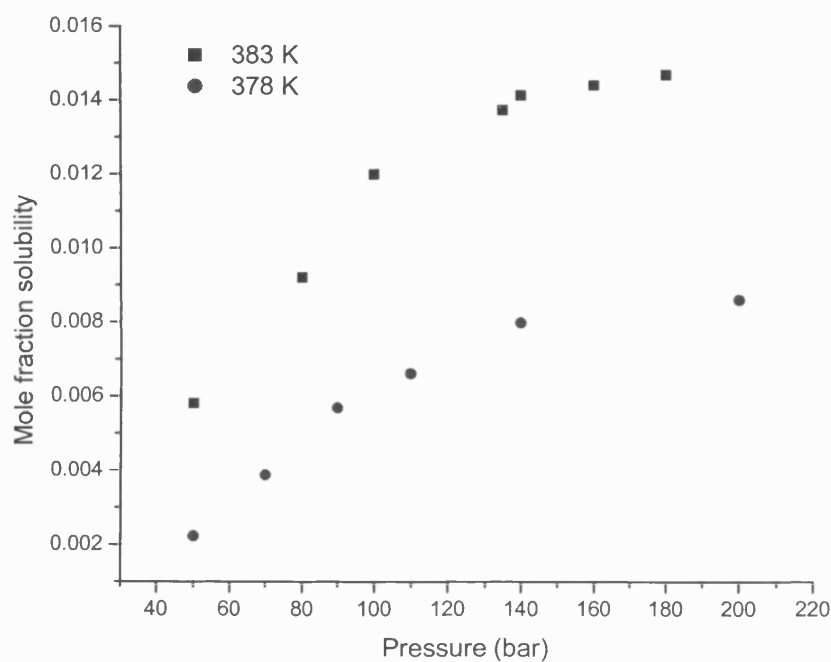


Figure 3.7 Temperature comparisons for methylsuccinic acid in HFC 134a and a variety of pressures.

3.2.2 Modelling Solubility in Supercritical HFC 134a

Kurnik and co-workers³² reported that the solubility of solid solutes in sc CO₂ could be correlated using the PR EOS. This PR model is used in this work to correlate the solubility of a number of solutes in HFC 134a using solute physical and chemical properties. The pure solute data used in the PR EOS model are summarised in Table 3.2. Tables 6-10 of the appendix and Figures 3.8-3.12 compare the experimental and theoretical solubilities for the solutes studied in this work and the results have a maximum root mean square correlation error of ± 0.0014 . It can be seen from these plots that there is good agreement between the experimental and theoretical data for the temperature and pressure ranges investigated. This is an indication that the PR EOS can be used to predict solute solubilities in sc HFC 134a.

It has been shown in this work that the dielectrometry technique is a rapid, *in situ* method for the determination of solubilities. It has been shown that the method can be used in sc HFC 134a and it is not limited by the solution concentration or appearance, which often limit spectroscopic measurements. The solubilities of the solutes studied are much higher in sc HFC 134a than in sc CO₂ (Figure 3.4) due to the higher dielectric constant of the HFC solvent. In order to obtain the same level of solubility in sc CO₂, polar modifiers or higher pressures would be required. The solvating power of HFC 134a suggests that it would be a useful solvent for sc extraction processes involving polar molecules and is a promising reaction medium for the production of industrially desirable products.

Solute	$\nu/\text{m}^3 \text{mol}^{-1}$ ^a	T_c/K	P/bar	ω	k_{ij} ^d
Crotonic acid	6.55×10^{-5}	647.5 ^b	47.0 ^b	0.572 ^b	-1.35
6-Methoxy-1-tetralone	1.13×10^{-4}	831.6 ^c	30.9 ^c	0.589 ^c	-0.98
Methylsuccinic acid	9.04×10^{-5}	817.2 ^c	41.1 ^c	1.033 ^c	-1.43
α -Acetamido-cinnamic acid	1.42×10^{-4}	963.2 ^c	28.3 ^c	1.015 ^c	-0.88
Itaconic acid	8.56×10^{-5}	821.0 ^b	42.4 ^b	0.925 ^b	-0.36

Table 3.2 Pure solute data used to model solubilities using the PR EOS.

^a Estimated using Spartan Pro⁵¹ ^b Published data⁵⁶ ^c Estimated using Cranium.⁵⁵

^d Obtained by fitting the experimental low pressure data to the PR EOS.

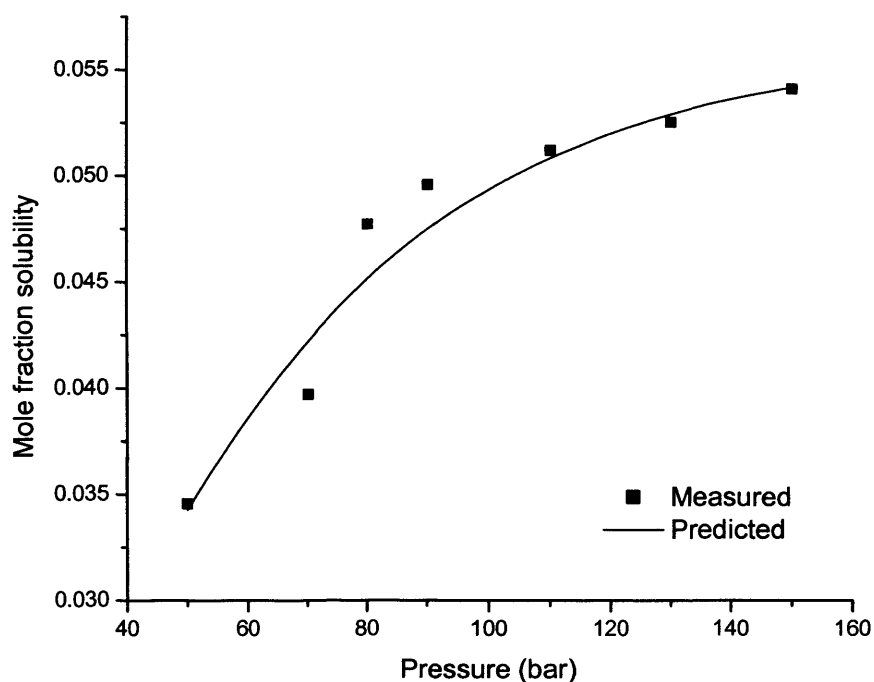


Figure 3.8 Comparison of experimental and theoretical solubility data for crotonic acid in HFC 134a at 378 K and a variety of pressures.

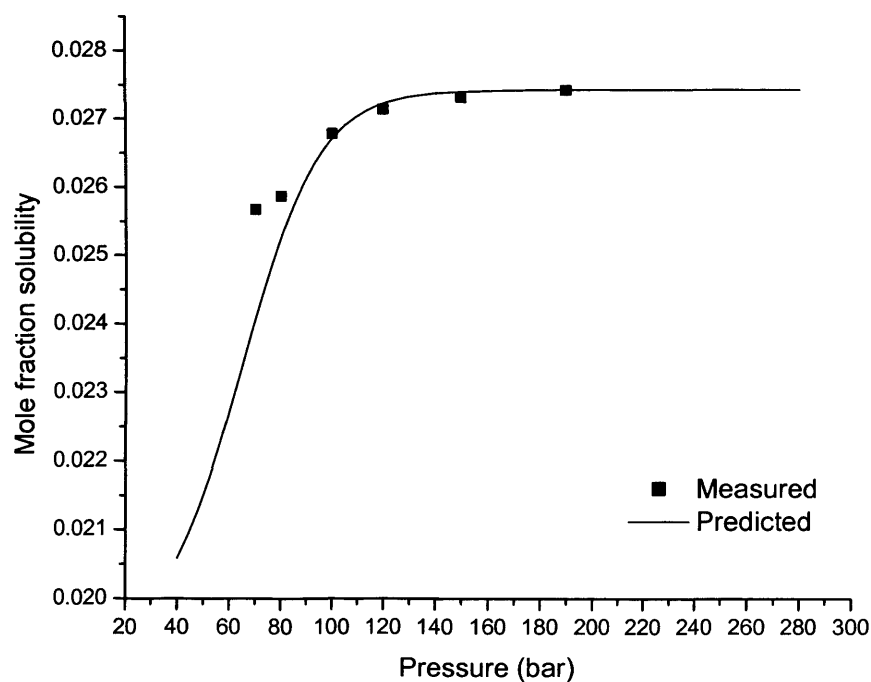


Figure 3.9 Comparison of experimental and theoretical solubility data for 6-methoxy-1-tetralone in HFC 134a at 378 K and a variety of pressures.

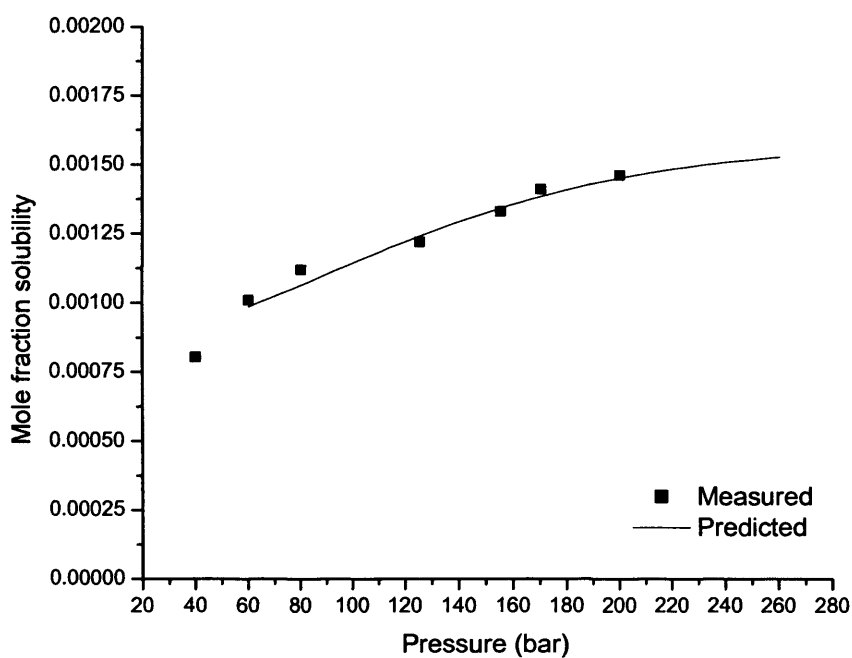


Figure 3.10 Comparison of experimental and theoretical solubility data for α -acetamido-cinnamic acid in HFC 134a at 378 K and a variety of pressures.

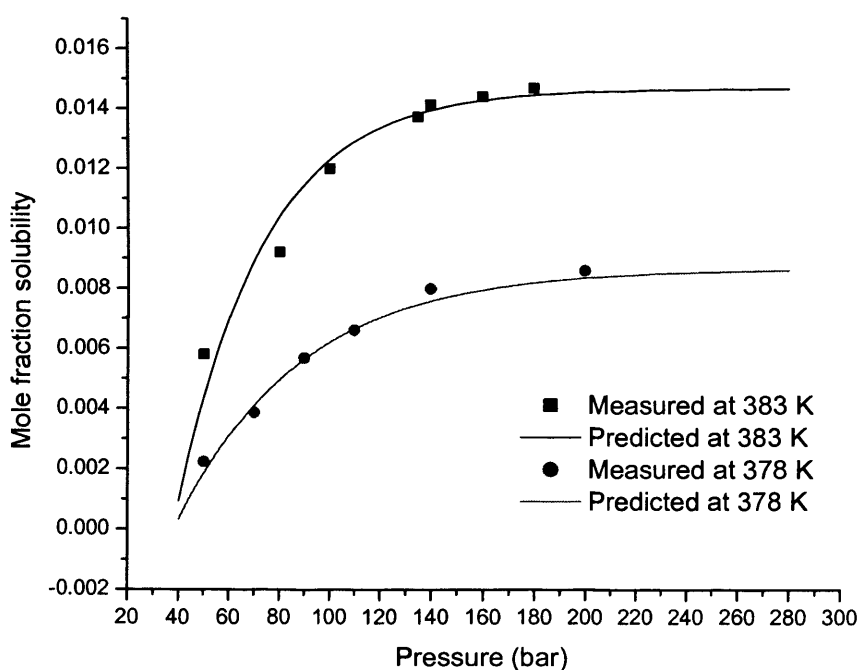


Figure 3.11 Comparison of experimental and theoretical solubility data for methylsuccinic acid in HFC 134a along two different isotherms and a variety of pressures.

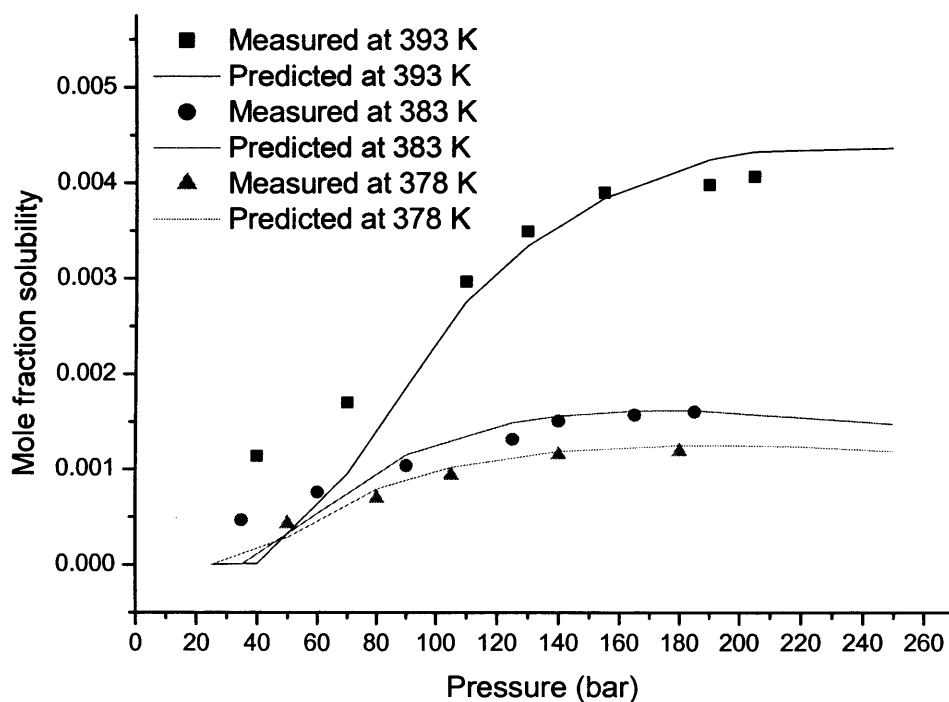


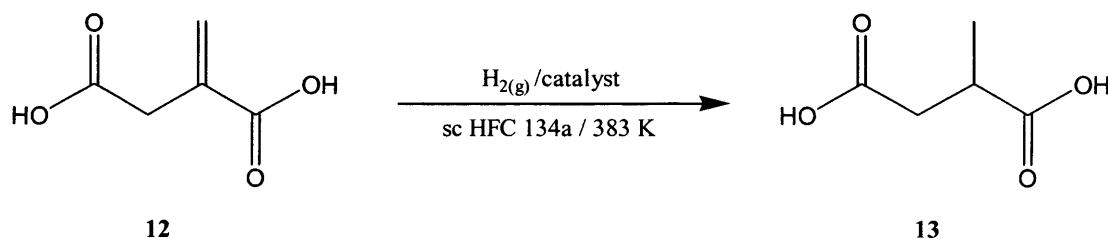
Figure 3.12 Comparison of experimental and theoretical solubility data for itaconic acid in HFC 134a along three different isotherms and a variety of pressures.

3.2.3 Designing a Separation Process

In Chapter 4 it is shown that alkenes can be effectively reduced in sc HFC 134a. It is therefore important to see if a methodology can be developed to separate the alkene substrate from the reduced product.

It is shown in Section 3.2.2 that the PR EOS can be used to adequately describe the solubility of the studied solutes in binary systems. Here we investigate the use of the PR EOS for ternary systems and use the results to design a model process for the separation of reagents and products for one of the hydrogenation reactions studied in Chapter 4 (Scheme 3.1).

A separation process for the reaction studied in Chapter 4 requires the inclusion of the homogeneous catalyst in the solubility studies and this gives rise to complicated phase considerations and mathematical analysis which is beyond the scope of this investigation. Therefore, for the purpose of this initial separation study only the solubility of the reagent and product will be considered. The concentration of catalyst in the system is assumed to be negligible and is ignored. Catalyst recovery by selective precipitation is a very important issue and the investigation of system conditions for such a process is the basis of future work. It is argued that sc HFC 134a can be used as a solvent in both the reaction and the subsequent separation by SFE. Such an integrated process combining the reaction and separation steps could prove to be effective in terms of engineering strategies and economy.



Scheme 3.1 The hydrogenation of itaconic acid in sc HFC 134a at 383 K and various pressures.

The separation strategy employed is based upon the difference in solubilities between the itaconic acid starting material **12** and the methylsuccinic acid product **13**. Due to the high conversions effected in the reactor, the concentration of methylsuccinic acid will be much higher than that of itaconic acid in the actual separation process. However, the solubility studies here employed an equimolar mixture of the two compounds in excess, so that a saturated solution was obtained giving an indication of the solvating ability and solvating preference of HFC 134a for each solute in this ternary system. Future work will focus on ternary solubility studies for various molar ratios of itaconic acid and methylsuccinic acid paving the way for a more detailed study of reagent-product separation and enabling the design of an efficient separation process.

It is important to realise that the solubilities of solutes can be greatly affected by the presence of species other than the solvent. This effect is shown in Figure 3.13 where the solubilities of itaconic acid and methylsuccinic acid in HFC 134a are given for both binary and ternary systems at 383 K and varying pressures.

It can be seen that the solubility of itaconic acid in the ternary system is enhanced (compared to the solubility in the binary system), whereas that of methylsuccinic acid is decreased. An appreciation of the solubility enhancement (*SE*) in ternary systems can be gained by using

$$SE = \frac{y_t - y_b}{y_b} \times 100 \% \quad (3.16)$$

where y_t and y_b are the mole fractions of the solute in solution for the ternary and binary systems respectively. At a given temperature there will be several values of *SE* for a given component and therefore average values will be used to quantify the solubility enhancement in this work.

The solubility enhancement for itaconic acid is calculated to be 109.3 % and that for methylsuccinic acid is calculated to be -53.7 %. The negative value for *SE* obtained for methylsuccinic acid denotes the observed decrease in solubility in the ternary system relative to the binary system (solubility diminution). Solubility diminution has been observed previously⁵⁷ but published data for such systems is scarce and to date, no explanations for this phenomenon have been proposed.

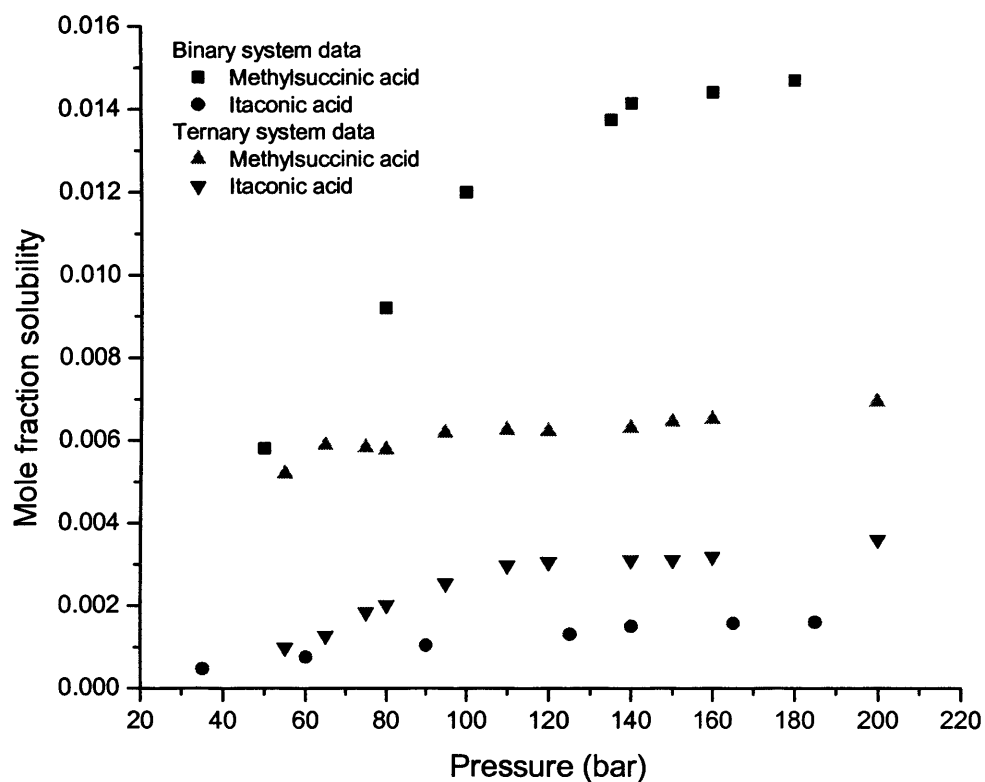


Figure 3.13 Comparison of binary (solvent and one pure solute; methylsuccinic acid or itaconic acid) and ternary (solvent, methylsuccinic acid and itaconic acid) system solubility data for itaconic acid and methylsuccinic acid in HFC 134a at 383 K.

The issue of solubility diminution requires further investigation of solute-solute and solute-solvent interactions and this is the basis of future work.

Positive solubility enhancement is more easily explained. It is well known that the addition of co-solvents (or entrainers) to sc fluid systems can lead to increased solubility for a given solute. Similarly, the presence of other components in mixed solute systems can enhance the solubility of one or more of the species due to solute-solute interactions. This is particularly applicable if the solutes contain potential hydrogen bonding sites,⁵⁸ which is the case with the solutes under investigation in this work and this explains the positive enhancement in the solubility of itaconic acid.

The difference in solubilities between the two compounds in the ternary system is much less than the differences in the binary systems and this will have an influence on the selection of separation conditions. Therefore, separation strategies based on solubility data should employ results obtained for systems in which all species are present in the mixture to be fractionated.

The applicability of the PR EOS to model solubility in the ternary system under investigation was tested and the results are shown in Figure 3.14 and Table 11 of the appendix. Quadratic mixing rules were used in conjunction with the PR EOS and the results had a maximum root mean square correlation error of ± 0.0003 . Although the PR EOS has previously been used to model ternary systems in CO₂,⁵⁹ this is the first time the model has been employed to model solubility in a ternary HFC 134a system comprising two solid components. It can be seen that this model adequately describes the solubilities of the solutes in this system and the PR EOS was therefore used to perform the required calculations in order to develop the separation process. All phase calculations were performed using the Phase Equilibria computer package⁶⁰ and the data required for the separation model was exported from the program. Figure 3.15 shows the saturation curves of the system under investigation and the figure contains an inset to show the vapour saturation curve more clearly (some example tie lines are shown).

The solubility data can be used to find optimum separation conditions. Since only one temperature has been studied in this work the temperature of the extraction is set to the experimental temperature of the reaction, which in this case is 383 K.

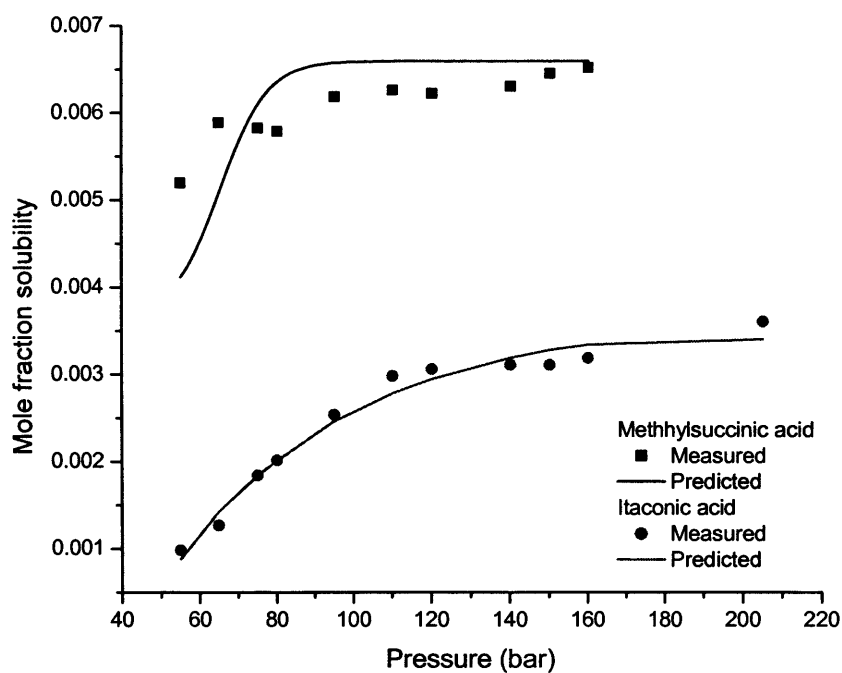


Figure 3.14 Comparison of experimental and theoretical solubility data for the ternary itaconic acid and methylsuccinic acid system in HFC 134a at 383 K.

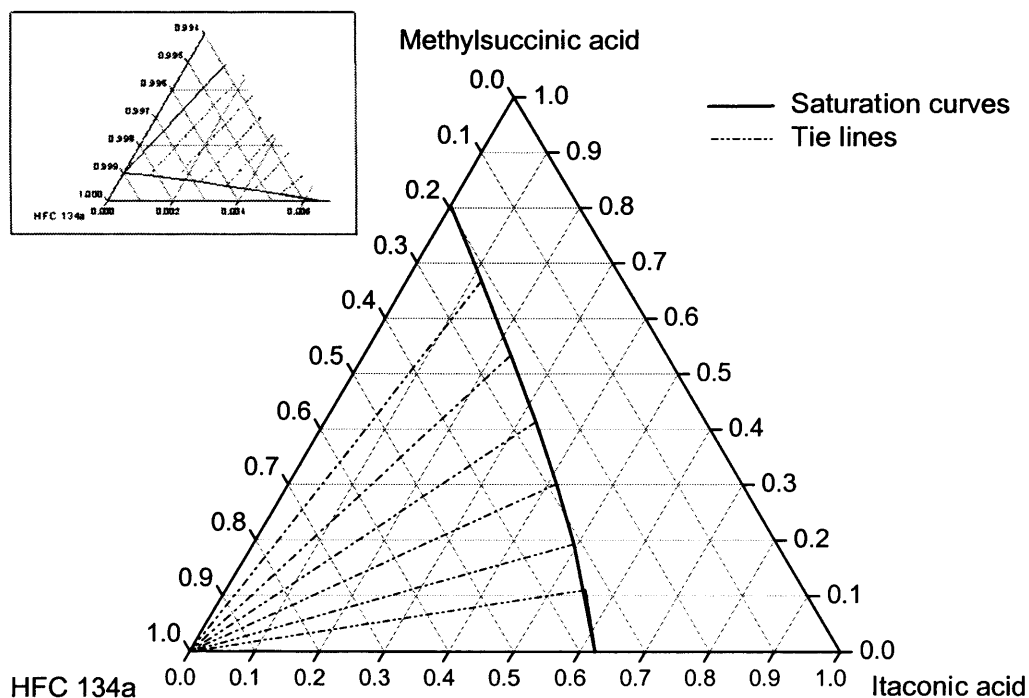


Figure 3.15 The saturation curves for the ternary system at 55 bar and 383 K. The inset shows the vapour saturation curve more clearly.

The extraction pressure is taken to be the pressure at which the selectivity (or separation factor) of the sc fluid is greatest. The selectivity is defined as the ratio of the more and less soluble solutes respectively. The selectivities based on the ternary system solubility data are shown in Figure 3.16 as a function of pressure. It can be seen that selectivity decreases with increasing pressure for this system and the greatest selectivity is observed at 55 bar. The percentage conversion in the reactor will give a product stream, which represents the feed, F , which must be dealt with in the SFE process.

The model described here for the separation process will employ a counter-current separating column as shown in Figure 3.17. The column is a multistage separation module in which the feed (HFC 134a, itaconic acid and methylsuccinic acid) enters the top of the column (entering at stage number 1), and the raffinate (HFC 134a and itaconic acid), R , leaves the bottom (stage number N). The raffinate is defined as the portion of the original feed left over once the desired component (methylsuccinic acid in this case) has been extracted with solvent.

The solvent stream, S , of HFC 134a enters the bottom of the column and flows counter-current to the descending raffinate phase, thus extracting the desired component. The extract phase (HFC 134a and methylsuccinic acid), E , exits the top of the column and the raffinate phase can be recycled to the reaction vessel and the starting material reused.

The remainder of this discussion will involve the determination of the required number of stages in the column to achieve the desired fractionation of components. Theoretical reaction conversion values of 50 % and 95 % are dealt with and the SFE process for intermediate conversions will require an intermediate number of stages in the separating column. The following assumptions are necessary in order to simplify the design process:⁶¹

1. The two flows, F and R , entering each stage are merged into a single flow.
2. The pressure and temperature for the SFE process are exerted externally and are the same for every stage. Energy balances are considered negligible and are neglected.

The extract and raffinate phases leaving each stage are in equilibrium and perfect homogeneity is assumed.

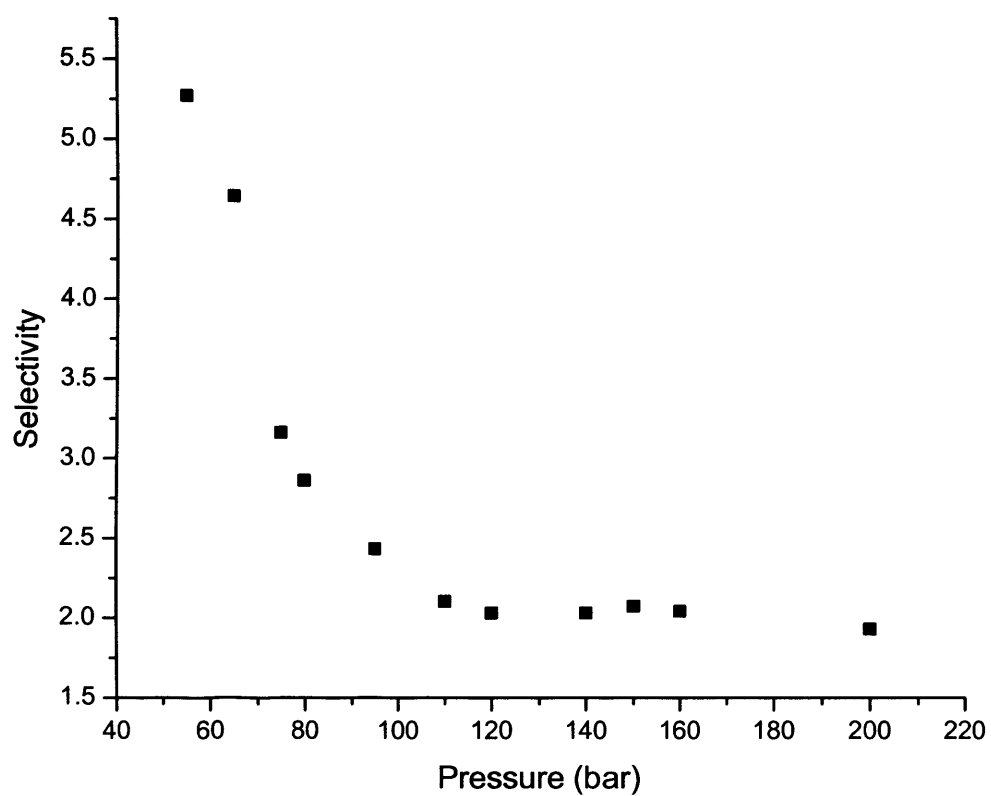


Figure 3.16 Selectivity as a function of pressure for itaconic acid and methylsuccinic acid in HFC 134a at 383 K.

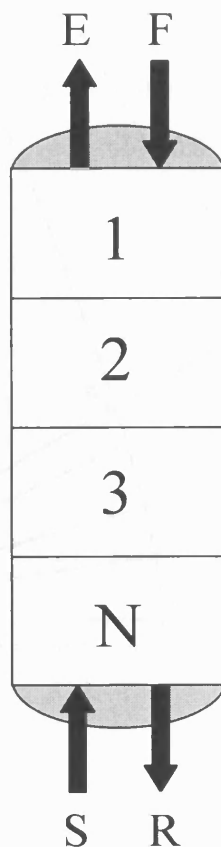


Figure 3.17 Representation of a counter-current separating column showing a number of N stages.

For a counter-current separating column the minimum number of theoretical stages required can be obtained by the construction of equilateral triangle diagrams, the method of which is described in detail elsewhere.^{62,63} Figures 3.18 and 3.19 show the equilateral triangle diagrams for the processes involving a 50 % and 95 % conversion respectively.

To simplify construction of the diagrams further, the minimum number of stages required to achieve separation is regarded as the point at which the methylsuccinic acid concentration in the raffinate becomes zero, which dictates the position of point R . This means that the construction lines run from point S in the diagram and reach their maximum value. The raffinate phase can be redirected back to the reaction vessel after leaving the separating column and the starting materials can be reused.

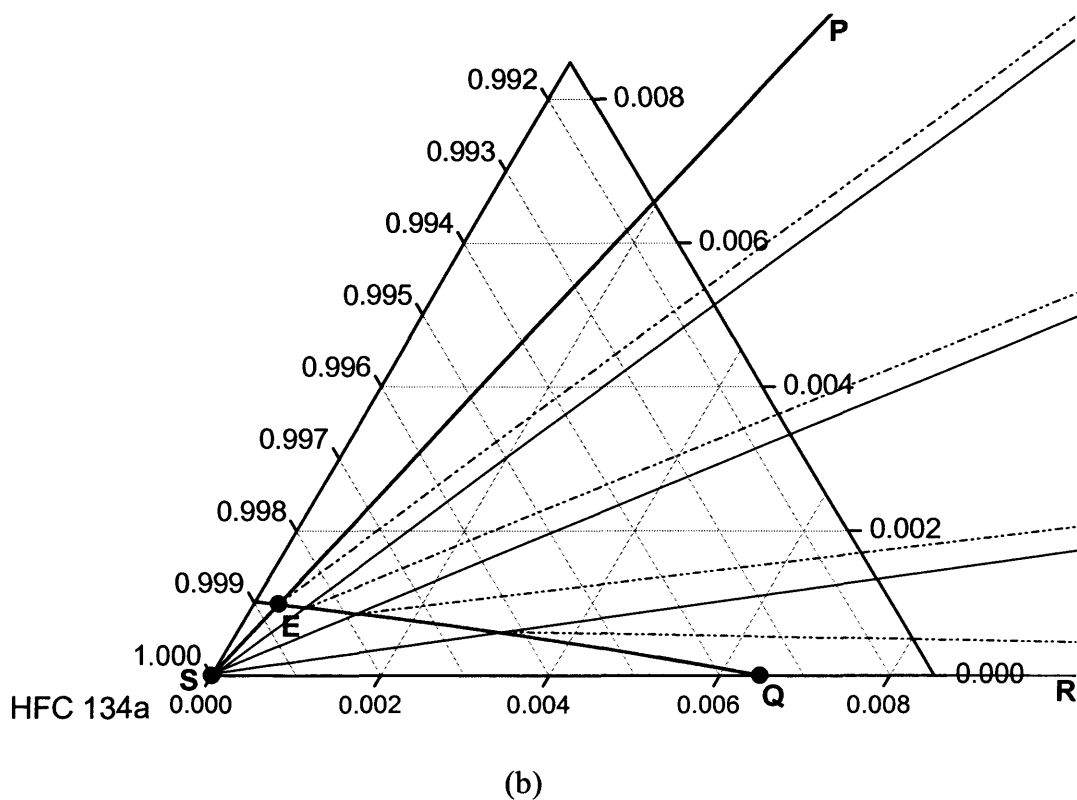
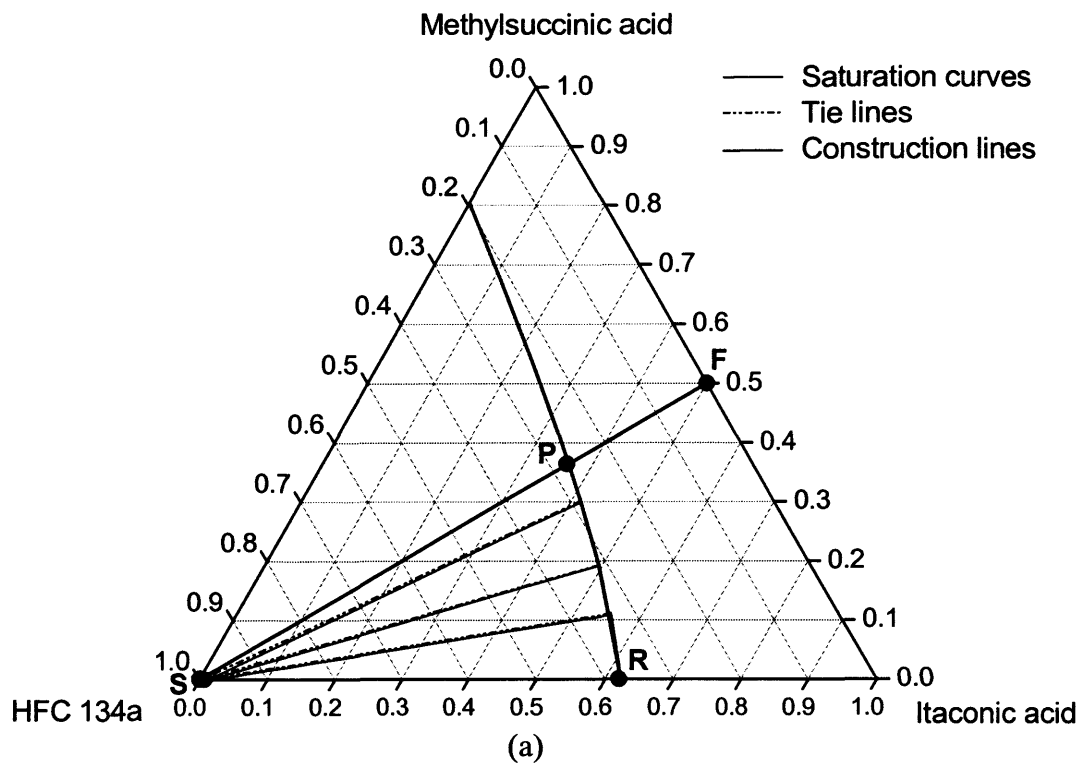


Figure 3.18 (a) The equilateral triangle diagram used to determine the minimum number of stages for counter-current separation of a 50:50 reagent to product feed.

(b) An enlargement showing the vapour saturation curve and the extract phase.

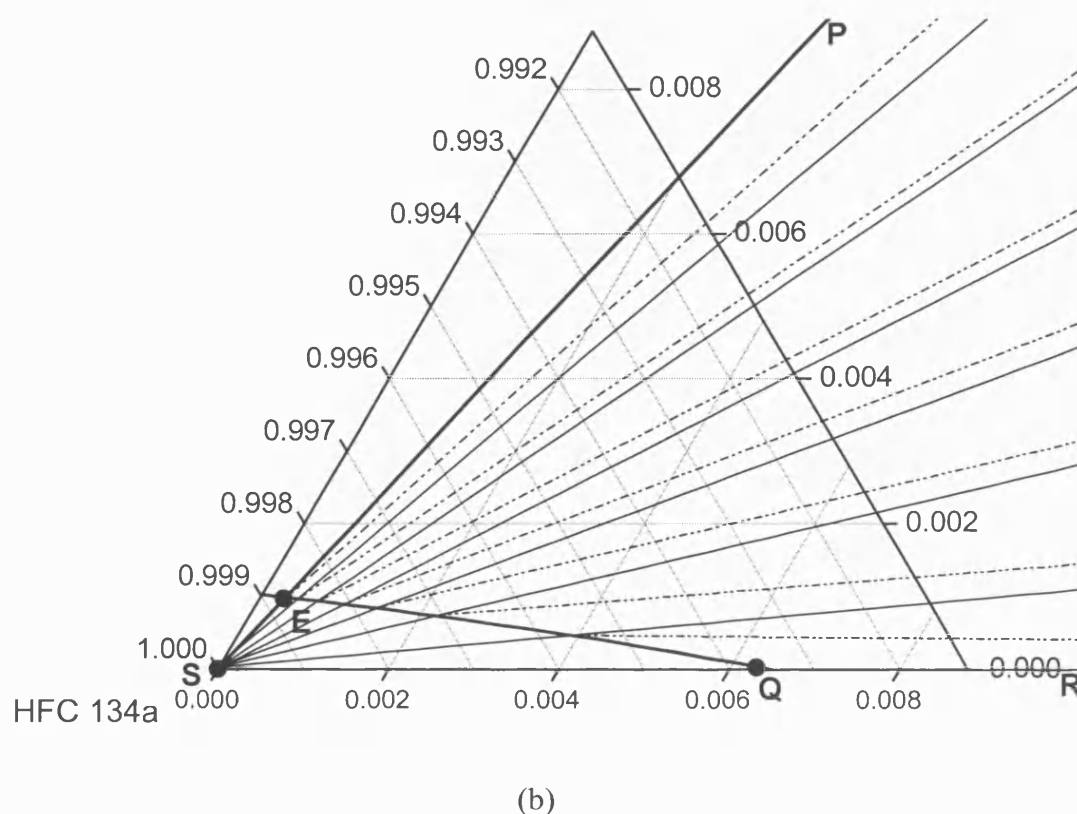
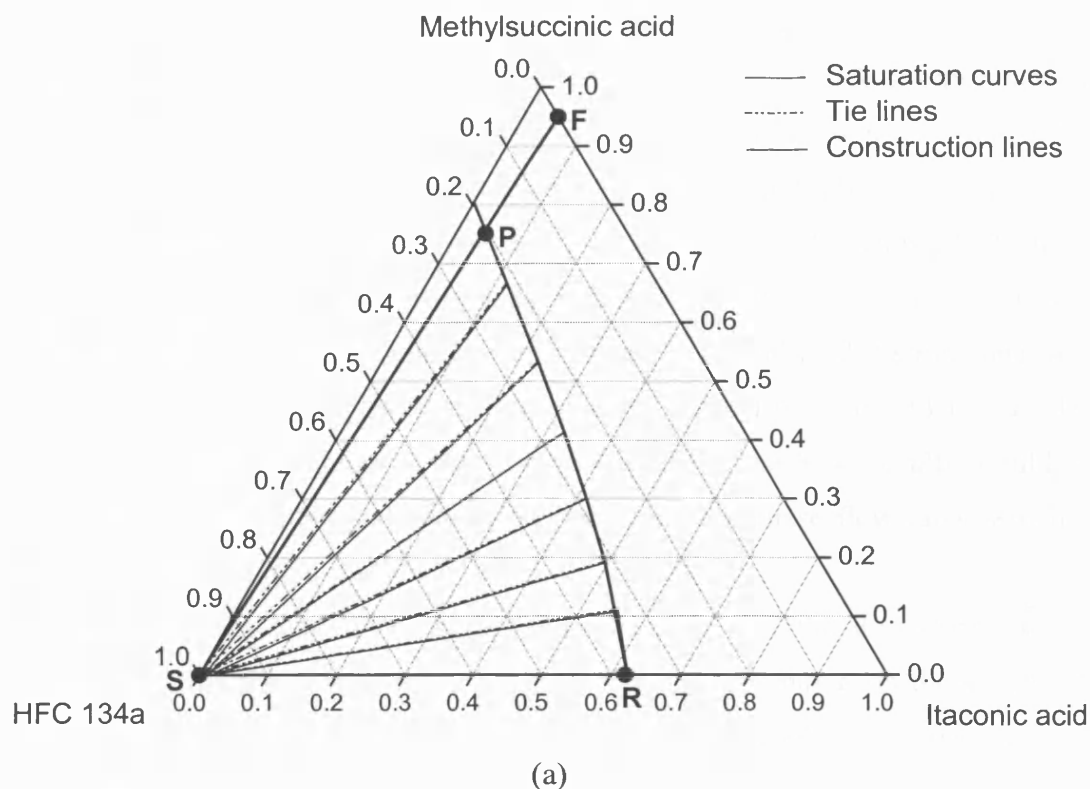


Figure 3.19 (a) The equilateral triangle diagram used to determine the minimum number of stages for counter-current separation of a 05:95 reagent to product feed.

(b) An enlargement showing the vapour saturation curve and the extract phase.

The lines $F-S$ and $R-S$ represent the upper and lower construction lines respectively and any other line that lies between $F-S$ and $R-S$ represents an intermediate construction line. The couples $R-Q$ and $P-E$ represent the start of the operating line and the end of the operating line respectively. The number of stepwise construction and tie lines in the diagram gives the number of stages required for separation. This corresponds to four stages for the 50 % methylsuccinic acid feed and seven steps for the 95 % methylsuccinic acid feed. Estimations from the triangle diagrams suggest that > 99 % of the methylsuccinic acid is extracted from each system, although a true representation of the SFE results would be obtained using computational simulations incorporating phase flow rates, which is beyond the scope of this study.

The discussion here is by no means exhaustive and the theoretical aspects employed during the design of the separation process are based on theoretical PR EOS calculations involving initial estimate data. The models have been made as simple as possible to serve as an example of how solubility data can be used in process design. A more detailed and realistic study should involve an experimental investigation of system phase behaviour of the components present in the mixture and this is the basis of future work.

These initial models do however suggest that it is possible to carry out sc fluid reactions in a system incorporating an in-line SFE process, which is beneficial in terms of economy and engineering strategies. It is shown that HFC 134a can be used not only as the reaction medium but also the extracting solvent and that efficient separation of reagents and products can be achieved, which greatly enhances the commercial applicability of this technology.

3.3 Conclusion

The solubilities of a range of polar solutes in HFC 134a have been investigated. It was shown that solubility increases with increasing pressure for all solutes studied and also with increasing temperature for itaconic acid and methylsuccinic acid. It has been reported previously that solubility decreases with increasing solute polarity.²³ This general trend was also observed in this work although it was shown that these trends are reversed if the experimental temperature exceeds the melting point temperature of the solute. The study also extends current data pertaining to the solvating power of HFCs, since publications to date are very limited.

It has been demonstrated that polar solutes have much higher solubilities in HFC 134a than in CO₂ and that the energy requirements needed to obtain similar solubilities in pure CO₂ are over an order of magnitude higher than those for the HFC 134a system. The higher energy requirement associated with CO₂ greatly reduces the attractiveness of this solvent for processes involving polar reagents, analytes or substrates and HFCs have been shown to be viable alternatives for such processes.

The higher solubilities in HFC 134a are due to the higher dielectric constant of this medium, which changes considerably with increasing pressure, especially around the critical point.⁵² This suggests that varying degrees of enantioselectivity can be achieved during asymmetric synthesis in this solvent.

It has been shown that the dielectrometry technique is a precise, simple, *in situ* method for the determination of solubilities of the solutes used in this study in supercritical fluids and measurements are not inhibited by solution concentration or appearance, which are often the limitations associated with spectroscopic techniques.

The data for the binary system was successfully modelled using the Peng-Robinson equation of state and for the first time this work applied the model to successfully correlate the solubilities of a ternary HFC 134a system comprising two solid solutes. This shows that the PR EOS could be a useful tool for predicting solute solubilities in HFC 134a and predictions of this sort may prove to be convenient alternatives to experimental data during initial process design.

The importance of solubility data was demonstrated by modelling an ideal supercritical fluid extraction process, for the separation of reagents and products, using a counter-current separating column.

It is suggested that supercritical HFC 134a can be used as both the reaction medium and extraction solvent, which enables in-line separation of compounds during supercritical fluid synthesis. Future work will focus on extended solubility and phase behaviour studies incorporating the asymmetric catalyst. Results from such a study, combined with the initial results obtained here, will provide a process in which facile catalyst/product/reagent separation will be possible using the principles of supercritical fluid extraction. Such a separation process coupled with enantioselective hydrogenation greatly enhances the commercial applicability of this work.

3.4 References

1. Hannay, J. B.; Hogarth, J. *Proc. R. Soc. London* **1879**, 29, 324.
2. Buckner, E. H. *Z. Phys. C* **1906**, 54, 665.
3. Jessop, P. G.; Leitner, W. *Chemical Synthesis using Supercritical Fluids*, Wiley-VCH, Weinheim, **1999**.
4. Anitescu, G.; Tavlarides, L. L. *J. Supercrit. Fluids* **1997**, 10, 175.
5. Anitescu, G.; Tavlarides, L. L. *J. Supercrit. Fluids* **1997**, 11, 37.
6. Anitescu, G.; Tavlarides, L. L. *J. Supercrit. Fluids* **1999**, 14, 197.
7. Rodrigues, S. V.; Nepamuceno, D.; Martins, L. V.; Baumann, W.; Fresenius, J. *Anal. Chem.* **1998**, 360, 58.
8. Lagalante, A. F.; Hansen, B. N.; Bruno, T. J.; Sievers, R. E. *Inorg. Chem.* **1995**, 34, 5781.
9. Jessop, P. G. *Topics in Catalysis* **1998**, 5, 95.
10. Yazdi, A. V.; Beckman, E. J. *Ind. Eng. Chem. Res.* **1997**, 36, 2368.
11. Kainz, S.; Koch, D.; Baumann, W.; Lietner, W. *Angew. Chem. Int. Ed. Engl.* **1997**, 36, 1628.
12. Kainz, S.; Brinkmann, A.; Leitner, W.; Pfaltz, A. *J. Am. Chem. Soc.* **1999**, 121, 6421.
13. Mochizuki, S.; Wada, N.; Smith, R. L.; Inomata, H. *Anal. Commun.* **1999**, 36, 51.
14. Vayssiere, P.; Wipff, G. *Phys. Chem. Chem. Phys.* **2003**, 5, 2842.
15. Burk, M. J.; Feng, S.; Gross, M. F.; Tumas, W. *J. Am. Chem. Soc.* **1995**, 117, 8277.
16. Dillow, A. K.; Hafner, K. P.; Yun, S. L. J.; Deng, F.; Kazarian, S. G.; Liotta, C. L.; Eckert, C. A. *AIChE J.* **1997**, 43, 515.
17. Lora, M.; Lim, J. S.; McHugh, M. A. *J. Phys. Chem.* **1999**, 103, 2818.
18. Reaves, J. T.; Roberts, C. B. *Chem. Eng. Comm.* **1999**, 171, 117.
19. Chialvo, A. A.; Cummings, P. T.; Kalyuzhnyi, Yu. V. *AIChE J.* **1998**, 44, 667.
20. Yamamoto, M.; Iwai, Y.; Nakajima, T.; Arai, Y. *J. Phys. Chem.* **1999**, 103, 3525.
21. Petsche, I. B.; Debenedette, P. G. *J. Chem. Phys.* **1989**, 91, 7075.
22. Zhang, X.; Han, B.; Hou, Z.; Zhang, J.; Liu, Z.; Jiang, T.; He, J.; Li, H. *Chem. Eur. J.* **2002**, 8, 5107.

23. Abbott, A. P.; Corr, S.; Durling, N. E.; Hope, E. G. *J. Chem. Eng. Data* **2002**, 47, 900.
24. Stahl, E.; Willing, E. *Mikrochim. Acta*. **1981**, 465.
25. Ashraf-Khorassani, M.; Combs, M. T.; Taylor, L. T.; Schweighardt, F. K.; Mathias, P. S. *J. Chem. Eng. Data* **1997**, 42, 636.
26. Abbott, A. P.; Eardley, C. A. *J. Phys. Chem. B* **1998**, 102, 8574.
27. Abbott, A. P.; Eardley, C. A.; Tooth, R. J. *J. Chem. Eng. Data* **1999**, 44, 112.
28. Abbott, A. P.; Eardley, C. A. *J. Phys. Chem. B* **1999**, 103, 2504.
29. Bartle, K. D.; Clifford, A. A.; Jafar, S. A.; Shilstone, G. F. *J. Phys. Chem. Ref. Data* **1991**, 20, 713.
30. Johnston, K. P.; Eckert, C. A. *AIChE J.* **1981**, 27, 773.
31. van Leer, R. A.; Paulaitis, M. E. *J. Chem. Eng. Data* **1980**, 25, 257.
32. Kurnik, R. T.; Holla, S. J.; Reid, R. C. *J. Chem. Eng. Data* **1981**, 26, 47.
33. Dobbs, J. M.; Wong, J. M.; Johnston, K. P. *J. Chem. Eng. Data* **1986**, 31, 303.
34. Hourri, A.; St-Arnaud, J. M.; Bose, T. K. *Rev. Sci. Instru.* **1998**, 69, 2732.
35. Fedotov, A. N.; Simonov, A. P.; Popov, V. K.; Bagratashvili, V. N. *Russian J. Phys. Chem.* **1996**, 70, 156.
36. Fedotov, A. N.; Simonov, A. P.; Popov, V. K.; Bagratashvili, V. N. *J. Phys. Chem. B* **1997**, 101, 2929.
37. Lu, B. C-Y.; Zhang, D.; Sheng, W. *Pure Appl. Chem.* **1990**, 62, 2277.
38. Joslin, C. G.; Gray, C. G.; Goldman, S.; Tomberli, B.; Li, W. *Mol. Phys.* **1996**, 89, 489.
39. Harvey, A. H. *Fluid Phase Equilibria* **1997**, 130, 87.
40. Alvarez, J. L.; Fernandez-Prini, R.; Japas, M. L. *Ind. Eng. Chem. Res.* **2000**, 39, 3625.
41. Sedlbauer, J.; O'Connell, J. P.; Wood, R. H. *Chem. Geol.* **2000**, 163, 43.
42. Politzer, P.; Murray, J. S.; Lane, P.; Brinck, J. *J. Phys. Chem.* **1993**, 97, 729.
43. Redlich, O.; Kwong, J. N. S. *Chem. Rev.* **1949**, 44, 233.
44. Guigard, S. E.; Stiver, W. H. *Ind. Eng. Chem. Res.* **1998**, 37, 3786.
45. Chrastil, J. *J. Phys. Chem.* **1982**, 86, 3016.
46. Peng, D-Y.; Robinson, D. B. *Ind. Eng. Chem. Fundam.* **1976**, 15, 59.
47. Yu, J-M.; Lu, B. C-Y. *Fluid Phase Equilibria* **1987**, 34, 1.
48. Adachi, Y.; Lu, B. C-Y. *Fluid Phase Equilibria* **1983**, 14, 147.

49. Smith, R. M. *J. Chromatogr. A* **1999**, 856, 83.
50. Hourri, A.; St-Arnaud, J. M.; Bose, T. K.; *Rev. Sci. Instru.* **1998**, 69, 2732.
51. Spartan Pro, Wavefunction Inc. Irvine, CA, USA.
52. Abbott, A. P.; Eardley, C. A.; Tooth, R. *J. Chem. Eng. Data* **1999**, 44, 112.
53. Sauceau, M.; Fages, J.; Letourneau, J-J.; Richon, D. *Ind. Eng. Chem. Res.* **2000**, 39, 4609.
54. Sigma-Aldrich Chemical Company.
55. Estimated using Cranium simulations program: Cranium, Molecular Knowledge Sytems Inc. Bedford, NH, USA.
56. Yaws, C. L. *Chemical Properties Handbook*, McGraw-Hill: New York, **1999**.
57. Lucien, F. P.; Foster, N. R. *J. Supercrit. Fluids* **2000**, 17, 111.
58. Lucien, F. P.; Foster, N. R. *Ind. Eng. Chem. Res.* **1996**, 35, 4686.
59. Chen, P-C.; Tang, M.; Chen, Y-P. *Ind. Eng. Chem. Res.* **1995**, 34, 332.
60. Brunner, G.; Pfhol, O.; Petkov, S. Phase Equilibira, Freeware, Technical University of Hamburg, Hamburg, Germany.
61. Chrisochoou, A.; Schaber, K.; *Chem. Eng. Process.* **1996**, 35, 271.
62. McHugh, M.; Krukoni, V. J. *Supercritical Fluid Extraction*, 2nd ed.; Butterworth-Heinemann: Boston, **1994**.
63. Blackadder, D. A.; Nedderman, R. M. *A Handbook of Unit Operations*, Academic Press, London, **1971**.

CHAPTER 4

HYDROGENATION IN HYDROFLUOROCARBON SOLVENTS

4.1 Introduction

4.1.1 Hydrogenation Reactions

4.1.2 Catalytic Systems for Asymmetric Hydrogenation

4.1.3 Heterogeneous Hydrogenation using Supercritical Fluids

4.1.4 Homogeneous Hydrogenation using Supercritical Fluids

4.1.5 Asymmetric Hydrogenation using Supercritical Fluids

4.1.6 Continuous Hydrogenation using Supercritical Fluids

4.2 Results and Discussion

4.2.1 Evaluating HFC 134a as a Solvent for Hydrogenation Processes

4.2.2 Asymmetric Hydrogenation in Supercritical HFC 134a

4.3 Conclusion

4.4 References

4.1 Introduction

Substances in the sc state have a unique set of physical properties that make them attractive, environmentally benign alternatives as reaction solvents. They have high miscibility with gases, liquid-like solvating power and better than liquid transport properties, which invariably suggests improved reaction rates.

Hydrofluorocarbons are polar media which allow the dissolution of a wider range of substrates than can be obtained in less polar solvents. Since solubility is dependent upon the density of the solvent, sc fluids have a tuneable solvent power, afforded by simple manipulation of temperature and/or pressure within the critical region. The tuneable solvent power will allow the heterogenisation of a homogeneous catalytic system. This provides a system which not only has high activity and selectivity towards industrially desirable products, but which will also allow facile catalyst/product separation using the principles of sc fluid extraction (Sections 1.4.2 and 3.2.2).

This aim of this chapter was to evaluate the potential of using sc HFCs as environmentally benign solvents for asymmetric hydrogenation. Work was carried out in sc HFC 134a using a range of substrates with a rhodium/monodentate-phosphine based catalyst (Section 2.3.2). The reactions were evaluated using NMR, GC and GC-MS techniques and the efficiency was evaluated with respect to selectivity and percentage conversion of reactants to products.

4.1.1 Hydrogenation Reactions

Hydrogenation of organic compounds is a reaction of great industrial importance. In the food industry the process is used in the production of edible fats from liquid oils and in the petroleum industry numerous processes involving in the manufacture of petrochemical products are based on the destructive hydrogenation of hydrocarbons. During the latter part of the 20th century the production of liquid fuels by hydrogenation of coal extract has become an attractive alternative to the extraction of petroleum.

The industrial importance of the hydrogenation process dates as far back as 1896, when the French chemist Paul Sabatier discovered that the introduction of a trace of nickel as a catalyst facilitated the addition of hydrogen to carbon based compounds.¹

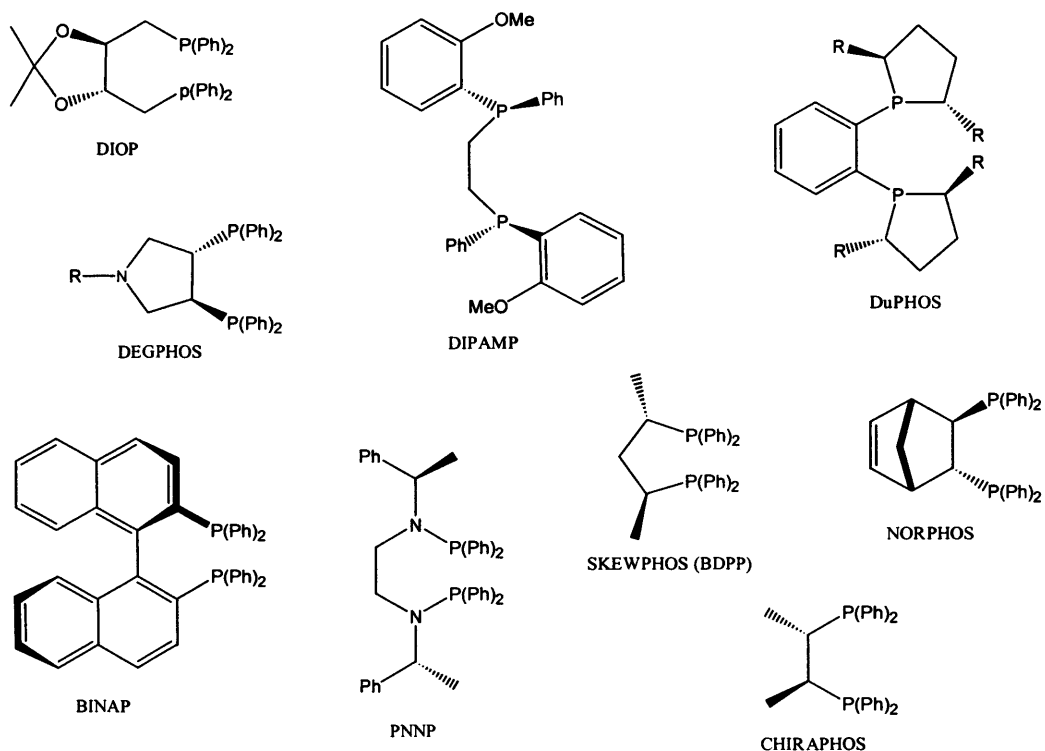
Since these early studies a phenomenal amount of research on hydrogenation reactions has been carried out with particular emphasis being placed on the design of efficient catalytic species. The scope for hydrogenation is very broad and many functional groups can be hydrogenated with high selectivities and high conversions. A book by Rylander gives a good account of many catalytic hydrogenation reactions.² The design of efficient reaction systems for asymmetric hydrogenation is critical in both the pharmaceutical and agrochemical industries.³ Asymmetric catalysis represents one of the most powerful and cost effective methods of producing enantiomerically enriched compounds⁴ and this has played a major role in establishing the economic strengths of the chemical industry.

4.1.2 Catalytic Systems for Asymmetric Hydrogenation

This discussion will focus on homogeneous catalysts although many examples of heterogeneous systems for asymmetric hydrogenation exist and a book by Jacobsen *et al.* covers heterogeneous hydrogenation reactions.⁵

The most effective homogeneous hydrogenation catalysts are complexes consisting of a central metal ion, one or more chiral ligands and anions that are able to activate molecular hydrogen, which can then be transferred to an acceptor substrate. The major influence controlling the catalytic properties of a given system is the nature of the ligating species, which can be varied to give maximum efficiency for a specific transformation. Research has shown that low-valent ruthenium, rhodium and iridium complexes stabilised by chiral phosphorus ligands are the most active and versatile catalysts⁵ and much of the current research is focused on these compounds.

The nature and structure of the ligand influences how the metal centre reacts with molecular hydrogen and the substrate *via* a number of elementary steps such as oxidative addition, insertion and reductive elimination. During these transformations the ligand must be able to stabilise various oxidation states and various coordination geometries. Some of the most common bidentate, chiral, phosphorus-based ligands are shown in Figure 4.1. Generally, ligand structures have the necessary flexibility to give high turnover rates and impart sufficient rigidity to control stereoselectivity.



Key

DIOP - (1*R,R*)-2,3-*O*-isopropylidene-2,3-dihydroxy-1,4-bis(diphenylphosphino)-butane

DEGPPOS - 1 substituted (1*S,S*)-3,4-bis(diphenylphosphino)pyrrolidine

DIPAMP - (1*R,R*)-1,2-bis[(*o*-methoxyphenyl)phenylphosphino]ethane

DuPHOS - substituted 1,2-bis(phospholano)benzene

BINAP - (1*R*)-2,2'-bis(diphenylphosphino)-1,1'-binaphthyl

PNNP - *N,N'*-bis(diphenylphosphino)-*N,N'*-bis[(*R*)-1-phenylethyl]ethylenediamine

SKEWPHOS - (1*S,S*)-bis(diphenylphosphino)pentane

NORPHOS - (1*R,R*)-5,6-bis(diphenylphosphino)-2-norbornene

CHIRAPHOS - (1*S,S*)-bis(diphenylphosphino)butane

Figure 4.1 Some of the most commonly used phosphorus-based ligands for homogeneous asymmetric hydrogenation.

More recently it has been suggested that monodentate ligands are promising alternatives to bidentate ones, since they are easily prepared from readily available starting materials, are inexpensive and can impart high reaction yields and enantioselectivities.⁶ Monodentate ligands are not a new concept and examples of monophosphines date back as far as 1968.^{7,8} However, these early examples gave low enantioselectivities and it was this deciding factor that directed research towards the more selective bidentate ligands. Some examples of recent monodentate ligands are shown in Figure 4.2 and these have been successfully applied to the asymmetric hydrogenation of a range of unsaturated substrates.⁹⁻¹⁴

Often the limitation of hydrogenation reactions is the limited solubility of gaseous hydrogen in liquid solvents. The complete miscibility of gases with sc fluids offers a potential solution to this problem and a brief review of hydrogenations carried out in sc fluids is discussed in the following sections.

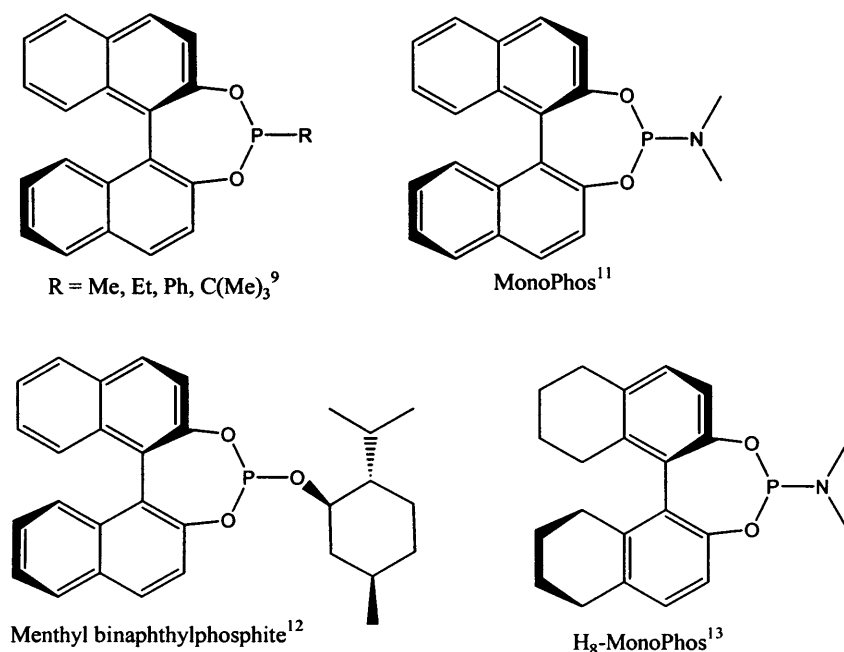


Figure 4.2 Examples of some monodentate phosphorous ligands employed in asymmetric hydrogenation.^{9,11-13}

4.1.3 Heterogeneous Hydrogenation using Supercritical Fluids

For a given amount of hydrogen the concentration in a sc fluid can be up to an order of magnitude higher than in a conventional solvent.¹⁵ This greatly increases the concentration of hydrogen at the catalyst surface, which in turn can lead to extremely high reaction rates compared to liquid phase systems. This has been used to particular advantage in the hydrogenation of fats and oils.^{16,17}

The problem associated with the use of hydrogen is its transport resistance with oils. This problem can be overcome with the use of a sc fluid as a reaction medium which is miscible with both the hydrogen and the oil, essentially forming a single homogeneous phase, which can then be fed into a fixed-bed reactor packed with a solid catalyst.^{18,19} A comprehensive review of heterogeneous hydrogenation in sc fluids is covered in work by Baiker¹⁵ and Jessop *et al.*^{20,21}

4.1.4 Homogeneous Hydrogenation using Supercritical Fluids

Gas miscibility and significant solubility of many liquid and solid substances allow sc fluids to bring reagents together in a single homogeneous phase. This offers a potential rate advantage for hydrogenation reactions over more conventional processes.

Most transition metal (M) catalysed homogeneous hydrogenation reactions take place by either an insertion mechanism or a hydrogen atom transfer (radical) mechanism (Figure 4.3). The route taken is dependent on the catalyst and substrate. The insertion mechanism is more common for hydridic MH complexes where M is rhodium or ruthenium for example. The radical mechanism is more common for acidic MH compounds such as $\text{Mn}(\text{CO})_5$ and $\text{CoH}(\text{CO})_4$.^{22,23}

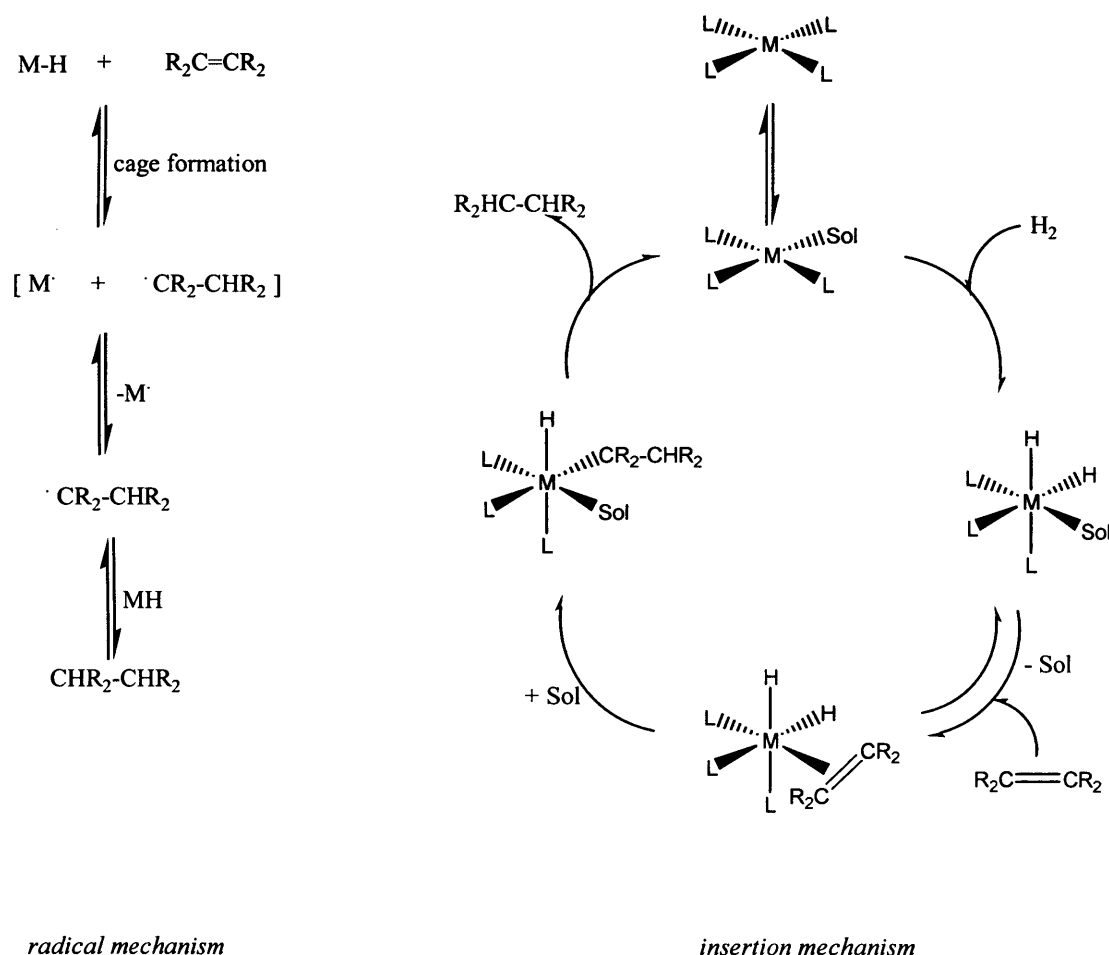
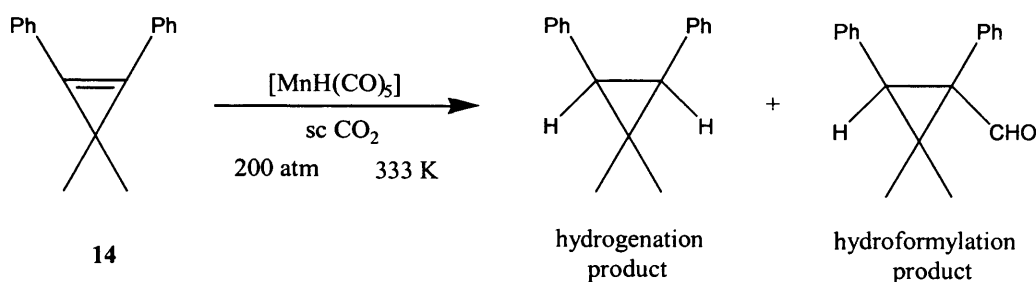


Figure 4.3 Generalised mechanism of metal catalysed homogeneous hydrogenation.

The rates of many hydrogenation reactions in liquid solvents are proportional to hydrogen concentration and are sometimes limited by the rate of diffusion of hydrogen from the gas to the liquid phase.²⁴ This problem can be overcome by the use of sc fluids as reaction media. It should be noted that in sc CO₂ the insertion of CO₂ into the metal-hydride bond of catalytic species to produce formate complexes is possible.^{25,26} This has the potential to inhibit hydrogenation reactions in sc CO₂ depending on the ability of the formate to revert back to the hydride and CO₂.

The first reported homogeneous hydrogenation of organic substrates in a sc fluid was a patent describing the hydrogenation of coal extract in sc H₂O.²⁷ The liquid hydrocarbons were extracted from the coal into the sc H₂O, which contained added hydrogen and dissolved catalysts such as NaOH, Na₄SiO₄ or KBO₂. The catalysts were recovered by precipitation induced by a pressure reduction. The use of sc H₂O in this reaction offered advantages over the earlier Bergius process²⁰ (which used liquid oils as the solvent) by preventing the coagulation of the coal, facilitating the separation of the hydrocarbon products from the solvent and rendering the coal residue more porous.

One of the first examples of hydrogenation in sc CO₂ was the hydrogenation of 3,3-dimethyl-1,2-diphenylcyclopropene **14** by [MnH(CO)₅] via a radical mechanism (Scheme 4.1).²⁸ Depending on the alkene and the solvent, either hydrogenation and/or hydroformylation products can be observed with this catalyst.^{28,29}



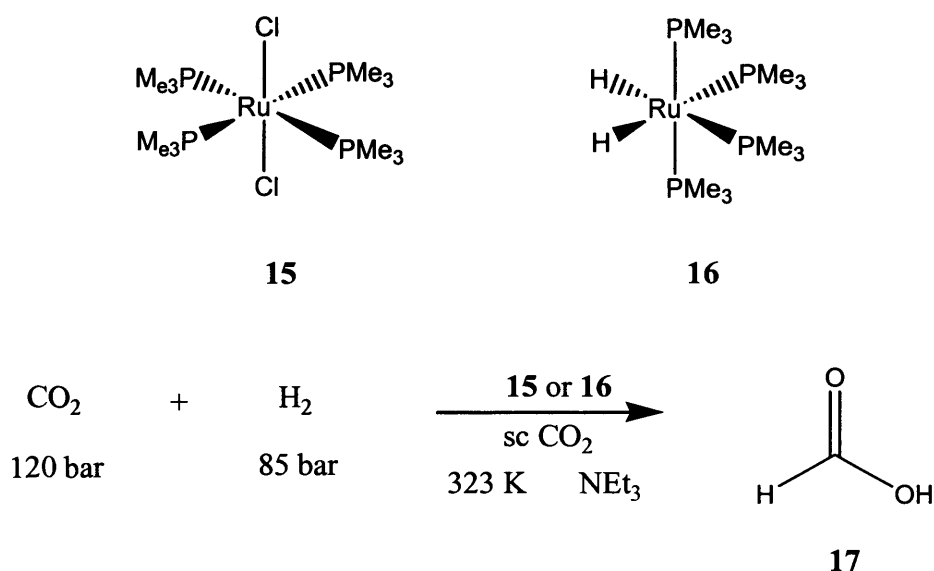
Scheme 4.1

The selectivity for hydrogenation over hydroformylation has been used as a measure of the strength of the solvent cage, with stronger cages favouring hydroformylation.^{28,30} The result of the study was that the selectivities obtained

from radical hydrogenations in sc CO₂ were similar to those obtained in liquid organic solvents.

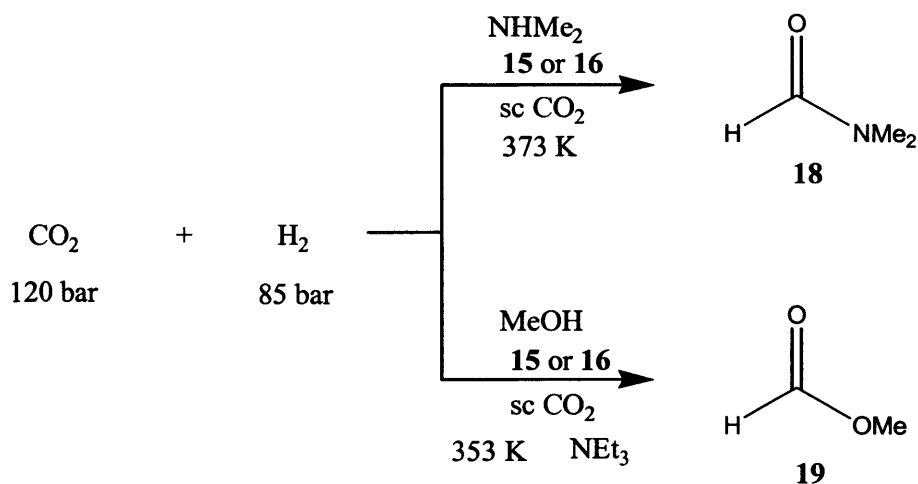
The use of CO₂ as a starting material for the synthesis of organic compounds has been of great interest to synthetic chemists. The hydrogenation of CO₂ has been particularly attractive but remains difficult under conventional gas phase conditions.

In 1994, Noyori *et al.* reported a hydrogenation reaction employing sc CO₂ as both solvent and substrate.²⁵ The system involved the use of ruthenium (II) phosphine catalysts **15** or **16** for the hydrogenation of CO₂ to formic acid **17** (Scheme 4.2).²⁵ The catalysts were chosen for their known solubility in non-polar solvents such as hexane and were shown to be more active than RuH₂[P(C₆H₅)₃]₄, which was considered to be the most active catalyst in benzene solution.



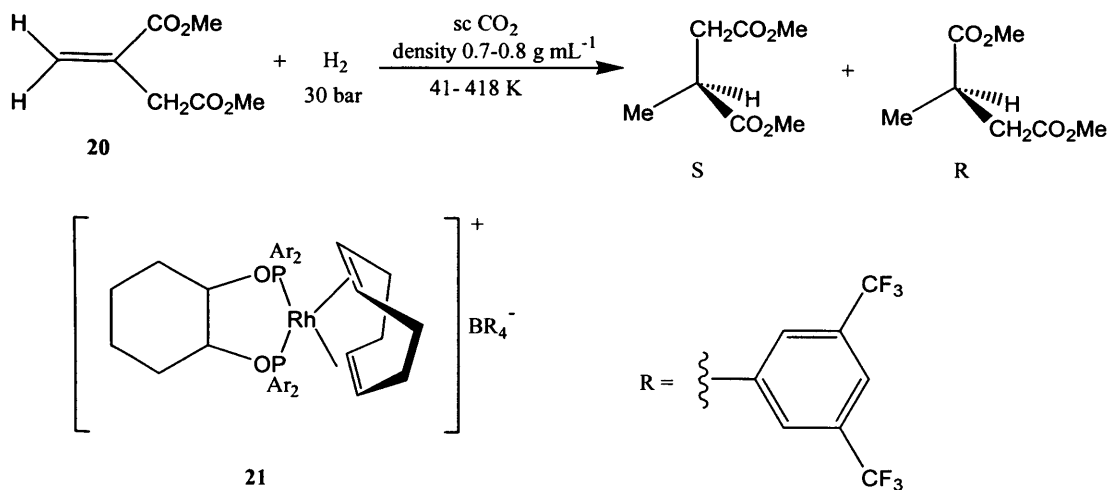
Scheme 4.2

Other reactions include the one-pot synthesis of dimethylformamide (DMF) **18** and methyl formate **19** from sc CO₂ (Scheme 4.3).²⁶ Catalyst **15** showed a catalytic activity which was two orders of magnitude greater than any reported in liquid solvents, giving 99% selectivity to DMF production and a conversion of 99% for the dimethylamine.³¹



Scheme 4.3

It is only over the last few years that the mechanistic aspects of homogeneous hydrogenation in sc fluids have been investigated. One of the first such investigations was carried out by Leitner and co-workers using dimethyl itaconate **20** and a rhodium based catalyst **21** as a model reaction (Scheme 4.4).³²

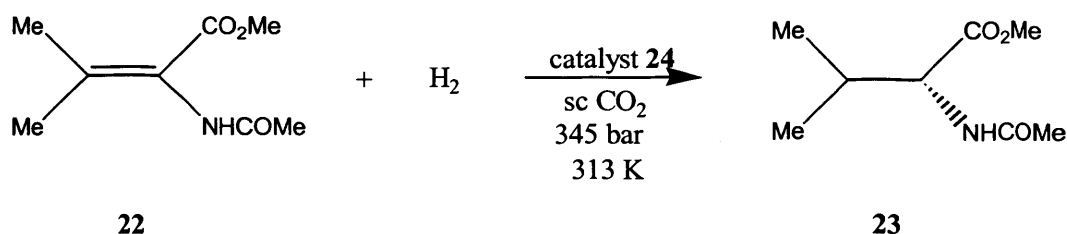


Scheme 4.4

The investigation was carried out in both hexane and sc CO_2 . They concluded that the mechanism (insertion mechanism of the type shown in Figure 4.3) was the same in both solvents and that CO_2 did not interfere with the activation and transfer of the hydrogen molecule at the activated catalytic species.

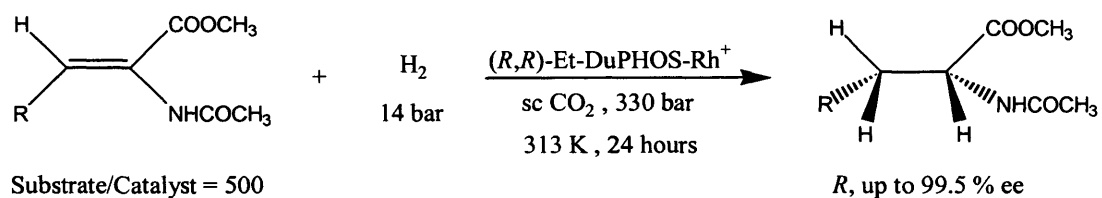
4.1.5 Asymmetric Hydrogenation using Supercritical Fluids

The enantioselectivity of asymmetric hydrogenation of a prochiral olefin depends strongly on the hydrogen concentration. Using higher concentrations of hydrogen can lead to higher, lower or reversed enantioselectivity.^{4,20} It was suggested by Burk and Tumas that the miscibility of hydrogen gas in sc fluids may lead to better enantioselectivity.³³ They studied the homogeneous asymmetric hydrogenation of β,β -disubstituted enamide **22** in sc CO₂, which gave the valine derivative (*R*)-**23** in 85 % enantiomeric excess (ee) (Scheme 4.5).³³ The highest previously reported enantioselectivity for this substrate was 55 % ee.³⁴ The same reaction was carried out in hexane pressurised to 345 bar with nitrogen. This additional experiment indicated that this enhancement of enantioselectivity was not a pressure effect but is associated with the use of sc CO₂. The asymmetric hydrogenation of several α -enamides in sc CO₂ using the cationic Rh complex **24** containing the Et-DuPHOS ligand along with a [BArF]⁻ **25** or CF₃SO₃⁻ counter-ion. (Scheme 4.6). The ee's obtained were comparable to those obtained in methanol and hexane.



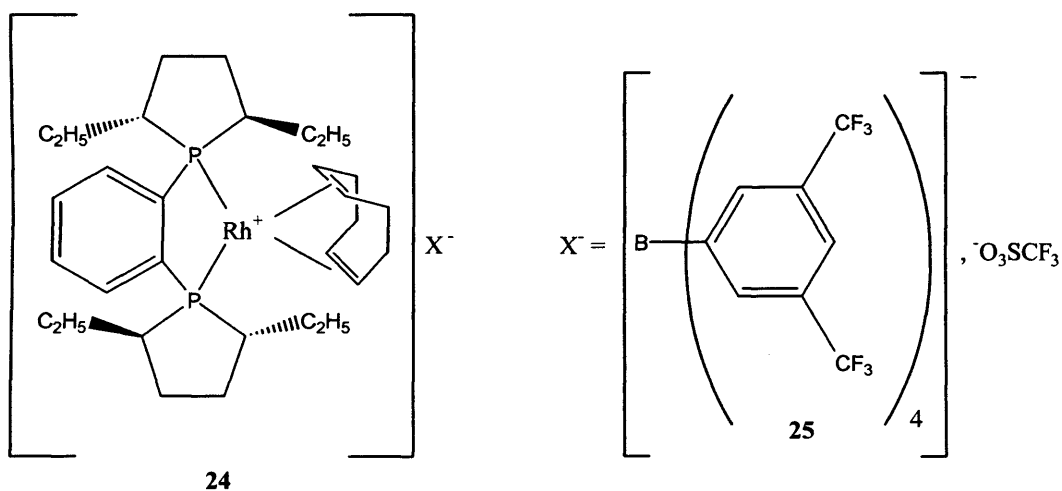
Scheme 4.5

Xiao *et al.* found that α,β -unsaturated carboxylic acids, such as tiglic acid **26**, could be hydrogenated in sc CO₂ by Ru(OCOCH₃)₂[(*S*)-H₈-binap] **28** to give (*S*)-2-methylbutanoic acid **27** (Scheme 4.7).³⁵ The product was obtained with an 81 % ee, which is comparable to that in methanol (82 %) and greater than that in hexane (73 %). The partially hydrogenated BINAP catalyst **28** (which gave 99 % yield) showed increased solubility in sc CO₂ over the fully aromatic derivative, which gave poorer yield (50 %) and selectivity (37 % ee). Adding the perfluorinated alcohol CF₃(CF₂)₆CH₂OH to **28** offered solubility enhancement and produced an increase in conversion (100 %) and enantioselectivity (89 % ee).

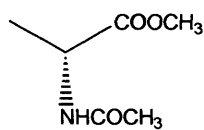


Rh 1 = [(*R,R*)-Et-DuPHOS-Rh](BARF)

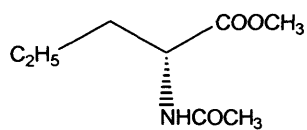
Rh 2 = [(*R,R*)-Et-DuPHOS-Rh](CF₃SO₃)



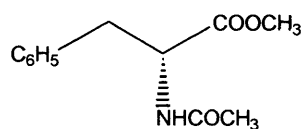
Examples (% ee)



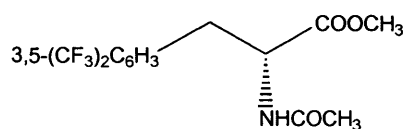
Rh 1 : 99.5
Rh 2 : 99.1



Rh 1 : 98.8
Rh 2 : 98.8

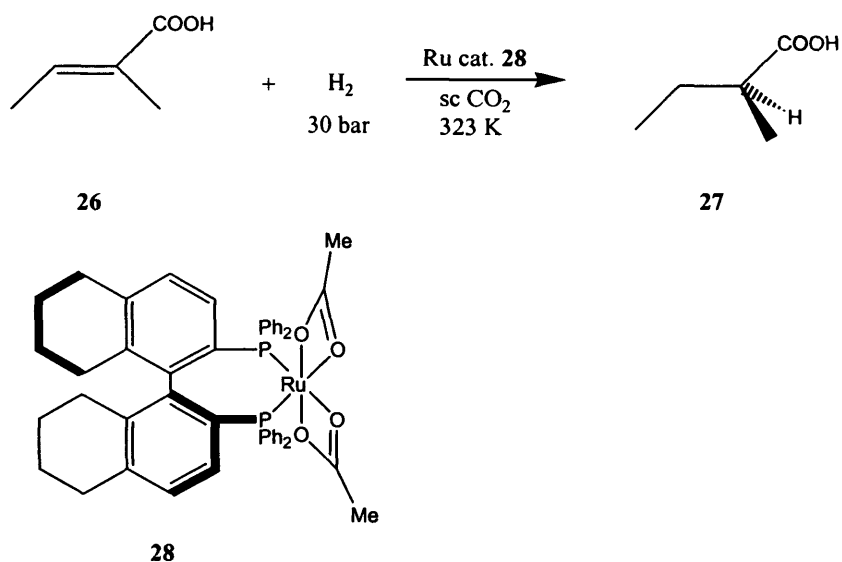


Rh 1 : 99.5
Rh 2 : 99.1



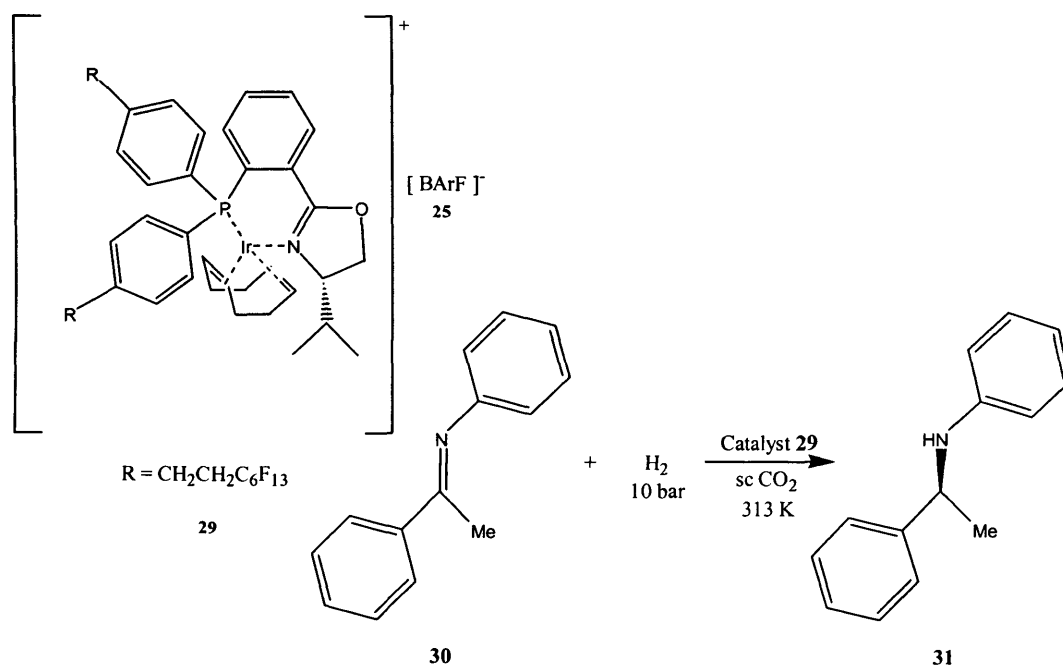
Rh 1 : 99.5
Rh 2 : 99.1

Scheme 4.6



Scheme 4.7

Leitner *et al.* have used $sc\ CO_2$ for the homogeneous iridium catalysed hydrogenation of prochiral imines.³⁶ Cationic iridium (I) complexes, modified with perfluoroalkyl groups **29** for increased CO_2 -philicity, were synthesised and used in the hydrogenation of *N*-(1-phenylethylidene)aniline **30** to give (*R*)-*N*-phenyl-1-phenyl-ethylamine **31** (Scheme 4.8).

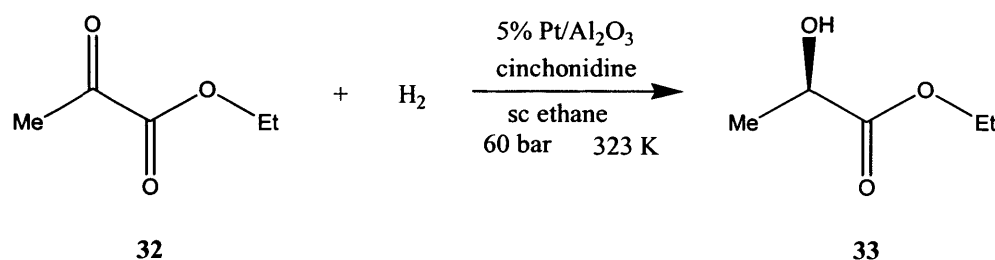


Scheme 4.8

The iridium complex containing the [BArF]⁻ counter-ion **25** gave the greatest asymmetric conversion with an 81% ee using 0.078 mol % catalyst over a period of 6 hours. In dichloromethane more than 22 hours and 5 times the amount of catalyst was required to give results comparable to those in sc CO₂.

The first reported asymmetric heterogeneous hydrogenation reaction performed in a sc fluid was carried out by Minder *et al.* in 1995.³⁷ They investigated the asymmetric hydrogenation of ethyl pyruvate **32** to ethyl (*R*)-lactate **33** under sc conditions using a heterogeneous catalytic system (Scheme 4.9). The reaction proceeded significantly faster in sc ethane when compared to the rate in toluene by a factor of over 3.5. Enantioselectivity was shown to be comparable to that obtained in toluene with ee values of around 75 %. The enantioselectivity is derived from a chiral cinchonidine modifier that is adsorbed on the surface of alumina-supported platinum. It was also noted that the reaction in sc ethane gave a slight increase in ee with increasing catalyst/reactant ratio. This was in contrast to the reaction in toluene or ethanol where an ee decrease is observed due to mass-transfer limitations at higher catalyst/reactant ratios.

The enantioselective hydrogenation in sc CO₂ showed strong catalyst deactivation. This was due to CO poisoning of the platinum following the reduction of CO₂ to CO on the catalyst surface.



Scheme 4.9

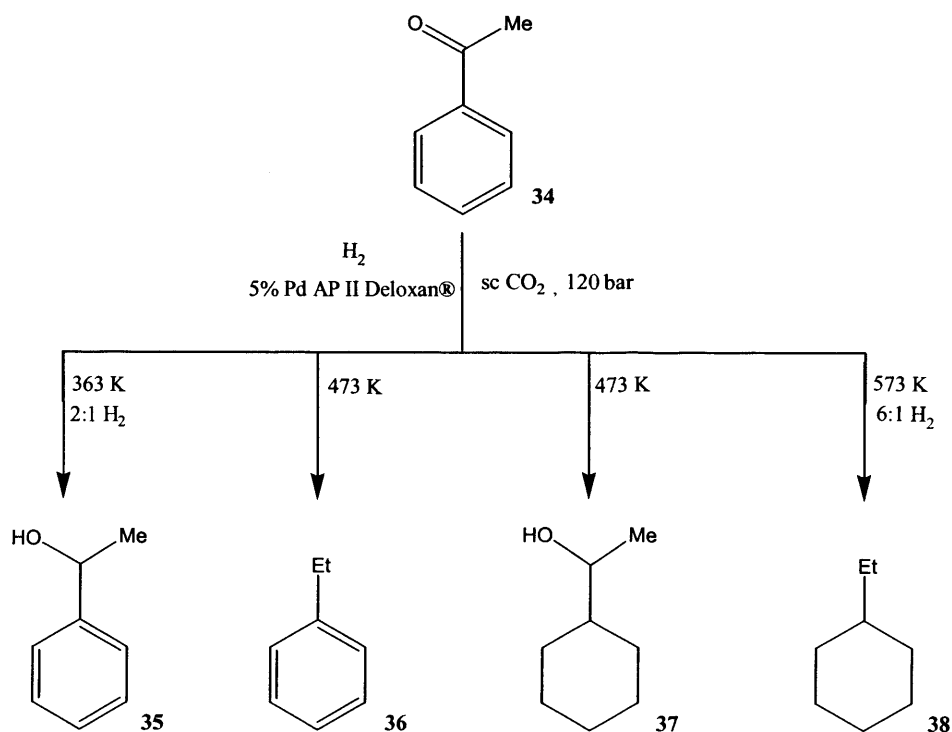
A later study by You and co-workers³⁸ investigated the same reaction shown in Scheme 4.9 and compared the results obtained for a continuous flow fixed-bed reactor to those obtained in a batch reactor. They obtained around 60 % ee and 90 % ee for the fixed-bed and batch process respectively, demonstrating the possibility of using a fixed-bed reactor for the asymmetric hydrogenation of ethyl pyruvate. It was

shown that the ee dropped over time in the continuous flow reactor since some of the chiral cinchonidine modifier was removed from the Pt/Al₂O₃ surface during the process.

4.1.6 Continuous Hydrogenation using Supercritical Fluids

Most sc hydrogenation work to date has been carried out as batch reactions in sealed autoclaves. The gas like nature of sc fluids makes them particularly suitable for continuous flow reactors. This can be advantageous because for a given reaction, a flow reactor can be smaller than the corresponding batch reactor required to produce a comparable amount of product. The reduction in reactor size is particularly attractive for the use of sc fluids because it reduces the cost and safety problems associated with high-pressure equipment.

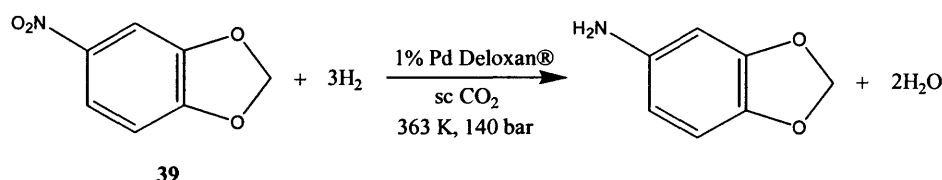
Poliakoff was the first to develop a system for the continuous hydrogenation in sc fluids using a polysiloxane supported palladium catalyst in the hydrogenation of acetophenone **34**.³⁹ Selectivity of products was achieved by adjusting the system temperature and hydrogen concentration (Scheme 4.10).



Scheme 4.10

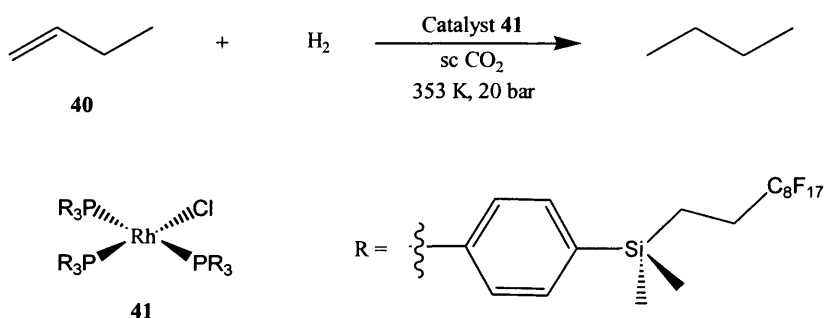
The products range from the aromatic alcohol **35** to the fully hydrogenated product **38**. The selective hydrogenation of other organic functionalities including aromatic and aliphatic alcohols, aldehydes, ketones, nitro-compounds, imines, oximes and olefins have been carried out using this system.⁴⁰

As well as the work carried out on the liquid acetophenone **34** shown in Scheme 4.10, Poliakoff and Hitzler demonstrated the ability to carry out continuous hydrogenation on a solid substrate dissolved in an inert organic solvent. One such reaction was the quantitative hydrogenation of 1,2-(methylenedioxy)-4-nitrobenzene **39** in sc CO₂ (Scheme 4.11).³⁹ The nitrobenzene compound **39** was pumped through the reactor in MeOH-THF (2:1 v/v).



Scheme 4.11

A membrane reactor was used by van den Broeke *et al.* to carry out the continuous, homogeneous hydrogenation of 1-butene **40** using a fluorinated derivative of Wilkinson's catalyst **41** in sc CO₂ (Scheme 4.12).⁴¹ The silica membrane in the reactor had a pore size of 0.5-0.8 nm whereas the catalyst was 2-4 nm in size. The substrate and product were able to diffuse through the membrane and therefore efficient catalyst recovery was facilitated. The catalyst was prepared *in situ* and conversions of around 40 % were obtained during the investigation.



Scheme 4.12

4.2 Results and Discussion

4.2.1 Evaluating HFC 134a as a Solvent for Hydrogenation Processes

The use of Wilkinson's catalyst **42** (Figure 4.4) for the hydrogenation of alkenes has often been used to evaluate the activity of new catalysts.⁴²⁻⁴⁴ A logical progression from this is therefore to use Wilkinson's catalyst to evaluate novel solvent systems for hydrogenation processes. Here, the hydrogenation of styrene **44** in sc HFC 134a is investigated and this is the first time the hydrogenation of unsaturated substrates has been carried out in this media.

The mechanism for the homogeneous hydrogenation of olefins using $[\text{RhCl}(\text{PPh}_3)_3]$ was elucidated by Halpern⁴⁵ to proceed *via* a hydride route and the mechanism for styrene is shown in Figure 4.4.

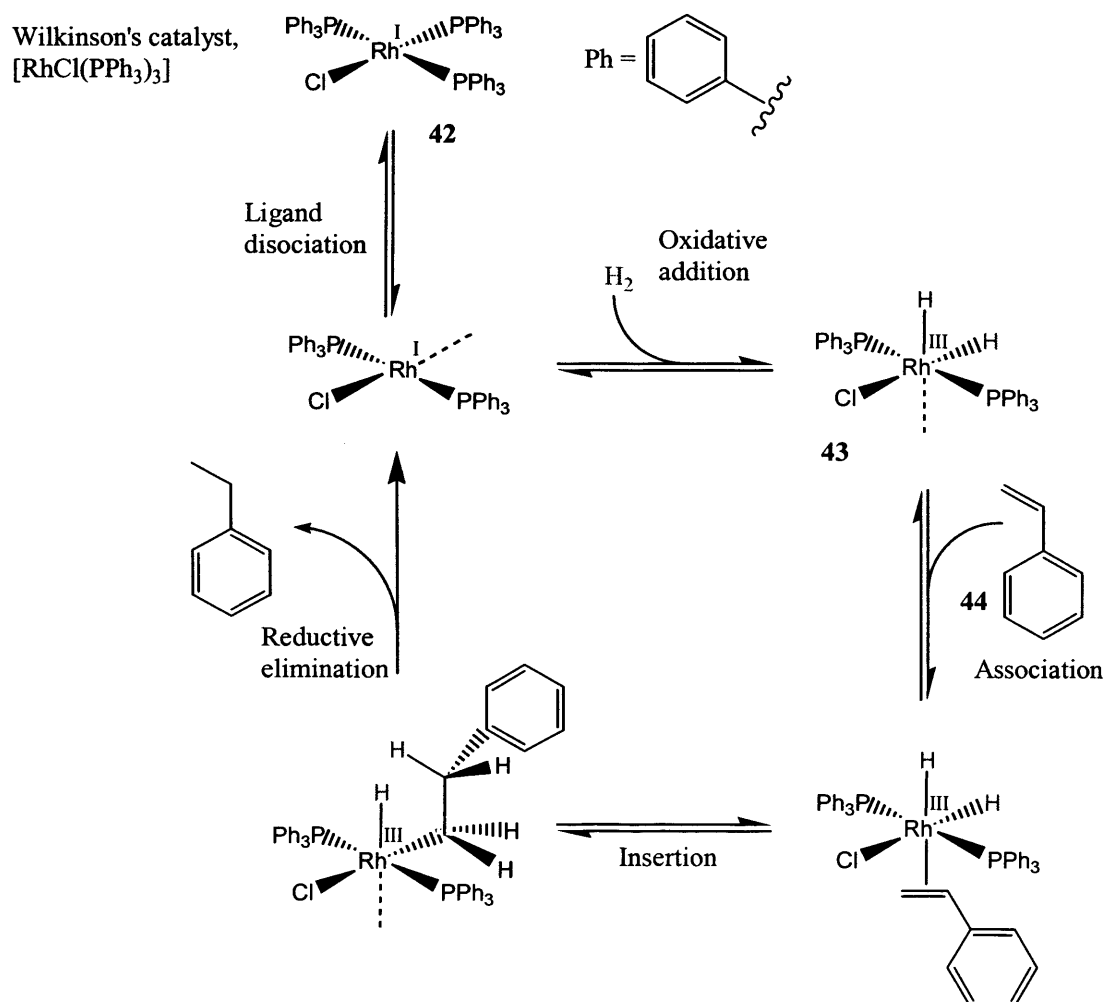


Figure 4.4 The catalytic cycle for the hydrogenation of styrene using $[\text{RhCl}(\text{PPh}_3)_3]$ as elucidated by Halpern.⁴⁵

Although the solubility of $[\text{RhCl}(\text{PPh}_3)_3]$ in HFC 134a was not measured quantitatively, a visual inspection using the cell shown in Figure 2.7 (page 33) showed that a concentration of $3 \times 10^{-3} \text{ mol dm}^{-3}$ could be dissolved in HFC 134a at 383 K in the pressure range of 50-280 bar. The solubility of $[\text{RhCl}(\text{PPh}_3)_3]$ in HFC 134a under the conditions employed in this study is more than sufficient to ensure a homogeneous reaction. A similar experiment was carried out using $1.3 \times 10^{-3} \text{ mol dm}^{-3}$ $[\text{RhCl}(\text{PPh}_3)_3]$ in CO_2 at 313 K in the pressure range 50-120 bar and an unnoticeable amount of catalyst was dissolved. This is a significant observation indicating that HFCs can be used as reaction media for homogeneous catalysis without the need for co-solvents or modification of catalytic species, such as the addition of perfluoroalkyl-ponytails, which is often a requirement for homogeneous catalytic reactions in sc CO_2 .

Firstly, the time dependency of the hydrogenation of **44** ($6.56 \times 10^{-3} \text{ mol dm}^{-3}$) in sc HFC 134a, using $2.20 \times 10^{-6} \text{ mol dm}^{-3}$ of $[\text{RhCl}(\text{PPh}_3)_3]$ and 0.57 mol dm^{-3} of hydrogen at 383 K and 100 bar total pressure, was investigated. Visual inspection of the reaction system using the view cell shown in Figure 2.7 (page 33) showed that the system was homogeneous under the conditions employed. The results are shown in Figure 4.5 and Table 12 of the appendix. It can be seen that the reaction reached maximum conversion after 1.75 hours and therefore subsequent hydrogenation reactions of **44** were carried out for 2 hours to ensure that the reaction had gone to completion. The time dependency results are generally the average of at least two determinations and a reproducibility of $\pm 3 \%$ was obtained.

Analysis of the initial data in Figure 4.5 yields a reaction rate of $167 \pm 5 \text{ mmol dm}^{-1} \text{ h}^{-1}$. Hope *et al.* studied the hydrogenation of **44** using Wilkinson's catalyst derivatives in a range of solvent systems.⁴⁴ The aim of their work was to evaluate the effect of perfluorocarbon solvents, organic solvents and perfluoroalkyl-ponytails on rhodium-catalysed hydrogenation in fluoruous biphasic systems. Some selected results are shown in Table 4.1.

The hydrogenation of **44** in the current work was carried out in a much more dilute solution than those used by Hope and co-workers (0.87 mol dm^{-3} of **44** *c.f.* $6.56 \times 10^{-3} \text{ mol dm}^{-3}$ used in this work), but it can be seen from Table 4.1 that the rate constant obtained in HFC 134a is comparable to some of those obtained in this previous study.

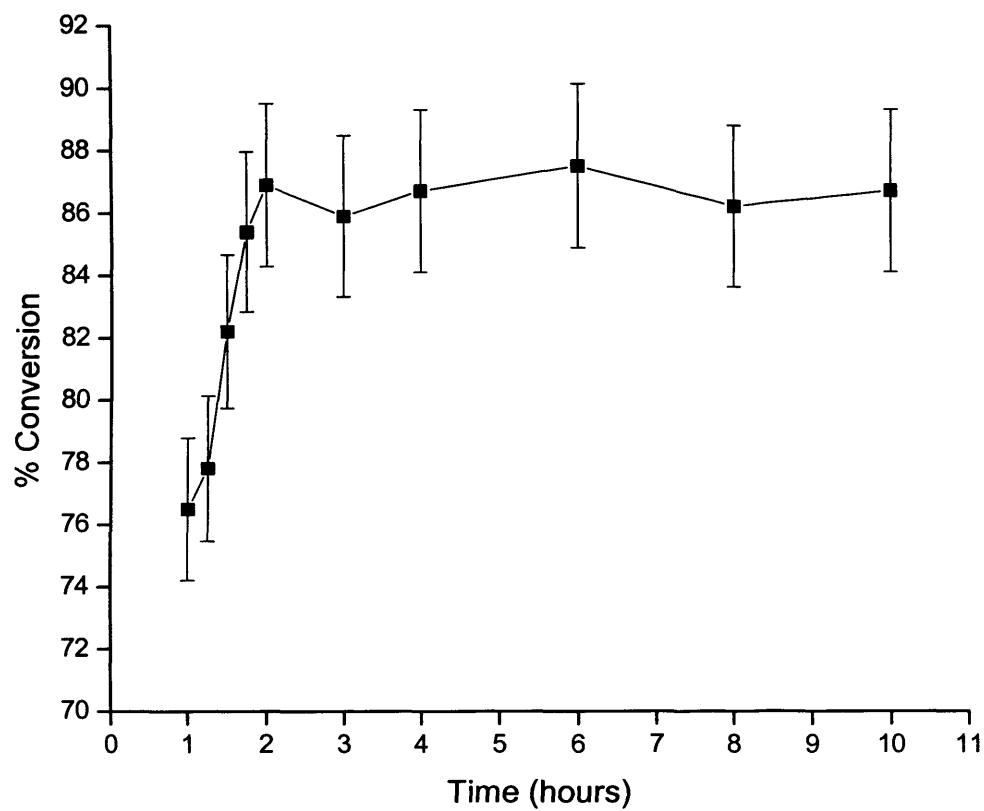


Figure 4.5 Time dependency of the hydrogenation of **44** in HFC 134 using $2.20 \times 10^{-6} \text{ mol dm}^{-3}$ of $[\text{RhCl}(\text{PPh}_3)_3]$ and 0.57 mol dm^{-3} of hydrogen at 383 K and 100 bar total pressure.

Temperature / K	Solvent system	Rate / mmol dm ⁻¹ h ⁻¹
298.3	Toluene	211
298.3	Toluene : PP3 ^a ; 0.8 : 1	276
348.3	Fluorobenzene : PP3 ^a ; 0.8 : 1	160
336.8	Toluene : Hexane : PP3 ^a ; 0.2 : 0.6 : 1	155

Table 4.1 Results obtained by Hope *et al.* for the hydrogenation of **44** in various solvent systems using [RhCl(PPh₃)₃].⁴⁴ ^aPerfluoro-1,3-dimethylcyclohexane.

Here, the comparable reaction rate in the dilute HFC 134a system is attributed to the higher diffusivity of hydrogen (compared to liquid solvent systems). It should be noted that the reactions in this work were carried out at temperatures much higher than those shown in Table 4.1 and this will also have a positive effect on the rate of reaction. It is however, expected that carrying out the reaction in a HFC 134a solution with concentrations comparable to those used by Hope *et al.* will increase the rate constant further and it is possible that results comparable to those in toluene may be obtained.

The pressure dependency of the hydrogenation of **44** at 383 K was also investigated and the results are shown in Figure 4.6 and Table 13 of the appendix. The results had a reproducibility of ± 3 % and the change in dielectric constant with pressure for the pure HFC 134a solvent at 383 K is also shown.⁴⁶ Reactions were carried out at constant mole fraction in order to observe the effect of pressure on the % conversion and rule out the possibility of dilution effects as pressure is increased. The mole fractions used are the same as those used in the time dependency study at 383 K and 100 bar (Figure 4.5).

It can be seen from Figure 4.6 that the % conversion increases with increasing pressure and this is attributed to the higher dielectric constant of HFC 134a at higher pressures. It was suggested by Wilkinson *et al.*^{47,48} that the rate determining step for the hydrogenation of olefins involves the formation of an activated complex, which has a greater dipole moment than the reacting species and that some charge separation is occurring during the formation of the activated intermediate.

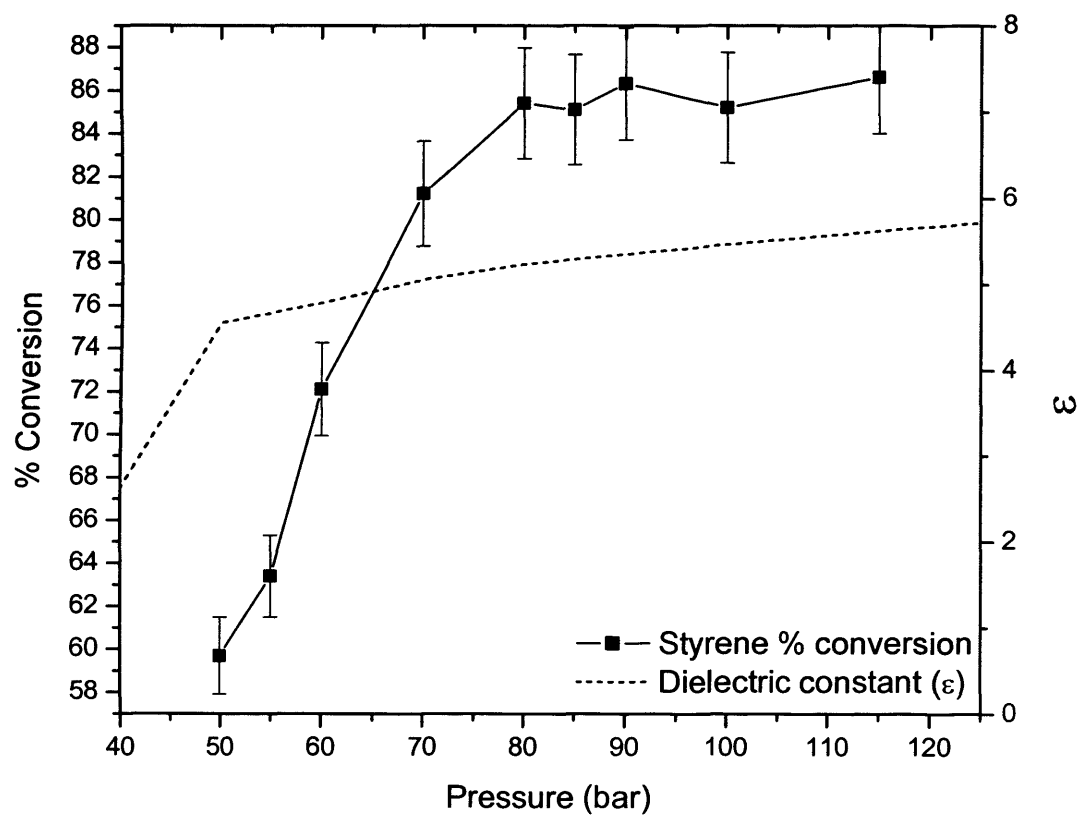


Figure 4.6 Pressure dependency of the hydrogenation of **44** using $[\text{RhCl}(\text{PPh}_3)_3]$ in HFC 134a at constant mole fraction and 383 K.

Such an effect may result from an increase in charge density on either one of the hydrogen atoms in **43** (Figure 4.4), perhaps due to the higher solvation of the chloride ion *trans* to hydrogen. Therefore, the formation of such an activated complex is more favourable in more polar solvents and is therefore more favourable in HFC 134a at higher pressures (higher dielectric constant). It should be noted that the dielectric constant of the reaction solution is higher than that of the pure HFC 134a fluid, however the discussion remains the same.

This initial study is the first to use HFC 134a as a reaction medium for the hydrogenation of olefins. It has been demonstrated that catalytic species and substrates have sufficient solubilities, affording homogeneous reaction conditions, and that reactions rates comparable to those in liquid solvents can be obtained.

4.2.2 Asymmetric Hydrogenation in Supercritical HFC 134a

In this work the industrially important area of asymmetric catalysis was investigated in sc HFC 134a. This is the first time asymmetric hydrogenation has been carried out in this media and it was decided that the process should be evaluated using a relatively simple catalytic system, which could be prepared *in situ*. Reactions were performed using $[\text{Rh}(\text{COD})_2\text{BF}_4]$ (bis(1,5-cyclo-octadiene)rhodium (I) tetrafluoro-borate) as the catalyst precursor and the monodentate (*R*)-MonoPhos (2,2-*O,O*-(1,1-Binaphthyl)-*O,O*-dioxo-*N,N*-dimethyl-phospholidine) ligand in a 1:2 ratio (**9** and **10** respectively in Scheme 2.1, page 35) (the optimum ratio for efficient catalysis). This was chosen because it was previously shown that BF_4 electrolytes are highly soluble and are extensively dissociated in HFC 134a.^{49,50} With less than 2 equivalents of MonoPhos, rhodium black is rapidly formed during catalytic hydrogenation, whereas no reaction occurs using 3 or more equivalents.^{11,51,52} It has been shown previously that the rhodium:ligand ratio has a large effect on reaction yield but has no effect on enantioselectivity.^{11,52} A mechanism to account for these observations has been proposed by de Vries *et al.* (Figure 4.7).^{51,52}

It was suggested by de Vries that the active catalytic species remained the same over the range of rhodium:ligand ratios studied. Assuming a mechanism in which the substrate is bound to the rhodium in a bidentate fashion (**45** in Figure 4.7), the oxidative addition of H_2 to the rhodium complex would be impossible if more than

two ligands are bound to the metal. Investigations using electrospray mass spectrometry (ES-MS) showed that species **46-49** were present during the course of hydrogenation reactions using rhodium/MonoPhos catalytic systems. From this information it can be deduced that the actual catalytic species contains one (**46**) or two ligands (**47**), although it is unclear at present which of these species is the active catalyst. Using lower ligand concentrations for hydrogenation reactions shifts the equilibrium shown in Figure 4.7 to the lower-ligated species, thus giving greater reaction conversions.

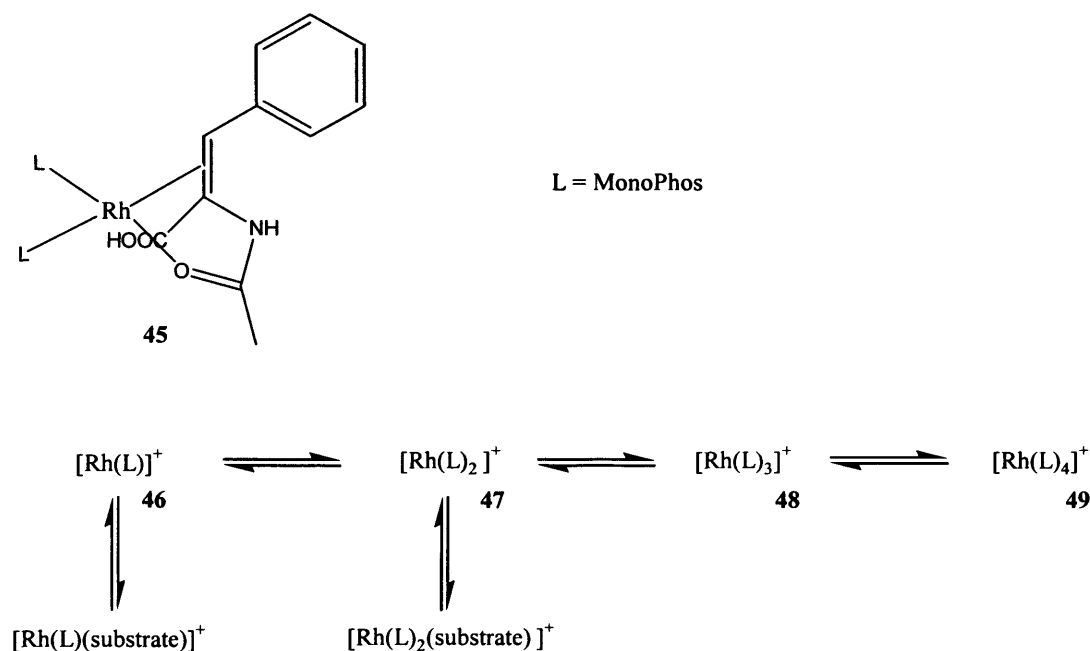
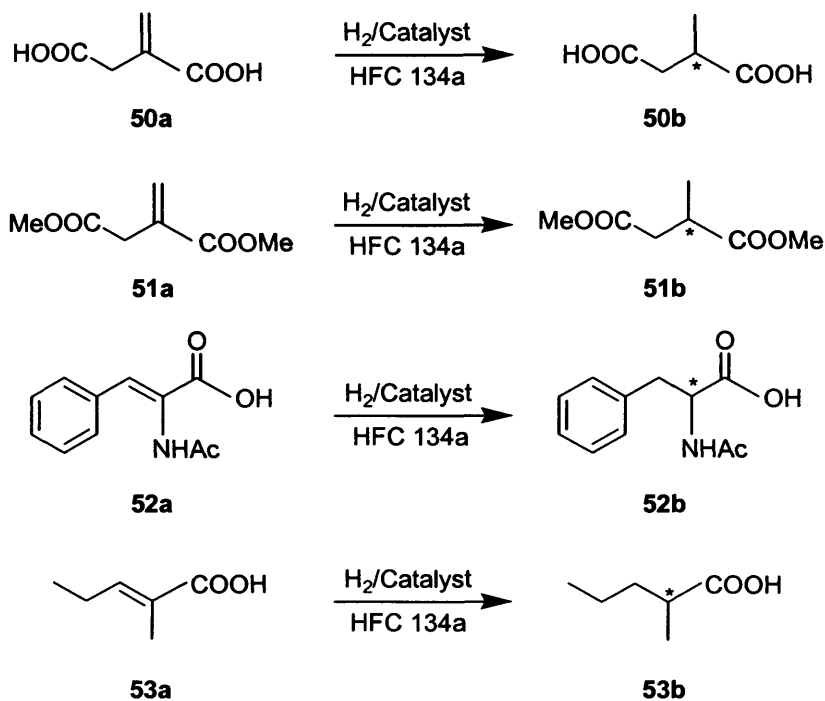


Figure 4.7 Species observed using ES-MS by Vries *et al.*⁵² during asymmetric hydrogenation reactions using a rhodium/MonoPhos catalytic system. The figure shows, as an example, how substrate **52a** (Scheme 4.13) binds to the rhodium centre of a di-ligated species.

MonoPhos is easily prepared from readily available starting materials and it has been shown that it can facilitate highly enantioselective rhodium-catalysed hydrogenations in conventional solvent systems.¹¹ It is a shelf stable compound, resistant to air and moisture and differs in this way to many other phosphine ligands, which are often prone to oxidation, and phosphites, which tend to hydrolyse in the presence of water. The features described above make rhodium/MonoPhos the ideal catalytic system for investigating asymmetric hydrogenation in novel

solvents. Reactions were carried out using itaconic acid, dimethyl itaconate, (*Z*)- α -acetamido-cinnamic acid and *trans*-2-methyl-2-pentenoic acid (**50a**, **51a**, **52a** and **53a** respectively in Scheme 4.13) as model substrates. Experimental details for all results obtained in this study are given in Section 2.3.2.



Scheme 4.13

Before reactions were carried out using HFC 134a, the rhodium/(*R*)-MonoPhos catalytic system was used to hydrogenate **50a-52a** in conventional organic solvents. This was done in order to evaluate the effectiveness of the catalytic species prepared in this work even though NMR, polarimetry and melting point data suggested that (*R*)-MonoPhos of high purity had been synthesised (Section 2.3.2). The results of the asymmetric hydrogenations using conventional solvents are shown in Table 4.2 along with some literature values for comparison.¹¹ Reactions were carried out at ambient hydrogen pressure and room temperature (294 ± 3 K) and the catalytic species was prepared *in situ*. The results in Table 4.2 from the current work compare well with those in the literature. This confirms the suitability of the (*R*)-MonoPhos ligand prepared in this work for the investigation of a novel solvent system.

Substrate	Solvent	% Conversion	% ee
50a^a	Ethyl acetate	100	95.7 (<i>R</i>)
50a^a	Ethanol	100	80.2 (<i>R</i>)
50a^a	THF	100	93.3 (<i>R</i>)
51a^a	Dichloromethane	100	94.2 (<i>R</i>)
52a^a	Ethyl acetate	100	96.5 (<i>S</i>)
52a^b	Ethyl acetate	100	97.1 (<i>S</i>)
52a^a	Diethyl ether	100	96.1 (<i>S</i>)
52a^a	Dichloromethane	100	90.2 (<i>S</i>)
52a^b	Dichloromethane	100	80.5 (<i>S</i>)

Table 4.2 Results for the asymmetric hydrogenation of substrates **50a-52a** in a range of organic solvents. Reactions were carried out at atmospheric hydrogen pressure and room temperature (294 ± 3 K) using $\text{Rh}(\text{COD})_2\text{BF}_4/(\text{R})\text{-MonoPhos}$.

^aResults from the current study. ^bLiterature results.¹¹

After confirming the suitability of the (*R*)-MonoPhos ligand, hydrogenations were carried out using HFC 134a as the solvating medium at 383 K and various pressures. Reactions were carried out at constant mole fraction so that dilution effects were ruled out and the influence of pressure could be observed.

The results are shown in Figures 4.8 and 4.9 and Tables 14-17 of the appendix. The results shown for the pressure dependency in Figure 4.8 had a reproducibility of ± 4 % whereas those for the enantiomeric excess in Figure 4.9 have a larger error of ± 8 %. It can be seen from Figure 4.8 that the % conversion during the asymmetric hydrogenation reactions shows a similar dependence on pressure as those seen for **44** using $[\text{RhCl}(\text{PPh}_3)_3]$ in Figure 4.6 and the same reasoning is offered to explain these trends. Poor NMR spectra were obtained for substrate **53a** and the error bars in Figure 4.8 show that the results had a very poor reproducibility and will therefore be ignored in the discussions that follow. For conversions less than 100 % it can be seen that the trend follows the order **50a** > **51a** > **52a** for a given pressure.

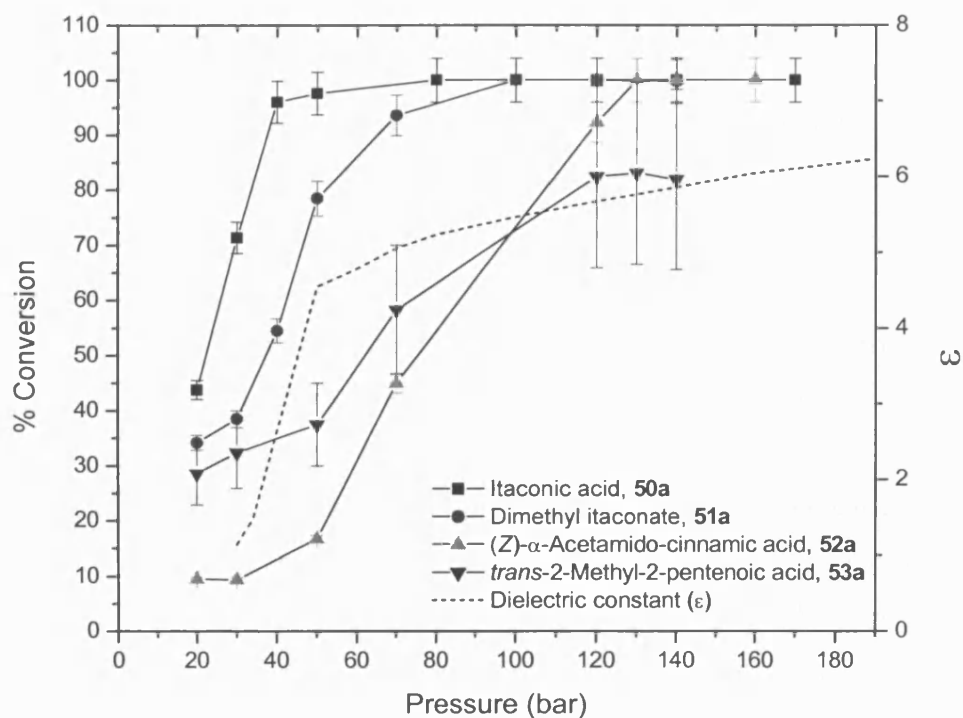


Figure 4.8 Pressure dependency of % conversion for the asymmetric hydrogenation of substrates **50a-53a** in HFC 134a at 383 K.

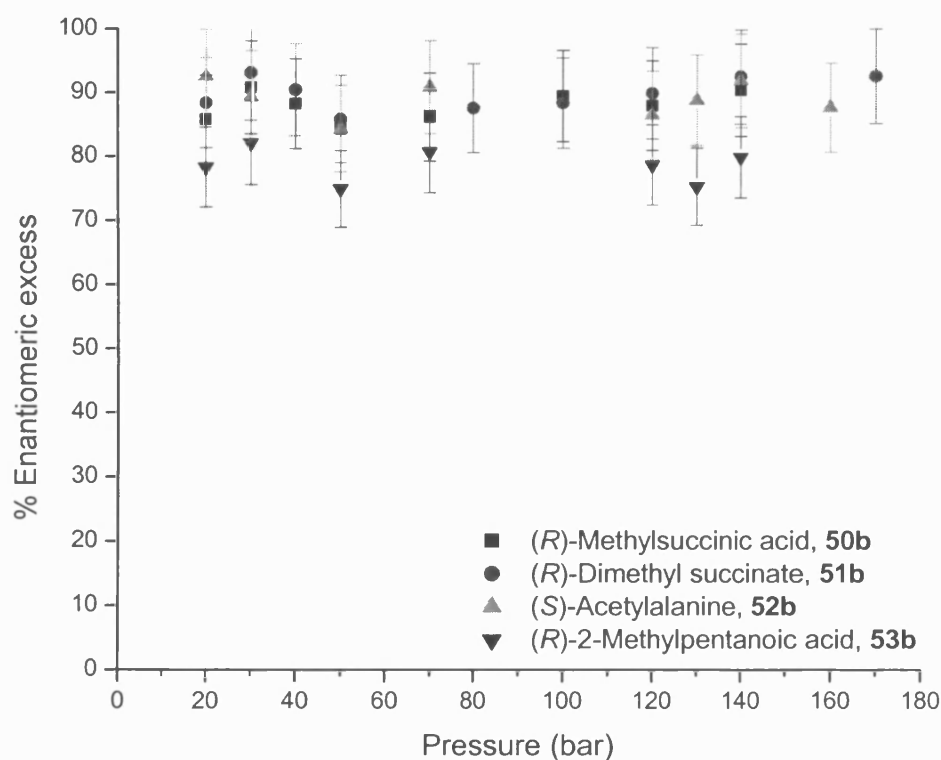


Figure 4.9 Pressure dependency of enantiomeric excess for products **50b-53b** in HFC 134a at 383 K.

One possible hypothesis for these observations is that there are two conflicting influences acting during the reaction; a negative steric effect and the positive effect of increasing dielectric constant. At lower pressures it is suggested that the reaction is under steric control and steric factors are hindering olefinic binding to the rhodium metal centre. The steric hindrance around the position of unsaturation for each substrate follows the trend **50a** < **51a** < **52a**. This trend is illustrated in Figure 4.10, which shows 3-dimensional, space-filling models of the substrates under investigation. It can be clearly seen that the site of unsaturation in substrate **52a** is much more hindered than those in substrates **50a** and **51a**.

At higher pressures the dielectric constant becomes the influencing factor and the % conversion increases to its maximum value of 100 %. It was mentioned earlier that the solution dielectric constant is higher than that of the pure HFC 134a solvent. Therefore, studies to obtain solution dielectric constant data will play an important role in gaining a greater understanding of the influence of reaction conditions on asymmetric hydrogenation in HFC solvents. Such an investigation was beyond the scope of this study and is the basis of future work.

de Vries and co-workers⁵¹ carried out solvent screening studies with the rhodium/MonoPhos catalyst using the methyl ester form of substrate **52a** and the results from this study are shown in Table 4.3.

Solvent	% ee
Methanol	70
Dichloromethane	95
Ethyl acetate	95
THF	93
Acetone	92
2-Propoxy ethanol	77

Table 4.3 Solvent screening results obtained by Vries *et al.* for the asymmetric hydrogenation of the methyl ester form of substrate **52a** using a rhodium/MonoPhos catalyst.⁵¹

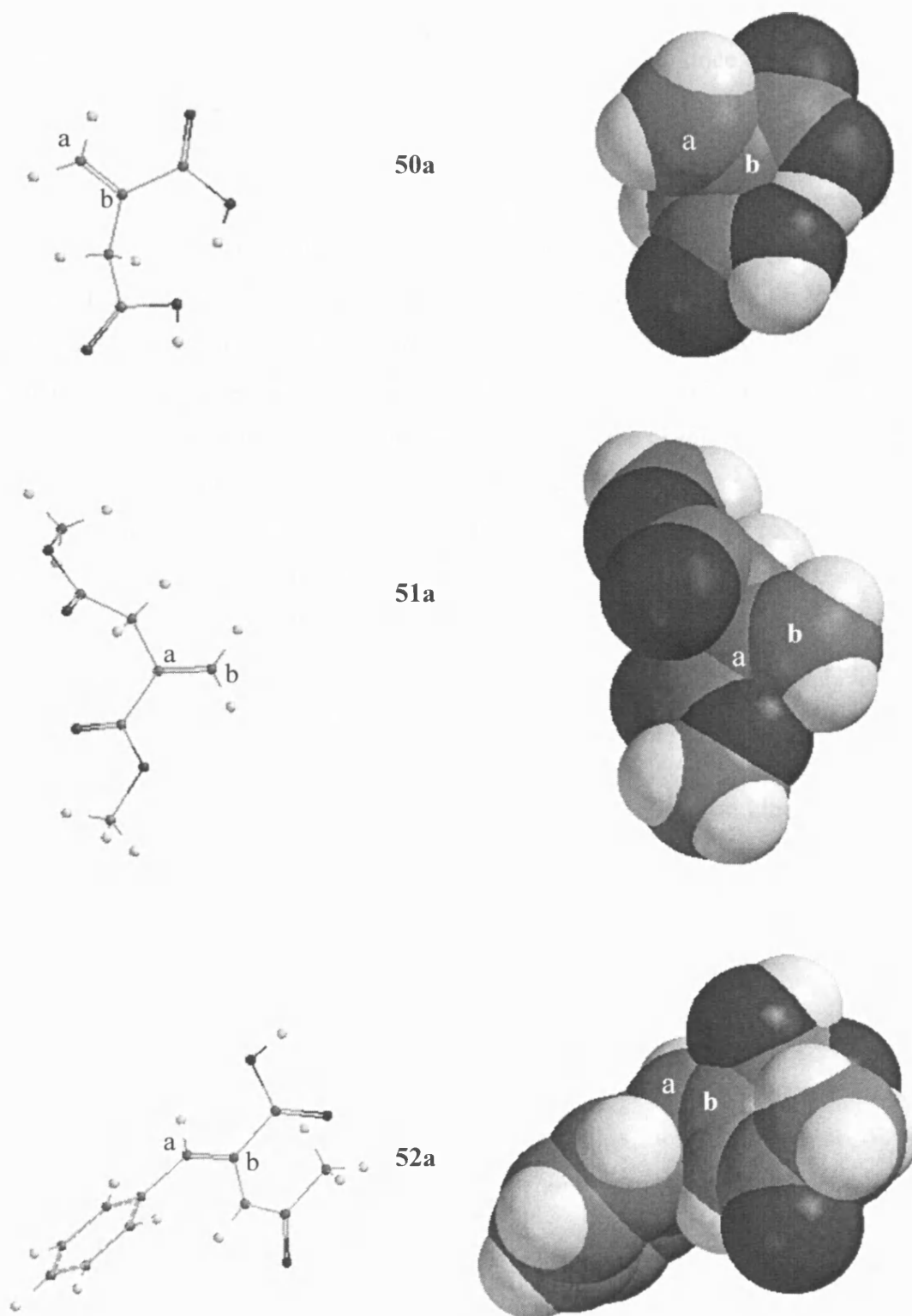


Figure 4.10 3-Dimensional, space-filling models illustrating the steric factors affecting olefinic binding to the catalytic rhodium metal centre. The steric hindrance around the position of unsaturation follows the trend **50a** < **51a** < **52a**.

It was concluded that non-protic solvents lead to higher enantioselectivities than protic ones. The effect of solvent polarity was ruled out since protic 2-propoxy ethanol ($\text{PrOCH}_2\text{CH}_2\text{OH}$) has a dipole moment (2.08)⁵³ intermediate to those of the non-protic solvents ethyl acetate (1.82)⁵³ and acetone (2.69)⁵³.

Within experimental error the % ee results at constant mole fraction shown in Figure 4.9 show no dependency on pressure and therefore, no dependency on the dielectric constant of HFC 134a. These results compliment those of de Vries in that the enantioselectivity induced by rhodium/MonoPhos is not affected by solvent polarity. The enantioselectivities obtained in HFC 134a for substrates **50a-52a** are comparable to some of those obtained in liquid solvents (Tables 4.2 and 4.3). This suggests that HFCs are promising alternative solvents for asymmetric hydrogenation of olefinic substrates. Furthermore, facile catalyst recovery should easily be achieved by precipitation, facilitated by system depressurisation.

It is well known that the concentration of hydrogen can have an effect on the enantioselectivity during asymmetric hydrogenation.⁴ Previous studies employing rhodium/MonoPhos^{11,51,52} and rhodium/MonoPhos-based¹³ catalysts have illustrated that the hydrogen pressure has no effect on enantioselectivity but using higher initial hydrogen pressures can afford greater rates of reaction. Reaction kinetics were not investigated in the current study and are to be studied in future work along with the effects of initial substrate and catalyst concentrations.

In order to give a more complete comparison of reactions carried out in HFC 134a to those carried out in conventional solvents, the effect of hydrogen concentration on enantioselectivity was investigated. The investigation was carried out using substrate **50a** since 100 % conversion was obtained at a moderate pressure and relatively high % ee values were achieved with this substrate. The reaction was carried out at 383 K and 100 bar total pressure and the results are shown in Figure 4.11 and Table 18 of the appendix. The reaction went to 100 % completion in each case and the results had a reproducibility of ± 7 %. It can be seen that within experimental error the initial hydrogen pressure has no effect on the enantiomeric excess and this compliments the results obtained using conventional organic solvents.

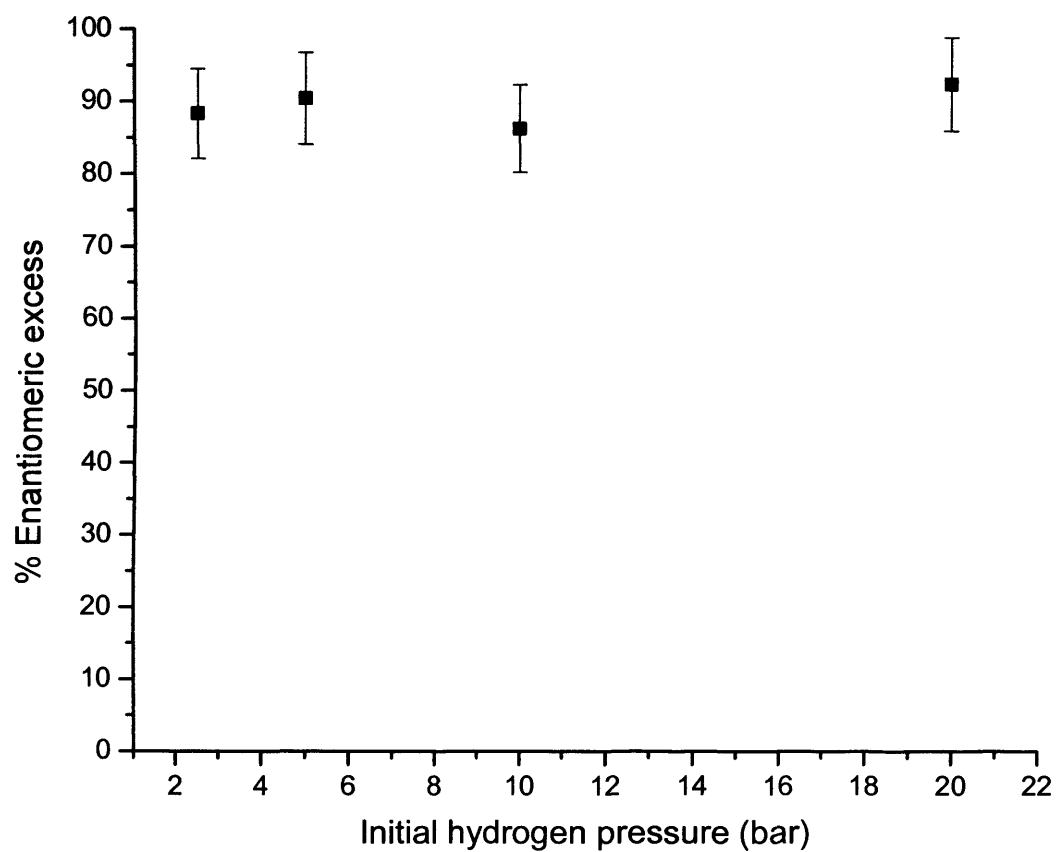


Figure 4.11 The dependence of enantioselectivity for **50b** on initial hydrogen pressure in HFC 134a at 383 K and 100 bar.

Although no direct mechanistic studies have been carried out in the current work, initial results suggest that the mechanism of rhodium/MonoPhos catalysis is the same in sc fluids as in liquid solvents, since similar solvent and hydrogen pressure effects are observed for these two media.

A study by Poliakoff *et al.* showed that the critical parameters of CO₂ were reduced during the hydrogenation of propane as the ratios of reagents to products changed.⁵⁴ Such an in depth study was not carried out here but this data is important in understanding the phase behaviour of sc fluid processes. This information is crucial to the design, application and efficiency of sc fluid applications and is therefore the basis of future work.

In this study a qualitative set of experiments were used to investigate the phase behaviour of the HFC 134a hydrogenation system. Only the system employing α -acetamido-cinnamic acid as the substrate was investigated, the reason being that this is the substrate with the highest measured solubility (Figure 3.3, page 50) and would therefore have the greatest effect on the critical parameters of HFC 134a. This statement is not strictly speaking true since dimethyl itaconate and *trans*-2-methyl-2-pentenoic acid are liquids at room temperature and thus, are expected to have higher solubilities.

The windowed vessel (Figure 2.7, page 33) was loaded with the same concentration amount of substrate and catalytic material used for the asymmetric hydrogenation reactions and the system was pressurised with HFC 134a. This process was repeated twice more using the same concentration amount of catalytic material but with a 50/50 substrate/product mixture and with product alone (emulating the reaction going to completion). It was found from these investigations that at 383 K the lowest pressure at which multi-phase behaviour was observed was around 35-38 bar, which is a small deviation from the critical pressure of HFC 134a (40.59 bar). Above 38 bar the system was in a single homogeneous phase.

Although no reactions using pure sc CO₂ were carried out for comparison, it is suggested by the current author that lower rates of reaction, lower % conversions and lower enantioselectivities will be obtained in this medium. This suggestion is based on the fact that rhodium metal catalysts (illustrated in Section 4.2.1 for [RhCl(PPh₃)₃]) and polar substrates (Figure 3.4, page 51) have very low solubilities in sc CO₂.

In order to achieve similar results in sc CO₂, to those obtained in sc HFC 134a, co-solvents or catalyst modification will be required and this will have negative practical and economic implications for such processes.

The rhodium MonoPhos catalyst has been shown to be an efficient catalytic system for the asymmetric hydrogenation of various polar substrates in HFC 134a. Although the % conversion and % ee values obtained were no higher than those obtained in liquid solvents, sc fluid reaction systems have the potential to afford simple catalyst reagent product separation as described in Chapter 3.

4.3 Conclusion

The applicability of HFC 134a for use as a reaction solvent for hydrogenation has been investigated. It was observed that rhodium based catalysts have sufficient solubility in this medium to afford homogeneous reaction conditions. Very little solvation of unmodified rhodium catalysts by carbon dioxide was obtained. Based on this observation and the solubility results in Chapter 3, it is suggested that pure carbon dioxide would be a poor choice of solvent for processes involving these catalytic systems.

Initial studies were carried out using the well-known hydrogenation of styrene with Wilkinson's catalyst. Reaction rates comparable to, and in some cases higher than, those in liquid solvents were obtained. The high reaction rates are attributed to the higher diffusivity of gaseous hydrogen in the supercritical media when compared to that in liquid solvents. It was shown that the percentage conversion was dependent on the solvent dielectric constant, which can be tuned by manipulating the HFC 134a system pressure.

The success achieved using Wilkinson's catalyst led to the investigation of asymmetric hydrogenation in HFC 134a. High conversions and enantioselectivities were obtained for a range of carboxylic acids and this initial study suggests that HFCs are promising alternatives as reaction media for the industrially important asymmetric hydrogenation process.

Furthermore, facile catalyst recovery can be achieved by precipitation afforded by system depressurisation. The combined advantages of catalyst recovery offered by heterogeneous catalysts and high selectivities offered by homogeneous catalytic systems add further support to the use of these fluids for reaction processes.

The enantioselectivity showed no dependence on solution dielectric constant or initial hydrogen pressure and this complements results obtained in liquid solvents. This suggests that the mechanism for asymmetric hydrogenation, facilitated by the rhodium/MonoPhos catalytic species, is the same in the supercritical regime as it is in liquid solvents.

Future work will build upon these promising initial results and will focus on the kinetics of reaction. Studies will be extended to ruthenium/BINAP and silica supported heterogeneous catalytic systems.

4.4 References

1. Sabatier, P.; Senderens, J. B. *Compt. Rend.* **1899**, 128, 1173.
2. Rylander, P. N. *Hydrogenation Methods*; Academic Press, New York, **1990**.
3. Nugent, W. A.; RajanBabu, T. V.; Burk, M. J. *Science* **1993**, 259, 479.
4. Noyori, R. *Asymmetric Catalysis in Organic Synthesis*; John Wiley and Sons; New York, **1994**.
5. Jacobsen, E. N.; Pfaltz, A.; Yamamoto, H. *Comprehensive Asymmetric Catalysis*, Vol. I-III; Springer, Berlin, **1999**.
6. Claver, C.; Fernandez, E.; Gillon, A.; Heslop, K.; Hyett, D. J.; Martorell, A.; Orpen, A. G.; Pringle, P. G. *Chem. Commun.* **2000**, 961.
7. Knowles, W. S.; Sabacky, M. J. *J. Chem. Soc. Chem. Commun.* **1968**, 1445.
8. Horner, L.; Siegel, H.; Büthe, H. *Angew. Chem. Int. Ed. Engl.* **1968**, 7, 942.
9. Reetz, M. T.; Sell, T. *Tetrahedron Lett.* **2000**, 41, 6333.
10. Reetz, M. T.; Mehler, G. *Angew. Chem. Int. Ed.* **2000**, 39, 3889.
11. van den Berg, M.; Minnaard, A. J.; Schudde, E. P.; van Esch, J.; de Vries, A. H. M.; de Vries, J. G.; Feringa, B. L. *J. Am. Chem. Soc.* **2000**, 122, 11539.
12. Xiao, J.; Chen, W. *Tetrahedron Lett.* **2001**, 42, 2879.
13. Zeng, Q.; Liu, H.; Mi, A.; Jiang, Y.; Li, X.; Choi, M. C. K.; Chan, A. S. C. *Tetrahedron* **2002**, 58, 8799.
14. Jia, X.; Guo, R.; Li, X.; Yao, X.; Chan, A. S. C. *Tetrahedron Lett.* **2002**, 43, 5541.
15. Baiker, A. *Chem. Rev.* **1999**, 99, 453.
16. King, J. W.; Holliday, R. L.; List, G. R.; Snyder, J. M. *J. A. Oil Chem. Soc.* **2001**, 78, 107.
17. Tacke, T.; Wieland, S.; Panster, P. *Process Technol. Proc.* **1996**, 12, 17.
18. van den Hark, S.; Haerrod, M. *Ind. Eng. Chem. Res.* **2001**, 40, 5052.
19. Macher, M-B.; Hogberg, J.; Moller, P.; Harrod, M. *Fett/Lipid* **1999**, 101, 301.
20. Jessop, P. G.; Ikariya, T.; Noyori, R. *Chem. Rev.* **1999**, 99, 475.
21. Jessop, P. G. *Topics in Catal.* **1998**, 5, 95.
22. Halpern, J. *J. Pure Appl. Chem.* **1979**, 51, 2171.
23. Crabtree, R. H. *The Organometallic Chemistry of the Transition Metals*, 2nd ed.; John Wiley: New York, **1994**.

-
24. Sun, Y.; LeBlond, C.; Wang, J.; Blackmond, D. G. *J. Am. Chem. Soc.* **1995**, 117, 12647.
 25. Jessop, P. G.; Ikariya, T.; Noyori, R. *Nature* **1994**, 368, 231.
 26. Jessop, P. G.; Hsiao, Y.; Ikariya, T.; Noyori, R. *J. Am. Chem. Soc.* **1996**, 118, 344.
 27. Coenen, H.; Hagen, R.; Kriegel, E. *U.S Patent* 4,485,003, **1984**.
 28. Jessop, P. G.; Ikariya, T.; Noyori, R. *Organometallics* **1995**, 14, 1510.
 29. Naesnik, T. E.; Freudenberger, J. H.; Orchin, M. *J. Organomet. Chem.* **1982**, 236, 95.
 30. Matsui, Y.; Orchin, M. *J. Organomet. Chem.* **1983**, 244, 369.
 31. Jessop, P. G.; Hsiao, Y.; Ikariya, T.; Noyori, R. *J. Am. Chem. Soc.* **1994**, 116, 8851.
 32. Lange, S.; Brinkmann, A.; Trautner, P.; Woelk, K.; Bargon, J.; Leitner, W. *Chirality* **2000**, 12, 450.
 33. Burk, M. J.; Feng, S.; Gross, M. F.; Tumas, W. *J. Am. Chem. Soc.* **1995**, 117, 8277.
 34. Oakes, R. S.; Clifford, A. A.; Rayner, C. M. *J. Chem. Soc., Perkin Trans. 1* **2001**, 917.
 35. Xiao, J.; Nefkens, S. C. A.; Jessop P. G.; Ikariya, T.; Noyori, R. *Tetrahedron Lett.* **1996**, 37, 2813.
 36. Kainz, S.; Brinkmann, A.; Leitner, W.; Pfaltz, A. *J. Am. Chem. Soc.* **1999**, 121, 6421.
 37. Minder, B.; Mallat, T.; Pickel, K. H.; Steiner, K.; Baiker, A. *Catal. Lett.* **1995**, 34, 1.
 38. You, X.; Li, X.; Xiang, S.; Zhang, S.; Xin, Q.; Li, X.; Li, C. *International Congress on Catalysis* **2000**, Pt, D.
 39. Hitzler, M. G.; Poliakov, M. *Chem. Commun.* **1997**, 1667.
 40. Koch, D.; Leitner, W. *J. Am. Chem. Soc.* **1998**, 120, 13398.
 41. Goetheer, E. L. V.; Verkerk, A. W.; van den Broeke, L. J. P.; de Wolf, E.; Deelman, B.-J.; van Koten, G.; Keurentjes, J. T. F. *J. Catal.* **2003**, 219, 126.
 42. Montelatici, S.; van der Ent, A.; Osborn, J. A.; Wilkinson, G. *J. Chem. Soc. A* **1968**, 1054.

-
43. Wilkinson, G.; Gillard, R. D.; McCleverty, J. A. *Comprehensive Coordination Chemistry*, Pergamon Press, Oxford, **1987**.
 44. Hope, E. G.; Kemmit, R. D. W.; Paige, D. R.; Stuart, A. M. *J. Fluorine Chem.* **1999**, 99, 197.
 45. Halpern, J. *Pure. Appl. Chem.* **2001**, 73, 209.
 46. Abbott, A. P.; Eardley, C. A.; Tooth, R. *J. Chem. Eng. Data* **1999**, 44, 112.
 47. Osborn, J. A.; Jardine, F. H.; Young, J. F.; Wilkinson, G. *J. Chem. Soc. A* **1966**, 1711.
 48. Jardine, F. H.; Osborn, J. A.; Wilkinson, G. *J. Chem. Soc. A* **1969**, 1574.
 49. Abbott, A. P.; Eardley, C. A. *J. Phys. Chem. B* **2000**, 104, 9351
 50. Abbott, A. P.; Eardley, C. A.; Harper, J. C.; Hope, E. G. *J. Electroanal. Chem.* **1998**, 457, 1
 51. van den Berg, M.; Minnard, A. J.; Haak, R. M.; Leeman, M.; Schudde, E. P.; Meetsma, A.; Feringa, B. L.; de Vries, A. H. M.; Maljaars, C. E. P.; Willans, C. E.; Hyett, D.; Boogers, J. A. F.; Henderickx, H. J. W.; de Vries, J. G. *Adv. Synth. Catal.* **2003**, 345.
 52. de Vries, J. G.; de Vries, A. H. M. *Eur. J. Org. Chem.* **2003**, 799.
 53. Riddick, J. A.; Bunger, W. B.; Sakano, T. K. *Organic Solvents: Physical Properties and Methods of Purification, Vol. II*, John Wiley & Sons, New York, **1986**.
 54. Ke, J.; George, W.; Poliakoff, M.; Han, B.; Yan, H. *J. Phys. Chem. B* **2002**, 106, 4496.

CHAPTER 5

POLYMER MODIFICATION USING SUPERCRITICAL FLUIDS

5.1 Introduction

5.1.1 Solid-State Properties of Polymers

5.1.2 Polymer Processing with Supercritical Fluids

5.1.3 Gas Sorption of Polymers

5.1.4 The Measurement of Gas Sorption using a Quartz Crystal Microbalance

5.1.5 Modelling Gas Sorption

5.2 Results and Discussion

5.2.1 Measurement of Gas Sorption by Polymers

5.2.2 Modelling the Gas Sorption Data

5.2.3 Kinetics of Gas Sorption

5.3 Conclusion

5.4 References

5.1 Introduction

It was noted during the hydrogenation and solubility experiments that the sc HFCs caused considerable swelling and deformation of several polymeric components within the high-pressure apparatus due to the high diffusivity of these fluids within these materials. Recent work within our group has also shown that the swelling of polymeric materials can be problematic when using HFCs as reaction media for polymerisations, since swelling and fragmentation of the polymeric products can occur.¹ These observations prompted the investigation into the swelling of polymers with HFCs and it was concluded that these gases could be used for polymer modification processes.

A quartz crystal microbalance (QCM) was used during the investigation. The application of a QCM to polymer thermodynamics was first reported by Bonner and Cheng² to measure the sorption of nitrogen in low-density polyethylene.

Here, a QCM is used to measure the sorption of CO₂ and HFC 32 in polystyrene (PS) and polyethylene (PE). The physical effects of the gases on each polymer are discussed and it is demonstrated for the first time how data relating to the kinetics of gas sorption in polymers can be extracted from QCM measurements.

5.1.1 Solid-State Properties of Polymers

The chemical structure of a polymer determines whether that polymer will be amorphous or crystalline in the solid-state. Completely amorphous polymers exist as long, randomly arranged chains that are capable of forming stable, flow-restricting entanglements at sufficiently high molecular weight. The critical molecular weight (M_c) for the formation of stable entanglements depends upon the flexibility of the polymer chains. Relatively flexible polymer chains, such as those in PS, have a high M_c whereas rigid chain polymers, such as polycarbonate, have a low M_c . In the glassy-state the long chains are motionless and the only movement occurring is the short-range motions of several short-chain segments or substituent groups. These can include limited motions of the main chain or rotations, vibrations and flips of substituents groups. These small-scale molecular motions are known as secondary relaxation processes and have been reported to have significant influences on glassy-state properties.³

Above a certain temperature, known as the glass-transition temperature, T_g , the polymer is in the melt and thermal energy is sufficiently high for long segments of each polymer chain to move in random micro-Brownian motions. The T_g of amorphous polymers varies widely depending on the chemical structure of the polymer chain. Generally, polymers with flexible backbones and small substituents groups have a low T_g , while those with rigid backbones have a high T_g . Some examples of T_g values for several important amorphous polymers are shown in Table 5.1.³

Crystalline polymers contain arrays of folded polymer chains that are organised into lamella giving a regular crystalline structure. No bulk polymer is completely crystalline although some, such as polyolefins, are highly crystalline materials with well-defined crystal morphology. In semi-crystalline polymers the regular crystalline units are linked by randomly orientated, irregular chains, which constitute amorphous regions. Polymers with a very low crystallinity are characterised by crystalline microstructures within an amorphous matrix. Due to the presence of unordered amorphous material within crystalline polymers, they can exhibit a T_g corresponding to long-range segmental motions in the amorphous regions. Crystalline polymers also exhibit a crystalline-melting temperature, T_m , which is the temperature at which crystallites are destroyed and an amorphous, unordered melt is formed. Some important semi-crystalline polymers with representative T_g and T_m values are shown in Table 5.2.³

Polymer morphologies have a significant influence on the mechanical, physical and thermal properties of polymeric materials and these properties in turn play an important role in the applicability of polymers for a given application. For a more in depth discussion regarding bulk polymer structure, polymer chain microstructure and the relationship between morphology, bulk polymer properties and inter-chain effects, the reader is directed elsewhere.³

Polymer	T_g / K	Applications
Polydimethylsiloxane	150	GC/HPLC columns, resin additive, plasticizer
Poly(vinyl acetate)	301	Carpet backing, water-based latex paints, adhesives, lacquers, cements
Polystyrene	373	Styrofoam® cups, food packaging, refrigerator insulation
Poly(methyl methacrylate)	378	Fibre optics, glass replacement, lubricating oil additive
Polycarbonate	423	Sheet glazing, riot shields, mobile telephones, safety goggles, safety helmets
Polysulfone	463	Plumbing materials, automotive parts, wire coatings

Table 5.1 Values of T_g for some important amorphous polymers.³

Polymer	T_g / K	T_m / K	Applications
Polyethylene (high-density)	153	408	Liquid containers, toys, detergent bottles
Polycaprolactone	213	334	Resin additive, plasticizer
Poly(vinylidene fluoride)	228	445	Transfer membranes, engineering components
Polyoxymethylene	188	468	Gears, casings, machine parts
Poly(vinyl alcohol)	358	531	Component in adhesives, emulsifiers, lacquers
Nylon-6,6	322	538	Bearings, gears, power tool castings

Table 5.2 Values of T_g and T_m for some important semi-crystalline polymers.³

5.1.2 Polymer Processing with Supercritical Fluids

Supercritical fluids are promising alternatives for materials processing due to the tuneable solvent power, high diffusivity, low viscosity and environmental advantages associated with these media. In particular sc fluids have received a great deal of attention for the processing of polymeric materials and it is the ability of these media to swell and plasticize polymers that is crucial to the impregnation, extraction and modification of the material.

Ipatiev⁴ reported some of the earliest work relating to polymer processing at the beginning of the 20th century. He discovered that when ethylene is heated above its T_c in a high-pressure autoclave, it oligomerizes noncatalytically into higher molecular mass alkanes. This process was developed further by ICI⁵ for the manufacture of PE using oxygen as the initiator. DuPont later took advantage of the tuneable density of sc ethylene and PE fractionation was carried out via selective precipitation.^{6,7} Since this early work, there has been a wealth of information pertaining to polymer synthesis published in the literature and for a more thorough treatise the reader is directed to a number of recent reviews.⁸⁻¹⁰

It has been recognised that the unique physical properties of sc fluids can be advantageous for the modification of polymeric materials. The sorption of sc fluids into polymers results in polymer swelling and this changes the mechanical and physical properties of the material. The most important of these effects is the reduction of T_g of glassy polymers and this is known as plasticization.¹¹

Many polymer-processing operations have taken advantage of plasticization and these include enhancement of monomer diffusion for synthesis, enhancement of additive diffusion through the polymer matrix for impregnation, viscosity reduction for polymer blending and extrusion, changes in morphology due to crystallization, and polymer foaming. Supercritical CO₂ has received the most attention for these applications because it is relatively inexpensive, non-toxic, non-flammable and is readily available in high purity.

The enhanced diffusion of monomers within a swollen polymer material allows polymerisation to occur within the polymer matrix. Watkins and McCarthy used sc CO₂ to make a variety of polymer blends by the infusion of styrene monomer and an initiator into several polymers including polychlorotrifluoroethylene (PCTFE), polymethylpentane (PMP) and PE.¹²

Several observations of enhanced diffusivity in sc CO₂ swollen polymers have been reported in the literature^{13,14} and sc fluids have found widespread applications for polymer impregnation. This is not only because of the enhanced diffusivity through the polymer matrix, but also because no solvent residues remain within the impregnated sample upon depressurisation. Pioneering work by Sand¹⁵ and Berens¹³ demonstrated that compressed CO₂ could accelerate the absorption of additives into a number of glassy polymers in which impregnation by conventional methods is difficult and slow. Since then a great deal of research for the impregnation of organometallic compounds,¹⁶ metal complexes¹⁷ and dyestuffs¹⁸ has been carried out as reviewed in detail by Kazarian.¹⁹

Impregnation of monomer and initiator from sc solution, followed by subsequent polymerisation within the polymer matrix, can be used to make polymer blends. Muth *et al.* prepared a poly(vinyl chloride) (PVC)/poly(methacrylic acid) blend using sc CO₂ impregnation.²⁰ It was suggested by the authors that this blend could not easily be obtained using conventional methods.

Conventional polymer extrusion has a large energy requirement and employs mechanical action, heat and plasticizers for polymer manipulation. The heat and plasticizers are used to reduce the polymer viscosity but these can have a negative effect on the process. Increased temperature can further increase the energy consumption and can also lead to polymer degradation and plasticizers can often remain in the end product affecting properties and performance. The use of sc fluids to reduce polymer viscosity is a promising alternative to increased temperatures and plasticizing additives.

Plasticization caused by sc CO₂ may induce crystallization in certain polymers. This occurs when induced mobility of the polymer chains allows them to rearrange into kinetically favoured configurations, therefore forming crystallites.¹⁹ It has been shown by various research groups that sc CO₂ can change the degree of crystallinity in poly(ethylene terephthalate) (PET).²¹⁻²⁵ The crystallinity and morphology of PET based materials is of particular interest because these materials are widely used in the production of drink bottles and synthetic polyester fibres. The degree of crystallinity affects the gas permeability of the material and this is of particular importance if the bottle is to contain carbonated drinks. The crystallinity of polyester fibres, used in the textile industry, affects the ability to dye the material

and the morphology can play an important role in determining the mechanical properties of the fibres.

Polymer foaming is achieved using substances called blowing agents and the resultant materials find widespread use as heat insulators, vehicle parts and cushioning materials in furniture. Chlorofluorocarbons were used extensively as blowing agents because they combine attractive properties such as volatility, chemical stability, non-flammability, low toxicity and high solubility within the polymer material. Unfortunately CFCs were implicated as the primary agent responsible for ozone depletion²⁶ and suitable alternatives had to be found. Hydrofluorocarbons represent a promising class of blowing agents because they retain many of the properties of CFCs but do not contribute to ozone depletion.²⁷

One of the most important factors influencing the final properties of the foam is the solubility of the blowing agent in the polymer. Computer simulations have shown that the solubility can affect the bubble size, size distribution and hence the density of the foam.²⁸

Gas induced plasticization of polymers has been studied by a variety of methods including *in situ* fourier transform infrared (FTIR) spectroscopy,^{29,30} fluorescence,³¹ NMR spectroscopy,^{32,33} molecular dynamics simulations,³⁴ X-ray diffraction,¹⁶ dielectric relaxation,³⁵ chromatography^{36,37} and QCM techniques.^{38,39} The first reported use of the QCM method for the study of gas sorption by polymers was in 1975 by Bonner and Cheng, who measured the solubility of nitrogen in PE.²

5.1.3 Gas Sorption of Polymers

Gas sorption refers to the permeation of gas molecules into a polymer matrix and it is important to note that gas molecules can be sorbed by different modes of sorption due to changes in concentration, temperature and polymer swelling. The most widely used model in the literature to describe gas sorption in polymers is the dual-mode sorption (DMS) model. The DMS model is based upon a combination of two distinct sorption mechanisms (Figure 5.1c): (a) gas dissolution in the bulk polymer described by Henry's law and (b) sorption of gas in molecular-scale microvoids due to the non-equilibrium nature of the glassy state, which is characterised by a Langmuir-type sorption.

Henry's law applies to rubbery polymers ($T > T_g$) when gas activities are low (specific interactions between the polymer and the gas molecules are low compared to the polymer-polymer interactions) and at low to moderate pressures (< 10 bar). Solubility shows a linear (Figure 5.1a) dependence on pressure and is given by Henry's law to be

$$C = Sp \quad (5.1)$$

where C is the concentration of the sorbed gas, S is the solubility coefficient and p is the pressure. Assuming that the solubility coefficient is constant at a given temperature and that the fugacity and pressure are equivalent then Equation 5.1 can be rewritten as

$$C = k_D p \quad (5.2)$$

where k_D is the Henry's law dissolution constant.

In the glassy state ($T < T_g$) a Langmuir-type sorption occurs and the solubility curve is concaved with respect to the pressure axis (Figure 5.1b). The gas solubility is given by

$$C = \frac{C_H' bp}{1 + bp} \quad (5.3)$$

where C_H' is the hole saturation constant and b is the hole affinity parameter. A combination of Equations 5.2 and 5.3 leads to the DMS model expression for the solubility of gases in glassy polymers.

$$C = k_D p + \frac{C_H' bp}{1 + bp} \quad (5.4)$$

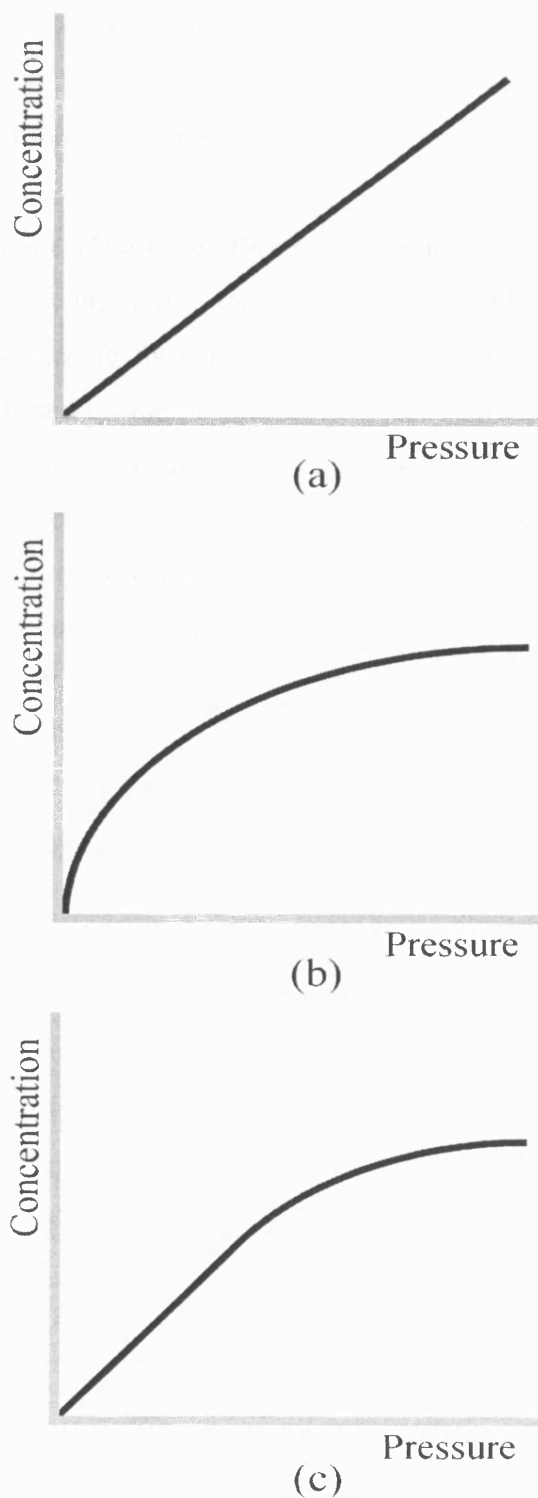


Figure 5.1 Concentration of sorbed gases versus pressure for (a) Henry's law (b) a Langmuir-type isotherm and (c) the DMS model.

For systems with greater penetrant activities, as is the case for highly condensable gases such as CO₂ at moderate to high pressures, Henry's law no longer applies. In this case the Flory-Huggins (F-H) lattice model and equation-of-state-based lattice models (Section 5.1.5) can be used to predict the increase in solubility of gases in rubbery polymers with increasing pressure.

5.1.4 The Measurement of Gas Sorption using a Quartz Crystal Microbalance

The QCM as a mass measuring technique was first introduced by Saurebrey⁴⁰ and owes widespread use to its extreme sensitivity, which lies in the nanogram range. The QCM is based on the piezoelectric effect observed in an AT-cut quartz crystal. Under the influence of an applied alternating electric voltage the crystal undergoes a shear deformation, and the frequency at which the deformation becomes a maximum is known as the resonance frequency. The resonance frequency depends on mass and therefore any change in mass will result in a frequency shift. Saurebrey developed an equation (Equation 5.5) relating the resonance frequency shift, Δf , to the change in mass at the electrode surface, Δm , in a vacuum.

$$\Delta f = \frac{-2\Delta m f_0^2}{A\sqrt{\mu_q \rho_q}} \quad (5.5)$$

where f_0 is the fundamental crystal frequency, A is the crystal area, μ_q is the shear modulus of the quartz and ρ_q is the quartz density. Assuming that the physical and geometrical properties of the crystal do not change, then Equation 5.5 can be written as

$$\Delta f = -k\Delta m \quad (5.6)$$

where k is a constant accounting for the characteristic crystal properties.

Let it be assumed that the bare quartz crystal has a resonance frequency in a vacuum of F_0 . If the crystal is loaded with polymer and the resonance frequency becomes F_l , then according to Equation 5.6 it follows that

$$F_l - F_0 = \Delta f_l = -k\Delta m_l \quad (5.7)$$

where Δm_l is the amount of polymer loaded onto the crystal surface.

If the polymer-loaded crystal is exposed to a gas at pressure p , then the polymer will absorb an amount of gas equal to Δm_p . The sorption of gas within the polymer will cause a further reduction in the resonance frequency. If the new frequency is denoted as F_p this gives

$$F_p - F_l = \Delta f_p = -k\Delta m_p \quad (5.8)$$

However, Equation 5.8 does not take into account the changes in the fundamental frequency of the crystal due to changes in temperature or pressure of the system. It is therefore necessary to incorporate such changes in any calculations by carrying out background measurements of the bare quartz crystal. If the bare crystal has a fundamental frequency of R_0 under vacuum and R_p under pressure p , then $R_p - R_0$ is the correction factor, which must be subtracted from $F_p - F_l$ to account for the system changes. Equation 5.8 now becomes

$$(F_p - F_l) - (R_p - R_0) = \Delta f_p = -k\Delta m_p \quad (5.9)$$

Combining Equations 5.7 and 5.9 gives

$$\frac{\Delta m_p}{\Delta m_l} = \frac{(F_p - F_l) - (R_p - R_0)}{F_l - F_0} \quad (5.10)$$

Equation 5.10 allows the calculation of fractional gas sorption (g of gas/g of polymer) directly from the resonance frequencies, without the need for the calculation of absolute masses.³⁹

5.1.5 Modelling Gas Sorption

There are several models in the literature to represent gas sorption in polymers: the DMS model²³ (Section 5.1.3), the F-H based models²⁴ and equation-of-state (EOS) models.^{43,44} The F-H model has been widely used to model the gas sorption of polymers using condensable gases at moderate to high pressures.^{45,46}

The gas-polymer sorption equilibrium for the F-H theory is described by

$$\ln\left(\frac{p}{p_0}\right) = \ln\phi_1 + (1 - \phi_1) + \chi_{12}(1 - \phi_1)^2 \quad (5.11)$$

where p and p_0 are the equilibrium gas pressure and saturated vapour pressure, at the experimental temperature, respectively, ϕ_1 is the volume fraction of gas dissolved in the polymer and χ_{12} is the Flory-Huggins binary interaction parameter. This theory assumes that χ_{12} is a constant for a given gas-polymer system and does not significantly depend upon temperature and concentration. Provided the polymer is in the rubbery state, if χ_{12} is known for a particular system, it is possible to calculate the solubility of the gas under any temperature and pressure conditions for that system.

Perhaps the most widely used model to describe gas solubility in polymers is the Sanchez-Lacombe (S-L) EOS.^{47,48} It has been used by several research groups to correlate data due to its simplicity, well defined physical meaning and the ability to extend available data to high temperature and pressure.⁴⁹⁻⁵³ The S-L EOS is derived from the F-H model and is given by

$$\tilde{p} = -\tilde{\rho}^2 - \tilde{T} \left[\ln(1 - \tilde{\rho}) + \left(1 - \frac{1}{r}\right) \tilde{\rho} \right] \quad (5.12)$$

where \tilde{p} , $\tilde{\rho}$, \tilde{T} and r are the reduced pressure, reduced mass density, reduced temperature and characteristic fluid chain length respectively. These parameters are given by

$$\tilde{p} = \frac{p}{p^*} \quad (5.13)$$

$$\rho = \frac{\rho}{\rho^*} \quad (5.14)$$

$$\tilde{T} = \frac{T}{T^*} \quad (5.15)$$

and

$$r = \frac{Mp^*}{(RT^*\rho^*)} \quad (5.16)$$

where M is the molecular weight of the fluid and the S-L EOS parameters p^* , ρ^* and T^* are evaluated with the following mixing rules:

$$p^* = \sum_i \sum_j \phi_i \phi_j p_{ij}^* \quad (5.17)$$

$$p_{ij}^* = (1 - k_{ij}) (p_i^* p_j^*)^{0.5} \quad (5.18)$$

$$T^* = p^* \sum_i \left(\frac{\phi_i^0 T_i^*}{p_i^*} \right) \quad (5.19)$$

$$\frac{1}{r} = \sum_i \left(\frac{\phi_i^0}{r_i^0} \right) \quad (5.20)$$

$$\phi_i^0 = \frac{\left(\frac{\phi_i p_i^*}{T_i^*} \right)}{\sum_j \left(\frac{\phi_j p_j^*}{T_j^*} \right)} \quad (5.21)$$

$$\phi_i = \frac{\left(\frac{w_i}{\rho_i^*} \right)}{\sum_j \left(\frac{w_j}{\rho_j^*} \right)} \quad (5.22)$$

The variables T_i^* , p_i^* , ρ_i^* , and r_i^0 in Equations 5.17-5.22 refer to the characteristic parameters of component i in the pure state and k_{ij} is the binary interaction parameter determined by fitting the EOS to experimental solubility data. This means you need experimental data to model the results obtained and extending the model to other temperature and pressure conditions will have an unknown error associated with such calculations.

Another EOS for describing gas-polymer phase behaviour is based on the statistical associating fluid theory (SAFT).⁵⁴⁻⁵⁷ This EOS is much more complex than the S-L EOS but has the advantage of being able to account for specific interactions such as hydrogen bonding between segments of polymer molecules or solvent molecules.

5.2 Results and Discussion

5.2.1 Measurement of Gas Sorption by Polymers

In this work the solubilities of CO₂ and HFC 32 were measured in PE and PS and the aim was to compare the effects each fluid had on the polymeric materials. This was carried out using a QCM as described in Chapter 2 and the gas sorption was calculated using Equation 5.10. Each sample was allowed to reach equilibrium under the conditions to be studied, which was indicated by the cessation of peak shift in the QCM scans. The study of equilibration times with a QCM can be used as an *in situ* technique for monitoring the kinetics of gas sorption and this is discussed in Section 5.2.3.

Some of the data from this study compare well with those previously published and Figure 5.2 and Table 19 of the appendix show that the results here compliment those obtained by Sato *et al.*⁴⁹ for the solubility of CO₂ in PS, which were acquired using a pressure decay method. The solubility isotherms show a similar dependence on temperature and pressure for both sets of data and this supports the validity of the experimental and analysis techniques used to measure the gas sorption of polymers in this work.

It was reported by Ensore *et al.* that glassy polymers, such as PS, exhibit a conditioning effect.⁵⁸ Conditioning is where the sorption ability of the sample appears to be greater in subsequent gas sorption experiments when compared to the first run with the unconditioned, as-cast sample. The effect is a result of the non-equilibrium nature of the glassy state. When the polymer is exposed to a gas, the polymer volume increases in order to accommodate the dissolved gas molecules and this results in a dilation of the polymer sample. Upon removal of the gas, by depressurisation, the polymer does not relax to its original volume but to a state having a larger free volume,⁵⁹ thus having a greater sorptive capability. This means that the sorption ability of the polymer is dependent on sample history (previous exposure to gas) and this has been verified in previous work.^{60,61} The conditioning effect was also observed in this work as shown in Figure 5.3 and Table 20 of the appendix. For this reason each set of experiments were carried out on new, as-cast samples in order to assess the plasticizing ability of the gas without the requirement for previous gas exposure.

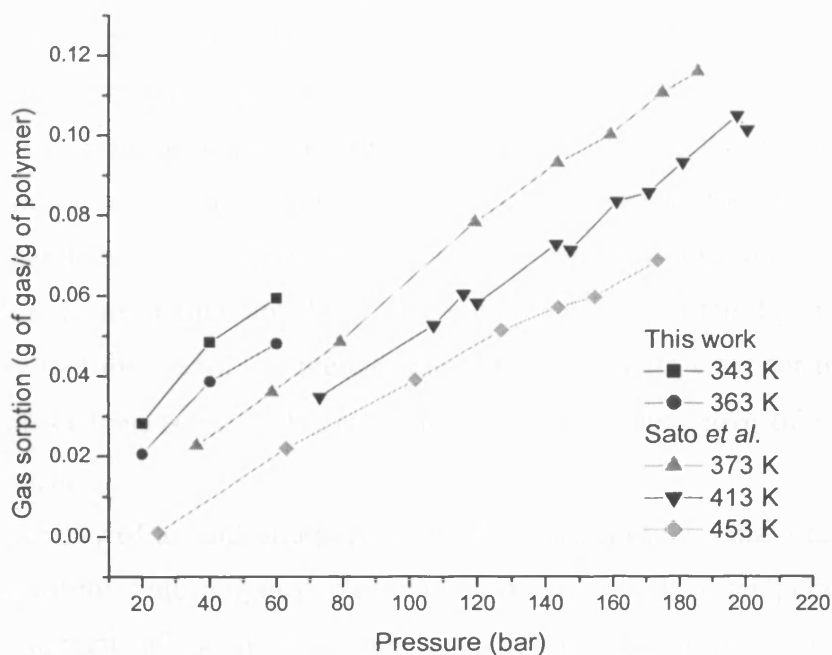


Figure 5.2 Gas sorption of CO₂ in PS for this work and that of Sato *et al.*⁴⁹ as a function of pressure along various isotherms.

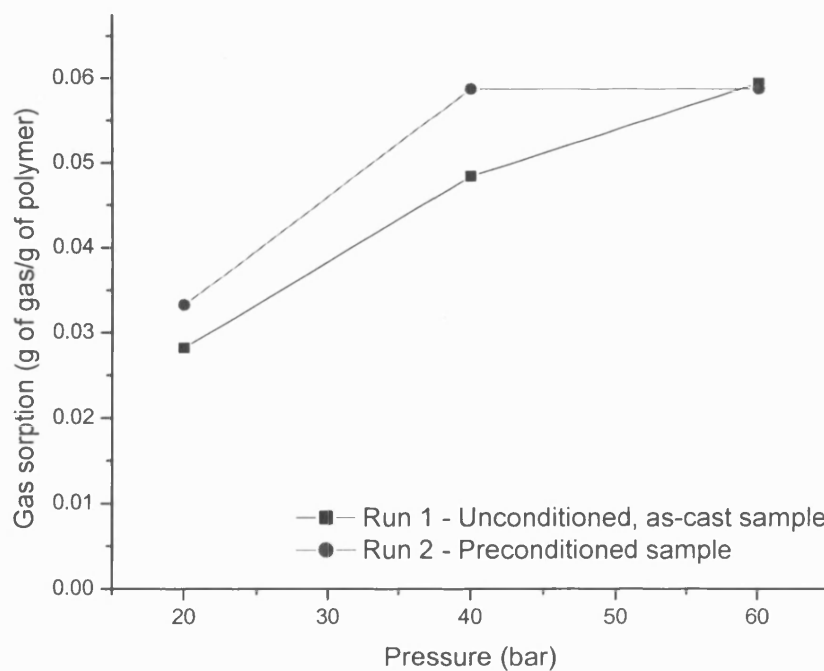


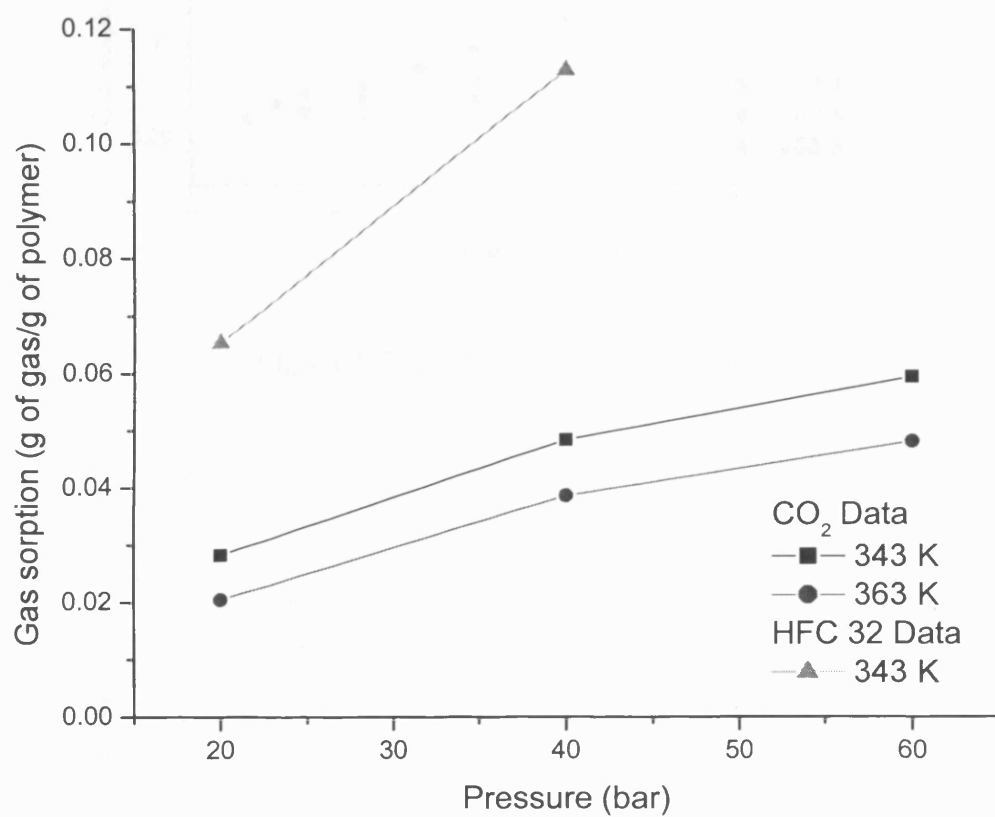
Figure 5.3 Successive sorption runs for the PS/CO₂ system at 343 K.

Conditioning of glassy polymer samples is also responsible for the hysteresis effect reported in previous studies.⁶² When hysteresis occurs a larger sorptive ability of the polymer is observed in the desorption process compared to the sorption process. Desorption was not measured in this work but the non-equilibrium behaviour of PS, suggested by Figure 5.3, implies that the effect would be observed during a complete sorption-desorption cycle. The complete sorption curves for the PS and PE systems studied are shown in Figures 5.4-5.6 and the data is presented numerically in Tables 21-28 of the appendix. The maximum error for the sorption results of all systems is $\pm 3\%$ based on an estimated reading error of ± 0.01 MHz for the frequency.

The solubility of a fluid in a polymer is determined by two main factors:⁶³ (a) the strength of the fluid-polymer interaction and (b) the critical temperature of the fluid. The strength of the fluid-polymer interaction is dependent on the types of interaction between the gas and the polymer. Both PS and PE are non-polar polymers and it would be expected that the solubility of non-polar CO₂ would be greater than that of the polar HFC 32 in these polymers. The data presented in Figures 5.4-5.6 shows that the reverse is true and this is due to the higher critical temperature of HFC 32 (Table 5.3).⁶⁴ The critical temperature can be used as a measure of the gas condensability and in general the solubility of a gas increases with increasing condensability.³ Boiling points or the Lennard-Jones well depth parameter, ϵ/k , can also be used as condensability measurements where, ϵ is the depth of the potential energy well (Figure 5.7) and k is the Boltzmann constant.³

Compound	T_c / K	T_b / K	μ / D
CO ₂	304.25 K	195.0	0
HFC 32	351.26	221.3	1.98

Table 5.3 Critical temperatures, boiling points and dipole moments of CO₂ and HFC 32.⁶⁴

**Figure 5.4** Gas sorption of PS.

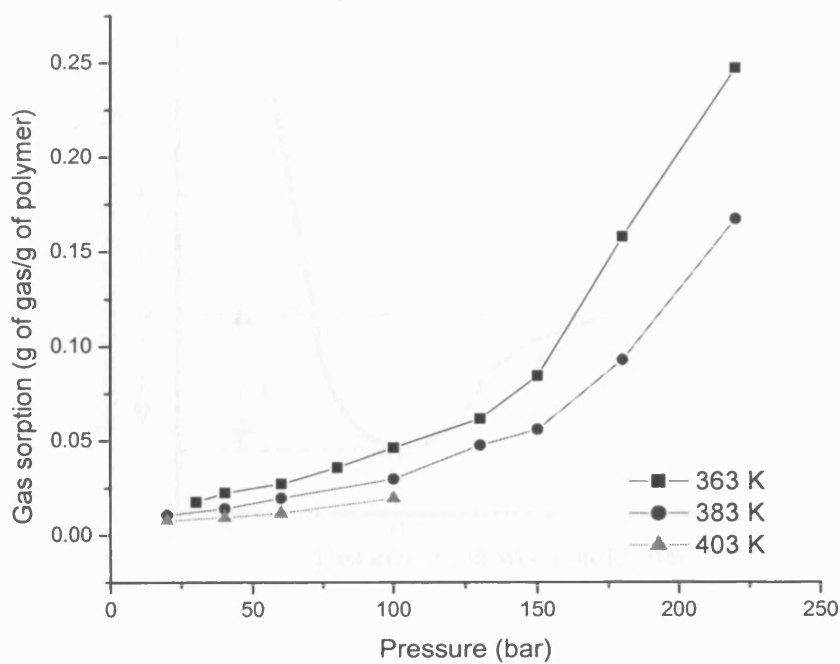


Figure 5.5 Gas sorption of CO₂ in PE.

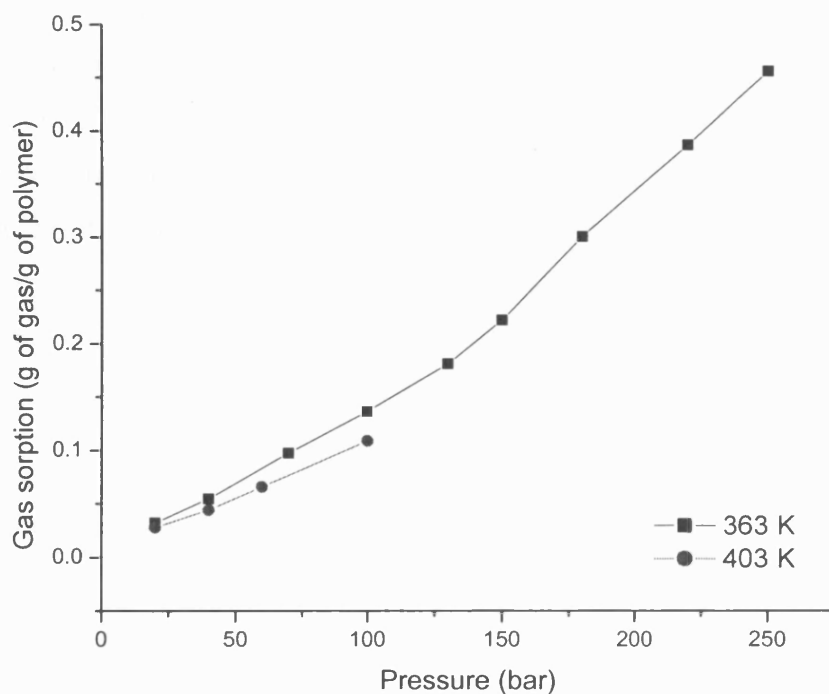


Figure 5.6 Gas sorption of HFC 32 in PE.

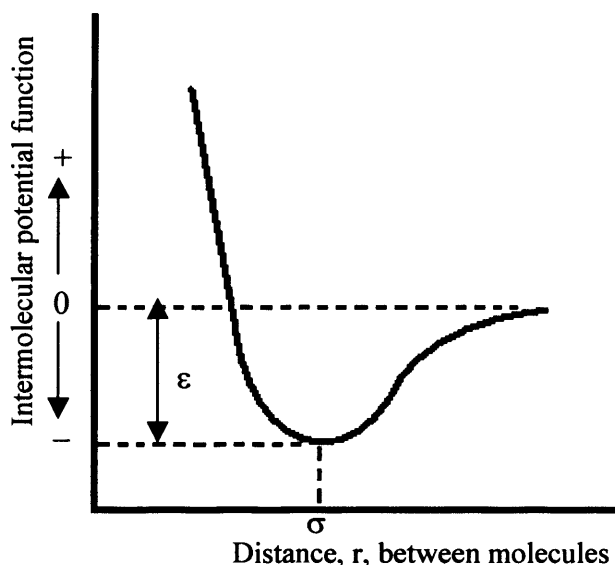


Figure 5.7 An intermolecular potential energy curve showing the distance of molecular separation at which the potential energy is minimum, σ .

The higher solubility of the more polar HFC medium suggests that these fluids are promising alternatives for polymer impregnation using polar solutes. Furthermore, residual solvents within the polymeric material after impregnation can be problematic when using conventional solvents or co-solvents with less polar fluids such as CO_2 . Complete removal of the HFC media can easily be attained by system depressurisation.

The solubilities of the gases in the polymer systems studied decrease with increasing temperature. This is a well-known phenomenon and is explained in terms of the condensability of the gas at lower temperatures. The solubility dependence of gas sorption is often written in terms of the Van't Hoff relationship:

$$S = S_0 \cdot \exp\left(\frac{-\Delta H_s}{RT}\right) \quad (5.23)$$

where S is the gas solubility, S_0 is a constant and ΔH_s is the partial molar enthalpy of sorption. The solubility in terms of thermodynamics is a two-step process.⁶⁵ The first step involves the condensation of the gas molecule within the polymeric material, followed by the formation of a molecular sized cavity for accommodation

of the gas molecule. The individual steps that contribute to the total enthalpy of sorption are represented by⁶⁵

$$\Delta H_s = \Delta H_{\text{condensation}} + \Delta H_{\text{mixing}} \quad (5.24)$$

For low molecular weight gases, low condensability causes sorption to be controlled by the enthalpy of mixing between the polymer and the gas. For weak interactions between the gas molecules and the polymer the change in the enthalpy of mixing is positive and this results in an increase in gas solubility with temperature. For condensable gases, as is the case for CO₂ and HFC 32, the enthalpy change of condensation is negative and dominant, hence the solubility of the gas in the polymer decreases with increasing temperature.⁶⁵

Polymers in the glassy state exhibit a concave sorption isotherm (relative to the pressure axis) as described by the DMS model (Section 5.1.3). When appreciable amounts of gas are dissolved in a glassy polymer a glass to liquid transition occurs because of solvent-induced plasticization. This effect is commonly referred to as isothermal glass transition^{62,66} and is denoted by an s-shaped sorption curve, being concave at lower pressures and convex at higher pressures, as shown in Figure 5.8. Many modifications of the DMS model have been proposed to account for gas-induced plasticization.^{67,68}

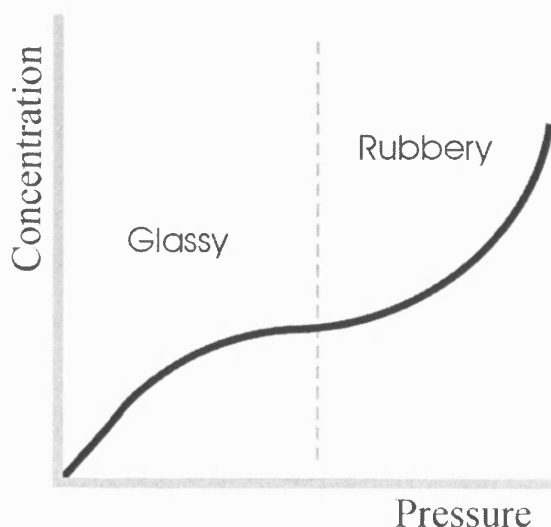


Figure 5.8 An s-shaped sorption curve where the inflection point denotes a glass to liquid transition due to gas-induced plasticization.

It can be seen in Figures 5.5-5.6 that the PE systems exhibit convex sorption isotherms over the temperature and pressure range studied. This implies that the polymer is in the rubbery state under the conditions employed, which is expected considering the T_g for PE is 143.5 K.⁶⁹ It is difficult to interpret the results obtained for the PS systems due to the small number of data points, but since T_g for PS is 358.8 K,⁶⁹ it is expected that the polymer is also in the rubbery state under the experimental conditions used. Only a few data points were acquired for the PS system because as the pressure was increased the QCM signal response was lost. This signal dampening is due to a significant increase in mass on the surface of the quartz crystal of the QCM due to sorption of gas within the PS sample.⁷⁰ A more informative interpretation of the acquired data can be obtained by calculating the reduction in T_g due to gas-induced plasticization. This will give an insight into the extent of plasticization in these systems and will also provide information on the states of the polymer samples (i.e. rubbery or glassy).

There are several theoretical approaches for the analysis of T_g depression available in the literature.⁷¹ These theoretical analyses use lattice fluid theory models such as the S-L (Section 5.1.5) to describe the gas-polymer thermodynamics for glass transition. One of the earliest and simplest to use methods for the calculation for T_g depression was that proposed by Chow⁷² and this is the approach that shall be employed here. This approach provides a theoretical estimate of polymer T_g depression by the addition of a diluent and is given by

$$\ln \left[\frac{T_g}{T_g^o} \right] = \beta [(1 - \theta) \ln(1 - \theta) + \theta \ln \theta] \quad (5.25)$$

where T_g^o is the glass transition temperature of the solvent free polymer. The parameters β and θ are given by

$$\beta = \frac{zR}{M_p \Delta C_p} \quad (5.26)$$

and

$$\theta = \frac{M_p}{zM_d} \frac{\omega}{1-\omega} \quad (5.27)$$

where z is the coordination number, R is the gas constant, M_p is the molecular weight of the polymer repeating unit, M_d is the diluent molecular weight, ΔC_p is the change in polymer heat capacity at T_g and ω is the diluent weight fraction. Goh and Lee⁷³ report ΔC_p for PS to be $6.45 \text{ J K}^{-1} \text{ mol}^{-1}$ and a value of $9.20 \text{ J K}^{-1} \text{ mol}^{-1}$ for PE has been extrapolated from work by Gaur and Wunderlich.⁷⁴ Figures 5.9-5.11 and Tables 29-31 of the appendix show the calculated T_g depression for the different gas-polymer systems studied in this work. It can be seen that for all systems the decrease in T_g with increasing gas sorption shows a linear relationship, which is independent of the working temperature. The calculated T_g values for both the PS and PE systems suggest that the polymers are in the rubbery state under all conditions studied.

At a given temperature HFC 32 causes 1.5 times more plasticization than CO_2 in both PS and PE (calculated as the ratio of the difference between the solvent free T_g and the gas-induced T_g for each system). Furthermore, the greater plasticization caused by HFC 32 occurs at much lower pressures than those required by CO_2 . This is a significant result and shows that HFCs have great potential as polymer modifying agents in terms of energy requirements, economy, safety considerations and equipment design.

A maximum error of 7.8 % is assigned to all calculated T_g values. This error includes the error associated with the gas sorption data and a maximum error of 5 %, which was assigned to the literature values for ΔC_p .

The knowledge of the variation of T_g with experimental conditions plays an important role in many practical applications of polymers. Glassy polymers are often used as separation membranes because of their high selectivities and T_g therefore, plays an important role in determining the physical state of such polymer membranes under operating conditions. A decrease in T_g when sufficient amounts of solutes or gases are dissolved within the polymer matrix causes a decrease in the rigidity of the polymer structure. This can have the undesired effect of reducing the molecular sieving ability (selectivity) of the separation membrane.

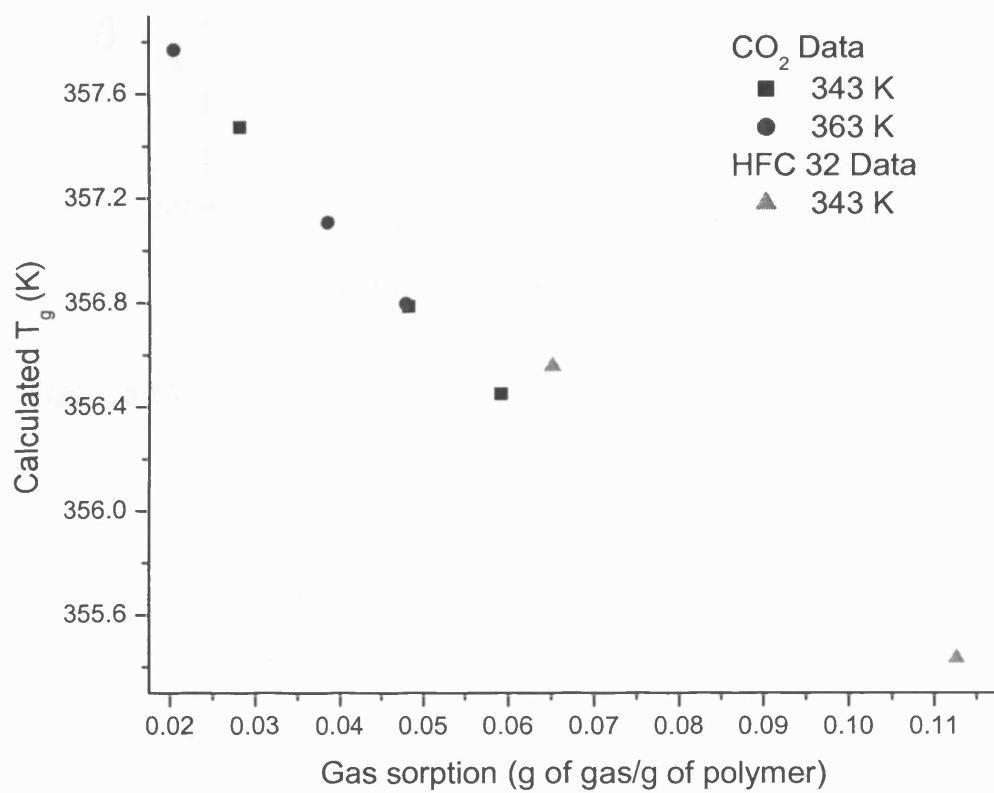


Figure 5.9 The reduction of T_g with gas sorption for the PS samples.

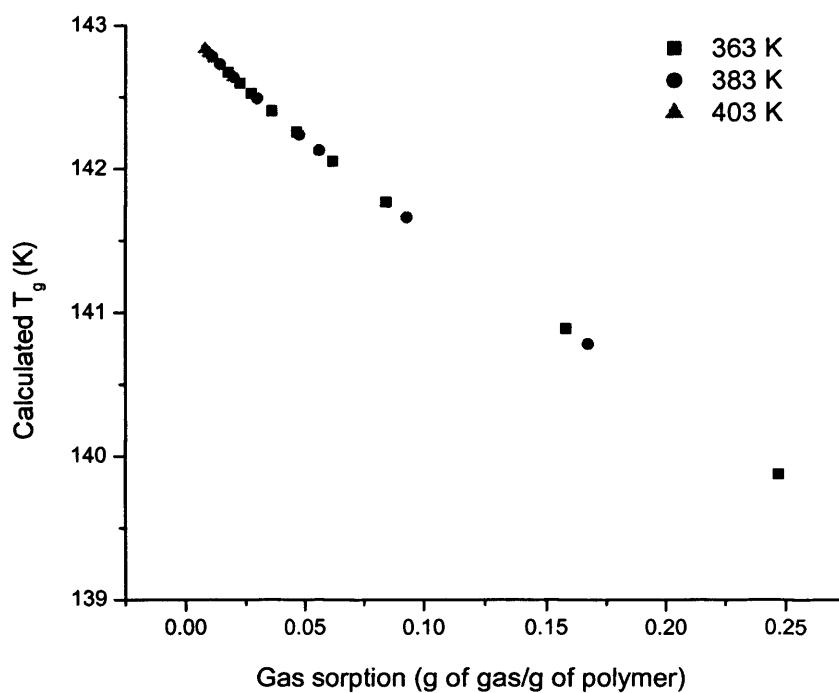


Figure 5.10 The reduction of T_g with gas sorption for the PE/CO₂ system.

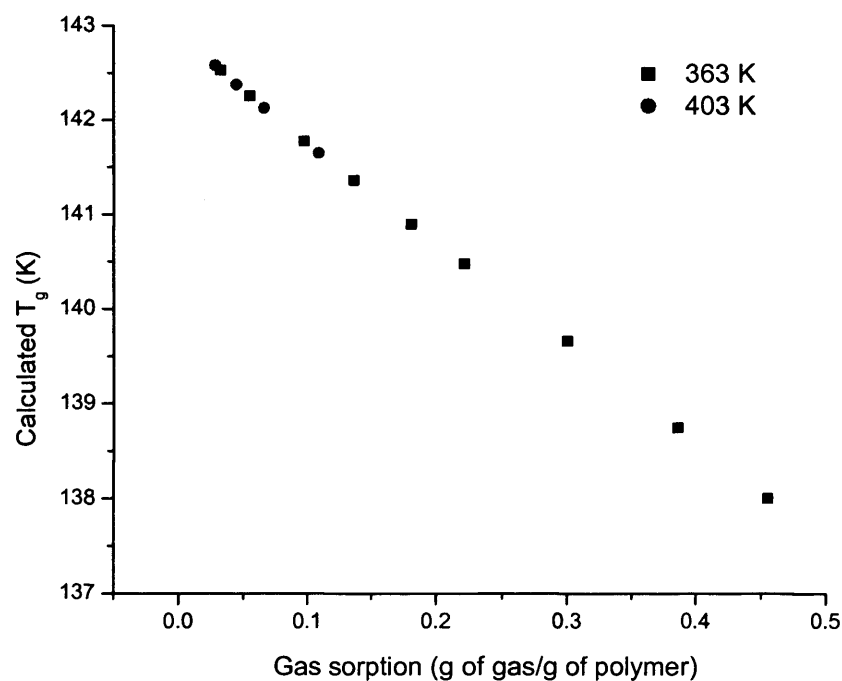


Figure 5.11 The reduction of T_g with gas sorption for the PE/HFC 32 system.

Plasticization of glassy polymers with high-pressure gases also plays an important role in the swelling of polymeric materials and in the formation of polymeric foams.

Swelling of the polymeric material was observed in this work and pictures of some of the samples, both before and after the experiments, are shown in Figures 5.12-5.14. No swelling of PS was observed when using HFC 32 but the sample volume increased approximately two-fold when using CO₂ as the plasticizing agent as shown in Figure 5.12. This implies that HFC 32 can be used as a plasticizing agent for the extrusion of PS without affecting the polymeric structure of the end product.

Both gases caused considerable swelling in the PE samples as shown in Figures 5.13 and 5.14 but swelling occurred by different mechanisms for each gas. In the case of CO₂, swelling was initiated by depressurisation of the high-pressure autoclave once the QCM signal was lost due to dampening. Depressurisation was carried out at two different rates and this gave two very different results in polymer morphology. Figure 5.13 shows the PE sample after a rapid depressurisation from 100 bar over a period of approximately 5 seconds.

The rapid escape of gas from the PE sample caused the nucleation and growth of bubbles within the polymer. Once a significant amount of gas had escaped from within the polymer matrix it caused the PE to “freeze” into a foamed structure. This phenomenon is known as anti-plasticization and the process was marked by total loss of QCM signal upon depressurisation, which signified the breaking of the quartz crystal as shown in Figure 5.13. Depressurisation was also carried out over a period of 20 minutes for this system and very little change in the morphology of the PE sample was observed (Figure 5.16c compared to Figure 5.16a).

Swelling of the PE sample by HFC 32 occurred under experimental conditions at 100 bar and 403 K. Again this swelling was marked by total loss of signal due to the breaking of the quartz crystal as shown in Figure 5.14. Figures 5.15 and 5.16 are cross-sectional SEM scans of each sample before and after treatment with the plasticizing gas. It can be seen in Figure 5.15 that the morphology of the PS sample has changed very little during the experiments, even in the sample treated with CO₂, which caused a two-fold increase in bulk volume.

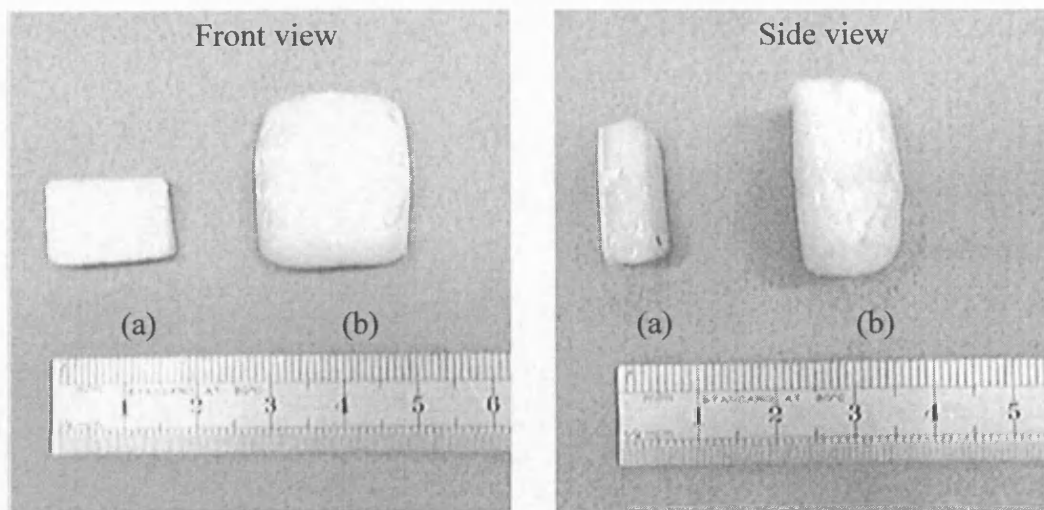


Figure 5.12 PS sample (a) before and (b) after treatment with CO₂ at 363 K.

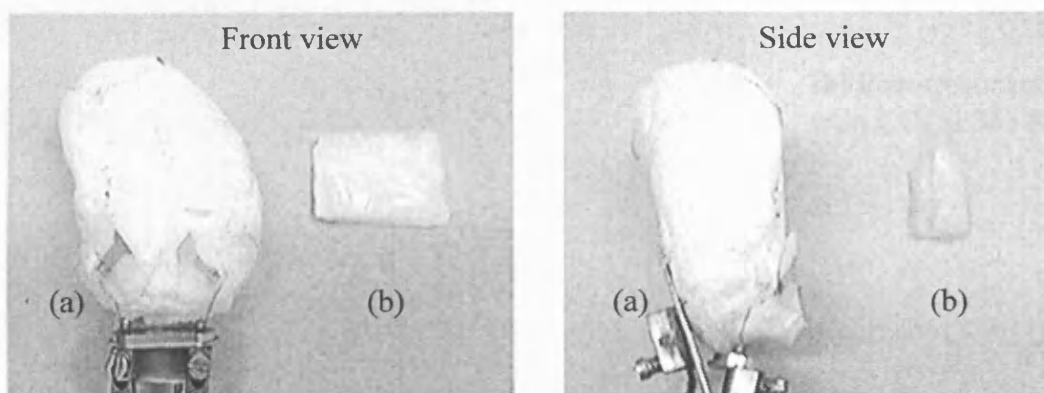


Figure 5.13 PE sample (a) after and (b) before treatment with CO₂ at 403 K.

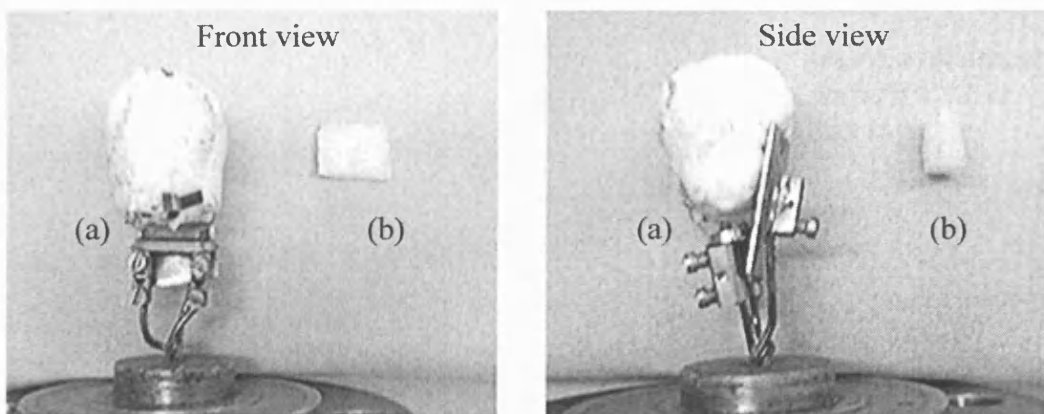
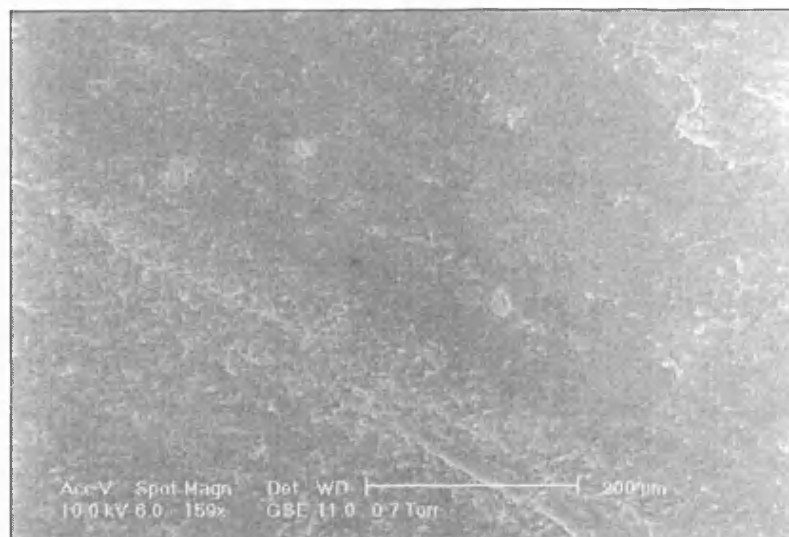
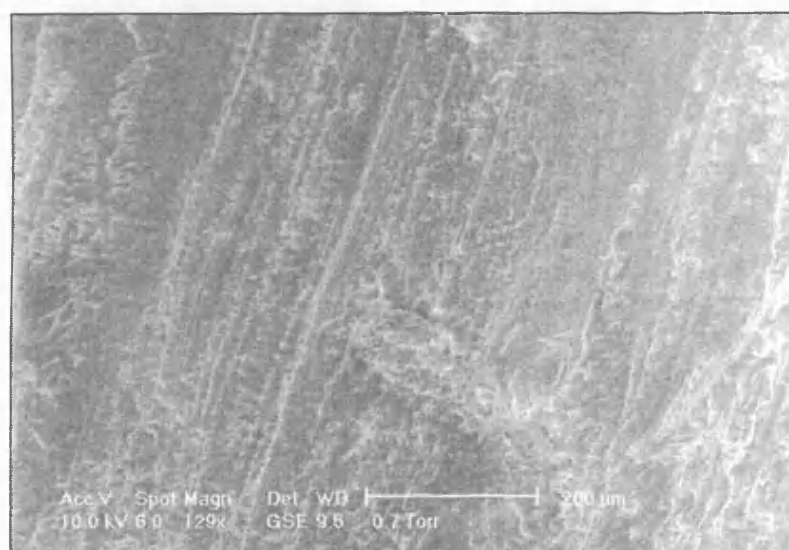


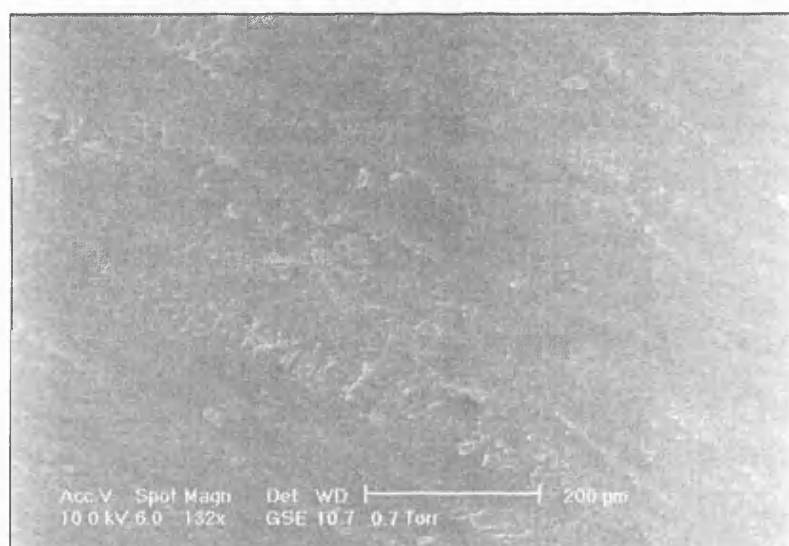
Figure 5.14 PE sample (a) after and (b) before treatment with HFC 32 at 403 K.



(a) Pre-treatment.



(b) Post-treatment
with CO₂ at 363 K.

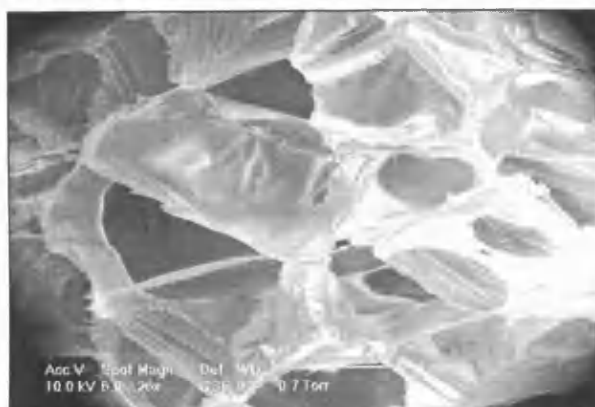


(c) Post-treatment
with HFC 32 at
343 K.

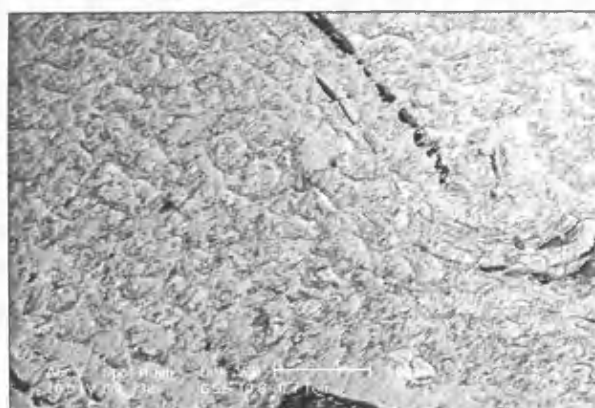
Figure 5.15 Cross-sectional SEM scans of the PS samples.



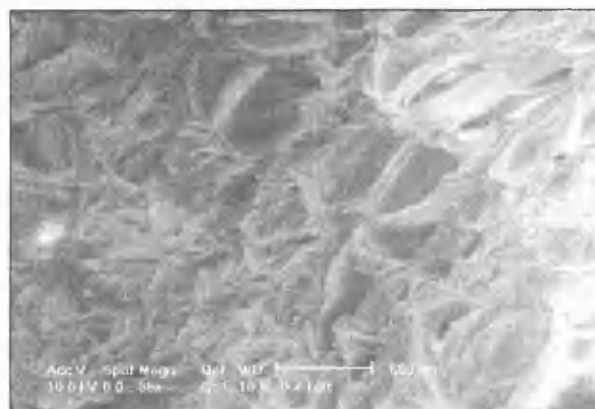
(a) Pre-treatment.



(b) Post-treatment with CO_2 at 403 K (rapid depressurisation over a period of 5 seconds).



(c) Post-treatment with CO_2 at 403 K (slow depressurisation over a period of 20 minutes).



(d) Post-treatment with HFC 32 at 403 K.

Figure 5.16 Cross-sectional SEM scans of the PE samples.

Figure 5.16 shows the differences in morphology for the PE samples when treated under different experimental conditions. Foaming of the sample exposed to CO₂ was achieved when the system was exposed to a rapid depressurisation and it can be seen in Figure 5.16b that the sample structure is considerably different to that of the starting material in Figure 5.16a.

Apart from the appearance of a few cracks in the PE sample exposed to a slow depressurisation (Figure 5.16c), the morphology appears relatively unchanged when compared to the SEM of the original sample. This suggests that it is possible to lower the T_g of the polymer, which is crucial for polymer modification processes such as impregnation and extraction, without seriously altering the physical structure of the polymeric material. The cracks shown in the sample may already have been present as defects in the original sample or may have been formed during the cutting process when the sample was prepared for cross-sectional SEM examination.

Figure 5.16d shows the foam structure formed when the PE was treated with HFC 32 at 403 K and 100 bar. The polymer structure is considerably different to the starting material but it is also interesting to note the scale on this SEM when compared to that for the CO₂ treated sample in Figure 5.16b. The bubbles in the CO₂ foamed sample are at least twice the size of the bubbles in the HFC 32 treated sample. The differences in morphologies obtained suggest that these systems can be used to form foams of varying structure depending on the temperature, pressure, rates of decompression and diluent gases used.

Polystyrene is regarded as an amorphous polymer and PE as a semi-crystalline one. It has been found that CO₂ solubility is higher in amorphous polymers when compared to the solubility of the same gas, under the same conditions, in more crystalline polymer systems.^{75,76} If the data for the sorption of CO₂ in PS is plotted on the same graph as that for the sorption of CO₂ in PE, then it can be seen from Figure 5.17 that this statement holds true for the conditions studied in this work. However, if it is assumed that the results in the current work follow the same trend as those obtained by Sato *et al.* (Figure 5.2), and the results for the PS system are extrapolated to higher pressures, it can be seen that at around 150-170 bar there will be cross over points where the solubilities of CO₂ in PE becomes higher than those in PS.

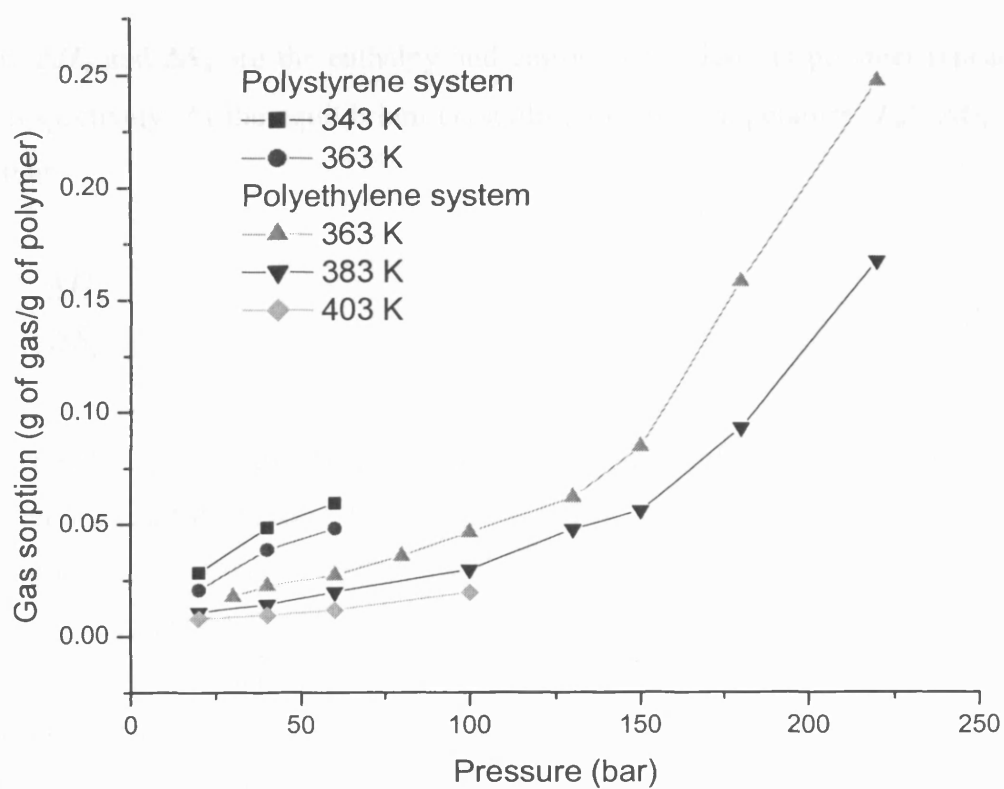


Figure 5.17 Comparison of the CO₂ sorption of PS and PE.

Here, the increase in CO₂ sorption in the PE system is attributed to the depression of the observed crystalline-melting temperature, T_m . The T_m is defined as the temperature at which polymer crystallites are destroyed and an amorphous, disordered melt is formed.³ From the first law of thermodynamics, the free energy of fusion per repeating unit of polymer, ΔG_u , is given by

$$\Delta G_u = \Delta H_u - T\Delta S_u \quad (5.28)$$

where ΔH_u and ΔS_u are the enthalpy and entropy of fusion per polymer repeating unit respectively. At the equilibrium crystalline-melting temperature, T_m^o , $\Delta G_u = 0$ and thus

$$T_m^o = \frac{\Delta H_u}{\Delta S_u} \quad (5.29)$$

Generally T_m is always lower than T_m^o and a number of factors can contribute to this melting-point depression. One is due to the kinetic effect of a finite heating or cooling rate and another is due to crystallite size, which can be influenced by the presence of impurities or the conditions of the crystallization process.³ A third contribution to this depression, and the one that is most important here, is the presence of a diluent or plasticizer. In this discussion the third factor applies to the sorption of CO₂ within the PE matrix. Using the F-H theory (Section 5.1.5), the relation for the melting-point depression due to the sorption of gas is given by

$$\frac{1}{T_m} - \frac{1}{T_m^o} = \left(\frac{R}{\Delta H_u} \right) \left(\frac{V_u}{V_l} \right) (\phi_l - \chi_{12}\phi_l^2) \quad (5.30)$$

where R is the ideal gas constant, V_u is the molar volume per polymer repeating unit, V_l is the molar volume of the diluent, ϕ_l is the volume fraction of the diluent and χ_{12} is the F-H interaction parameter between the diluent (component 1) and the polymer (component 2). The F-H theory generally assumes χ_{12} to be independent of

temperature but the calculations here use the temperature-dependent values shown in Table 5.4, which were calculated for this system.

Using Equation 5.30 along with the parameters in Table 5.5 and Tables 32-34 of the appendix, it is possible to calculate the depression of T_m for the PE/CO₂ system and the results are shown in Figure 5.18. The weight of PE used in each of these experiments was 1.012 ± 0.05 g. The weight of PE remained unchanged after each experiment when compared to that of the pre-experimental sample and this showed that the diluent had not removed any of the polymeric material from within the PE matrix.

Temperature / K	363	383	403
χ_{12}	1.36	1.25	1.17

Table 5.4 Temperature-dependent F-H interaction parameter for the PE/CO₂.

T_m^o / K	ΔH_u / J mol ⁻¹	$V_u \times 10^{25}$ / Å ³	$V_l \times 10^{25}$ / Å ³
419	229.15	3.50 ^a	2.84 ^a

Table 5.5 The parameters used in Equation 3.9 to calculate the depression in T_m for the PE/CO₂ system.³ ^a Estimated using PC Spartan Pro molecular modelling package.⁷⁷

It can be seen from Figure 5.18 that the experimental temperatures used in this study exceed those of T_m for the PE sample. This means that the crystallites in the polymer matrix are being destroyed under the conditions studied and an unordered, amorphous polymer melt is being formed. This is used to account for the observation that the solubility of CO₂ in PE may exceed that of PS at elevated gas pressures, since gas sorption only occurs in the amorphous region of polymers.

If the depression of T_m is plotted against gas sorption (Figure 5.19) it is possible to see that T_m decreases uniformly and is independent of temperature. The maximum error in χ_{12} was calculated to be ± 6 %. Including the error in χ_{12} , the error associated with the sorption data and a maximum error of ± 5 % for the

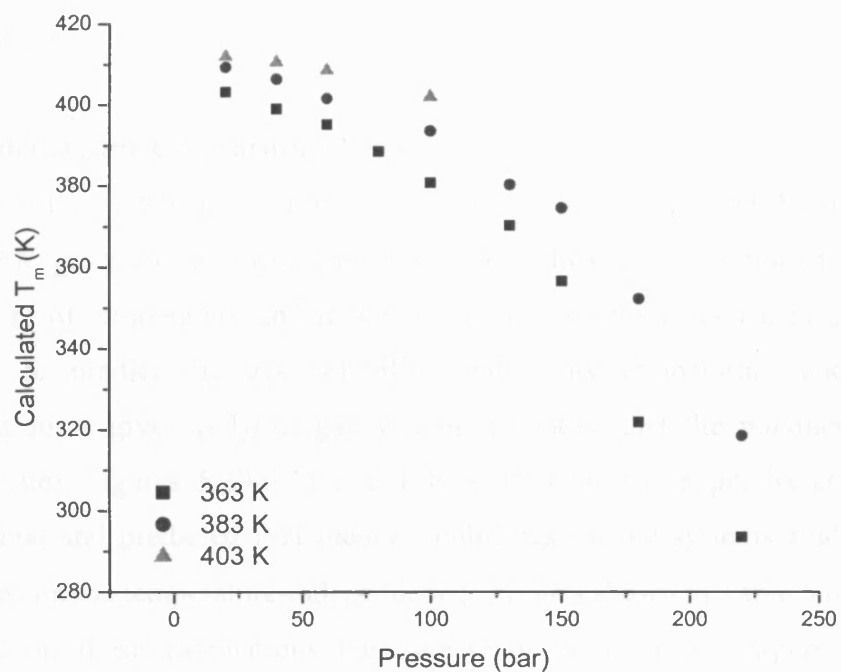


Figure 5.18 Correlation of T_m reduction with pressure for the PE/CO₂ system.

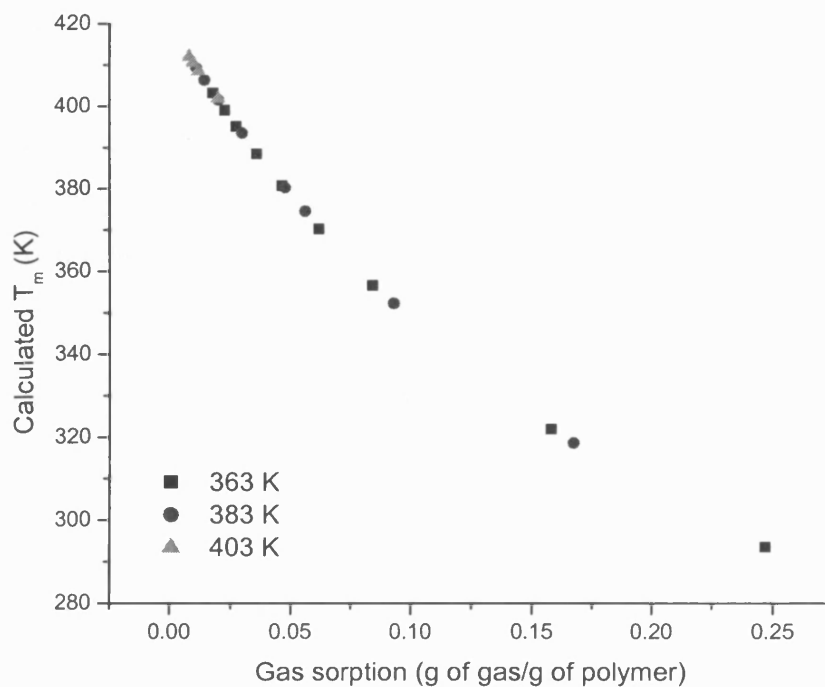


Figure 5.19 The variation of T_m with gas sorption for the PE/CO₂ system.

literature values, the maximum error assigned to the calculated T_m values was calculated to be $\pm 6.5\%$.

5.2.2 Modelling the Gas Sorption Data

The F-H theory (Section 5.1.5) has been widely used to predict the solubility of condensable gases in polymers. In classical F-H theory it is assumed that χ_{12} is independent of temperature and if this parameter is known then it is possible, in principle, to predict the gas solubility under any temperature and pressure conditions for a given polymer-gas system (provided that the polymer is in the rubbery state). Figures 5.20-5.22 and Tables 35-37 of the appendix compare the experimental and predicted F-H theory solubilities for the systems studied in this work based on the temperature-independent χ_{12} values shown in Table 5.6.

Based on these calculations the agreement between the experimental and predicted solubilities is poor in the PE systems. Strictly speaking χ_{12} is not independent of temperature since³

$$\chi_{12} = \frac{zr_1\Delta\omega_{12}}{kT} \quad (5.31)$$

where z is the lattice coordination number, r_1 is the number of polymer segments, ω_{12} is the energy of interaction between the diluent and the polymer, k is the Boltzmann constant and T is the experimental temperature.

System	χ_{12}
PS/CO ₂	0.99
PS/HFC 32	1.25
PE/CO ₂	1.31
PE/HFC 32	1.51

Table 5.6 Calculated temperature-independent F-H parameters for the systems studied.

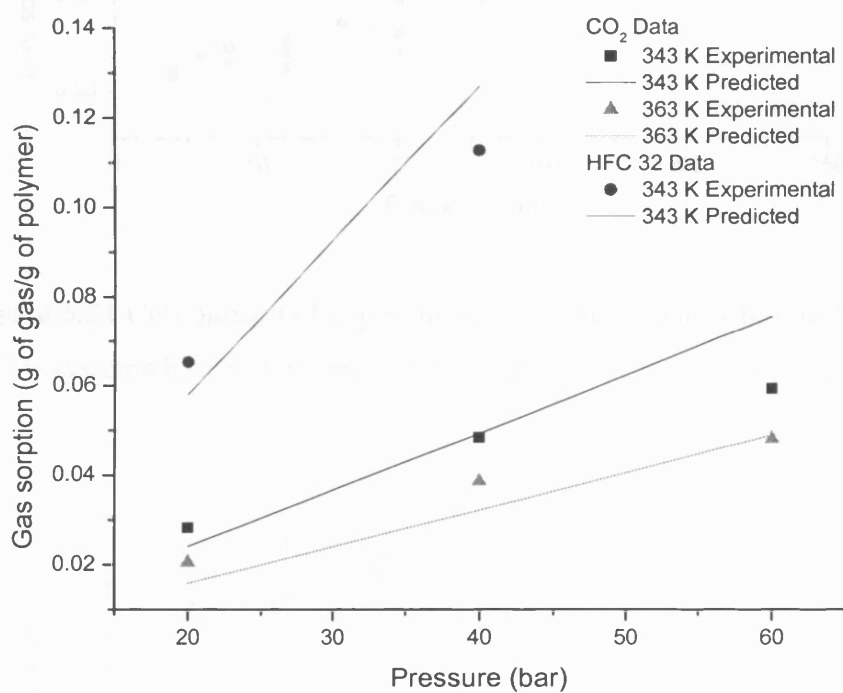


Figure 5.20 Comparison of experimental and theoretical solubilities for the PS systems based on temperature-independent interaction parameters.

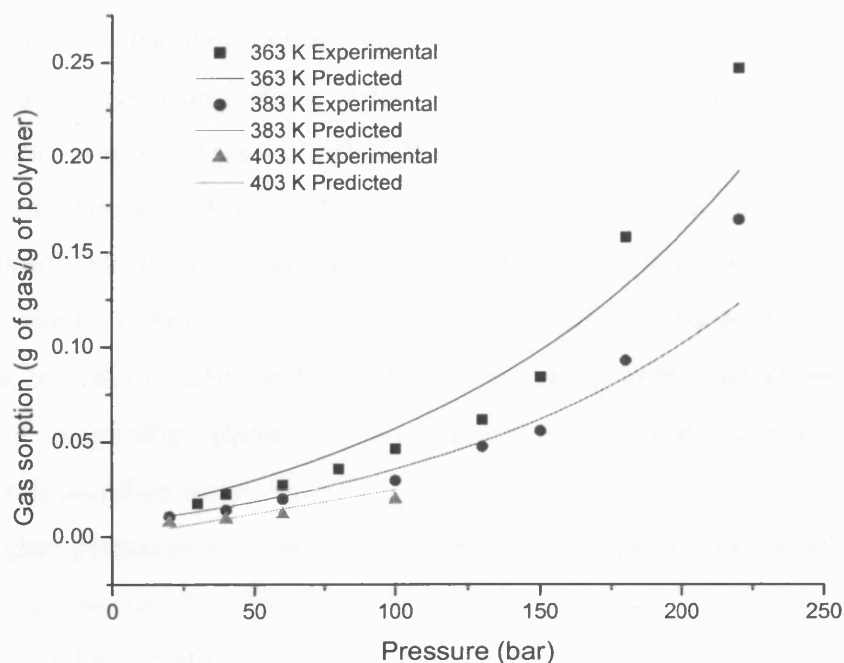


Figure 5.21 Comparison of experimental and theoretical solubilities for the PE/CO₂ systems based on temperature-independent interaction parameters.

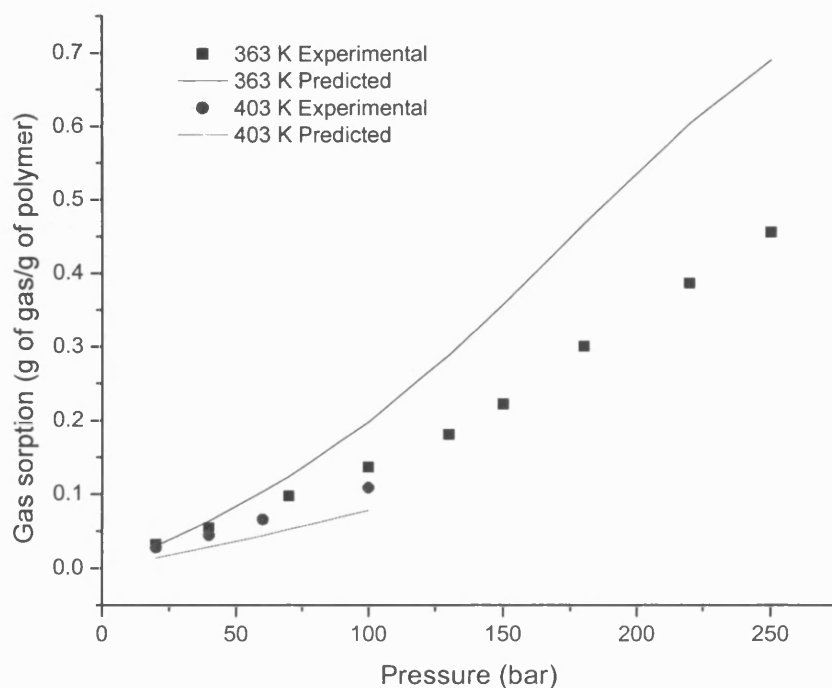


Figure 5.22 Comparison of experimental and theoretical solubilities for the PE/HFC 32 systems based on temperature-independent interaction parameters.

Therefore, temperature-dependent χ_{12} values for each of the systems studied in this work were calculated and are shown in Table 5.7. The predicted solubilities were re-calculated using these values and the results are compared to the experimental values in Figures 5.23-5.25 and Tables 35-37 of the appendix. It can be seen that the agreement between the experimental and calculated values is greatly improved and the maximum root mean square error in the correlation is decreased from ± 0.09 to ± 0.06 g of gas/g of polymer. It is shown here that the F-H model can be used to adequately predict the solubility of the gas-polymer systems although a temperature-dependent χ_{12} gives a much better correlation between experimental and theoretical data.

At higher pressures (> 150 bar) the correlation between the experimental and predicted data for the PE/HFC 32 system at 363 K (Figure 5.25) is less accurate. If the model for the PE/HFC 32 system is excluded from the error calculations, then the maximum root mean square error in the correlation for the temperature dependent models is reduced from ± 0.06 to ± 0.008 g of gas/g of polymer, which demonstrates a very good correlation for all other systems studied. In the case of the PE/HFC 32 system the EOS of Sanchez and Lacombe may provide a better correlation. However, due to the lack of information on the variables required for such calculations, it was not possible to predict the gas solubilities of the systems studied here using models any more complex than the F-H model.

Temperature / K	System			
	PS/CO ₂	PS/HFC 32	PE/CO ₂	PE/HFC 32
343	1.13	1.25	-	-
363	0.85	-	1.36	1.96
383	-	-	1.25	-
403	-	-	1.17	1.03

Table 5.7 Calculated temperature-dependent F-H parameters for the systems studied.

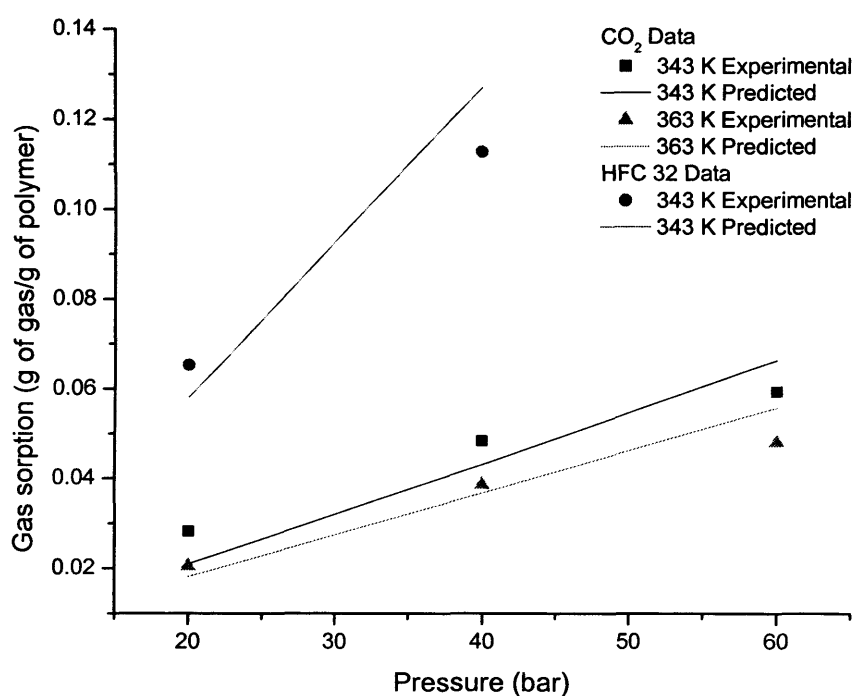


Figure 5.23 Comparison of experimental and theoretical solubilities for the PS systems based on temperature-dependent interaction parameters.

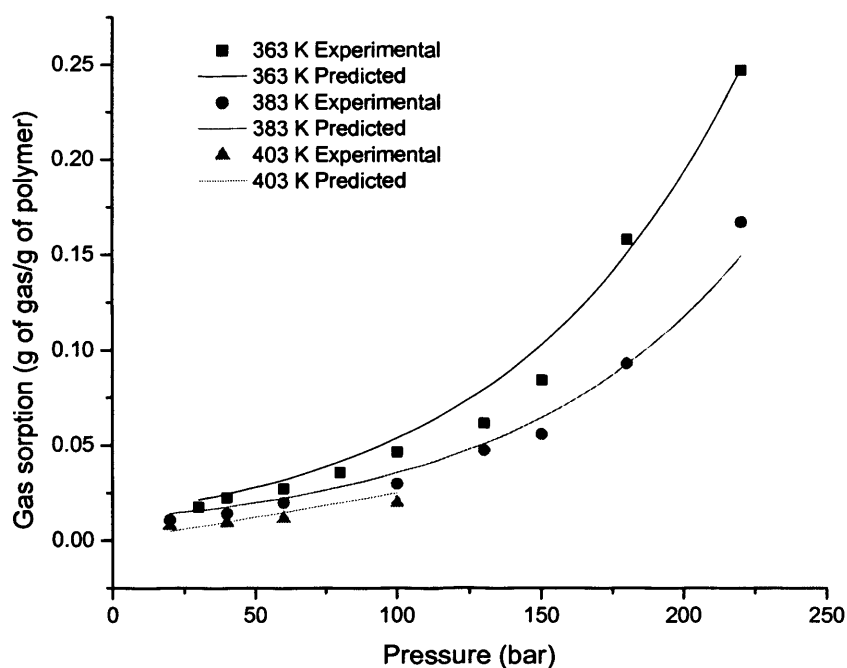


Figure 5.24 Comparison of experimental and theoretical solubilities for the PE/CO₂ systems based on temperature-dependent interaction parameters.

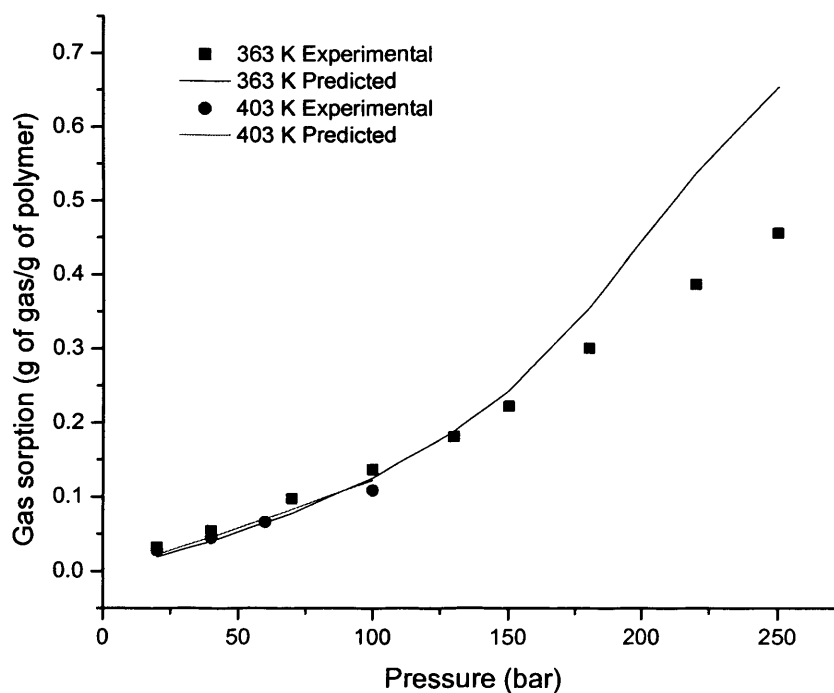


Figure 5.25 Comparison of experimental and theoretical solubilities for the PE/HFC 32 systems based on temperature-dependent interaction parameters.

5.2.3 Kinetics of Gas Sorption

The QCM technique can also be used to measure the kinetics of gas sorption by monitoring the change in peak shift with time. Some typical QCM scans for the gas sorption of CO₂ in PS, at 363 K and 60 bar, are shown in Figure 5.26. It can be seen that the system reaches equilibrium after 220 minutes (overlapping of peaks in the QCM scan) and this information can be used to calculate the rate of gas sorption for the system under these conditions. The gas sorption for each of the peaks shown in Figure 5.26 has been calculated using Equation 5.10 and the rate of change of gas sorption with time is shown in Figure 5.27 and Table 38 of the appendix.

In order to calculate the rate constant for the sorption of gas within the polymer matrix the gas uptake was considered as a consumption of CO₂ within the PS sample. The data for the consumption of CO₂, in g of gas/g of polymer, is shown as an inset on Figure 5.27. The data can now be treated as a change in concentration with time for the calculation of the rate constant. The first-order rate law for the consumption of CO₂ is given by

$$\frac{d[CO_2]}{dt} = -k[CO_2] \quad (5.32)$$

which rearranges to

$$\frac{d[CO_2]}{[CO_2]} = -kdt \quad (5.33)$$

The differential rate law in Equation 5.33 can be integrated to give the solution shown in Equation 5.34 where $[CO_2]_0$ is the concentration of CO₂ at $t = 0$, $[CO_2]$ is the concentration at time t and k is the rate constant.

$$\ln\left(\frac{[CO_2]}{[CO_2]_0}\right) = -kt \quad (5.34)$$

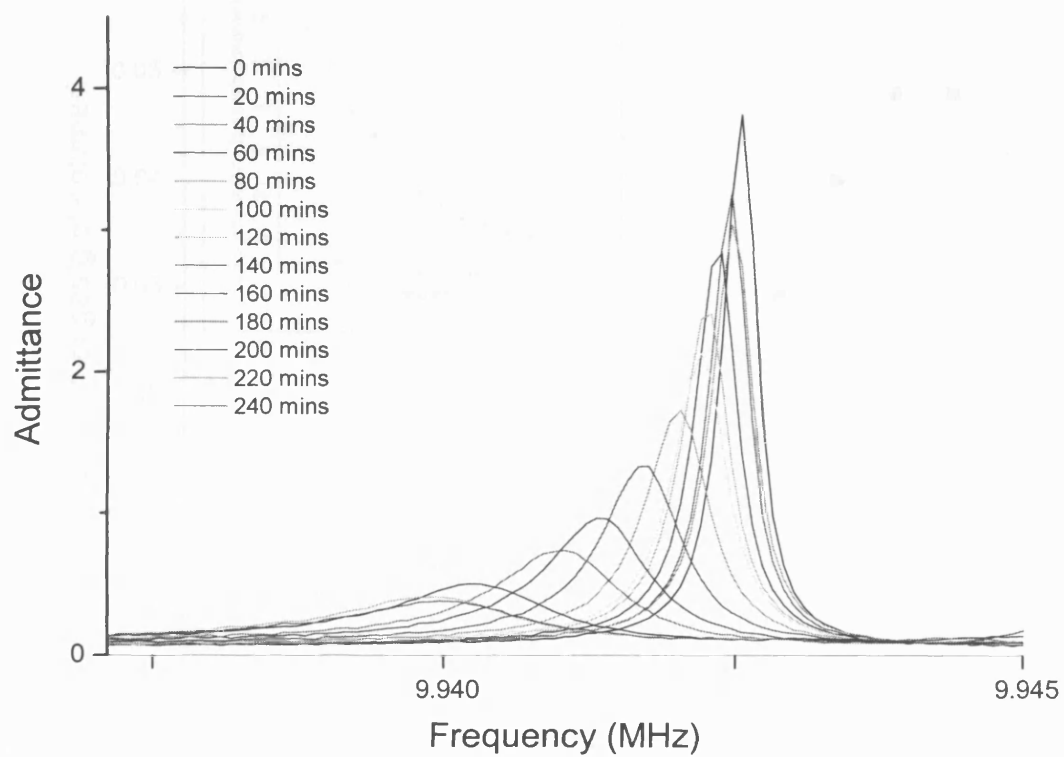


Figure 5.26 QCM scans of CO₂ sorption of PS, at 363 K and 60 bar for various time intervals.

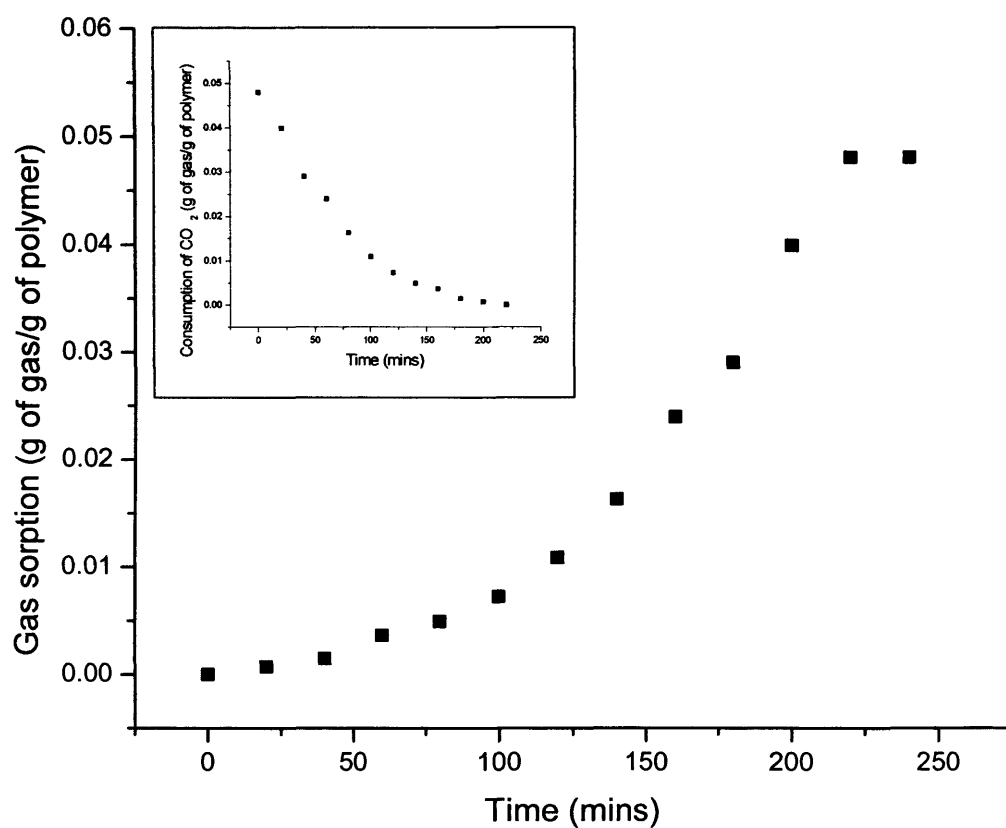


Figure 5.27 Rate of change of gas sorption with time for the PS/CO₂ system at 363 K and 60 bar. The inset shows the consumption of CO₂ with time as it is sorbed into the polymer matrix.

If $\ln([CO_2]/[CO_2]_0)$ is plotted against t , then a first-order process will give a straight line of slope $-k$. Figure 5.28 is a plot of pre-equilibrium data for the PS/CO₂ data under investigation here and it can be seen that a straight line is obtained with a correlation of 0.995. From the graph the rate constant for gas sorption is calculated to be $2.80 \pm 0.3 \times 10^{-4} \text{ s}^{-1}$. This is the first time that *in situ* rate constant data has been calculated for gas-polymer systems and no literature values for the PS/CO₂ system could be found for comparison.

Diffusion coefficients are important parameters in foam processing and in establishing the ability of polymers to act as diffusivity-selective separation membranes and barrier materials. Glassy polymers exhibit more restricted torsional mobility of the polymer backbones than rubbery ones and are therefore more useful for diffusion-controlled separations.⁷⁸ Diffusion coefficients can be calculated using various methods and two examples are given here. Equation 5.35 converges rapidly at short times and is truncated after the first term on the right hand side, whereas Equation 5.36 converges at long times and is truncated after the first two terms on the right hand side.⁷⁹

$$\frac{M_t}{M_\infty} = \frac{4}{L} \left(\frac{Dt}{\pi} \right)^{0.5} + \frac{8}{L} (Dt)^{0.5} \sum_{n=1}^{\infty} (-1)^n \text{ierfc} \left(\frac{nL}{2(Dt)^{0.5}} \right) \quad (5.35)$$

$$\frac{M_t}{M_\infty} = 1 - \frac{8}{\pi^2} \sum_{n=0}^{\infty} \frac{1}{(2n+1)^2} \cdot \exp \left(\frac{-(2n+1)^2 \pi^2 Dt}{L^2} \right) \quad (5.36)$$

These two methods have been shown to be unsatisfactory since they do not use the full sorption curve^{80,81} and a hybrid method combining Equations 5.35 and 5.36 was introduced.⁸¹

However, the investigation here is by no means exhaustive and the aim is to simply demonstrate the applicability of the QCM technique as a simple method for the determination of the diffusion coefficient, using the PS/CO₂ system at 363 K and 60 bar as an example.

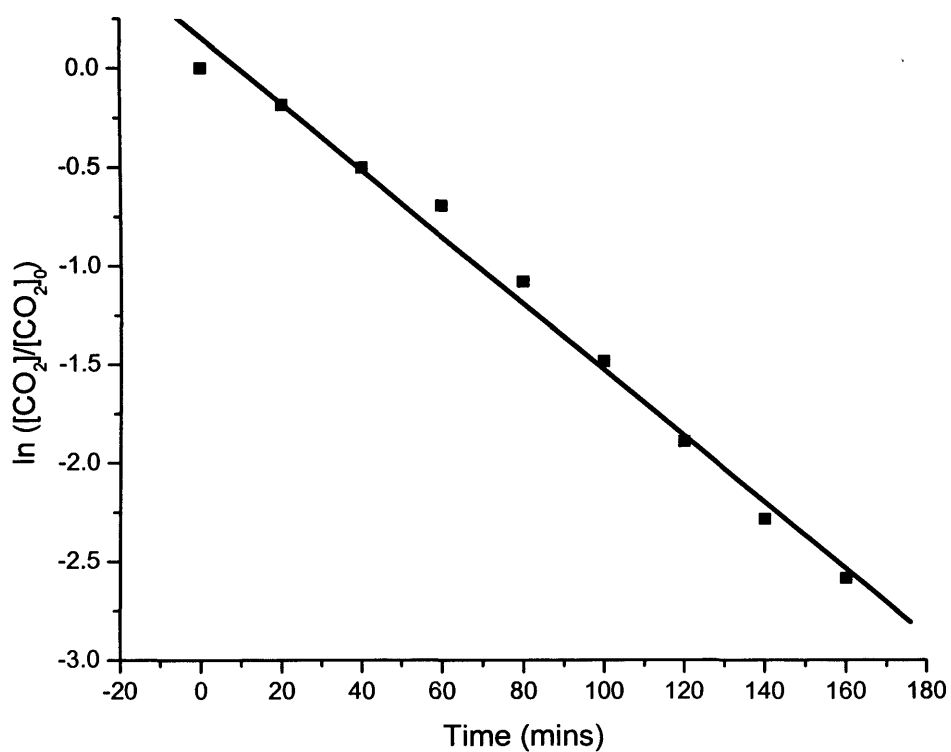


Figure 5.28 A first order plot of $\ln([\text{CO}_2]/[\text{CO}_2]_0)$ against time in order to calculate the rate constant for the sorption of CO_2 by PS at 363 K and 60 bar.

The diffusion coefficient is given by the simplified version of Equation 5.35:

$$\frac{M_t}{M_\infty} = 4 \left(\frac{D}{\pi} \right)^{0.5} \left(\frac{t^{0.5}}{L} \right) \quad (5.37)$$

where M_t is the mass of sorbed gas at time t , M_∞ is the mass of sorbed gas at t_∞ (the equilibrium solubility under experimental conditions), D is the diffusion coefficient and L is the polymer sample thickness. A plot of M_t/M_∞ against $t^{0.5}/L$ yields a sorption curve with the earlier part of the graph having a slope of $4(D/\pi)^{0.5}$. The value of the slope can be used to calculate the diffusion coefficient and the plot for the system under investigation here is shown in Figure 5.29. Here D was calculated to be $8.17 \pm 0.9 \times 10^{-7} \text{ cm}^2 \text{ s}^{-1}$. Sato *et al.*⁵¹ measured the solubility of CO_2 in PS using a pressure decay method and they reported the diffusion coefficients of CO_2 in PS to be $1.46 \times 10^{-6} \text{ cm}^2 \text{ s}^{-1}$ at 373 K and 64 bar and $4.42 \times 10^{-6} \text{ cm}^2 \text{ s}^{-1}$ at 423 K and 62.9 bar.

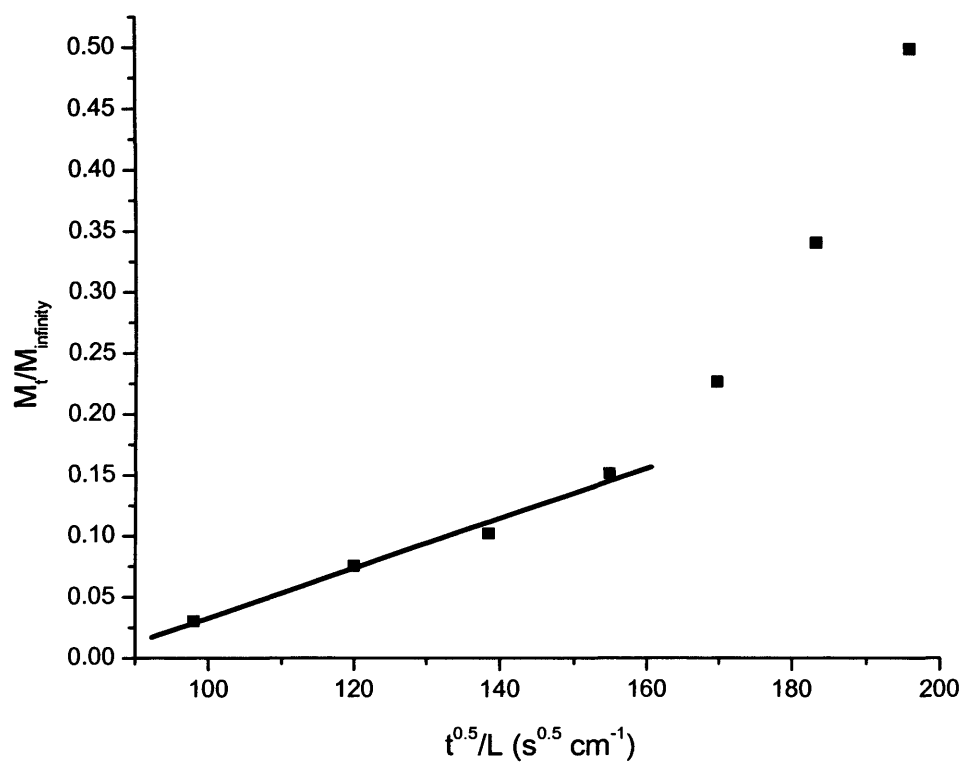


Figure 5.29 A plot used to estimate the diffusion coefficient for the PS/CO₂ system at 363 K and 60 bar.

5.3 Conclusion

A quartz crystal microbalance has been used to assess the swelling ability of HFC 32 in polystyrene and polyethylene and the results have been compared to the swelling obtained with CO₂ in the same polymers. This is the first time that HFC 32 has been investigated for use as a polymer modifying agent.

It was demonstrated that the gas sorption of polymers is dependent on sample history (previous exposure to gas) due to the non-equilibrium nature of the glassy state. It was also shown that gas condensability was the major factor in determining gas solubility since the more polar HFC 32, with its higher critical constants, had a greater solubility than CO₂ in the non-polar polymeric materials. The high condensability of CO₂ and HFC 32 lead to a decrease in solubility with increasing temperature in accordance with the Van't Hoff equation.

The greater solubility of HFC 32 in the polymers suggests that HFCs are promising media for modification processes involving the impregnation of polar solutes. Furthermore, the HFC solvent is easily removed from the polymeric materials by depressurisation.

At sufficiently high pressures the absorption of gases caused swelling of the polymer samples due to gas-induced plasticization. Plasticization was investigated by the calculation of the glass transition temperature depression for each gas-polymer system and it was found that all systems were in the rubbery state under the experimental conditions employed. It was shown that HFC 32 could plasticize polystyrene and polyethylene to a greater extent than CO₂, even at lower pressures. This is significant in terms of energy requirements and economy of polymer modification processes.

Carbon dioxide and HFC 32 caused polymer swelling by two different processes. Swelling by CO₂ required decompression whereas HFC 32 caused swelling of the polymeric materials under experimental conditions, due to the high levels of gas dissolved in the samples.

It has been shown that decompression time plays an important role in the morphology of the polymer during processing. Polymeric foams were formed by rapidly decompressing the polyethylene sample exposed to CO₂. A process in which no polymer deformation occurs requires a slow decompression time and it was demonstrated that this can leave the sample unchanged when compared to the original sample, even though a reasonable amount of plasticization had occurred. It

was also found that HFC 32 could cause significant plasticization without affecting the morphology of polystyrene. The practical aspects of this work therefore demonstrate that the rate of decompression, or the appropriate selection of diluent, plays an important role in the cleaning of polymer containing components with high-pressure gases, since an overall change in the material is undesirable. This can also have implications in polymer extrusion processes allowing the use of lower temperatures leading to lower energy consumption.

The reduction of the crystalline-melting temperature due to the sorption of gas within semi-crystalline polymers can further enhance gas sorption since absorption only occurs in the amorphous regions.

It has been shown that the gas sorption in these systems can be adequately modelled using Flory-Huggins theory. This model usually assumes the Flory-Huggins interaction parameter to be independent of temperature but a better correlation between the experimental and theoretical data was obtained when temperature-dependent parameters were used.

It was demonstrated for the first time how data relating to the kinetics of gas sorption could be extracted quickly and easily from *in situ* quartz crystal microbalance measurements. It was shown, using CO₂ and polystyrene at 363 K and 60 bar as an example, how time *versus* frequency data could be converted into gas sorption *versus* time data, which could then be used to calculate the rate constant for gas sorption and the diffusion coefficient.

5.4 References

1. Abbott, A. P.; Durling, N. E.; Dyer, P. W.; Hope, E. G.; Lange, S.; Vukusic, S. *Green Chem.* **2004**, 6, 81.
2. Bonner, D. C.; Cheng, Y. *J. Polym. Sci. Polym. Lett. Ed.* **1975**, 13, 259.
3. Fried, J. R. *Polymer Science and Technology*, Prentice Hall PTR, New Jersey, **1995**.
4. Ipatiev, V.; Rutala, O. *Ber. Dtsch. Chem.* **1913**, 46, 1748.
5. Perrin, M. W. *Research* **1953**, 6, 111.
6. Krase, N. W. *US Patent* **1945**, US 2396791.
7. Ehrlich, P.; Mortimer, G. A. *Adv. Polymer Sci.* **1970**, 7, 386.
8. Cooper, A. I. *J. Mater. Chem.* **2000**, 10, 207.
9. Kendall, J. L.; Canelas, D. A.; Young, J. L.; DeSimone, J. M. *Chem. Rev.* **1999**, 99, 543.
10. Cooper, A. I.; Desimone, J. M. *Current Opinion in Solid State & Materials Sci.* **1996**, 1, 761.
11. Alessi, P.; Cortesi, A.; Kikic, I.; Vecchione, F. *J. Appl. Polym. Sci.* **2003**, 88, 2189.
12. Watkins, J. J.; McCarthy, T. J. *Macromolecules* **1994**, 27, 4845.
13. Berens, A. R.; Huvar, G. S.; Korsmeyer, R. W.; Kunig, R. W. *J. Appl. Polym. Sci.* **1992**, 46, 231.
14. Cotton, N. J.; Bartle, K. D.; Clifford, A. A.; Dowle, C. J. *J. Appl. Polym. Sci.* **1993**, 48, 1607.
15. Sand, M. L. *US Patent* **1986**, US 4598006.
16. Poliakoff, M.; Howdle, S. M.; Kazarian, S. G. *Angew. Chem. Int. Engl.* **1995**, 34, 1275.
17. Watkins, J. J.; McCarthy, T. J. *Chem. Mater.* **1995**, 7, 1991.
18. Von Schnitzler, J.; Eggers, R. *J. Supercrit. Fluids* **1999**, 16, 81.
19. Kazarian, S. G. *Polym. Sci. Ser. C* **2000**, 42, 78.
20. Muth, O.; Hirth, T.; Vogel, H. *J. Supercrit. Fluids* **2000**, 17, 65.
21. Zhong, Z.; Zheng, S.; Mi, Y. *Polymer* **1999**, 40, 3829.
22. Mensitieri, G.; Del Nobile, N. A.; Guerra, G.; Apicella, A.; Al Ghatta, H. *Polym. Eng. Sci.* **1995**, 35, 506.
23. Kazarian, S. G.; Brantley, N. H.; Eckert, C. A. *Vibr. Spectrosc.* **1999**, 19, 277.

24. Mizoguchi, K.; Hirose, T.; Naito, Y.; Kamiya, Y. *Polymer* **1987**, 28, 1298.
25. Lambert, S. M.; Paulaitis, M. E. *J. Supercrit. Fluids* **1999**, 4, 15.
26. Molina, J. M.; Rowland, F. S. *Nature* **1974**, 249, 810.
27. <http://www.afeas.org/>
28. Shafi, M. A.; Joshi, K.; Flumerfelt, R. W. *Chem. Eng. Sci.* **1997**, 52, 635.
29. Kazarian, S. G.; Vincent, M. F.; Bright, F. V.; Liotta, C. L.; Eckert, C. A. *J. Am. Chem. Soc.* **1996**, 118, 1729.
30. Kazarian, S. G.; Brantley, N. H.; West, B. L.; Vincent, M. F.; Eckert, C. A. *Appl. Spectrosc.* **1997**, 51, 491.
31. Li, M.; Bright, F. V. *Appl. Spectrosc.* **1996**, 50, 740.
32. Miyoshi, T.; Takegoshi, K.; Terao, T. *Macromolecules* **1997**, 30, 6582.
33. Nealey, P. F.; Cohen, R. E.; Argon, A. S. *Macromolecules* **1994**, 27, 4193.
34. Van der Vegt, N. F. A.; Briels, W. J.; Wessling, M.; Strathmann, H. *J. Chem. Phys.* **1999**, 110, 11061.
35. Kamiya, Y.; Mizoguchi, K.; Naito, Y. *J. Polym. Sci. Part B: Polym. Phys.* **1990**, 28, 1955.
36. Edwards, R. R.; Tao, Y.; Xu, S.; Wells, P. S.; Yun, K. S.; Parcher, J. F. *J. Phys. Chem.* **1998**, 1287.
37. Edwards, R. R.; Tao, Y.; Xu, S.; Wells, P. S.; Yun, K. S.; Parcher, J. F. *J. Polym. Sci. Part B: Polym. Phys.* **1998**, 36, 2537.
38. Kim, J-M.; Chang, S-M.; Muramatsu, H. *Polymer* **1999**, 40, 3291.
39. Boudouris, D.; Prinos, J.; Bridakis, M.; Pantoula, M.; Panayiotou, C. *Ind. Eng. Chem. Res.* **2001**, 40, 604.
40. Saurebrey, G. Z.; *J. Phys.* **1959**, 155, 206.
41. Koros, W. J.; Smith, G. N.; Stannet, V. *J. Appl. Polym. Sci.* **1981**, 26, 159.
42. Shim, J-J.; Johnston, K. P. *AIChE J.* **1989**, 35, 1097.
43. Doghieri, F.; Sarti, G. C. *Macromolecules* **1996**, 29, 7885.
44. Wissinger, R. G.; Paulaitis, M. E.; *Ind. Eng. Chem. Res.* **1991**, 30, 842.
45. Suwandi, M. S.; Stern, S. A. *J. Polym. Sci., Polym. Phys. Ed.* **1973**, 11, 663.
46. Kamiya, Y.; Naito, Y.; Terada, K.; Mizoguchi, K. *Macromolecules* **2000**, 33, 3111.
47. Sanchez, I. C.; Lacombe, R. H. *J. Phys. Chem.* **1976**, 80, 2352.
48. Sanchez, I. C.; Lacombe, R. H. *Stat. Thermo. Polym. Sol.* **1978**, 11, 1145.

49. Sato, Y.; Yurugi, M.; Fujiwara, K.; Takishima, S.; Masuoka, H. *Fluid Phase Equilibria* **1996**, 125, 129.
50. Garg, A, Gulari, E.; Manke, C. W. *Macromolecules* **1994**, 27, 5643.
51. Sato, Y.; Takikawa, T.; Takishima, S.; Masuoka, H. *J. Supercrit. Fluids* **2001**, 19, 187.
52. Zhang, Y.; Gangwani, K. K.; Lemert, R. M. *J. Supercrit. Fluids* **1997**, 11, 115.
53. Sato, Y.; Fujiwara, K.; Takikawa, T.; Sumarno.; Takishima, S.; Masuoka, H. *Fluid Phase Equilibria* **1999**, 162, 261.
54. Chapman, W. G.; Gubbins, K. E.; Jackson, G.; Radosz, M. *Fluid Phase Equilibria* **1989**, 52, 31.
55. Chapman, W. G.; Gubbins, K. E.; Jackson, G.; Radosz, M. *Ind. Eng. Chem. Res.* **1990**, 29, 1709.
56. Miller, E. A.; Gubbins, K. E. *Ind. Eng. Chem. Res.* **2001**, 40, 2193.
57. Colina, C. M.; Hall, C. K.; Gubbins, K. E. *Fluid Phase Equilibria* **2002**, 194, 553.
58. Ensore, D. J.; Hopfenberg, H. B.; Stannett, V. T.; Berens, A. R. *Polymer* **1977**, 18, 1105.
59. Sefik, M. D. *J. Polym. Sci. Polym. Phys.* **1986**, 24, 935.
60. Kamiya, Y.; Mizoguchi, K.; Terada, K.; Fujiwara, Y.; Wang, J. S. *Macromolecules* **1998**, 31, 472.
61. Pope, D. S.; Fleming, G. K.; Koros, W. J. *Macromolecules* **1990**, 23, 2988.
62. Fleming, G. K.; Koros, W. J. *Macromolecules* **1986**, 19, 2285.
63. Condo, P. D.; Sanchez, I. C.; Panayiotou, C. G.; Johnston, K. P. *Macromolecules* **1992**, 25, 6119.
64. Jessop, P. G.; Leitner, W. *Chemical Synthesis using Supercritical Fluids*, Wiley-VCH, Weinheim, **1999**.
65. Ghosal, K.; Freeman, B. D. *Polym. Adv. Technol.* **1994**, 5, 673.
66. Kamiya, Y.; Mizoguchi, K.; Takuji, H.; Yasutoshi, N. *J. Polym. Sci. Polym. Phys.* **1989**, 27, 879.
67. Kamiya, Y.; Hirose, T.; Mizoguchi, K.; Naito, Y. *J. Polym. Sci. Polym. Phys.* **1986**, 24, 1525.
68. Mauze, G. R.; Stern, S. A. *Polym. Eng. Sci.* **1983**, 23, 548
69. Values supplied by Rapra Technology Ltd.

-
70. French, R. N.; Koplos, G. J. *Fluid Phase Equilibria* **1999**, 158, 879.
 71. Banerjee, T.; Lipscomb, G. G. *J. Appl. Polym. Sci.* **1998**, 68, 1441.
 72. Chow, T. S. *Macromolecules* **1980**, 13, 362.
 73. Goh, S. H.; Lee, S. Y. *Thermochimica Acta.* **1990**, 161, 119.
 74. Gaur, U.; Wunderlich, B. *Macromolecules* **1980**, 13, 445.
 75. Shieh, Y-T.; Su, J-H.; Manivannan, G.; Lee, P. H. C.; Sawan, S. P.; Spall, W. *D. J. Appl. Polym. Sci.* **1996**, 59, 707.
 76. Shieh, Y-T.; Su, J-H.; Manivannan, G.; Lee, P. H. C.; Sawan, S. P.; Spall, W. *D. J. Appl. Polym. Sci.* **1996**, 59, 695.
 77. Spartan Pro, Wave Function Inc, Irvine Ca, USA.
 78. Freeman, B.; Pinnau, I. *Reviews* **1997**, 5, 167.
 79. Wong, B.; Zhang, Z.; Handa, Y. P. *J. Polym. Sci. Part B Polym. Phys.* **1998**, 36, 2025.
 80. Felder, R. M. *J. Membr. Sci.* **1978**, 3, 15.
 81. Balik, C. M. *Macromolecules* **1996**, 29, 3025.

CHAPTER 6

SUMMARY AND FUTURE WORK

6.1 Summary

6.1.1 Solubility Studies

6.1.2 Hydrogenation Reactions

6.1.3 Polymer Modification

6.2 Future Work

6.2.1 Solubility and Separation Studies

6.2.2 Hydrogenation Reactions

6.2.3 Polymer Processing

6.1 Summary

This study has shown that hydrofluorocarbons (HFCs) are promising alternatives to conventional liquid solvents for hydrogenation and polymer modification processes. These media have accessible critical constants, relatively high dielectric constant values and are able to facilitate the dissolution of polar solutes and rhodium based catalysts without the need for co-solvents or fluorinated ponytails. Furthermore, the investigation suggests that reactions carried out in the supercritical (sc) regime can allow facile reagent/product separation and it is logical to assume that a similar methodology can be applied to catalyst recovery.

It was also shown that difluoromethane (HFC 32) can cause significant plasticization in polystyrene (PS) and polyethylene (PE) at moderately low pressures and this shows potential for a range of applications such as foaming, impregnation and a reduction in the energy required for polymer extrusion.

6.1.1 Solubility Studies

The solubility of a range of unsaturated carboxylic acids was measured in 1,1,1,2-tetrafluoroethane (HFC 134a) using dielectrometry and gravimetric techniques. It was shown that this medium could dissolve polar solutes to a greater extent than carbon dioxide and the results were explained in terms of dipole moment and vapour pressure considerations. Measurements were carried out for both binary and ternary systems and it was demonstrated that the Peng-Robinson equation of state (PR EOS) could adequately model solubilities in these systems.

The PR EOS model was used to devise a methodology for the separation of itaconic acid (unsaturated substrate) and methylsuccinic acid (hydrogenation product). The theoretical separation method employs a counter-current separation column and it was suggested that HFC 134a could be used as both the reaction solvent and extracting medium, which enables in-line separation of compounds during sc synthesis.

6.1.2 Hydrogenation Reactions

For the first time hydrogenation of unsaturated substrates has been carried out in sc HFC 134a. The work showed that this medium is a suitable solvent for asymmetric hydrogenation of polar substrates employing a rhodium/MonoPhos based catalyst (Section 2.3.2, page 35). The catalyst had a high degree of solubility

in this medium without the need for co-solvents or fluorinated ponytails, which has positive practical and economic implications. High yields and enantioselectivities comparable to those in liquid solvents were obtained and this coupled with the separation technique makes this a commercially attractive process. The enantioselectivity showed no dependence on solution dielectric constant or initial hydrogen pressure and this complements results obtained in liquid solvents. This suggests that the mechanism for asymmetric hydrogenation, facilitated by the rhodium/MonoPhos catalytic species, is the same in the sc regime as it is in liquid solvents.

6.1.3 Polymer Modification

A quartz crystal microbalance (QCM) was used to assess the sorption of HFC 32 in PS and PE and the results were compared to the sorption of carbon dioxide in the same polymeric materials. This is the first time that HFC 32 has been investigated for use as a polymer modifying agent.

For both polymers it was shown that HFC 32 has a higher solubility than carbon dioxide within the samples and this suggests that HFCs are promising media for the impregnation of polar solutes. It was shown that the infusion of gas into the polymers can reduce the glass transition temperature and this plasticization could be significant in terms of economy and energy requirements for polymer modification processes.

Manipulating system conditions can facilitate plasticization with or without changes in polymer morphology and this suggests that HFCs could be used for a range of applications such as foaming, impregnation and cleaning of polymer-containing materials.

The results were adequately described by Flory-Huggins theory and it was demonstrated for the first time how data relating to the kinetics of gas sorption could be extracted quickly and easily from *in situ* quartz crystal microbalance measurements.

6.2 Future Work

6.2.1 Solubility and Separation Studies

Knowledge of the ability of a sc fluid to dissolve a particular solute is essential in process design. Recovery of precious metal catalysts is very important for synthetic processes and future work will focus on quantitative determinations of the solubilities of these compounds. Solubility studies in ternary systems with varying molar ratios of reagent (itaconic acid) and product (methylsuccinic acid) along with experimental investigations of system phase behaviour would allow the design of a more detailed and realistic separation process.

Although solubility diminution has been observed previously, no explanation for this phenomenon has been offered. Solvatochromic investigations can be used to study solution interactions and this would give a greater understanding of this process.

6.2.2 Hydrogenation Reactions

Promising results for asymmetric hydrogenation in HFC 134a have been obtained in this study. Future work should build upon these initial results and focus on the effects of pressure, temperature and reagent concentration on reaction kinetics. Solution dielectric constant values need to be evaluated in order to provide a greater understanding of the influence of reaction conditions on asymmetric hydrogenation in HFC solvents.

Studies should be extended to ruthenium/BINAP catalytic systems since initial hydrogen concentration can have a significant effect on enantioselectivities with these catalysts in liquid solvents. It is hoped that results would show that enantioselectivity in the sc regime can be fine tuned due to the complete miscibility of gaseous hydrogen with sc solvents.

6.2.3 Polymer Processing

It has been shown that HFC 32 can cause significant plasticization and changes in morphology for PS and PE and this is a promising result for a range of polymer modification processes. Future work will focus on altering polymer morphology and producing foams of specific pore size, facilitated by manipulation of system conditions.

APPENDIX

Item	Quantity	Unit Price	Total Price
1.00	1.00	1.00	1.00
2.00	2.00	2.00	4.00
3.00	3.00	3.00	9.00
4.00	4.00	4.00	16.00
5.00	5.00	5.00	25.00
6.00	6.00	6.00	36.00
7.00	7.00	7.00	49.00
8.00	8.00	8.00	64.00
9.00	9.00	9.00	81.00
10.00	10.00	10.00	100.00

APPENDIX A - Summary of the data collected during the field study.

Item	Quantity	Unit Price	Total Price
1.00	1.00	1.00	1.00
2.00	2.00	2.00	4.00
3.00	3.00	3.00	9.00
4.00	4.00	4.00	16.00
5.00	5.00	5.00	25.00
6.00	6.00	6.00	36.00
7.00	7.00	7.00	49.00
8.00	8.00	8.00	64.00
9.00	9.00	9.00	81.00
10.00	10.00	10.00	100.00

Pressure / bar	Molarity / Mol L ⁻¹	Mole fraction solubility
50	0.263	0.03457
70	0.350	0.03971
80	0.439	0.04770
90	0.469	0.04956
110	0.504	0.05116
130	0.534	0.05249
150	0.564	0.05404

Table 1 Solubility data for crotonic acid in HFC 134a at 378 K.

Pressure / bar	Molarity / Mol L ⁻¹	Mole fraction solubility
70	0.223	0.02567
80	0.233	0.02586
100	0.253	0.02678
120	0.265	0.02714
150	0.277	0.02731
190	0.289	0.02742

Table 2 Solubility data for 6-methoxy-1-tetralone in HFC 134a at 378 K.

Temperature / K	Pressure / bar	Molarity / Mol L ⁻¹	Mole fraction solubility
378	50	0.016	0.00223
378	70	0.033	0.00387
378	90	0.051	0.00568
378	110	0.062	0.00661
378	140	0.079	0.00799
378	200	0.089	0.00859
383	50	0.0348	0.00580
383	80	0.078	0.00920
383	100	0.108	0.01199
383	135	0.132	0.01373
383	140	0.137	0.01413
383	160	0.143	0.01439
383	180	0.149	0.01468

Table 3 Solubility data for methylsuccinic acid in HFC 134a.

Pressure / bar	Molarity / Mol L ⁻¹	Mole fraction solubility
40	0.001	5.0376E-4
60	0.008	0.00101
80	0.010	0.00112
125	0.012	0.00122
155	0.013	0.00133
170	0.014	0.00141
200	0.015	0.00146

Table 4 Solubility data for α -acetamidocinnamic acid in HFC 134a at 378 K.

Temperature / K	Pressure / bar	Molarity / Mol L ⁻¹	Mole fraction solubility
378	50	0.003	4.2992E-4
378	80	0.006	6.9520E-4
378	105	0.009	9.3769E-4
378	140	0.0112	0.00115
378	180	0.012	0.00116
383	35	8.14E-4	4.6902E-4
383	60	0.006	7.5921E-4
383	90	0.009	0.00104
383	125	0.012	0.00131
383	140	0.014	0.00151
383	165	0.015	0.00157
383	185	0.016	0.00160
393	40	0.002	0.00114
393	70	0.012	0.00170
393	110	0.025	0.00296
393	130	0.031	0.00349
393	155	0.037	0.00390
393	190	0.039	0.00398
393	205	0.040	0.00406

Table 5 Solubility data for itaconic acid in HFC 134a.

Pressure / bar	Experimental mole fraction solubility	Predicted mole fraction solubility
50	0.03457	0.03356
70	0.03971	0.04316
80	0.04770	0.04701
90	0.04956	0.04892
110	0.05116	0.04947
130	0.05249	0.05269
150	0.05404	0.05489

Table 6 Comparison of experimental and theoretical solubility data for crotonic acid in HFC 134a at 378 K and a variety of pressures.

Pressure / bar	Experimental mole fraction solubility	Predicted mole fraction solubility
70	0.02567	0.02398
80	0.02586	0.02548
100	0.02678	0.02642
120	0.02714	0.02744
150	0.02731	0.02763
190	0.02742	0.02735

Table 7 Comparison of experimental and theoretical solubility data for 6-methoxy-1-tetralone in HFC 134a at 378 K and a variety of pressures.

Pressure / bar	Experimental mole fraction solubility	Predicted mole fraction solubility
40	8.04E-4	8.9800E-4
60	0.00101	9.8400E-4
80	0.00112	0.00111
125	0.00122	0.00123
155	0.00133	0.00135
170	0.00141	0.00139
200	0.00146	0.00145

Table 8 Comparison of experimental and theoretical solubility data for α -acetamido-cinnamic acid in HFC 134a at 378 K and a variety of pressures.

Temperature / K	Pressure / bar	Experimental mole fraction solubility	Predicted mole fraction solubility
383	50	0.0058	0.00585
383	80	0.0092	0.01042
383	100	0.01199	0.01120
383	135	0.01373	0.01390
383	140	0.01413	0.01404
383	160	0.01439	0.01426
383	180	0.01468	0.01448
378	50	0.00223	0.00202
378	70	0.00387	0.00477
378	90	0.00568	0.00552
378	110	0.00661	0.00614
378	140	0.00799	0.00737
378	200	0.00859	0.00836

Table 9 Comparison of experimental and theoretical solubility data for methylsuccinic acid in HFC 134a along at two different temperatures and a variety of pressures.

Temperature / K	Pressure / bar	Experimental mole fraction solubility	Predicted mole fraction solubility
393	40	0.00114	1.0370E-5
393	70	0.00170	9.5349E-4
393	110	0.00296	0.00276
393	130	0.00349	0.00334
393	155	0.00390	0.00384
393	190	0.00398	0.00424
393	205	0.00406	0.00432
383	35	4.6900E-4	4.2878E-6
383	60	7.5921E-4	5.36858E-4
383	90	0.00104	0.00115
383	125	0.00131	0.00149
383	140	0.00151	0.00156
383	165	0.00157	0.00161
383	185	0.00160	0.00162
378	50	4.2991E-4	2.8747E-4
378	80	6.952E-4	7.9139E-4
378	105	9.3769E-4	0.00102
378	140	0.00115	0.00119
378	180	0.00119	0.00125

Table 10 Comparison of experimental and theoretical solubility data for itaconic acid in HFC 134a at three different temperatures and a variety of pressures.

Solute	Pressure / bar	Experimental mole fraction solubility	Predicted mole fraction solubility
Methylsuccinic acid	55	0.00519	0.00411
Methylsuccinic acid	65	0.00589	0.00509
Methylsuccinic acid	75	0.00582	0.00605
Methylsuccinic acid	80	0.00578	0.00644
Methylsuccinic acid	95	0.00618	0.00643
Methylsuccinic acid	110	0.00626	0.00657
Methylsuccinic acid	120	0.00622	0.00676
Methylsuccinic acid	140	0.00630	0.00677
Methylsuccinic acid	150	0.00645	0.00654
Methylsuccinic acid	160	0.00651	0.00641
Itaconic acid	55	9.8390E-4	8.8039E-4
Itaconic acid	65	0.00127	0.00143
Itaconic acid	75	0.00184	0.00184
Itaconic acid	80	0.00202	0.00201
Itaconic acid	95	0.00254	0.00246
Itaconic acid	110	0.00298	0.00278
Itaconic acid	120	0.00306	0.00294
Itaconic acid	140	0.00311	0.00319
Itaconic acid	150	0.00311	0.00328
Itaconic acid	160	0.00319	0.00334
Itaconic acid	205	0.00360	0.00340

Table 11 Comparison of experimental and theoretical solubility data for the ternary itaconic acid and methylsuccinic acid system in HFC 134a at 383 K.

Time / hours	% Conversion
1.00	76.5
1.25	77.8
1.50	82.2
1.75	85.4
2.00	86.9
3.00	85.9
4.00	86.7
6.00	87.5
8.00	86.2
10.00	86.7

Table 12 Time dependency of the hydrogenation of **44** in HFC 134 using 2.20×10^{-6} mol dm⁻³ of [RhCl(PPh₃)₃] and 0.57 mol dm⁻³ of hydrogen at 383 K and 100 bar total pressure.

Pressure / bar	% Conversion
50	59.7
55	63.4
60	72.1
70	81.2
80	85.4
85	85.1
90	86.3
100	85.2
115	86.6

Table 13 Pressure dependency of the hydrogenation of styrene using [RhCl(PPh₃)₃] in HFC 134a at constant mole fraction and 383 K.

Pressure / bar	% Conversion	% ee (<i>R</i>)
20	43.8	88.4
30	71.4	93.1
40	96.0	90.4
50	97.6	85.8
80	100	87.5
100	100	88.3
120	100	89.8
140	100	92.4
170	100	92.5

Table 14 Results for the pressure dependency of asymmetric hydrogenation of itaconic acid in HFC 134a at 383 K.

Pressure / bar	% Conversion	% ee (<i>R</i>)
20	34.2	85.8
30	38.5	90.8
40	54.5	88.2
50	78.5	84.3
70	93.6	86.1
100	100	89.4
120	100	87.9
140	99.7	90.3

Table 15 Results for the pressure dependency of asymmetric hydrogenation of dimethyl itaconate in HFC 134a at 383 K.

Pressure / bar	% Conversion	% ee (<i>S</i>)
20	9.5	92.5
30	9.4	89.4
50	16.7	84.3
70	45.0	90.8
120	92.3	86.4
130	100	88.7
140	100	91.8
160	100	87.6

Table 16 Results for the pressure dependency of asymmetric hydrogenation of α -acetamido-cinnamic acid in HFC 134a at 383 K.

Pressure / bar	% Conversion	% ee (<i>R</i>)
20	28.6	78.3
30	32.4	82.1
50	37.5	74.9
70	58.3	80.7
120	82.4	78.6
130	83.1	75.2
140	81.9	79.8

Table 17 Results for the pressure dependency of asymmetric hydrogenation of *trans*-2-methyl-2-pentenoic acid in HFC 134a at 383 K.

Hydrogen gas pressure / bar	% ee (<i>R</i>)
2.5	88.3
5	90.4
10	86.2
20	92.3

Table 18 The dependence of enantioselectivity for (*R*)-methylsuccinic acid on initial hydrogen pressure in HFC 134a at 383 K and 100 bar.

373 K		413 K		453 K	
Pressure / bar	Gas sorption / g gas/g of polymer	Pressure / bar	Gas sorption / g gas/g of polymer	Pressure / bar	Gas sorption / g gas/g of polymer
36.17	0.0226	72.90	0.0347	24.72	0.0009
58.60	0.0359	107.21	0.0526	62.76	0.0219
79.21	0.0484	115.94	0.0602	101.88	0.0389
119.28	0.0781	119.94	0.058	127.04	0.0513
143.48	0.0929	143.16	0.0727	143.79	0.0570
159.08	0.1000	147.38	0.0713	154.44	0.0596
174.76	0.1104	161.10	0.0833	173.72	0.0687
185.54	0.1157	170.87	0.0857	-	-
-	-	180.97	0.0931	-	-
-	-	197.39	0.1048	-	-
-	-	200.36	0.1012	-	-

Table 19 Data for the reported gas sorption of CO₂ in polystyrene by Sato *et al.* used for method verification in Section 5.2.1.

Pressure / bar	Gas sorption / g of gas/g of polymer	
	Run 1	Run 2
20	0.02822	0.03324
40	0.04837	0.05864
60	0.05931	0.05866

Table 20 Data for successive sorption runs for the CO₂-polystyrene system at 343 K.

P / bar	F _p	F ₁	R _p	R ₀	F ₀	Gas sorption / g gas/g polymer
	/ MHz					
20	9.98791	9.995	9.9984	10.0052	10.0052	0.02822
40	9.98756	9.995	9.99825	10.0052	10.0052	0.04837
60	9.9869	9.995	9.9977	10.0052	10.0052	0.05931

Table 21 Data for CO₂ solubility in polystyrene at 343 K.

P / bar	F _p	F ₁	R _p	R ₀	F ₀	Gas sorption / g gas/g polymer
	/ MHz					
20	9.94207	9.95	9.9984	10.0052	10.0052	0.02048
40	9.94092	9.95	9.99825	10.0052	10.0052	0.03857
60	9.93985	9.95	9.9977	10.0052	10.0052	0.04801

Table 22 Data for CO₂ solubility in polystyrene at 363 K.

P / bar	F _p	F _l	R _p	R ₀	F ₀	Gas sorption / g gas/g polymer
	/ MHz					
20	9.98753	9.995	9.9984	10.0052	10.0052	0.06525
40	9.9869	9.995	9.99825	10.0052	10.0052	0.11265

Table 23 Data for HFC 32 solubility in polystyrene at 343 K.

P / bar	F _p	F _l	R _p	R ₀	F ₀	Gas sorption / g gas/g polymer
	/ MHz					
30	9.99019	9.9986	9.99795	10.0052	10.0052	0.01755
40	9.98981	9.9986	9.9979	10.0052	10.0052	0.02253
60	9.98915	9.9986	9.99755	10.0052	10.0052	0.0273
80	9.98764	9.9986	9.9966	10.0052	10.0052	0.03581
100	9.98564	9.9986	9.9953	10.0052	10.0052	0.04632
130	9.98438	9.9986	9.99505	10.0052	10.0052	0.0617
150	9.98269	9.9986	9.99485	10.0052	10.0052	0.08421
180	9.97773	9.9986	9.99475	10.0052	10.0052	0.15787
220	9.97181	9.9986	9.9947	10.0052	10.0052	0.24681

Table 24 Data for CO₂ solubility in polyethylene at 363 K.

P / bar	F _p	F _l	R _p	R ₀	F ₀	Gas sorption / g gas/g polymer
	/ MHz					
20	9.98704	9.9925	10.0011	10.0052	10.0052	0.01072
40	9.98601	9.9925	10.0005	10.0052	10.0052	0.01413
60	9.98439	9.9925	9.9996	10.0052	10.0052	0.0198
100	9.98173	9.9925	9.9982	10.0052	10.0052	0.0297
130	9.97751	9.9925	9.99625	10.0052	10.0052	0.04752
150	9.97509	9.9925	9.9949	10.0052	10.0052	0.05595
180	9.96811	9.9925	9.9926	10.0052	10.0052	0.09286
220	9.95508	9.9925	9.989	10.0052	10.0052	0.16709

Table 25 Data for CO₂ solubility in polyethylene at 383 K.

P / bar	F _p	F _l	R _p	R ₀	F ₀	Gas sorption / g gas/g polymer
	/ MHz					
20	9.98418	9.99	9.9995	10.0052	10.0052	0.0078
40	9.97956	9.99	9.9949	10.0052	10.0052	0.00945
60	9.97022	9.99	9.9856	10.0052	10.0052	0.01174
100	9.957	9.99	9.9725	10.0052	10.0052	0.01964

Table 26 Data for CO₂ solubility in polyethylene at 403 K.

P / bar	F _p	F _l	R _p	R ₀	F ₀	Gas sorption / g gas/g polymer
	/ MHz					
20	9.98792	9.995	9.99845	10.0052	10.0052	0.03208
40	9.98744	9.995	9.9982	10.0052	10.0052	0.05455
70	9.98681	9.995	9.998	10.0052	10.0052	0.09725
100	9.98606	9.995	9.99765	10.0052	10.0052	0.13637
130	9.98426	9.995	9.9963	10.0052	10.0052	0.18078
150	9.98354	9.995	9.996	10.0052	10.0052	0.22157
180	9.98194	9.995	9.9952	10.0052	10.0052	0.29996
220	9.98057	9.995	9.9947	10.0052	10.0052	0.38578
250	9.97946	9.995	9.9943	10.0052	10.0052	0.4551

Table 27 Data for HFC 32 solubility in polyethylene at 363 K.

P / bar	F _p	F _l	R _p	R ₀	F ₀	Gas sorption / g gas/g polymer
	/ MHz					
20	10.02195	9.9925	10.035	10.0052	10.0052	0.02792
40	10.01824	9.9925	10.0315	10.0052	10.0052	0.04411
60	10.01497	9.9925	10.0285	10.0052	10.0052	0.06562
100	10.00842	9.9925	10.0225	10.0052	10.0052	0.10865

Table 28 Data for HFC 32 solubility in polyethylene at 403 K.

Gas	Temperature / K	Pressure / bar	ω	Calculated T_g / K
CO ₂	343	20	0.02822	357.47
CO ₂	343	40	0.04837	356.79
CO ₂	343	60	0.05931	356.45
CO ₂	363	20	0.02048	357.77
CO ₂	363	40	0.03857	357.11
CO ₂	363	60	0.04801	356.80
HFC 32	343	20	0.06525	356.56
HFC 32	343	40	0.11265	355.43

Table 29 The Parameters used in Equation 5.25 to calculate T_g depression for the polystyrene systems.

Temperature / K	Pressure / bar	ω	Calculated T_g / K
363	30	0.01755	142.67
363	40	0.02253	142.60
363	60	0.0273	142.52
363	80	0.03581	142.40
363	100	0.04632	142.26
363	130	0.0617	142.05
363	150	0.08421	141.77
363	180	0.15787	140.89
363	220	0.24681	139.87
383	20	0.01072	142.79
383	40	0.01413	142.73
383	60	0.0198	142.64
383	100	0.0297	142.49
383	130	0.04752	142.24
383	150	0.05595	142.13
383	180	0.09286	141.66
383	220	0.16709	140.78
403	20	0.0078	142.84
403	40	0.00945	142.81
403	60	0.01174	142.77
403	100	0.01964	142.64

Table 30 The Parameters used in Equation 5.25 to calculate T_g depression for the CO₂-polyethylene systems.

Temperature / K	Pressure / bar	ω	Calculated T_g / K
363	20	0.03208	142.52
363	40	0.05455	142.25
363	70	0.09725	141.77
363	100	0.13637	141.36
363	130	0.18078	140.90
363	150	0.22157	140.47
363	180	0.29996	139.66
363	220	0.38578	138.75
363	250	0.4551	138.00
403	20	0.02792	142.58
403	40	0.04411	142.38
403	60	0.06562	142.12
403	100	0.10865	141.65

Table 31 The Parameters used in Equation 5.25 to calculate T_g depression for the HFC 32-polyethylene systems.

Pressure	Vol. of CO ₂ / cm ³	Vol. of PE / cm ³	ϕ_l	Calculated T _m / K
20	0.0115	1.27827	0.00889	403.17
40	0.0147	1.27742	0.0114	399.00
60	0.0178	1.2765	0.0138	395.12
80	0.0234	1.27502	0.018	388.48
100	0.0302	1.27355	0.0232	380.74
130	0.0403	1.2718	0.0307	370.27
150	0.055	1.27033	0.0415	356.57
180	0.103	1.26858	0.0752	321.87
220	0.161	1.26564	0.113	293.51

Table 32 The parameters used in Equation 3.9 to calculate T_m depression for the CO₂-polyethylene system at 363 K.

Pressure	Vol. of CO ₂ / cm ³	Vol. of PE / cm ³	ϕ_l	Calculated T _m / K
30	0.007	1.3017	0.00535	409.27
40	0.00923	1.29948	0.00705	406.30
60	0.0129	1.29836	0.00986	401.51
100	0.0194	1.29501	0.0148	393.51
130	0.031	1.29305	0.0234	380.30
150	0.0365	1.29138	0.0275	374.49
180	0.0607	1.28943	0.0449	352.21
220	0.109	1.28608	0.0782	318.48

Table 33 The parameters used in Equation 3.9 to calculate T_m depression for the CO₂-polyethylene system at 383 K.

Pressure	Vol. of CO ₂ / cm ³	Vol. of PE / cm ³	ϕ_l	Calculated T _m / K
20	0.00509	1.32396	0.00383	411.97
40	0.00617	1.32154	0.00465	410.52
60	0.00767	1.32021	0.00578	408.53
100	0.0128	1.31646	0.00965	401.87

Table 34 The parameters used in Equation 3.9 to calculate T_m depression for the CO₂-polyethylene system at 403 K.

Gas	Temperature / K	Pressure / bar	Experimental gas sorption / g of gas/g of polymer	Predicted gas sorption / g of gas/g of polymer	
				T.I.	T.D.
CO ₂	343	20	0.02822	0.02405	0.02097
CO ₂	343	40	0.04837	0.04922	0.04306
CO ₂	343	60	0.05931	0.07551	0.06632
CO ₂	363	20	0.02048	0.01583	0.01815
CO ₂	363	40	0.03857	0.03214	0.03675
CO ₂	363	60	0.04801	0.04894	0.05578
HFC 32	343	20	0.06525	0.05813	0.05813
HFC 32	343	40	0.11265	0.12685	0.12685

Table 35 Comparison of the experimental and predicted gas solubility in the polystyrene systems (T.I.: data using temperature independent interaction parameters; T.D.: data using temperature dependent interaction parameters).

Temperature / K	Pressure / bar	Experimental gas sorption / g of gas/g of polymer	Predicted gas sorption / g of gas/g of polymer	
			T.I.	T.D.
363	30	0.01755	0.01746	0.01661
363	40	0.02253	0.0235	0.02236
363	60	0.0273	0.03593	0.0342
363	80	0.03581	0.04885	0.04652
363	100	0.04632	0.06228	0.05933
363	130	0.0617	0.08345	0.07956
363	150	0.08421	0.09829	0.09375
363	180	0.15787	0.12168	0.15445
363	220	0.24681	0.19742	0.24791
383	20	0.01072	0.00761	0.00808
383	40	0.01413	0.01542	0.01636
383	60	0.0198	0.02341	0.02484
383	100	0.0297	0.04003	0.04245
383	130	0.04752	0.05307	0.05625
383	150	0.05595	0.06205	0.06574
383	180	0.09286	0.07596	0.08042
383	220	0.16709	0.1259	0.15363
403	20	0.0078	0.00484	0.00556
403	40	0.00945	0.00975	0.0112
403	60	0.01174	0.01474	0.01693
403	100	0.01964	0.02496	0.02864

Table 36 Comparison of the experimental and predicted gas solubility in the CO₂-polyethylene systems (T.I.: data using temperature independent interaction parameters; T.D.: data using temperature dependent interaction parameters).

Temperature / K	Pressure / bar	Experimental gas sorption / g of gas/g of polymer	Predicted gas sorption / g of gas/g of polymer	
			T.I.	T.D.
363	20	0.03208	0.02977	0.0189
363	40	0.05455	0.06343	0.04012
363	70	0.09725	0.12315	0.07767
363	100	0.13637	0.19709	0.12505
363	130	0.18078	0.28805	0.18794
363	150	0.22157	0.35734	0.2432
363	180	0.29996	0.4668	0.35459
363	220	0.38578	0.60283	0.53653
363	250	0.4551	0.68914	0.65293
403	20	0.02792	0.01384	0.02227
403	40	0.04411	0.02849	0.04558
403	60	0.06562	0.04403	0.06996
403	100	0.10865	0.07812	0.12194

Table 37 Comparison of the experimental and predicted gas solubility in the HFC 32-polyethylene systems (T.I.: data using temperature independent interaction parameters; T.D.: data using temperature dependent interaction parameters).

Frequency / MHz	Gas sorption / g of gas/g of polymer	Time / mins
9.9425	1E-6	0
9.94246	7.2464E-4	20
9.94242	0.00145	40
9.9423	0.00362	60
9.94223	0.00489	80
9.9421	0.00725	100
9.9419	0.01087	120
9.9416	0.01630	140
9.94118	0.02391	160
9.9409	0.02899	180
9.9403	0.03986	200
9.93985	0.04801	220
9.93985	0.04801	240

Table 38 The change in QCM scan frequency and gas sorption with time for CO₂ in polystyrene at 363 K and 60 bar.